# Characterization and Remobilization of Sediment Deposits in Reservoirs

by

Yannick Dück

from Cologne (Germany)

Accepted Dissertation thesis for the partial fulfillment of the requirements for a

Doctor of Natural Sciences

Fachbereich 7: Natur- und Umweltwissenschaften

Universität Koblenz-Landau

Thesis examiners:

Prof. Dr. rer. nat. Andreas Lorke (Landau, Germany)

Prof. Dr.-Ing. Christian Jokiel (Cologne, Germany)

Date of oral examination: May 10th 2019

This dissertation is based on the following publication and manuscripts (ordered by date). I was the lead author of the articles. The contributions of all authors are stated in *Appendices I-IV*.

1. Dück, Y., Fahlenbock, T., Frings, R., and C. Jokiel. 2017. DENSE: Semicontinuous Automated, Gravimetric Measurement Device for Suspended Sediment Concentrations. International Journal of Hydraulic Engineering. 143(12), doi: doi.org/10.1061/(ASCE)HY.1943-7900.0001374.
2. Dück, Y., Liu, L., Lorke, A., Ostrovsky, I., Katsman, R., and C. Jokiel. 2019. A novel freeze corer for characterization of methane bubbles and assessment of coring disturbances. Limnology and Oceanography: Methods, 17: 305-319, doi: 10.1002/lom3.10315.
3. Dück, Y., Lorke, A., Jokiel, C., and J. Gierse. Laboratory and Field Investigations on Freeze and Gravity Core Sampling and Assessment of Coring Disturbances with Implications on Gas Bubble Characterization. Submitted for publication in: Limnology and Oceanography: Methods.
4. Dück, Y., Bolsenkötter, L., Lorke, A., and C. Jokiel. Experimental Investigation of Impinged, Oblique Submerged Cavitating Water Jets with Pressure Measurement Sensing. Submitted for publication in: International Journal of Hydraulic Engineering.

# Table of Contents

## Abstract

Sediment transport contributes to the movement of inorganic and organic material in rivers. The construction of a dam interrupts the continuity of this sediment transport through rivers, causing sediments to accumulate within the reservoir. Reservoirs can also act as carbon sinks and methane can be released when organic matter in the sediment is degraded under anoxic conditions. Reservoir sedimentation poses a great threat to the sustainability of reservoirs worldwide, and can emit the potent greenhouse gas methane into the atmosphere. Sediment management measures to rehabilitate silted reservoirs are required to achieve both better water quantity and quality, as well as to mitigate greenhouse gas emissions.

This thesis aims at the improvement of sediment sampling techniques to characterize sediment deposits as a basis for accurate and efficient water jet dredging and to monitor the dredging efficiency by measuring the sediment concentration. To achieve this, we investigated freeze coring as a method to sample (gas-bearing) sediment *in situ.* The freeze cores from three reservoirs obtained were scanned using a non-destructive X-Ray CT scan technique. This allows the determination of sediment stratification and characterization of gas bubbles to quantify methane emissions and serve as a basis for the identification of specific (i.e. contaminated) sediment layers to be dredged. The results demonstrate the capability of freeze coring as a method for the characterization of (gas-bearing) sediment and overcomes certain limitations of commonly used gravity cores. Even though the core's structure showed coring disturbances related to the freezing process, the general core integrity seems to not have been disturbed. For dredging purposes, we analyzed the impact pressure distribution and spray pattern of submerged cavitating water jets and determined the effects of impinging distances and angles, pump pressures and spray angles. We used an adapted Pressure Measurement Sensing technique to enhance the spatial distribution, which proved to be a comparatively easy-to-use measurement method for an improved understanding of the governing factors on the erosional capacity of cavitating water jets. Based on this data, the multiple linear regression model can be used to predict the impact pressure distribution of those water jets to achieve higher dredging accuracy and efficiency. To determine the dredging operational efficiency, we developed a semi-continuous automated measurement device to measure the sediment concentration of the slurry. This simple and robust device has lower costs, compared to traditional and surrogate sediment concentration measurement technologies, and can be monitored and controlled remotely under a wide range of concentrations and grain-sizes, unaffected by entrained gas bubbles

# 1 Introduction

## 1.1 Reservoir Sedimentation and Greenhouse Gas Emissions

In natural river systems in dynamic equilibrium with stable catchments, the processes of erosion, transport, and sedimentation are relatively balanced. The construction of a dam structure interrupts the suspended particle and bedload transport of river systems, causing sediments to accumulate within the reservoir and reduce reservoir storage capacity (Annandale et al. 2016; Kondolf et al. 2014; Vörösmarty et al. 2003). As reservoirs are used for various purposes, such as hydropower, flood mitigation, water supply and irrigation (Lempérière 2006; Morris & Fan 1998), reservoir sedimentation negatively affects those distinct functions. The trapped sediments necessary to maintain its morphology and support riparian ecosystems are lacking downstream from the dam (Kondolf et al. 2014). Even though human interference has increased the sediment transport through soil erosion globally, sediment retention in reservoirs has decreased the sediment flux to downstream deltas of approx. 1.5 billion tons of sediment per year (Syvitski et al. 2005; Vörösmarty et al. 2003). Dam construction worldwide has increased substantially during the second decade of the last century. At present, about 58,000 dams larger than 15 meters in height exist, 9,595 of which were either solely or partially purposed for hydropower (ICOLD 2016, Lehner et al. 2011). With 16% of the worldwide energy production, hydropower is the world's largest source of renewable electricity production (International Hydropower Association 2018; Zarfl et al. 2014). Global annual storage capacity loss due to sedimentation varies from 0.1% to 2.3%, with an average annual world storage loss of about 1% (Walling 2006). Therefore, the worldwide annual loss of storage capacity to sedimentation is higher than the increase in capacity from the construction of new reservoirs (Schleiss et al. 2010; Sumi & Hirose 2009), and this issue poses a significant threat to the longevity, usefulness, and sustainable operation of existing reservoirs (Palmiere et al. 2003).

Sediment accumulations can be a sink of organic carbon and be mineralized to gas, consisting mainly of methane ($CH_4$), nitrogen ($N_2$) and a little carbon dioxide ($CO_2$) (Casper et al. 2000; Walter et al. 2008) through anaerobic decomposition (Sobek et al. 2009). In shallow waters, ebullition can be a dominant pathway for methane flux (DelSontro et al. 2010; Maeck et al. 2013; Xiao et al. 2014). Ebullition-mediated flux is often highly variable in space and time (Maeck et al. 2014; Varadharajan & Hemond 2012; Wilkinson et al. 2015), which is

directly linked to sediment gas storage (Liu et al. 2016) and sedimentation rate (Maeck et al. 2013). Many studies confirmed the relevance of greenhouse gas (GHG) emissions from freshwater systems (e.g. Barros et al. 2011; Bastviken et al. 2011; Beaulieu et al. 2014; Maeck et al. 2013; Wilkinson et al. 2015). Although quite a number of researchers published data about reservoir-specific GHG emissions as well as regional and global estimates, the real extent of GHG emissions from anthropogenic surface water bodies and especially from hydroelectric reservoirs is still poorly understood (Barros et al. 2011; Deemer et al. 2016), and there is a large variability of estimates among different studies (St. Louis et al. 2000). Efforts to quantify, model, and manage these emissions have been limited by data availability and inconsistencies in methodological approach (Deemer et al. 2016). Considering that hydropower is the major renewable energy source worldwide, this green energy source may be a significant contributor of GHG emissions. This effect will even be intensified as gas generation in sediments is expected to increase globally due to increasing temperatures (Aben et al. 2017; Yvon-Durocher et al. 2014), the increasing number of reservoirs worldwide (Zarfl et al. 2014), as well as due to the increasing supply and trapping of sediments and organic matter from rivers.

## 1.2 Reservoir Sedimentation Survey

Understanding the spatial distribution and characteristics of sediment deposits in reservoirs is required for various scientific and technical purposes. Both physical and biological in-lake processes influence the pattern of organic sediment deposition (Morris & Fan 1998), where $CH_4$ is formed through anaerobic decomposition (Martens & Berner 1974). The spatial heterogeneity of sedimentation patterns in lakes and reservoirs has been found to be related to the ebullitive flux (DelSontro et al. 2011; de Mello et al. 2018; Maeck et al. 2013). For scientific purposes, considerable effort is required to obtain accurate estimates for whole-lake emissions (Natchimuthu et al. 2016) and to reduce the remaining uncertainties of $CH_4$ estimations (Bastviken et al. 2011), as ebullition measurements are difficult, time consuming, and costly to accurately quantify due to temporal and spatial heterogeneity (Wik et al. 2013). Nearly all investigation relies on the use of bubble traps (e.g. Delwiche et al. 2015; Varadharajan et al. 2010), incubation experiments (Wilkinson et al. 2015, 2019), and echo sounding (DelSontro et al. 2015; Ostrovsky et al. 2008). Very little is known about the *in situ* gas content and vertical gas bubble distribution. For technical purposes, determining sediment depositional characteristics for the identification, design and implementation of sediment

management measures is required. It is important to understand the basic patterns and driving forces for sediment distribution in a reservoir, since those patterns have a strong influence on the hydropower schemes as well as biochemical processes like GHG production (De Cesare et al. 2001). Knowledge of both the rate and pattern of sediment deposition in a reservoir is required to predict the types of service impairments which will occur, the time frame in which they will occur, and the types of remedial strategies which may be practicable (Morris & Fan 1998).

The rapid specification and mapping of spatial sediment characteristics over large areas is usually determined by performing hydroacoustic surveys (Ostrovsky & Tęgowski 2010; Tęgowski 2005; Wienberg & Bartholomä 2005). Hydroacoustic methods allow a quantification of sediment deposits, document the decline in storage capacity over time, and determine physical and chemical sediment properties to help to assess the extent, distribution and volume of contaminated aquatic systems sediments (Anderson et al. 2013). Thus, hydroacoustics are a valuable tool for water quality management and lake restoration (Anderson & Pacheco 2011), and provide efficient and cost-effective site remediation (Anderson et al. 2013). Even though hydroacoustic measurement can be related to sediment properties (e.g. Ostrovsky & Tęgowski 2010; Tęgowski 2005), sediments with similar granulometric composition may differ considerably in their physio-chemical properties, particle composition and gas bubble content (Wilkens & Richardson 1998), all influencing the shape and energetic characteristics of the hydroacoustic signal. To overcome this issue, hydroacoustic surveys need essential ground-truth information for the sediment sample. Thus, it is essential to correlate hydroacoustic data with corresponding lakebed sample data (Amiri-Simkooei et al. 2011; Poulain et al. 2011).

In many cases, sediment investigations are descriptive studies simply designed to investigate the spatial and temporal distribution of contaminants for “state of the environment” reporting, for compliance monitoring, or to guide management actions such as dredging (Simpson & Batley 2016). Sediment characterization should be site specific (U.S. ACE 2007) and encompass the identification and evaluation of sediments characteristic for scientific purposes and for technical purposes, and predict environmental impacts due to dredging. This characterization may include physical, chemical, or biological sampling and/or testing, or any combination of these forms of characterization. As the most direct and convenient method, coring has been widely used for characterizing aquatic sediment (HELCOM 2000). Sediment cores are used to determine the sediment stratigraphy (i.e. vertical contaminated sediment concentration profiles) for the reconstruction of pollution history, for dating sediments, for the

estimation of gas fluxes and for the determination of sedimentation rates (Morris & Fan 1998; Simpson & Batley 2016). In areas of highly variable spatial sediment properties, increased spatial resolution is needed to properly characterize the sediment properties, especially when determining the possibility of an area being dredged (Spigolon 1995). Consequently, for a sound characterization, it is necessary to preserve both the *in situ* sediment's structural integrity and its sedimentological, biogeochemical, and biological conditions, which reflect the ambient condition (Mogg et al. 2017). The ability to extract sediment samples from aquatic ecosystems is therefore a fundamental prerequisite in various research and engineering fields. Many authors have questioned the validity of results obtained from *ex situ* sediment analyses because of the sampling bias associated with the coring device used (Baxter et al. 1981; Blomqvist 1985; Buckley et al. 1994). For example, core shortening may lead to the misinterpretation of sediment rates (Nevissi et al. 1989; Rongve & Erlandsen 1979), as shortening can be up to 50% (Wright 1993; Skinner & McCave 2003).

To avoid coring related biases and to minimize the misinterpretation of gas bubble size and distribution in sediments, the preservation of gas bubbles with minimal disturbance requires an appropriate coring technique. In recent years, a variety of coring techniques have been developed for different purposes (e.g. gravity corers, percussion corers, vibra-corers and drill corers) (Glew et al. 2002). Particularly in lakes and reservoirs with organic-rich sediments that favor $CH_4$ production under anaerobic conditions, freeze coring can facilitate the sampling of undisturbed sediment cores. Freezing the sediment *in situ* preventing a dissolution of gases that can occur due to the change in hydrostatic pressure and sample temperature where rising bubbles are destroying the stratigraphy (Rymer & Neale 1981; Verschuren et al. 2000). Also, expansion of free gas can occur in response to the decreasing hydrostatic pressure associated with reducing depth during core withdrawal (Lane & Taffs 2002). A rise in sample temperature causes the formation of additional gas bubbles, as temperature severely affects sediment methanogenesis (Zeikus & Winfrey 1976). As a consequence, expansion and a relocation of existing bubbles as well as the formation of new bubbles can be expected, which significantly biases the characterization of *in situ* sediment gas bubbles and stratigraphy. Therefore, the applicability and validity of regular, non-pressurized cores is questionable for taking intact cores without significant disturbance of gas-bearing sediment, as they are very sensitive to being influenced by pressure and temperature, which are required to be preserved at *in situ* values (Abegg & Anderson 1997).

These drawbacks can be avoided by preserving *in situ* hydrostatic pressure in closed coring devices. A pressure corer has been developed for characterizing gas-bearing sediment, and

was tested in Eckernförde Bay, Germany (Abegg & Anderson 1997). The *in situ* hydrostatic pressure was preserved by capping a pressure tight aluminum transfer chamber on the seabed with the help of divers. However, the application of pressurized cores obtained by divers is limited to shallow depths (Abegg & Anderson 1997) and is generally very costly. Various other pressurized corers have been developed and deployed in marine science, such as the Pressure Coring Barrel, developed within the Deep-Sea Drilling Project, and the Pressure Coring Sampler, developed in the course of the Ocean Drilling Program (Li et al. 2016). Besides their ability to sample gassy sediment, pressurized corers used in marine science require expertise and a proper platform to operate, which makes them expensive.

Freeze coring was introduced as an alternative method to take sediment cores for detailed stratigraphic analysis, even if they have a low cohesion (Lisle 1989) and for the sampling of muddy or gassy sediment (Verschuren 2000). The technique is based on the principle of freezing the sediment on the surface of a metallic surfaced coring device and held in position long enough to freeze the surrounding sediment (e.g. Huttunen & Meriläinen 1978; Pachur et al. 1984; Renberg 1981; Shapiro 1958). To freeze the sediment, the device is filled with a coolant such as liquid nitrogen (Pachur et al. 1984) or dry ice, preferably mixed with ethanol (this mixture has better energy transmission and heat capacity compared to solid dry ice). In principle, freezing preserves sediment gas bubbles under *in situ* hydrostatic pressure, prevents $CH_4$ porewater dissolution and gas bubble expansion upon lifting the corer through the water column (Wright 1993) and therefore the formation of new gas bubbles after withdrawal (Lane & Taffs 2002; Miskimmin et al. 1996; Wright 1980). Freeze coring can thus provide information on the *in situ* bubble population in sediment samples.

## 1.3 Reservoir Sedimentation Countermeasures

An awareness of the sustainable management of sedimentation in the planning phase of reservoirs has frequently been neglected in the past, and also today, many dams are planned and built without any consideration for sedimentation (Kondolf et al. 2014). Thus, sedimentation problems affect the vast majority of existing reservoirs. The problem of sedimentation tends to increase due to the siltation of existing reservoirs and the acceleration of new dam construction globally (Kondolf et al. 2014). Various techniques to counteract the problem of reservoir sedimentation are available, and can be classified into three groups (Fig. 1): (i) minimizing the sediment load entering the reservoir, (ii) reducing the further deposition of sediments, and (iii) removing previously accumulated sediments from a reservoir.

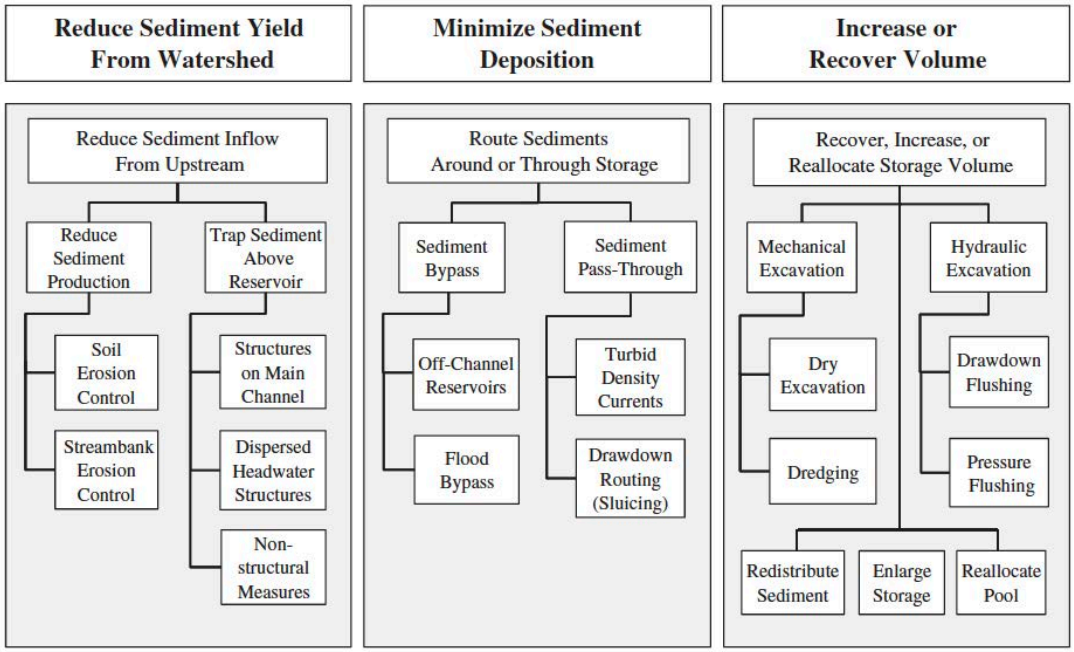


**Figure 1.** Classification of strategies for sediment management from the perspective of sustaining reservoir capacity (Kondolf et al. 2014).

As the majority of the worldwide reservoir capacity has already been reduced by sediment deposits, the focus is on the removal of deposits, either by mechanical or hydraulic dredging. Mechanical dredges remove sediment through the direct application of a mechanical force to dislodge and excavate sediment (U.S. ACE 1983; U.S. EPA 1994). This technique is generally limited to shallow water depths or requires the dewatering of the reservoir to dredge at deeper depths. Releasing water for mechanical dredging makes it economically unfavorable. The applicability of this method is further limited by a combination of high costs plus the scarcity of sites suitable for the disposal of the large amount of sediment excavated (Randle et al. 2017). Hydraulic dredging can be conducted continuously, where the loosened mixture of sediment and water (called slurry) is sucked from its *in situ* state in suspension through a pipeline and is then transferred to a disposal site using one or more pumps (Turner 1996; Van Eeten 2011). Hydraulic dredging has the advantages of (i) working at current water levels and without lowering the reservoir; (ii) less adverse ecological impacts compared to excavation measures, i.e. due to little or no turbidity or resuspension at the dredge suction head; (iii) low unit costs of sediment removal; (iv) effective dredging of both fine and coarse material; and (v) the prevention of damage to vulnerable infrastructure (i.e. pipelines, cables). This technique has also proven in many cases to be efficient in the dredging of contaminated sediment layers, as the re-suspension of sediment is limited and the dredged material can be piped directly to the disposal area (U.S. EPA 1991). Such environmental dredging, however, aims to accurately remove thin layers and minimize turbidity, so that there is

less dredged material to be disposed of. Additionally, the increase in dredging accuracy helps to minimize over-dredging. Environmental disruption can be assumed to be inversely proportional to the efficiency of the dredging operation (Turner 1996). This is a valuable development, as less over-dredging means less material to be dredged and treated. From a financial perspective it results in lower costs, which can lead to reduced tender prices.

For loose material, suction can be sufficient to pump the slurry, whereas consolidated bed material may require loosening by mechanical action or the use of water jets. To enhance the dredging production rate, or in projects where cohesive sediment has led to consolidation, water jets are used to penetrate the sediment's surface and loosen up the (consolidated) bed material, so the fluidized material can be dredged afterward (Hogg et al. 1997; Nobel & Talmon 2012; Turner 1996; Wyatt & Miller 2013) and to achieve a high penetration for cohesive material (Schouten 2016; Zhang et al. 2017). For dredging, water jets use relatively low pressures with large flow rates, on the order of magnitude of 10 bar at 30 l/s per jet (Nobel 2013). Even though water jets in hydraulic dredging are widely used, literature on the investigation of submerged water jets and their effect on the bed material is limited. Sediment removal by water jets is a complex physical process that involves several parameters. Most studies deal empirically with sediment erosion, and others attempt to understand the physics of the process using submerged water jets (Hou et al. 2016). The behavior of cohesive sediment (e.g. Mitchell & Soga 2005) and the behavior of submerged water jets (Rajaratnam 1976) has been investigated in various studies, but literature on the interaction between both is rather limited. Fundamental research is limited to the erosion of cohesive sediment induced by a turbulent flow parallel to the sediment surface (Winterwerp & van Kesteren 2004) and erosion induced by a stationary low-pressure jet (Mazurek et al. 2001, 2006). Only simple experimental correlations between the most important sediment and water jet parameters have been published (e.g. Machin et al. 2001; Machin & Allan 2011).

High erosional forces make cavitating water jets a promising technique for sediment dredging due to high erosional forces: the emission of shock waves upon the collapse of the cavitation bubble and the generation of a high-speed liquid jet (Nobel 2013). Given the fact that numerous cavitating bubbles implode in a timescale of microseconds at the spatial scale of a micrometer, measuring the impact pressure and determining the position of impact remains a huge challenge (Peng et al. 2018). At the interface of the jet and the ambient water, a zone of incompressible water and unsteady compressible vapor bubbles exists (Schouten 2016). Because of this complexity, numerical simulation is challenging and no numerical description

can be found in the literature for a fully developed cavitating water jet. Here, the impact of pressure distribution and the spray pattern at a specific impinging distance and angle are important parameters to model the dredging process (Nobel 2013), and is a crucial aspect for the design of dredging operations. Traditional pressure transducers are limited in spatial resolution, as the signal comes from a sensor whose area is much larger than the size of a typical cavitation impact (Peng et al. 2018). Thus, no information about the impact pressure distribution for submerged water jets is given. A technique is required to measure the impact pressure distribution of submerged cavitating water jets with a high resolution to overcome those limitations.

Knowledge of both the characteristics of the water jet and the sediment is key to the development and implementation of a suitable dredging technique for the efficient and precise dredging of sediment deposits in reservoirs. Information on the critical shear stress of bed material is essential for the design of dredging operations. For sediment, many widely used erosion prediction models are based on the concept that sediment transport begins at a constant value of the non-dimensional bed-shear stress or the critical shear stress (Meyer-Peter & Müller 1948; Engelund & Fredsoe 1976; Wilcock & Crowe 2003). This research is based on the fundamental research of Shields (1936). A variety of bed properties have an effect on the erosional behavior of mud beds in natural systems. Experiments by Mitchener & Torfs (1996), Panagiotopoulos et al. (1997) and Torfs et al. (1996) have shown that a small amount of mud added to a sand bed can dramatically change its erosional properties. However, there are currently no reliable methods to accurately estimate the critical shear stress based on sediment properties. For quantification of the influence of cohesion on the critical shear stress of non-uniform sediment, having gravel and clay sizes together in their mixture, no studies are available (Kothyari & Jain 2008). Besides the grain size, many factors affect resistance to erosion, including density, clay content, clay mineralogy, pore and eroding fluid chemistry, temperature, fabric, water content, organic content, and matric suction, etc. (Hanson & Cook 1998; Kimiaghalam et al. 2016; Paaswell 1973; Righetti & Lucarelli 2007). In natural sediments, vegetation (Black et al. 2002), several biological (e.g. biofilms, organic content) and chemical parameters (e.g. chlorinity, pH) also have an effect on the critical shear stress (Berlamont et al. 1993; Partheniades 1979). Biological modification through slimes produced by diatoms and cyanobacteria, or tubes produced by sessile suspension feeders (Newell et al. 1998), can increase the critical shear stress to erode the sediment deposits. On the other hand, bioturbation can cause the erosion shear strength to be reduced (Cadée 2001). With regard to gas-bearing sediment, the erosion resistance has been found

to increase with organic content (Young & Southard 1978), whereas Jepsen et al. (2000) demonstrated that with gas in reconstructed sediments, the critical shear stress for erosion can decrease by as much as a factor of twenty compared to sediments without gas. Moreover, in natural sediment, the above-mentioned multiple parameters interact, and this affects the shear strength of the cohesive sediment. These effects are still not fully understood and analytical approaches can barely handle the uncertainties involved (Silva et al. 2017).

## 1.4 Sediment Concentration Measurement

The dredging process should be optimized – in terms of mass of solids passing through the dredging pipeline – at the lowest operating costs and with the lowest environmental impact. The efficiency is monitored by measuring the sediment concentration in the dredging pipeline. The sediment concentration, respectively the density of the slurry, is the most basic and crucial parameter monitored (Zych & Osnabrugge 2017), and primarily used for process control and production calculation (Scott 1993; Van Eeten 2011). The accuracy of the monitoring systems varies according to the instrument used and the knowledge of the sediment and water properties associated with the dredging activity. Furthermore, the variation in concentration and grain size is prone to error in dredging projects, as both vary due to the spatial distribution pattern of sediment deposition and gas bubbles within reservoir sediments.

Sediment concentration measurement methods can be classified into two categories: traditional (or direct) and surrogate (or indirect) methods (Gray & Gartner 2009). Traditional methods involve the collection of water samples and the subsequent determination (sample weighing after drying or filtration) of the suspended sediment properties in a laboratory (Rai & Kumar 2015). These methods allow for measurements over a wide range of concentrations and particle-sizes with high accuracy, under the assumption that the requirements of representative sampling are met (Gray & Simões 2008; Topping et al. 2011). Although the gravimetric measurement method is the most accurate for determining the sediment concentration, it is unable to provide temporally high-resolution data and hence also spatial sediment characteristics, because it requires frequent, manual sampling. Demanding a higher temporal resolution makes traditional methods of sediment concentration monitoring expensive, as well as time and labor intensive (Gray & Gartner 2009). Surrogate methods, such as pressure difference, optical or acoustic backscatter, transmission methods, Coriolis flow meter, and gamma radiation meter measure suspended sediment properties indirectly. They allow, in comparison to traditional methods, a less expensive measurement with a high temporal and

spatial resolution, but are limited in concentration and particle-size measurement range. Due to natural variations in sediment characteristics, such as particle-size, density, and organic material content, as well as gas concentration, these methods require a site-specific calibration and periodic validation of the instrument with traditionally collected samples (Gray & Landers 2014). Surrogate techniques are subject to at least one of the following limitations: (i) small concentration and particle-size range; (ii) particle-size dependency; (iii) high costs and fragility in a fluvial environment; (iv) special training on radiation safety and/or licenses, (v) the accuracy is affected by multiphase flows, or (vi) expenses of installation and operation. Taking into account that dredging operations are carried out in sites of intense GHG emissions (e.g. Barros et al. 2011; Deemer et al. 2016; Giles 2006), enclosed gas bubbles within the dredging pipeline can affect the accuracy of the measurement technique (Wang & Baker 2014). Thus, the development of a new method for quick and efficient measurement of sediment concentrations is of interest (Ban et al. 2017). Therefore, a monitoring technique that overcomes the limitations of currently available measurement technologies and closes the gap between both methods is needed.

# 2 Objectives and Hypotheses

Even though reservoir sedimentation and $CH_4$ emissions are widely discussed, research is still needed to identify the spatial (horizontal and vertical) pattern of (gas-bearing) sediment deposits for the design and implementation of appropriate sediment management techniques. In this regard, environmentally friendly, cost-efficient and accurate techniques need to be developed to restore the reservoir capacity and mitigate $CH_4$ emissions. Based on the gaps in the current state of scientific and technical knowledge outlined in Section 1, this thesis addresses three major research objectives: (i) *in situ* sediment freeze core sampling, (ii) hydraulic dredging with cavitating water jets and (iii) sediment concentration measurement. The contribution of each objective of this thesis to the verification of the stated hypotheses is described in the following and is schematically presented in Figure 2.

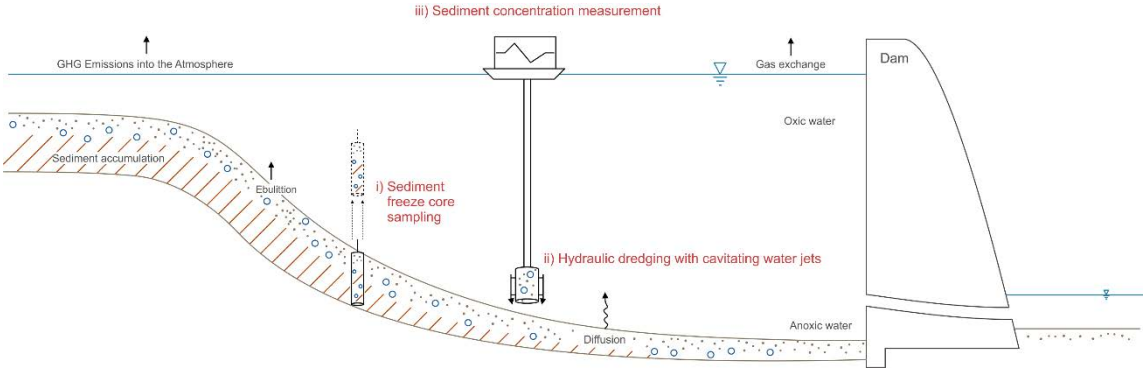


**Figure 2.** Schematic presentation. i) *in situ* sediment freeze core sampling for the characterization of the sediment deposits, ii) remobilization of distinct (gas-bearing) sediment layer by hydraulic dredging with cavitating water jets and iii) the measurement of the sediment concentration in the dredging pipeline.

A prerequisite for the implementation of the appropriate sediment management technique is the identification of the sediment stratigraphy, which allows the investigation of the spatial distribution, vertical sediment (contamination) concentration profiles, as well as gas bubble characteristics. It is therefore required to preserve the *in situ* sediment characteristics to minimize changes to the structural integrity of the collected sediment sample, because any disruption of the structure and integrity can bias the results and the subsequent measures. We assume that *in situ* freeze coring facilitates the sampling and characterization of (gas-bearing) sediment (*Hypothesis 1*), without being affected by changes in hydrostatic pressure and sample temperature.

It is hypothesized that freezing affects the sediment stratigraphy and bubble structure, as the thermal and hydraulic properties of the sediment and pore water are influenced by subzero temperature (*Hypothesis 2*). Thus, the objective (*Objective 1*) was to develop a freeze coring technique to sample sediment cores under *in situ* conditions, to evaluate the effect of

freezing under laboratory conditions, test the applicability of freeze coring under field conditions and analyze the core stratigraphy and gas characteristics.

Based on the knowledge gained from the first part of this thesis, hydraulic dredging with water jets to erode and fluidize distinct sediment deposits to enhance the dredging efficiency of the (gas-bearing) sediment layer was investigated. We assumed that submerged cavitating water jets achieve high erosional forces and thus can be used to dredge at specific depths of distinct sediment layers (*Hypothesis 3*). To test this hypothesis, we adapted a Pressure Measuring Sensing (PMS) technique to investigate the impact pressure distribution of water jets and to evaluate the factors involved (*Objective 2*).

To measure and control the effectiveness of the water jet assisted hydraulic dredging operation, the sediment concentration in the dredging pipeline needs to be measured under a wide range of concentration and particle-sizes, unaffected by entrained gas bubbles. We hypothesize that the autonomous weighing of a sample taken out of the dredging pipeline with a defined volume allows the quasi-continuous sediment concentration measurement, unaffected by entrained gas bubbles (*Hypothesis 4*). Thus, the objective (*Objective 3*) was to develop a simple, robust and cost-efficient technique to measure the sediment concentration of hydraulic dredging operations. Table 1 gives an overview of the thesis's objectives and hypotheses.

**Table 1.** Thesis objectives and hypotheses.

| | | |
|---|---|---|
| **Part 1** | **Objective 1:** Development and testing of a sediment freeze coring technique to sample sediment cores under *in situ* conditions. | |
| | **Hypothesis 1:** *In situ* freeze coring facilitates the sampling and characterization of (gas-bearing) sediment. | **Hypothesis 2:** Freezing sediment *in situ* affects the sediment stratigraphy and gas bubble structure. |
| | ➔ *Appendix II and III* | |
| **Part 2** | **Objective 2:** Investigation of the impact pressure distribution of submerged cavitating water jets and the evaluation of the factors involved with the impact pressure. | |
| | **Hypothesis 3:** Submerged cavitating water jets achieve high erosional forces and can be used to dredge at specific depths of distinct (gas-bearing) sediment layers. | |
| | ➔ *Appendix IV* | |
| **Part 3** | **Objective 3:** Development of a simple, robust and cost-efficient method to measure the sediment concentration of hydraulic dredging operations. | |
| | **Hypothesis 4:** Autonomous weighing of a sample with a defined volume allows the measurement of sediment concentrations, unaffected by entrained gas bubbles. | |
| | ➔ *Appendix I* | |

# 3 Outline

The present thesis comprises four publications/manuscripts that are either published in or have been submitted to peer-reviewed journals and are provided in *Appendencies I-IV*.

### A novel freeze corer for characterization of methane bubbles and assessment of coring disturbances

Dück, Y., Liu, L., Lorke, A., Ostrovsky, I., Katsman, R., and C. Jokiel. 2019. A novel freeze corer for characterization of methane bubbles and assessment of coring disturbances. Limnology and Oceanography: Methods, 17: 305-319, doi: 10.1002/lom3.10315. *(Appendix II)*

In this part of the thesis, the development of a freeze coring technique to sample sediment under *in situ* conditions to determine sediment layer stratification and characterize the gas bubble distribution is described (*Objective 1*).

In order to test *Hypothesis 1*, the applicability and performance of the freeze coring technique to sample sediment for gas bubble characterization was initially tested under field conditions in Lake Kinneret (Israel). The freeze cores were sampled along a transect from shallow to deep water to cover the spatial variability in sediment depositional characteristics. The cores were X-Ray CT scanned to visualize the sediment structure as well as characterize and quantify sediment methane bubbles. We compared our data with results obtained in other studies on the spatial organic carbon distribution, hydroacoustic measurements and visual inspection of gravity core data to validate our results qualitatively. To test *Hypothesis 2*, the freeze coring technique was investigated under laboratory conditions to evaluate quantitatively the effect of freezing on the number and size distribution of gas bubbles by comparing non-destructive X-Ray CT scans of frozen and unfrozen cores with different types of homogenized sediment with organic carbon to fuel biogenic gas production.

### Laboratory and Field Investigations on Freeze and Gravity Core Sampling and Assessment of Coring Disturbances with Implications on Gas Bubble Characterization

Dück, Y., Lorke, A., Jokiel, C., and J. Gierse. Laboratory and Field Investigations on Freeze and Gravity Core Sampling and Assessment of Coring Disturbances with Implications on Gas Bubble Characterization. Submitted for publication in: Limnology and Oceanography: Methods. *(Appendix III)*

Based on the findings of the first part of the thesis, this part extends the laboratory experiments to investigate the effect of freezing on the sediment's structural integrity and to identify related coring disturbances to test *Hypothesis 2*. Laboratory experiments were conducted

with (i) artificial sediment and (ii) sediments sampled from two reservoir sites in Germany. Additional field investigations enabled the evaluation of the freeze corer performance in comparison to a commonly used gravity coring technique.

To further verify *Hypothesis 2*, additional laboratory experiments were conducted to investigate the causes, effects, and extent of coring disturbances, with an emphasis on the effect of freezing. This was achieved by comparing X-Ray CT scans of both freeze and gravity cores. Cores were sampled from sediment with known stratigraphy, which differs predominantly in grain-size distribution, water content and organic matter. To evaluate the possibility of the effect of freezing on gas bubble nucleation and particle migration, freezing rate experiments were conducted. To visualize the effect of freezing on the core structure, real-time X-Ray CT scans were conducted, which allow a non-destructive temporal visualization of the freezing process.

To test *Hypothesis 1*, with emphasis on the comparison of *in situ* freeze coring technique to gravity coring, sediment cores were sampled at two reservoirs in Germany, which differ in sediment deposition pattern and reservoir characteristics. The sampling locations were chosen to cover a gradient of hydrostatic pressure and sediment temperature. To identify the influence of freezing on the sediment and gas structure, freeze cores, gravity cores, and gravity cores frozen after withdrawal were sampled some meters apart from each other. The cores were X-Ray CT scanned, coring disturbances were identified and quantified, and the bubble sizes and their distribution resulting from each different coring method were examined.

## Experimental Investigation of Impinged, Oblique Submerged Cavitating Water Jets with Pressure Measurement Sensing

Dück, Y., Bolsenkötter, L., Lorke, A., and C. Jokiel. Experimental Investigation of Impinged, Oblique Submerged Cavitating Water Jets with Pressure Measurement Sensing. Submitted for publication in: International Journal of Hydraulic Engineering. *(Appendix IV)*

The third part of the thesis investigates the impact pressure distribution and flow field of submerged cavitating water jets. The water jets are intended for the remobilization of defined (gas-bearing) sediment layers that were investigated under *Objective 1*. To test *Hypothesis 3*, an adapted design of the PMS technique was used to measure and visualize the impact pressure distribution of submerged cavitating water jets. This technique enhances the spatial resolution compared to commonly used pressure transducers and allows a precise identification of the spray pattern. The effect of standoff distances, impinging angles, pump pressures and spray angles on the impact pressure and spray pattern was investigated (*Objective 2*). The

findings of those tests are discussed in respect to the practical application of cavitating water jets to efficiently and precisely remobilize defined sediment layers and bubbles, as identified within the techniques related to *Objective 1*.

## DENSE: Semicontinuous Automated, Gravimetric Measurement Device for Suspended Sediment Concentrations

Dück, Y., Fahlenbock, T., Frings, R., and C. Jokiel. 2017. DENSE: Semicontinuous Automated, Gravimetric Measurement Device for Suspended Sediment Concentrations. International Journal of Hydraulic Engineering. 143(12), doi: doi.org/10.1061/(ASCE)HY.1943-7900.0001374. *(Appendix I)*

The last part deals with the development and tests of a sediment concentration measurement device (*Objective 3*) to control the dredging process and evaluate its efficiency. The sediment concentration is the quantity of sediments of a specific layer, which has been identified under *Objective 1*, and is assumed to be remobilized by water jets under *Objective 2*, and the dredged water. A technique was developed that overcomes the limitation of traditional and surrogate methods to measure wide ranges in concentration and grain-size, unaffected by entrained gas bubbles. To examine *Hypothesis 4*, laboratory tests have been conducted to evaluate the performance and precision of the technique. Within these tests, we can identify the influencing factors on the accuracy of the technique. The validity of the results was confirmed by manual gravimetric analysis. Additionally, the performance data were compared with the published data of other techniques and acceptance criteria for sediment concentration data acquisition.

# 4 Synthesis

## 4.1 In situ sediment freeze coring technique for sampling and characterization of (gas-bearing) sediment

Within this thesis, a freeze coring technique was developed to overcome some of the limitations of non-pressurized coring techniques for sampling (gas-bearing) sediment and provide a simple, robust and cost-efficient method. Coring disturbances, in particular those related to the freezing process, were investigated in laboratory experiments. The freeze coring technique was successfully tested under field conditions and produced verified results.

Freeze coring in combination with non-destructive X-Ray CT scanning (*Appendices II and III*) has proved to be a promising technique for sediment stratigraphy and gas bubble characterization (Liu et al. 2016) from laboratory experiments and *in situ* field investigations. Sediment sampling with the freeze coring technique can increase sediment characterization accuracy, because coring disturbances due to liquefaction, depressurization, gas dissolution, and handling can be minimized. Field studies (*Appendix II* and *III*) revealed a high variability of occurrence and extent of freeze and gravity coring disturbances. Therefore, we recommend X-ray CT scanning to identify zones of disturbances that should not be taken into consideration for the subsequent core analysis, as recommended by Liernur et al. (2017). A visual inspection of the core stratigraphy and an exclusion of a buffer zone around the corer (e.g. Strasser et al. 2015; Franchini & Zeyer 2012) only allow the identification of coring disturbances in texturally and structurally homogenous sediments of just one cross-section through the core, and does not take into account the spatial structure of disturbances. This is necessary because of various possible coring disturbances and the fact that their analysis is not a routine aspect of data analysis in the majority of studies published, which used sediment core data. The validity of results in those studies obtained from field cores is questionable with regard to the sampling bias associated with the coring devices (Baxter et al. 1981; Blomqvist 1985; Buckley et al. 1994), as any disruption of the sediment sample integrity during its removal, transport, storage, and testing in the laboratory complicates interpretations of treatment effects, causative factors, and *in situ* comparisons (U.S. EPA 2001).

The results of volumetric gas content ($\theta$) measurement of Lake Kinneret freeze cores (*Appendix II*) was compared with those obtained in other studies of organic carbon content (Ostrovsky & Tęgowski 2010; Ostrovsky & Yacobi 2010; Sobek et al. 2011), as well as acoustic measurements (Katsnelson et al. 2017). The organic carbon content of the uppermost sediment layer and the $\theta$ measured by hydroacoustic measurements increases from the profundal

zone towards zones of deeper water: this correlates with the directly measured $\theta$ of the freeze cores. Given that our findings are based on limited knowledge about free gas in Lake Kinneret, the results showed a good agreement (*Hypothesis 1 corroborated*).

The field investigations at Urft Reservoir showed that the $\theta$ of the freeze cores increased (0.2% to 1.2%) with decreasing water level (31 m to 5 m) towards the littoral zone. The $\theta$ of the frozen gravity cores increases (0.3% to 5.6%) along this transect and shows a similar trend as the freeze cores, in contrast to the increasing $\theta$ *of* gravity cores (10.5% to 10.9%), respectively. Differences in $\theta$ between the freeze and gravity cores were also observed at Olsberg Reservoir. The $\theta$ of Olsberg Reservoir gravity cores ranged from 4.5% to 12.4% and from 0.6% to 1.2% for the freeze cores, respectively. Only a few studies have quantified *in situ* the amount of gas retained in sediments (e.g. Huttunen et al. 2001; Martinez & Anderson 2013) or have been determined indirectly with hydroacoustic measurements and can only be considered as a first step toward a more profound understanding of the spatial $\theta$ distribution. The vertical gas bubble distribution remains unclear. Thus, a validation of the $\theta$ of Urft and Olsberg Reservoir core data (*Appendix III*) with other studies can only be done on a qualitative basis.

Even though ebullition is spatially heterogeneous (Bastviken et al. 2008; Beaulieu et al. 2016; Tušer et al. 2017) and a sporadic event unpredictable in time (Scandella et al. 2016; Wik et al. 2013), many studies have found that ebullition is often found to be most active in the littoral zone (Bastviken et al. 2008; Duc et al. 2010; Murase et al. 2005; Natchimuthu et al. 2016; Torres et al. 2010; Wik et al. 2013). Higher water temperatures are often observed in the littoral zone of deep, stratified lakes, which enhances $CH_4$ production in the sediment relative to deeper waters. Like Urft Reservoir, water and sediment temperatures are more likely to be warmer in shallow zones, which stimulates methanogenesis (Duc et al. 2010) and makes $CH_4$ less soluble (Yamamoto et al. 1976). In addition, lower dissolved gas concentrations are required at those zones with lower hydrostatic pressure for reaching oversaturation and bubble formation. Labile allochthonous organic loading is also likely to have a shorter residence time in the water column and a higher likelihood of being deposited into sediments in shallow zones (Wik et al. 2013). This is in accordance with our results, where the organic matter measured in the freeze cores in the shallower zone of Urft Reservoir (16.9%) is higher than in the deeper parts (11.9%). At depth, it eventually accumulates in a more decomposed state after a longer transit time and a prolonged period in the water column (Torres et al. 2010). It has been demonstrated that littoral sediments are particularly important, since $CH_4$ produced in littoral sediments is much more likely to reach the

atmosphere than $CH_4$ produced in deeper profundal sediments (Bastviken et al. 2008; Murase et al. 2005). However, when comparing our results to those in temperate freshwater systems, the spatial $\theta$ distribution of the Urft Reservoir freeze cores fits those findings, which observed that ebullition is often found to be most active in the littoral zone. When comparing our results to those mentioned above, it must be pointed out that the surface area of the lakes, water depths, water level fluctuations and other boundary condition of the sites in their studies differ from our sites, which may result in different $\theta$ values.

Nevertheless, coring disturbances of both the gravity and freeze cores has to be taken into consideration. Under *in situ* conditions, predominantly $CH_4$ and small amounts of other gases may occur dissolved in pore water or as free gas bubbles. During core recovery, the pressure on the sediment sample decreases immediately unlike temperature, which is governed by heat transport and hence subject to time lags (Mogollón et al. 2011), causing a considerable shift in the partitioning between the dissolved and gaseous phases. According to Henry's Law, the amount of dissolved $CH_4$ is proportional to the increasing water depth (Abegg & Anderson 1997), thus the solubility of $CH_4$ decreases with decreasing hydrostatic pressure (Edwards 1991). Free gas bubbles expand with decreasing pressure linearly in proportion to water depth according to Boyle's Law, where pressure is inversely proportional to the volume. Existing gas bubbles will expand from absolute pressure (4 bar at 31 m of water depth) to atmospheric pressure (1 bar), resulting in a fourfold increase in $\theta$. The rising temperature in the sample reduces $CH_4$ solubility (Lane & Taffs 2002) and the methanogenic decomposition activities increase (Kelly & Chynoweth 1981; Thebrath et al. 1993). For example, at Urft Reservoir sampling location 1, under surface conditions (1 bar at 5°C), $CH_4$ saturation in pore water is 34 mg/L (Lewin & Bradshaw 1993). At hydrostatic pressure associated with 31 m of water depth, approximately 134 mg/L of $CH_4$ are required to saturate the pore water at 5°C. Thus, there is more than a factor of four of change in the $CH_4$ saturation concentration between the lakebed and surface at this site. Therefore, most of the $CH_4$ that was originally dissolved will be transferred into a free gas phase. The change in sample temperature from the lakebed ($T_{Sediment,Urft}$ = 5.1°C) to the ambient air temperature ($T_{Ambient,Urft,Dam}$ = 21.2°C) decreases the solubility of $CH_4$ from 34.4 mg/L to 23.7 mg/L over time, resulting in the formation of additional gas bubbles. Both pressure and temperature effects will lead to a (partial) ebullition or relocation of gas bubbles within the gravity core, resulting in a disturbance of the stratigraphy and an overestimation of the *in situ* $\theta$. There are also important differences between the gravity and frozen gravity core at Urft sampling site 1, with $\theta$ of 10.5% and 0.3%, respectively. This difference might be related to the reduction in $CH_4$

solubility and additional methane formation (MF) due to the rise in the sample temperature over time, which occurred during sample transportation until the cores were scanned. MF is potentially regulated through microbial activity by several environmental factors including temperature, organic substrate quality, supply nutrient availability and oxygen concentration (Megonigal et al. 2005). Duc et al. (2010) observed that the potential MF rates were sensitive to temperature and increased 10- to 100-fold over a temperature range from 4°C to 30°C. Based on incubation experiments of Urft Reservoir freeze cores, following the procedure of Saarnio et al. (1997) and Wilkinson et al. (2019), MF is approx. 7.8 mL for Urft Reservoir sampling site 4 (freeze core volume: 1315 mL) due to the change in temperature from the lakebed of 4°C to an ambient temperature of 21.2°C and a time of 36h. Therefore, the effect of MF due to a rise in sediment sample additionally negatively affected the *in situ* $\theta$, even though this effect is less pronounced than the solubility of $CH_4$. These factors may explain the rather contradictory $\theta$ between the freeze and gravity core at Urft Reservoir, which is more pronounced with regard to the variation in hydrostatic pressure and sediment temperature than to the results obtained at Olsberg Reservoir. Sampling depth varies at Urft Reservoir from 31 m ($T_{Sediment,Urft,Dam}$ = 5.1°C) to 9 m ($T_{Sediment,Urft,Inflow}$ = 7.9°C) of water depth in contrast to the shallow (< 2 m water depth) Olsberg Reservoir, which is a nearly uniform, deep reservoir with homogeneous sediment temperatures ($T_{Sediment,Olsberg}$ = 14.2°C). The $\theta$ of the Urft Reservoir freeze cores is therefore more affected by the sudden degassing of $CH_4$ due to the higher differences in hydrostatic pressure (Verschuren et al. 2000; Wever et al. 1998). However, it remains unclear as to what extent the above-mentioned pressure and temperature dependent effects have on $\theta$. Even though freezing changes the $\theta$ *in situ*, it can be mathematically corrected following Charles's Law, which is a relevant advantage of the freeze coring technique in contrast to the gravity coring technique. Due to the lack of data and the associated sampling biases of the coring devices, more research with a comparative study between frozen, non-frozen, pressurized and non-pressurized coring techniques needs to be undertaken before the association between the related coring disturbances is more clearly understood. In particular, the use of a pressurized corer may allow a clearer distinction between the coring disturbances associated with the change of hydrostatic pressure (volume expansion) and temperature (solubility of $CH_4$ and the increase in MF).

The differences of $\theta$ between the freeze and gravity cores at both sites can also be explained by the spatial heterogeneity and extended pore network of gas bubbles. Studies have demonstrated spatial heterogeneity of ebullitive flux related to sedimentation pattern in lakes

and reservoirs, albeit at a larger spatial scale (de Mello et al. 2018; Maeck et al. 2013). Bubble release from soft sediments can be focused at vent outlets, which may be long-lived (Bussmann et al. 2011; Scandella et al. 2017). If a bubble vent is fed by an extended pore network analogous to root-like macropore structures as field (Scandella et al. 2017) and laboratory (Liu et al. 2018) observations suggest, the area feeding such a bubble vent would be difficult to define (Wilkinson et al. 2019). Consequently, the areal density and distribution of bubble vents in relation to the sample location may result in different $\theta$ between the coring techniques used, even though the cores were taken just some meters apart from each other.

This study indicates that the majority of freeze cores in the structure were affected due to the freezing process (*Hypothesis 2 corroborated*), and that the freezing rate is correlated to the extent of the vertical displacement of the sediment layer. Until recently only the Rutledge & Fleeger study (1988) described similar observations of disturbances due to freezing. They have shown that the distortion of the vertical sediment profile by freezing is strongly related to the temperature. They stated that fast-freezing tends to cause greater disruption, whereas the layer deformation of slow-freezing is probably not distinguishable from that caused by core compaction or due to the drag of the corer wall upon insertion. Apart from this study, there is a general lack of research on coring disturbances due to freezing, although freeze coring has been widely used in studies such as for sampling of macroinvertebrates (Hill 1999), the sediment-water interface (Pachur et al. 1984), characterization of microbial community structure in wetland soils (Franchini & Zeyer 2012), and geohydraulic characterization of river bed sediment (Strasser et al. 2015). Because of the lack of studies, we discussed the observed effects in this study based on the findings of publications on frost heave, which refers to the volume expansion of the water content when a soil freezes (e.g. Peppin & Style 2013; Sheng et al. 2013) or in the special case of dewatering of sludge by freezing (e.g. Chen et al. 2001; Franceschini 2010; Hjorth 2004). However, due to different cooling temperatures, freezing rates, and other boundary conditions, caution must be applied, as the findings might only be partially transferable to gassy sediments in aquatic sediments. Nevertheless, the effects described in those studies can explain some of the disturbances, but the extent of each effect cannot be determined precisely.

Besides the effect of a disturbance of the sediment structure due to freezing, the results (*Appendix II and III*) suggest that future studies should investigate the effect of particle and bubble migration, as well as bubble nucleation due to freezing and its major influencing factors. The solidification front, which represents the phase-transition from water to ice due to the freezing process, may interact with bubbles and particles. The front either pushes the

particles indefinitely and segregates them in the liquid that is frozen last, or the front may engulf the particles after having pushed them over some distance, or instantaneously upon contact (e.g. Asthana & Tewari 1993; Lipp & Körber 1993). Freezing can also be expected to cause bubble nucleation, which occurs as the gas solubility in ice is at least two orders of magnitude smaller than in water (Killawee et al. 1998). Studies have shown that the freezing rate is related to the size of nucleated gas bubbles. Lipp et al. (1987) found that the bubbles are < 20 µm for freezing velocities exceeding 65 µm/s, which is the slowest freezing rate measured in their laboratory experiments. Most of the studies (e.g. Carte 1961; Lipp et al. 1987) on this topic deal with nucleation in an advancing ice-water interface or consider different freezing rates, as in this study. Within those studies, the freezing rate is reported to be an important parameter for the number and size of nucleated bubbles. However, those studies can only give an indication that this issue can occur within freeze coring, and this phenomenon should be investigated in greater detail. Due to the limitation in spatial resolution of the X-Ray CT scan in this study (voxel dimension: 0.04 mm³ (*Appendix II)* and 0.126 mm³ *(Appendix III*)), caution must be applied, as the findings may not show nucleated gas bubbles if present. It can also not be excluded that several small gas bubbles have joined together to form larger ones, which cannot be differentiated from *in situ* bubbles. Therefore, future studies should investigate the effect of the freezing rate (with dry-ice and ethanol as coolant) on bubble nucleation, and scanning with high-resolution X-Ray CTs (which are commonly used in materials science and are less available and more expensive as medical CT scanners, as used in this study) of frozen and non-frozen cores may answer this question.

Laboratory experiments (*Appendix III*) have indicated that nearly all freeze and gravity cores exhibit sediment core shortening. As the freeze corer's cutting-edge is sharper and the ratio between the sampler and soil area is higher than that of the compared gravity corer, the overall freeze core shortening (17.0%) is less than the gravity corer's (29.7%), and therefore in line with the observation of Andresen (1981) and Clayton et al. (1995). Besides the correlation between the coring techniques and shortening, various authors stated that sediment characteristics also have an effect on shortening. Emery & Dietz (1941), Emery & Hülsemann (1964) and Lebel et al. (1982) further claim that sediment core shortening is a linear function of the depth of sediment penetrated by the corer. Non-linear (curved) relationships have been found by Piggot (1941) and Weaver & Schultheiss (1990). Those results reflect the high variability in sediment stratigraphy, resulting in various shortening patterns, which could relate not only to the coring technique of the laboratory experiment cores. This

pattern cannot be measured in field studies, as the shortening of each layer cannot be determined independent of the coring technique. Measurement of the penetration depth of the gravity corer is most difficult *in situ* and often seems impossible in practice (Blomqvist 1991). This problem has been overcome by measuring the penetration depth of the corer (a scale is attached to the outside of the corer) with an attached underwater video camera at the tripod. The measurement of the penetration depth allows the calculation of the overall core shortening.

The results in this study (*Appendix II* and *III*) showed, the freeze coring technique can enhance the precision of sediment characterization needed in the planning process of the dredging operation to determine the volume, thickness, location, and physical and chemical properties (U.S. ACE 2007). Thus applying, the sediment core data is extrapolated over large areas in reservoirs by using hydroacoustic measurement. This is due to the fact as sediment can adsorb and retain contaminants and also act as a sink for organic carbon (US Geological Survey 2004), and it can retain nutrients, including nitrogen and phosphorus (Moss et al. 1996), and heavy metals such as zinc, lead, copper, etc. (Manap & Voulvoulis 2015), persistent organic chemicals, fallout radio-nuclides (Klös & Schoch 1993), and pathogenic organisms (Burton et al. 1987). This is required to comply with environmental guidelines. Even though sediment quality guideline values are not a regulatory requirement (Burton et al. 2002; Wenning & Ingersoll 2005), those guidelines are used (Manap & Voulvoulis 2015). The freeze coring technique can also enhance the spatial mapping of gas-bearing sediments. Although the acoustic response of gas-bearing sediments has been studied theoretically (Anderson & Hampton 1980), there are few well-constrained experimental data sets to validate and improve these models. Even fewer data are available for validating acoustic estimates of sediment $\theta$ using direct measurements or they did not consider coring disturbances in their analysis. While bubble formations and migration have been studied under laboratory conditions (Boudreau 2012; Johnson et al. 2002), *in situ* observations are constrained by gas expansion and ebullition in response to the change in hydrostatic pressure when sampled sediment cores are retrieved for analysis. Thus, sound sediment core data from the freeze coring technique can improve the characterization of dredging sites in order to achieve efficient and environmentally friendly dredging operations.

## 4.2 Submerged cavitating water jets for hydraulic dredging

Hydraulic dredging in combination with submerged cavitating water jets is assumed to efficiently dredge (e.g., gassy, consolidated or contaminated) sediment layers at distinct depths. For the design and planning of a dredging operation, knowledge of the impact pressure distribution and spray pattern of the water jet is required. Therefore, the governing parameter and its effect on the impact pressure distribution were obtained with an adapted Pressure Measurement Sensing method.

The findings on the parameters affecting the impact pressure, obtained in this study (*Appendix IV*), agree with the investigations of e.g. Mortensen (2013), Nobel & Talmon (2012), Soyama & Lichtarowicz (1998), Soyama (2011), and Yamaguchi & Shimizu (1987), who found that the impinging distance and angle, and the pump pressure are crucial parameters affecting the (cavitational) forces of the water jets. However, the results of this study go beyond previous studies by providing a higher spatial resolution of the impact pressure distribution. This is particularly needed because various flat fan water jets with different spraying angles were investigated. The results of the experiments found clear correlations between the impact pressure and standoff distance, spray angle, pump pressure, and impinging angle, which have been used for the multiple linear regression (MLR) model. The MLR can be used to roughly predict the average ($R^2$=0.81) and peak impact pressure ($R^2$=0.86) of submerged cavitating water jets. It is shown that a technique to control the impact pressure of the water jet on the sediment, such as by controlling the pump pressure and impinging distance, is required to achieve a constant high dredging efficiency. However, it was not possible to investigate all parameters affecting the impact pressure in detail in this study. For example, the ambient pressure and salinity also have an effect on the impact pressure (Nobel & Talmon 2012). However, those ambient conditions were not varied in this study, as they cannot be controlled during the dredging process, even though those parameters should be taken into consideration for further analysis.

This study has shown that an increase in pump pressure increases the impact pressure, which positively correlates with the number and density of cavitation bubbles. The impact pressure seems to be optimized in terms of maximum output (impact pressure) by minimum input (energy of the pump pressure) of between 60 bar and 90 bar pump pressure. This corresponds to the results of Nobel & Talmon (2012). They observed that at a certain pressure, the effectiveness of the cavitation cone reaches a near maximum value and a further increase in pressure results only in a negligible increase in stagnation pressure. The same trend –

even though they studied non-cavitating jets – was observed by Shen & Sun (1988). Thus, applying the optimized pressure can reduce costs in dredging operations.

The results showed that the submerged cavitating water jets achieve high impact pressures, as the collapsing cavitation bubbles create a much higher working pressure than pump pressure alone (Soyama & Lichtarowicz 1998). In line with the idea of Nobel (2013), it can be concluded that cavitating water jet can increase the dredging efficiency and penetration depth in contrast to non-cavitating jets. This is due to fact that water jets which are widely used in dredging operation uses large flow rates and low-pressure (Nobel 2013), but at such low jet pressures, the resistance of the ambient water hinder the jet development and destroy the integrity of the jet (Kang et al. 2019). It can therefore be reasonably assumed that cavitational water jets achieve high energy impacts to enhance the erosional capacity, as demonstrated in this study (*Hypothesis 3 corroborated*).

A surprising result of the study was that at an inclination of 22.5°, the water jet positively but not significantly affected the average and peak impact pressure, whereas a further inclination to 45° significantly decreased the impact pressure. When the water jet approaches the wall, a rise in static pressure forces the water jet to decelerate until the stagnation point is reached, where static pressure is highest when the velocity is zero, according to the Bernoulli equation. Upon approaching the wall, the water jet flow velocity decreases and the jet flow turns radially and induces eddies of various sizes around the impingement point (Peng et al. 2018). The inclination of the water jet reduces the thickness of a stagnation zone which provides resistance to the approaching jet flow, as the jet flow can turn radially more easily. This effect shifts the stagnation point to a closer distance towards the wall. It is assumed that this change in flow velocity, respectively the stagnation point, might be attributed to the collapse of the cavitation bubbles, resulting in a change of impact pressure. Our findings corroborates those of Al Naib & Sanders (1997) and Chuan et al. (2017), who investigated the effect of impinging angles on a fully-submerged, oblique impinging water jet, but those studies have been restricted to non-cavitating water jets. Thus, the transferability of the explanations of the effects to those in this study should be made with caution, in particular because the impact pressure due to the flow velocity and implosion of cavitation bubbles may significant differ. Nevertheless, the results indicate that an inclined water jet can achieve higher erosional forces to erode sediment deposits. This suspicion is supported by the findings reported by Hou et al. (2016), who found that the scour depth (50 mm silica powder as experimental sediment) of the submerged water jet increases with an increase in impinging angle. It will be important that future research investigate the effect of the impinging angle on

the average and peak impact pressure to confirm the hypothesis, that a certain water jet inclination positively affects the impact pressure. If this hypothesis were confirmed, an inclination of the water jet can increase the dredging efficiency without generating costs.

In general, the findings in this study (*Appendix IV*) can only be applied cautiously to *in situ* sediment. In this regime, the results obtained for the oblique, impinging water jet may be significantly different when applied to erodible sediment beds. As this study describes an experimental method for impact pressure measurement on an impermeable, non-erodible and non-deforming wall, there is clearly a different situation to a cavitating water jet penetrating into the sediment. Therefore, as the erosion process starts in natural sediment, the relevant parameters will vary with increasing dredging depth.

In order to control the scouring effects of impinging jets, detailed knowledge of both the flow field and the scouring effect for the given flow configuration is necessary (Kobus et al. 1979). There are various studies on sediment erosion by submerged impinging vertical turbulent jets such as Aderibigbe & Rajaratnum (1996) and Beltaos & Rajaratnam (1974). Regarding the limitations of those studies, as they are restricted to non-cohesive sediment and non-cavitating water jets, the findings of this study support the results obtained on the influencing factors of standoff distance and jet velocity. Nevertheless, sediment parameters have to be measured *in situ* to optimize the precision and efficiency of dredging operations. However, literature concerning the erodibility of sediment that might be used for the prediction of sediment erodibility is very limited. Even though the relevant parameters might be measured, it remains unclear to what degree each parameter is attributed to an increasing or decreasing shear stress resistance in the sediments. Consequently, the best approach might be to measure the *in situ* erosional resistance of these sediments. A wide variety of techniques for determining sediment erodibility exist, but no test is accepted as the standard for *in situ* measurements (e.g. Tolhurst et al. 1999). There is currently no reliable method to estimate the critical shear stress for clay-rich or cohesive sediments based on soil properties (Cossette et al. 2012). This is, as already mentioned, because there are many factors that affect a clayey soil's erosion resistance including the soil density, clay content, clay mineralogy, pore and eroding fluid chemistry, temperature, water content and organic content (Hanson & Cook 1998; Paaswell 1973). It will be important that future research investigates a reliable method for measuring the critical shear stress *in situ* to provide sound data for the design of dredging operations.

## 4.3 Sediment concentration measurement for the determination of the efficiency of water jet dredging

The measurement of the dredged sediment concentration in the dredging pipeline is required to control the dredging operation and to measure its efficiency. It helps to prevent under- and over-dredging, reduces environmental impacts, reduces the dredging time and helps to achieve optimal utilization rates.

This study (*Appendix I*) has shown that the DENSE technique (densimeter of semicontinuous suspended sediment concentration measurements) combines the strengths of traditional and surrogate methods. Laboratory experiments proved that an autonomous weighing of a solid-water mixture with a defined sample volume allows the accurate measurement of its concentration, unaffected by entrained gas (*Hypothesis 4 corroborated*). DENSE achieves the accuracy of traditional methods and enhance the temporal resolution, such as surrogate methods without the requirement of site calibration. It has been shown that the sediment concentration can be calculated by Eq. (1), derived from the relationship between fluid density and the mass concentration of suspended sediment (suspended sediment concentration described the concentration of solid-phase material suspended in a water-sediment mixture (Gray et al. 2000)) of Lewis & Rasmussen (1999):

$$SSC = \frac{M_S}{V_w} = \frac{\left(\frac{M_T - V_T * \rho}{\rho_s - \rho}\right) * \rho_s}{V_T - \left(\frac{M_T - V_T * \rho}{\rho_S - \rho}\right)} \qquad \text{Eq. (1)}$$

$M_T$ Total mass of the water and sediment sample
$M_S$ Mass of the sediment
$V_T$ Total volume of the water and sediment
$V_W$ Volume of the water
$\rho_s$ Density of the sediment
$\rho$ Density of the water

The temperature (which correlates to the sample's volume), mass and volume of the sample obtained affect the accuracy of the DENSE method calculation. The study revealed that the decisive factor for the sediment concentration measurement relies on the accurate determination of the weight of the sample and on the design of the overflow apparatus to ensure a constant sample volume. Surprisingly, the study revealed that the temperature curve does not fit the theoretical temperature-density curve. No explanation for this has been found so far, but due to the strong correlation of the laboratory data, a temperature correction was possible. It has to be noted that this assumption is only valid for the current design of DENSE, whereas a change or optimization of the design would require a new validation. Greater precision can be achieved by enhancing the accuracy of the load cell or by increasing the sample

volume. By increasing the sample's volume, specifically the weight, small changes in the weight of the sample can be measured more precisely.

In this study (Eq. 1) – and used widely elsewhere (e.g. Armanini 2018; Guillén et al. 2014; Mehta 2013) – the solid density was assumed to be 2,650 kg $m^{-3}$. The majority of mineral-rich and organic material-poor particles are composed of quartz, with a density of nearly 2,600 – 2,700 kg $m^{-3}$, or calcareous material with a density of ~2,900 kg $m^{-3}$ (Armanini 2018). Mineral-poor and organic material-rich sediments have densities between 1,000 and 1,500 kg $m^{-3}$ (Wakeham & Canuel 2016). Variation in sediment density may, therefore, affect the accuracy of DENSE. In particular, low density organic matter may negatively skew particle density estimates. In this study, the variation of particle density was not investigated, but it is necessary for future studies to understand how the sediment particle density and, in particular, the organic matter influences the measurement of sediment concentration.

Isokinetic sampling from a dredging pipeline is important because otherwise, sediment concentration and particle-sizes are over- or underestimated, essentially for particles coarser than silt (Edwards & Glysson 1999). To avoid such biases, the velocity of the pipeline and the sampling pipe should be the same, and the sampling flow should be taken in the direction of the approaching flow (Felix 2017). In the laboratory experiments of this study, samples were taken from a closed-loop system with a centrifugal pump, which ensures a uniform distribution of concentration within the cross-section of the pipeline. If DENSE is applied in dredging operations, an isokinetic sampling is required, which has to be adapted to the specific application.

The dredging operation is affected by the high spatial variation in sediment characteristics as well as the experience and working state of the operator (Tang et al. 2009). The operator controls the dredging operation based on the slurry flow rate and density. The DENSE technique allows quasi-continuous sediment concentration measurement, thus providing the required data in real-time for optimizing the dredging operation. This allows the automatization of the dredging process (e.g. automated adaption of the pump pressure or the standoff distance), and enables a faster reaction to changes in the boundary conditions, such as the sediment composition. It is also a desired performance parameter (e.g. slurry density), thereby increasing the dredging efficiency.

# 5 Conclusion

The present thesis advances the understanding of sediment sampling for the characterization of (gas-bearing) sediment layer and provides a scientific and technical basis for submerged cavitating water jet dredging, as well as the measurement of the dredged sediment concentration in order to assess and control the dredging efficiency.

This thesis reveals that the freeze coring technique developed, in combination with non-destructive X-Ray CT scans, adds significant value for the understanding of sediment depositional features, especially for the gas bubble characterization. This freeze coring technique delivers significantly better results, as it is less susceptible to be affected by changes in pressure and temperature, and in combination with a coring disturbance analysis, increases the accuracy of the sediment analysis. These methods allow the quantification of sediment gas content *in situ*, for which no cost-efficient methods exist, and only a very limited number of studies have estimated the *in situ* gas content. The results of the field studies showed that the sediment gas content of freeze cores generally follows previously described spatial patterns in sediment organic carbon content and hydroacoustic gas content estimates, and corresponds to the findings of various studies where higher gas content is pronounced in the littoral zone (*Hypothesis 1 corroborated*). Although freeze cores are affected by coring disturbances due to the freezing process (*Hypothesis 2 corroborated*), the results indicate that the sediment stratigraphy and gas bubble integrity are less affected by changes in the hydrostatic pressure and sample temperature compared to the gravity coring technique. The X-Ray CT scans have proven to be a non-destructive technique to analyze (gassy) sediment core samples. It also allows the identification of zones of coring disturbances where the structural integrity is affected. The findings indicate that without corrections for disturbances, the validity of data obtained from non-frozen and non-pressurized coring in studies can be compromised, and should become a routine aspect in data analysis.

This study proves that the adapted design of a Pressure Measurement Sensing technique allows the impact pressure measurement and visualization of the spray pattern from the submerged oblique, impinging cavitating water jets at a high spatial resolution. In combination with the multiple linear regression model, the average and peak impact pressure distribution, depending on the governing parameter (impinging angle, standoff distance, spray angle and pump pressure) can be determined. The results provide a scientific and technical basis for the design of hydraulic dredging operations, where water jets are needed to erode and/or fluidize sediment deposits. The cavitating water jets can achieve high erosional forces and

showed their potential to precisely and efficiently erode (gas-bearing) sediment layers (*Hypothesis 3 corroborated*). However, the laboratory conditions represent a clearly different situation to *in situ* sediment. The results obtained need to be related to (variable) *in situ* sediment parameters to use the data for the purposes of dredging operations. In this context, it remains unclear to what extent water jets can remobilize defined sediment layers, as the interaction of a water jet with the sediment is a highly complex and dynamic process. Future studies are required to identify the *in situ* critical shear stress of the sediment to be dredged, for the transferability of the results is obtained from the impact pressure distribution.

Traditional and surrogate methods for sediment concentration measurement are limited in the range of concentration and particle-sizes, and they can be biased by entrained gas bubbles. The innovative DENSE technique developed here overcomes these limitations and closes the gap between traditional and surrogate sediment concentration measurement methods. The results show that an autonomous weighing of a solid-water mixture sample with a defined volume allows the semi-continuous measurement of sediment concentrations unaffected by entrained gas bubbles (*Hypothesis 4 corroborated*). The laboratory results confirmed its performance and the required accuracy of the method. Future research should confirm the applicability of the DENSE method under *in situ* conditions, as the laboratory conditions do not reflect the changing sediment concentration, particle density and particle-size.

Within the scope of this thesis, three different methods (i) freeze coring for sampling and characterization of (gas-bearing) sediments; (ii) Pressure Measurement Sensing for the visualization and investigation of the impact pressure of submerged cavitating water jets; and (iii) the DENSE technique for measuring the sediment concentration have been developed, which enhances technical and scientific processes within the field of reservoir sedimentation and sediment management techniques. These easy-to-use and relatively cost-efficient methods produce sound information, which can be used in the context of reservoir sedimentation analysis and countermeasures.

# References


Abegg, F., and A. L. Anderson. 1997. The acoustic turbid layer in muddy sediments of Eckernfoerde Bay, Western Baltic: methane concentration, saturation and bubble characteristics. Marine Geology. 137: 137-147, doi: doi.org/10.1016/S0025-3227(96)00084-9.

Aben, R. C., Barros, N., Donk, E. V., Frenken, T., Hilt, S., Kazanjian, G., Lamers, L. P., Peeters, E. T., Roelofs, J. G., Domis, L. N., Stephan, S., Velthuis, M., Waal, D. B., Wik, M., Thornton, B. F., Wilkinson, J., DelSontro, T., and S. Kosten. 2017. Cross continental increase in methane ebullition under climate change. Nature Communications. 8: 1682, doi: 10.1038/s41467-017-01535-y.

Aderibigbe, O. O., and N. Rajaratnum. 1996. Erosion of loose beds by submerged circular impinging jets. Journal of Hydraulic Research. 34: 19-33, doi: doi.org/10.1080/00221689609498762.

Al Naib, S., and J. Sanders. 1997. Oblique and vertical jet dispersion in channels. Journal of Hydraulic Engineering. 123: 456-462, doi: doi.org/10.1061/(ASCE)0733-9429(1997)123:5(456).

Amiri-Simkooei, A. R., Snellen, M., and D. G. Simons. 2011. Principal Component Analysis of Single-Beam Echo-Sounder Signal Features for Seafloor Classification. Oceanic Engineering. 36(2): 259-272, doi: 10.1109/JOE.2011.2122630.

Anderson, A. L., and L. D. Hampton. 1980. Acoustics of gas-bearing sediments I. Background. The Journal of the Acoustical Society of America. 67: 1865-1889, doi: doi.org/10.1121/1.384453.

Anderson, M. A., and P. Pacheco. 2011. Characterization of bottom sediments in lakes using hydroacoustic methods and comparison with laboratory measurements. Water Research. 45(15): 4399-4408. doi: 10.1016/j.watres.2011.05.029.

Anderson, M. A., Conkle, J. L., Pacheco, P., and J. Gan. 2013. Use of hydroacoustic measurements to characterize bottom sediments and guide sampling and remediation of organic contaminants in lake sediments. Science of The Total Environment. 458-460: 117-124, doi: 10.1016/j.scitotenv.2013.04.009.

Andresen, A. 1981. Exploration, sampling and in-situ testing of soft clay, p. 245-308. In, Brand, E.W., Brenner, R.P [eds.], Soft clay engineering, Elsevier.

Annandale, G. W., Karki, P., and G. L. Morris. 2016. Technical guidance note: Extending the life of reservoirs - Sustainable sediment management for run-of-river hydropower and dams. World Bank Report, Washington, DC.

Armanini, A. 2018. Introduction to Sediment Transport, p. 33-47. In Principles of River Hydraulics. Springer.

Asthana, R., and S. N. Tewari. 1993. The engulfment of foreign particles by a freezing interface. Journal of Material Science. 28: 5414, doi: doi.org/10.1007/BF00367810.

Ban, Y., Chen, T., Yan, J., and T. Lei. 2017. Accurate mass replacement method for the sediment concentration measurement with a constant volume container. Measurement Science and Technology. 28(4), doi: doi.org/10.1088/1361-6501/aa5b23.

Barros, N., Cole, J. J., Tranvik, L. J., Prairie, Y. T., Bastviken, D., Huszar, V. L. M., del Giorgio, P., and F. Roland. 2011. Carbon emission from hydroelectric reservoirs linked to reservoir age and latitude. Nature Geoscience. 4: 593-596, doi: 10.1038/ngeo1211.

Bastviken, D., Cole, J. J., Pace, M. L., and M. C. Van de Bogert. 2008. Fate of methane from different lake habitats: Connecting whole-lake budgets and $CH_4$ emissions. Journal Geophysical Research. 113: G02024, doi: 10.1029/2007JG000608.

Bastviken, D., Tranvik, L., Downing, J. A., Crill, P. M., and A. Enrich-Prast. 2011. Freshwater methane emissions offset the continental carbon sink. Science. 331: 50, doi: 10.1126/science.1196808.

Baxter, M. S., Farmer, J. G., McKinley, I. G., Swan, D. S., and W. Jack. 1981. Evidence of the unsuitability of gravity coring for collecting sediment in pollution and sedimentation rate studies. Environmental Science and Technology. 15: 843-846, doi: doi/pdf/10.1021/es00089a014.

Beaulieu, J. J., McManus, M. G., and C. T. Nietch. 2016. Estimates of reservoir methane emissions based on spatially balanced probabilistic – survey. Limnology and Oceanography. 61: S27-S40, doi: 10.1002/lno.10284.

Beaulieu, J. J., Smolenski, R. L., Nietch, C. T., Townsend-Small, A., and M. S. Elovitz. 2014. High methane emissions from a midlatitude reservoir draining an agricultural watershed. Enviro. Sci. Technol. 48(19): 259-272, doi: doi.org/10.1021/es501871g.

Beltaos, S., and N. Rajaratnam. 1974. Impinging circular turbulent jets. Journal of the hydraulics division. 100: 1313-1328.

Berlamont, J., Ockenden, M. Toorman, E., and J. Winterwerp. 1993. The characterisation of cohesive sediment properties. Coastal Engineering. 21: 105-128, doi: doi.org/10.1016/0378-3839(93)90047-C.

Black, K. S., Tolhurst, T. J., Paterson, D. M., and S. E. Hagerthey. 2002. Working with Natural Cohesive Sediments. Journal of Hydraulic Engineering. 128(1): 2-8, doi: 10.1061/(ASCE)0733-9429(2002)128:1(2).

Blomqvist, S. 1985. Reliability of core sampling of soft bottom sediment - an in situ study. Sedimentology. 32: 605-612, doi: 10.1111/j.1365-3091.1985.tb00474.x.

Blomqvist, S. 1991. Quantitative sampling of soft-bottom sediments: Problems and solutions. Marine Ecology Progress Series. 72: 295-304, doi: 10.3354/meps072295.

Boudreau, B. P. 2012. The physics of bubbles in surficial, soft, cohesive sediments. Marine and Petroleum Geology. 38(1): 1-18, doi: 10.1016/j.marpetgeo.2012.07.002.

Buckley, D. E., MacKinnon, W. G., Cranston, R. E., and H. A. Christian. 1994. Problems with piston core sampling: Mechanical and geochemical diagnosis. Marine Geology. 117: 95-106, doi: 10.1016/0025-3227(94)90008-6.

Burton, G. A., Batley, G. E., Chapman, P. M., Forbes, V. E., Smith, E. P., Reynoldson, et al. 2002. A weight-of-evidence framework for assessing sediment (or other) contamination: Improving certainty in the decision-making process. Human and Ecological Risk Assessment. 8(7): 1675-1696, doi: doi.org/10.1080/20028091056854.

Burton, G. A., Gunnison, D., and G. Lanza. 1987. Survival of Pathogenic Bacteria in Various Freshwater Sediments. Applied and environmental microbiology. 53: 633-638.

Bussmann, I., Schlömer, S., Schlüter, M., and M. Wessels. 2011. Active pockmarks in a large lake (Lake Constance, Germany): effects on methane distribution and turnover in the sediment. Limnology Oceanography. 56: 379-393, doi: doi.org/10.4319/lo.2011.56.1.0379.

Cadée, G.C. 2001. Sediment dynamics by bioturbating organisms, p. 127-148. In, Reise, K. [eds.], Ecological comparison of sedimentary shores, Verlag Berlin Heidelberg.

Carte, A. E. 1961. Air bubbles in Ice. Proceedings of the Physical Society. 77(3): 757-768, doi: 10.1088/0370-1328/77/3/327.

Casper, P., Maberly, S. C., Hall, G. H., and B. J. Finlay. 2000. Fluxes of methane and carbon dioxide from a small productive lake to the atmosphere. Biogeochemistry. 49: 1-19, doi: 10.1023/A:1006269900174.

Chen, L. C., Chian, C. Y., Yen, P. S., Chu, C. P., and D. J. Lee. 2001. High-speed sludge freezing. Water Resources. 35(14): 3502-3507, doi: doi.org/10.1016/S0043-1354(01)00048-3.

Chuan, W., Xikun, W., Weidong, S., Weigang, L., Soon, K. E., and Z. Ling. 2017. Experimental investigation on impingement of a submerged circular water jet at varying impinging angles and Reynolds numbers. Experimental Thermal and Fluid Science. 89: 189-19, doi: doi.org/10.1016/j.expthermflusci.2017.08.005.

Clayton, C. R. I., Matthews, M. C., and N. E. Simons. 1995. Site Investigations, 2nd ed. Blackwell Science.

Cossette, D., Mazurek, K. A., and C. D. Rennie. 2012. Critical shear stress from varied methods of analysis of a submerged circular turbulent impinging jet test for determining erosion resistance of cohesive soils. In Proceedings of the 6th Intl. Conf. on Scour and Erosion (ICSE6), Paris, France.

De Cesare, G., Schleiss, A., and F. Hermann. 2001. Impact of turbidity currents on reservoir sedimentation. Journal of Hydraulic Engineering. 127(1): 6-16, doi: doi.org/10.1061/(ASCE)0733-9429(2001)127:1(6).

de Mello, N. A. S. T., Brighenti, L. S., Barbosa, F. A. R., Staehr, P. A., and J. F. B. Neto. 2018. Spatial variability of methane (CH4) ebullition in a tropical hypereutrophic reservoir: silted areas as a bubble hot spot. Lake and Reservoir Management. 34(2): 105-114, doi: doi.org/10.1080/10402381.2017.1390018.

Deemer, B. R., Harrison, J. A., Li, S., Beaulieu, J. J., DelSontro, T., Barros, N., Bezerra-Neto, J., Powers, S., Dos Santos, M., and J. Vonk. 2016. Greenhouse gas emissions from reservoir water surfaces: A new global synthesis. BioScience. 66(11): 949−964, doi: doi.org/10.1093/biosci/biw117.

DelSontro, T., Kunz, M. J., Kempter, T., Wüst, A., Wehrli, B., and D. B. Senn. 2011. Spatial Heterogeneity of Methane Ebullition in a Large Tropical Reservoir. Environmental Science & Technology. 45(23): 9866-9873, doi: 10.1021/es2005545.

DelSontro, T., McGinnis D. F., Sobek S., Ostrovsky I., and B. Wehrli. 2010. Extreme methane emissions from a Swiss hydropower reservoir: contribution from bubbling sediments. Environmental Science & Technology. 44(7): 2419-2425, doi: 10.1021/es9031369.

DelSontro, T., McGinnis, D. F., Wehrli, B., and I. Ostrovsky. 2015. Size does matter: Importance of large bubbles and small-scale hot spots for methane transport. Environmental Science & Technology. 49 (3): 1268-1276.

Delwiche, K., Senft-Grupp, S., and H. Hemond. 2015. A novel optical sensor designed to measure methane bubble sizes in situ. Limnology and Oceanography: Methods. 13: 712-721, doi: 10.1002/lom3.10060.

Duc, N., Crill, P., and D. Bastviken. 2010. Implications of temperature and sediment characteristics on methane formation and oxidation in lake sediments. Biogeochemistry. 100(1-3): 185-196.

Edwards, J. S. 1991. Potential hazards resulting from the presence of methane dissolved in groundwater. In, Proceedings of the 4th International Mine Water Congress, Ljubljana, Slovenia, Yugoslavia.

Edwards, T. K., and G. D. Glysson. 1999. Field methods for measurement of fluvial sediment, p. 89. In Techniques of Water-Resources Investigations, Book 3. U.S. Geological Survey.

Emery, K. O., and J. Hülsemann. 1964. Shortening of sediment cores collected in open-barrel gravity cores. Sedimentology. 3: 144-154, doi: doi.org/10.1111/j.1365-3091.1964.tb00639.x.

Emery, K. O., and R. S. Dietz. 1941. Gravity coring instrument and mechanics of sediment coring. Geological Society of America Bulletin. 53: 1685-1714, doi: doi.org/10.1130/GSAB-52-1685.

Engelund, F., and J. Fredsoe .1976. A Sediment Transport Model for Straight Alluvial Channels. Hydrology Research. 7(5), 293-306, doi: doi.org/10.2166/nh.1976.0019.

Felix, D. 2017. Experimental investigation on suspended sediment hydro-abrasive erosion and efficiency reductions of coated Pelton turbines. Ph.D. thesis. Swiss Federal Institute of Technology in Zurich.

Fleischer, P., Orsi, T., Richardson, M., and A. Anderson. 2001. Distribution of free gas in marine sediments: a global overview. Geo-Marine Letters. 21: 103-122, doi: 10.1007/s003670100072.

Franceschini, O. 2010. Dewatering of sludge by freezing. Master thesis. Luleå University of Technology.

Franchini, A. G., and J. Zeyer. 2012. Freeze-Coring Method for Characterization of Microbial Community Structure and Function in Wetland Soilds at High Spatial Resolution. Applied and Environmental Microbiology. 78(12): 4501-4504, doi: 10.1128/AEM.00133-12.

Giles, J. 2006. Methane quashes green credentials of hydropower. Nature. 444: 524-525, doi: 10.1038/444524a.

Glew J. R., Smol J. P., and W. M. Last. 2002. Sediment Core Collection and Extrusion. In Last W.M., Smol J.P. [eds.] Tracking Environmental Change Using Lake Sediments. Developments in Paleoenvironmental Research, 1st ed. Springer.

Gray, J. R., and F. J. M. Simões. 2008. Estimating sediment discharge. Sedimentation engineering - Processes, measurements, modeling, and practice, p. 1067-1088. M. Garcia [eds.], ASCE.

Gray, J. R., and J. W. Gartner. 2009. Technological advances in suspended sediment surrogate monitoring. Water Resources Research. 45(4), doi: dx.doi.org/10.1029/2008wr007063.

Gray, J. R., and M. N. Landers. 2014. Measuring suspended sediment, p. 157-204. In S. Ahuja [eds.], Comprehensive water quality and purification, Elsevier.

Gray. J. R., Glysson, G. D., Turcios, L. M., and G. E. Schwarz. 2000. Comparability of suspended-sediment concentration and total suspended solids data. U.S. Dept. of the Interior, U.S. Geological Survey, doi: 10.3133/wri004191.

Guillén, S., Franca, M. J., Schleiss, A. J., and A. H. Cardoso. 2014. Morphodynamic differences induced by difference confluence angles in widen confluences. In, Proceedings of the International Conference on Fluvial Hydraulics, Lyon, France.

Hanson, G. J., and K. R. Cook. 1998. Relationship of soil suction and erodibility of a compacted soil, Paper No. 982065. In, ASAE Annual Int. Meeting, Orlando, USA.

HELCOM, 2000. Intercomparison of sediment sampling devices using artificial radionuclides in Baltic Sea sediments The MOSSIE Report. Baltic Sea Environment Proceedings No. 21(80).

Hill, M. T. R. 1999. A freeze-corer for simultaneous sampling of benthic macroinvertebrates and bed sediment from shallow streams. Hydrobiologia. 412: 213-215, doi: doi.org/10.1023/A:1003820920670.

Hjorth, T. 2004. Effects of freeze-drying on partitioning patterns of major elements and trace metals in lake sediments. Analytica Chimica Acta. 526: 95-102, doi: 10.1016/j.aca.2004.08.007.

Hogg, A. J., Huppert, H. E., and W. B. Dade. 1997. Erosion by planar turbulent wall jets. Journal Fluid Mechanics. 338: 317-340, doi: doi.org/10.1017/S0022112097005077.

Hongve, D., and A. H. Erlandsen. 1979. Shortening of surface sediment cores during sampling. Hydrobiologia. 65: 283-287, doi: doi.org/10.1007/BF00038869.

Hou, J., Zhang, L., Gong, Y., Ning, D., and Z. Zhang. 2016. Theoretical and experimental study of scour depth by submerged water jet. Advances in Mechanical Engineering. 8(12), doi: doi.org/10.1177/1687814016682392.

Huttenen, J. T., Lappalainen, K. M., Saarijarvi, E., Vaisanen, T., and P. Martikainen. 2001. A novel sed-iment gas sampler and a subsurface gas collector used for measurement of the ebullition of methane and carbon dioxide from a eutrophied lake. Science of the Total Environment. 266: 153-158, doi: doi.org/10.1016/S0048-9697(00)00749-X.

Huttunen, P., and J. Meriläinen. 1978. New freezing device providing large unmixed sediment samples from lakes. Annales Botanici Fennici. 15(2): 128-130.

ICOLD. 2016. Register of Dams - General Synthesis. Retrieved April 25, 2016, from http://www.icold- cigb.org/GB/World_register/general_synthesis.asp

International Hydropower Association. 2018. Hydropower Status Report. Sector trends and insights.

Jepsen, R., McNeil, J., Lick, and W. Lick. 2000. Effects of gas generation on the density and erosion of sediments from the Grand River. Journal of Great Lakes Research. 26(2): 209-219, doi: doi.org/10.1016/S0380-1330(00)70687-3.

Johnson, B. D., Boudreau, B. P., Gardiner, B. S., and R. Maass. 2002. Mechanical response of sediments to bubble growth. Marine Geology. 187: 347-363, doi: doi.org/10.1016/S0025-3227(02)00383-3.

Kang, C., Liu, H., Mao, N., and Y. Zhang. 2019. Submerged Waterjet. Methods for Solving Complex Problems in Fluids Engineering. 27-69. doi:10.1007/978-981-13-2649-3_3.

Katsnelson, B., Katsman, R., Lunkov, A., and I. Ostrovsky. 2017. Acoustical methodology for determination of gas content in aquatic sediments, with application to Lake Kinneret, Israel, as a case study. Limnology Oceanography: Methods. 15: 531-541, doi: 10.1002/lom3.10178.

Kelly, C. A., and D. P. Chynoweth. 1981. The contributions of temperature and of the input of organic matter in controlling rates of sediment methanogenesis. Limnology Oceanography. 26: 891-897, doi: 10.4319/lo.1981.26.5.0891.

Killawee, J. A., Fairchild, I. J., Tison, J.-L., Janssens L., and R. R. Lorrain. 1998. Segregation of solutes and gases in experimental freezing of dilute solutions: Implications for natural glacial systems. Geochim. Cosmochim. Acta. 62: 3637-3655, doi: doi.org/10.1016/S0016-7037(98)00268-3.

Kimiaghalam, N., Clark, S. P., and H. Ahmari. 2016. An experimental study on the effects of physical, mechanical, and electrochemical properties of natural cohesive soils on critical shear stress and erosion rate. International Journal of Sediment Research. 31: 1-15, doi: 10.1016/j.ijsrc.2015.01.001.

Klös, H., and C. Schoch. 1993. Einfache Methoden zur Radiodatierung limnischer Sedimente. Z. Umweltchem. Ökotox. 5(1):2-6.

Kobus, H., Leister, P., and B. Westrich. 1979. Flow field and scouring effects of steady and pulsating jets impinging on a movable bed. Journal of Hydraulic Research. 17(3): 175-192, doi: doi.org/10.1080/00221687909499582.

Kondolf, G. M. et al. 2014. Sustainable sediment management in reservoirs and regulated rivers: Experiences from five continents. Earth's Future. 2, doi: doi.org/10.1002/2013EF000184.

Kothyari, U. C., and R. K. Jain. 2008. Influence of cohesion on the incipient motion condition of sediment mixtures. Water Resources Research. 44: W04410, doi: doi.org/10.1029/2007WR006326.

Lane. M. C., and K. H. Taffs. 2002. The LOG corer - a new device for obtaining short cores in soft lacustrine sediments. Journal of Paleolimnology. 27: 145-150, doi: doi.org/10.1023/A:1013547028068.

Lebel, J., Silverberg, N., and B. Sundby. 1982. Gravity core shortening and pore water chemical gradients. Deep Sea Research. 29: 1365-1372, doi: doi.org/10.1016/0198-0149(82)90014-0.

Lehner, B. et al. 2011. High-resolution mapping of the world's reservoirs and dams for sustainable river-flow management. Front. Ecol. Environ. 9: 494-502, doi: 10.1890/100125.

Lempérière, F. 2006. The role of dams in the XXI century Achieving a sustainable development target, p. 99-109. In, Proceedings of the 26th Annual USSD Conference San Antonio, Texas, United States of America.

Lewin, K., and K. Bradshaw. 1993. Continuous Monitoring of Methane in Groundwater. HSE Contract Research Report No. 49.

Lewis, A. J., and T. C. Rasmussen. 1999. Determination of suspended sediment concentrations and particle size distributions using pressure measurements. Journal of Environmental Quality. 28(5): 1490-1496, doi: 10.2134/jeq1999.00472425002800050014x.

Li, L., Peng, J., Gao, Q., Sun, M., Liu, Y., Li, M., Chen. B., and K. Bo. 2016. Pressure retaining method based on phase change of coring of gas hydrate bearing sediments in offshore drilling. Applied Thermal Engineering. 107: 633-641, doi: doi.org/10.1016/j.applthermaleng.2016.06.174.

Liernur, A., et al. 2017. Coupling X-ray computed tomography and freeze-coring for the analysis of fine-grained low-cohesive soils. Geoderma. 308: 171-186, doi: doi.org/10.1016/j.geoderma.2017.08.010.

Lipp, G. and C. Körber. 1993. On the Engulfment of Spherical Particles by a Mobing Solid Liquid Interface. Journal of Crystal Growth. 130(3-4): 475-489, doi: 10.1016/0022-0248(93)90536-6.

Lipp, G., Körber, C., Englich, S., Hartmann, U., and G. Rau. 1987. Investigation of the behavior of dissolved gases during freezing. Journal of Cryobiology. 24: 489-503, doi: doi.org/10.1016/0011-2240(87)90053-8.

Lisle, T. E. 1989. Sediment transport and resulting deposition in spawning gravels, north coastal. California. Water Resources Research. 25: 1303-1319, doi: 10.1029/WR025i006p01303.

Liu, L., De Kock, T., Wilkinson, J., Cnudde, V., Xiao, S., Buchmann, C., et al. 2018. Methane bubble growth and migration in aquatic sediments observed by X-ray μCT. Environmental Science & Technology. 52 (4): 2007-2015, doi: 10.1021/acs.est.7b06061.

Liu, L., J. Wilkinson, K. Koca, C. Buchmann, and A. Lorke. 2016. The role of sediment structure in gas bubble storage and release. Journal of Geophysical Research: Biogeosciences. 121: 1992-2005, doi: 10.1002/2016JG003456.

Machin, J. B., and P. A. Allan. 2011. State-of-the-art jet trenching analysis in stiff clays., p. 871-876, Gourvenec, S., and D. White [eds.], Frontiers in offshore Geotechnics II, Taylor and Francis Group.

Machin, J. B., Messina, F. D., Mangal, J. K., and J. Girard. 2001. Recent research in stiff clay jetting. In, Proceedings of Offshore Technology Conference, Houston, Texas.

Maeck, A., DelSontro, T., McGinnis, D. F., Fischer, H., Flury, S., Schmidt, M., Fietzek, P., and A. Lorke. 2013. Sediment trapping by dams creates methane emission hot spots. Environmental Science & Technology. 47: 8130-8137, doi: 10.1021/es4003907.

Maeck, A., Hofmann, H., and A. Lorke. 2014. Pumping methane out of aquatic sediments: Ebullition forcing mechanisms in an impounded river. Biogeosciences. 11: 2925-2938, doi: doi.org/10.5194/bg-11-2925-2014.

Manap, N., and N. Voulvoulis. 2015. Environmental management for dredging sediments - The requirement of developing nations. Journal of environmental management. 147: 338-348, doi: 10.1016/j.jenvman.2014.09.024.

Martens, C. S., and R. A. Berner. 1974. Methane production in the interstitial waters of sulfate-depleted marine sediments. Science. 185: 1167-1169, doi: 10.1126/science.185.4157.1167.

Martinez, D., and M. A. Anderson. 2013. Methane production and ebullition in a shallow, artificially aerated, eutrophic temperate lake (Lake Elsinore, CA). Science of the Total Environment. 454-455: 457-465, doi: 10.1016/j.scitotenv.2013.03.040.

Mazurek, K. A., N. Rajaratnam, and D. C. Sego. 2001. Scour of cohesive soil by submerged vertical circular turbulent impinging jets. Journal of Hydraulic Engineering. 127(7): 598-606, doi: doi.org/10.1061/(ASCE)0733-9429(2001)127:7(598).

Mazurek, K. A., N. Rajaratnam, and D. C. Sego. 2006. Time development of scour in a cohesive material due to a submerged circular impinging jet. In, 3th International Conference on Scour and Erosion, Amsterdam.

Megonigal, J. P., Mines, M. E., and P. T. Visscher. 2005. Linkages to trace gases and aerobic processes. Biogeochemistry. 8: 350-362.

Mehta, A. J. 2013. An Introduction to Hydraulics of Fine Sediment Transport, World Scientific.

Meyer-Peter, E., and R. Müller. 1948. Formulas for Bed Load Transport. In, Proceedings of the 2nd meeting of the International Association for Hydraulic Structures Research, Delft, Netherlands.

Miskimmin, B. M., Curtis, P. J., Schindler, D. W., and N. Lafaut. 1996. A new hammer-driven freeze corer. Journal Paleolimnology. 15: 265-269, doi: doi.org/10.1007/BF00213045.

Mitchell, K. J., and K. Soga. 2005. Fundamentals of soil behavior. 3rd Edition [eds.]. John Wiley & Sons, Inc.

Mitchener, H., and H. Torfs. 1996. Erosion of mud/sand mixtures. Coastal Engineering. 30(3-4): 319, doi: doi.org/10.1016/S0378-3839(96)00002-6.

Mogg, A. O., Attard, K. M., Stahl, H., Brand, T., Turnewitsch, R., and M. D. Sayer. 2017. The influence of coring method on the preservation of sedimentary and biogeochemical features when sampling soft-bottom, shallow coastal environments. Limnology Oceanography: Methods. 15: 905-915, doi: 10.1002/lom3.10211.

Mogollón, J. M., Dale, A. W., L'Heureux, I., and P. Regnier. 2011. Impact of seasonal temperature and pressure changes on methane gas production, dissolution, and transport in unfractured sediments. Journal of Geophysical Research. 116: G03031, doi: 10.1029/2010JG001592.

Morris, G. L., and J. Fan. 1998. Reservoir Sedimentation Handbook: Design and Management of Dams, Reservoirs and Watersheds for Sustainable Use. McGraw-Hill Book Co., New York.

Mortensen, J. 2013. Resistance of Protective Coatings and Pipe Linings to High-Pressure Water Jets Used for Invasive Mussel Removal and Cleaning. Hydraulic Laboratory Technical Memorandum PAP-1074.

Moss, B., Madgwick, J., and G. Phillips. 1996. A Guide to the Restoration of Nutrienten-riched Shallow Lakes, p. 180, Broads Authority, 18 Colegate, Norwich, Norfolk NR3 1BQ, UK.

Murase, J., Sakai, Y., Kametani, A., and A. Sugimoto. 2005. Dynamics of methane in mesotrophic Lake Biwa. In Kohyama T., Canadell J., Ojima D.S., Pitelka L.F. [eds.], Forest Ecosystems and Environments. Springer.

Natchimuthu, S., I. Sundgren, M. Gålfalk, L. Klemedtsson, P. Crill, Å. Danielsson, and D. Bastviken. 2016. Spatiotemporal variability of lake CH4 fluxes and its influence on annual whole lake emission estimates. Limnology Oceanography. 61: S13-S26, doi: 10.1002/lno.10222.

Nevissi, A. E., Schott, G. J., and E. A. Crecelius. 1989. Comparision of two gravity coring devices for sedimentation rate measurement by 210Pb dating techniques. Hydrobiologia. 179: 261-269.

Newell, R. C., Seiderer, L. J., and D. R. Hitchcok. 1998. The impact of dredging works in coastal waters: a review of the sensitivity to disturbance and subsequent recovery of biological resources on the seabed. Oceanography and Marine Biology: an Annual Review. 36: 128-178.

Nobel, A. J. 2013. On the excavation process of a moving vertical jet in cohesive soil. Ph.D thesis. Delft University of Technology.

Nobel, A. J., and A. M. Talmon. 2012. Measurements of the stagnation pressure in the center of a cavitating jet. Experiments in Fluids. 52(2): 403-415, doi: doi.org/10.1007/s00348-011-1231-y.

Ostrovsky, I., and J. Tegowski. 2010. Hydroacoustic analysis of spatial and temporal variability of bottom sediment characteristics in Lake Kinneret in relation to water level fluctuation. Geo-Mar. Lett. 30: 261-269, doi: 10.1007/s00367-009-0180-4.

Ostrovsky, I., and Y. Z. Yacobi. 2010. Sedimentation flux in a large subtropical lake: Spatio-temporal variations and relation to primary productivity. Limnology and Oceanography. 55: 1918-1931, doi: 10.4319/lo.2010.55.5.1918.

Ostrovsky, I., McGinnis, D. F., Lapidus, L., and W. Eckert. 2008. Quantifying gas ebullition with echosounder: the role of methane transport by bubbles in a medium-sized lake. Limnology & Oceanography: Methods. 6: 105-118, doi: 110.4319/lom.2008.4316.4105.

Paaswell, R. E. 1973. Causes and Mechanisms of Cohesive Soil Erosion: The State of the Art. P. 8-19, Soil Erosion: Causes and Mechanisms: Prevention and Control, Conference Workshop on Soil Erosion, Highway Research Board Special Report 135, Washington, D.C.

Pachur, H. J., Denner, H. D., and H. Walter. 1984. A freezing device for sampling the sediment-water interface of lakes. Catena. 11: 65-70, doi: doi.org/10.1016/S0341-8162(84)80006-5.

Palmiere, A., Shah, F., Annandale, G. W., and A. Dina. 2003. Reservoir Conversation Vol. I: The RESCON Approach. World Bank, Washington DC.

Panagiotopoulos, I. Voulgaris, G., and B. Collins. 1997. The influence of clay on the threshold of movement of fine sandy beds. Coastal Engineering. 32(1): 19-43, doi: doi.org/10.1016/S0378-3839(97)00013-6.

Partheniades, E. 1979. Cohesive Sediment Transport Mechanics and Estuarine Sedimentation. Lecture Notes, International Course on Sediment Transport in Estuarine and Coastal Environment, Poona, India.

Peng, K., Tian, S., Li, G., and H. Alehossein. 2018. Mapping Cavitation Impact Field in a Submerged Cavitating Jet. Wear. 396-397: 22-33, doi: doi.org/10.1016/j.wear.2017.11.006.

Peppin, S. S. L., and R. W. Style. 2013. The Physics of Frost Heave and Ice-Lens Growth. Vadose Zone Journal. 12(1): vzj2012.0049, doi: doi.org/10.2136/vzj2012.0049.

Piggot, C. S. 1941. Factors involved in submarine core sampling. Bulletin of the Geological, Society of America. 52: 1513-1523, doi: doi.org/10.1130/GSAB-52-1513.or.

Poulain, T., Argillier, C., Gevrey, M. and J. Guillard, J. 2011. Identifying lakebed nature: is it feasible with a combination of echosounder and Sonar5-pro?. Advances in Oceanography and Limnology. 2 (1): 49-53.

Rai, A. A., and A. Kumar. 2015. Continuous measurement of suspended sediment concentration: Technological advancement and future outlook. Measurement. 76: 209-227, doi: doi.org/10.1016/j.measurement.2015.08.013.

Rajaratnam, N. 1976. Turbulent jets. 1st ed. Elsevier.

Randle, T., et al. 2017. Frequently Asked Questions about Reservoir Sedimentation and Sustainability, https://acwi.gov/sos/faqs_2017-05-30.pdf.

Renberg, I. 1981. Improved methods for sampling, photographing and varve-counting of varved lake sediments. Boreas. 10: 255-258, doi: doi.org/10.1111/j.1502-3885.1981.tb00486.x.

Righetti, M., and Lucarelli, C. 2007. May the Shields theory be extended to cohesive and adhesive benthic sediments?. Journal of Geophysical Research. 112: C05039, doi: 10.1029/2006JC003669.

Rongve, D., and A. H. Erlandsen. 1979. Shortening of surface sediment cores during sampling. Hydrobiologia. 65(3): 283-287, doi: 10.1007/bf00038869.

Rutledge, P. A., and J. W. Fleeger. 1988. Laboratory studies on core sampling with application to subtidal meiobenthos collection. Limnology and Oceanography. 33: 274-280, doi: doi.org/10.4319/lo.1988.33.2.0274.

Rymer, L., and J. Neale. 1981. Freeze coring as a method of collecting unconsolidated lake sediments. Australian Journal of Ecology. 6: 123-126, doi: doi.org/10.1111/j.1442-9993.1981.tb01279.x.

Saarnio, S., Alm, J., Silvola, J., Lohila, A., Nykänen, H., and P. J. Martikainen. 1997. Seasonal variation in CH4 emissions and production and oxidation potentials at microsites on an oligotrophic pine fen. Oecologia. 110: 414-422.

Scandella, B. P, Pillsbury, E., Weber, T., Ruppel, C., Hemond, H. F., and R. Juanes. 2016. Ephemerality of discrete methane vents in lake sediments. Geophyscial Research Letters. 43: 4374-4381, doi: 4310.1002/2016GL068668.

Scandella, B. P., Delwiche, K., Hemond, H. F., and R. Juanes. 2017. Persistence of bubble outlets in soft, methane-generating sediments. Journal of Geophysical Research: Biogeosciences. 122: 1298-1320, doi: 10.1002/2016JG003717.

Schleiss A., De Cesare G., and J. Jenzer Althaus. 2010. Verlandung der Stauseen gefährdet die nachhaltige Nutzung der Wasserkraft. Wasser, Energie, Luft - Eau, Energie, Air. 102(1): 31-40.

Schouten, T. 2016. Numerical simulation of a cavitating jet. Master thesis. Delft University of Technology.

Scott, S. H. 1993. Uncertainty Analysis of Dredge-Production Measurement and Calculation. Journal of Waterway, Port, Coastal, and Ocean Engineering. 119(2): 193-203, doi: 10.1061/(asce)0733-950x(1993)119:2(193).

Shapiro, J. 1958. The core-freezer - a new sampler for lake sediments. Ecology. 39: 758, doi: doi.org/10.2307/1931618.

Shen Z., and Q. Sun. 1988. Study of pressure attenuation of a submerged nonfree jet and a method of calculation for bottomhole hydraulic parameters. SPE Drilling Engineering. 3: 69-76, doi: doi.org/10.2118/14869-PA.

Sheng, D., Zhang, S., Yu, Z., and J. Zhang. 2013. Assessing frost susceptibility of soils using PCHeave. Cold Regions Science and Technology. 95: 27-38, doi: doi.org/10.1016/j.coldregions.2013.08.003.

Shields, A. 1936. Awendung der Aehnlichkeitsmechanik und der Turbulenzforschung auf die Geschiebebewegung. Mitt. Preuss. Versuchsanst. Wasserbau Schiffbau, 26.

Silva, A. S. R., Noack, M., Schlabing, D., and S. Wieprecht. 2017. A data-driven fuzzy approach to simulate the critical shear stress of cohesive sediments. In, International Symposium of River Sedimentation, Stuttgart, Germany.

Simpson, S., and Batley, Graeme. 2016. Sediment Quality Assessment A Practical guide, 2nd ed. CSIRO Publishing.

Skinner, L. C., and I. N. McCave. 2003. Analysis and modelling of gravity- and piston coring based on soil mechanics. Marine Geology. 199: 181-204, doi: 10.1016/S0025-3227(03)00127-0.

Sobek, S., Del Sontro, T., Wongfun, N., and B. Wehrli. 2012. Extreme organic carbon burial fuels intense methane bubbling in a temperate reservoir. Geophysical Research Letter. 39, doi: 10.1029/2011GL050144.

Sobek, S., Durisch-Kaiser, E., Zurbrügg, R., Wongfun, N., Wessels, M., Pasche, N., and B. Wehrli. 2009. Organic carbon burial efficiency in lake sediments controlled by oxygen exposure time and sediment source. Limnolology Oceanography. 54: 2243-2254, doi: 10.4319/lo.2009.54.6.2243.

Sobek, S., Zurbrügg, R., and I. Ostrovsky. 2011. The burial efficiency of organic carbon in the sediments of Lake Kinneret. Aquatic Sciences. 73(3): 355-364, doi: 10.1007/s00027-011-0183-x.

Soyama H., and A. Lichtarowicz. 1998. Cavitating jets - similarity correlations. Journal of Jet Flow Engineering. 12: 9-19.

Soyama, H. 2011. Enhancing the aggressive intensity of a cavitating jet by means of the nozzle outlet geometry. ASME Journal of Fluids Engineering. 133: 1-11, doi: dx.doi.org/10.1115/1.4004905.

Spigolon, S. J. 1995. Geotechnical descriptors for dredgeability. Technical Note DRP-2-13. Vicksburg, MS: U.S. Army Engineer Waterways Experiment Station.

St. Louis, V. L., Kelly, C. A., Duchemin, E., Rudd, J. W. M., and D. M. Rosenberg. 2000. Reservoir surfaces as sources of greenhouse gases to the atmosphere: A global estimate. Bioscience. 50: 766-775.

Strasser, D., Lensing, H. J., Nuber, T., Richter, D., Frank, S., Goeppert, N., and N. Goldscheider. 2015. Improved geohydraulic characterization of river bed sediments based on freeze-core sampling - development and evaluation of a new measurement approach. Journal of Hydrology. 527: 133-141, doi: 10.1016/j.jhydrol.2015.04.074.

Sumi, T., and T. Hirose. 2009. Accumulation of sediment in reservoirs, in Water Storage, Transport, and Distribution, p. 489. Yutaka Takahasi [eds.], Encyclopedia of Life Support Systems. UNESCO Publishing-Eolss Publishers.

Syvitski, J. P. M., Vörösmarty, C. J., Kettner, A. J., and P. Green. 2005. Impact of humans on the flux of terrestrial sediment to the global coastal ocean. Science 308: 376-380, doi: 10.1126/science.1109454.

Tang, J., Wang, Q., and T. Zhong. 2009. Automatic monitoring and control of cutter suction dredger. Automation in Construction. 18(2): 194-203, doi: 10.1016/j.autcon.2008.07.006.

Tęgowski, J. 2005. Acoustical classification of the bottom sediments in the Southern Baltic Sea. Quaternary International. 130(1): 153-161, doi.org/10.1016/j.quaint.2004.04.038.

Thebrath, B., Rothfuss, F., Whiticar, M. J., and R. Conrad. 1993. Methane production in littoral sediment of Lake Constance. FEMS Microbiology Ecology. 102: 279-289, doi: doi.org/10.1016/0378-1097(93)90210-S.

Tolhurst, T. J., Black, K. S., Shayler, S. A., Mather, S., Black, I., Baker, K., and D. M. Paterson. 1999. Measuring the in situ Erosion Shear Stress of Intertidal Sediments with the Cohesive Strength Meter (CSM). Estuarine, Coastal, and Shelf Service. 49: 281-294, doi: doi.org/10.1006/ecss.1999.0512.

Topping, D. J., Rubin, D. M., Wright, S. A., and T. S. Melis. 2011. Field evaluation of the error arising from inadequate time averaging in the standard use of depth-integrating suspended-sediment samplers, U.S. Geological Survey, Reston, VA, 95.

Torfs, H., Mitchener, H., Huysentruyt, H., and E. Toorman. 1996. Settling and consolidation of mud/sand mixtures. Coastal Engineering. 29: 27-45, doi: 10.1016/S0378-3839(96)00013-0.

Torres, I. C., Inglett, K. S., and K. R. Reddy. 2010. Heterotrophic microbial activity in lake sediments: Effects of organic electron donors. Biogeochemistry. 104(1-3): 165-181, doi: 10.1007/s10533-010-9494-6.

Turner, T. T. 1996. Fundamentals of Hydraulic Dredging. 2nd ed. ASCE Press.

Tušer, M., Picek, T., Sajdlová, Z., Jůza, T., Muška, M., and J. Frouzová. 2017. Seasonal and Spatial Dynamics of Gas Ebullition in a Temperate Water-Storage Reservoir. Water Resources Research. 53: 8266-8276, doi: 8210.1002/2017WR020694.

U. S. Army Corps of Engineers (USACE). 1983. Dredging and dredged material disposal. EM 1110-2-5025. Washington, DC: USACE Office, Chief of Engineers.

U. S. Army Corps of Engineers (USACE). 2007. Overdepth Dredging and Characterization Depth Recommendations. WRAP Technical Notes Collection (ERDC/TN EEDP-04-37), U. S. Army Engineer Research and Development Center, Vicksburg, MS.

U.S. EPA. 1991. Handbook: Remediation of contaminated sediments. EPA/625/6-91/028. U.S. Environmental Protection Agency, Office of Water, Washington, DC.

U.S. EPA. 1994. Remediation guidance document. EPA 905-R94-003. Assessment and Remediation of Contaminated Sediments Program. Chicago, Il: EPA Great Lakes National Program Office.

U.S. EPA. 2001. Methods for Collection, Storage and Manipulation of Sediments for Chemical and Toxicological Analyses: Technical Manual. EPA 823-B-01-002. U.S. Environmental Protection Agency, Office of Water, Washington, DC.

US Geological Survey. 2004. Chesapeake Bay river input monitoring program. In, US Geological Survey.

Van Eeten, M. J. C. 2011. Radio-Frequency Slurry-Density Measurements for Dredging Pipelines. Ph.D. thesis. Eindhoven University of Technology.

Varadharajan, C., and H. F. Hemond. 2012. Time series analysis of high resolution ebullition fluxes from a stratified, freshwater lake. Journal of Geophysical Research: Biogeosciences. 117: G02004, doi: 10.1029/2011JG001866.

Varadharajan, C., Hermosillo, R., and H. F. Hemond. 2010. A low-cost automated trap to measure bubbling gas fluxes. Limnology and Oceanography: Methods. 8: 363-375, doi: doi.org/10.4319/lom.2010.8.363.

Verschuren, D., Tibby, J., Sabbe, K., and N. Roberts. 2000. Effects of depth, salinity, and substrate on the invertebrate community of a fluctuating tropical lake. Ecology. 81: 164-182, doi: 10.1890/0012-9658(2000)081[0164:EODSAS]2.0.CO;2.

Vörösmarty, C. J., Meybeck, M., Fekete, B., Sharma, K., Green, P., and J. P. M. Syvitski. 2003. Anthropogenic sediment retention: major global impact from registered river impoundments. Global and Planetary Change 39: 169-190, doi: doi.org/10.1016/S0921-8181(03)00023-7.

Wakeham, S. G., and E. A. Canuel. 2016. The nature of organic carbon in density-fractionated sediments in the Sacramento-San Joaquin River Delta (California). Biogeosciences. 13: 567-582, doi: doi.org/10.5194/bg-13-567-2016, 2016.

Walling, D. E. 2006. Human impact on land-oceam sediment transfer by the world's rivers. Geomorphology. 79: 192-216, doi: 10.1016/j.geomorph.2006.06.019.

Walter, K. M., Chanton, J. P., Chapin, F. S., Schuur, E. A. G., and S. A. Zimov. 2008. Methane production and bubble emissions from arctic lakes: Isotopic implications for source pathways and ages. Journal of Geophysical Research. 113: G00A08. doi: 10.1029/2007JG000569.

Wang, T., and R. Baker. 2014. Coriolis flowmeters: a review of developments over the past 20 years, and an assessment of the state of the art and likely future directions. Flow Measurement and Instrumentation. 40: 99-123, doi: doi.org/10.1016/j.flowmeasinst.2014.08.015.

Weaver, P. P. E., and P. J. Schultheiss. 1990. Current methods for obtaining, logging and splitting marine sediment cores. Marine Geophysical Research. 12: 83-100, doi: 10.1007/BF00310565.

Wenning, R. J., and C. G. Ingersoll. 2005. Use of sediment quality guidelines and related tools for the asssessment of contaminated sediments. Executive Summary of a SETAC Pellston Workshop on Use of Sediment Quality Guidelines and Related Tools for the Assessment of Contaminated Sediment, Montana, USA.

Wever, T. F., Abegg, F., Fiedler, H. M., Fechner, G., and I. H. Stender. 1998. Shallow gas in the muddy sediments of Eckernförde Bay, Germany. Continental Shelf Research. 18: 1715-1739, doi: doi.org/10.1016/S0278-4343(98)00055-7.

Wienberg, C., and A. Bartholomä. 2005. Acoustic seabed classification in a coastal environment (outer Weser Estuary, German Bight) - a new approach to monitor dredging and dredge spoil disposal. Continental Shelf Research. 25: 1143-1156, doi: doi.org/10.1016/j.csr.2004.12.015.

Wik, M., Crill, P. M., Varner, R. K., and D. Bastviken. 2013. Multiyear measurements of ebullitive methane flux from three subarctic lakes. Journal of Geophysical Research: Biogeosciences. 118(3): 1307-1321, doi: doi.org/10.1002/jgrg.20103.

Wilcock, P. R., and J. C. Crowe. 2003. Surface-based transport model for mixed-size sediment. International Journal of Hydraulic Engineering. 129(2): 120-128, doi: 10.1061/(ASCE)0733-9429(2003)129:2(120).

Wilkens, R. H., and M. D. Richardson. 1998. The influence of gas bubbles on sediment acoustic properties: In situ, laboratory, and theoretical results from Eckernförde Bay, Baltic sea. Continental Shelf Research. 18: 1859-1892, doi: doi.org/10.1016/S0278-4343(98)00061-2.

Wilkinson, J., Bodmer, P., and A. Lorke. 2019. Methane dynamics and thermal response in impoundments of the Rhine River, Germany. Science of the Total Environment. 659: 1045-1057, doi: doi.org/10.1016/j.scitotenv.2018.12.424.

Wilkinson, J., Maeck, A., Alshboul, Z., and A. Lorke. 2015. Continuous seasonal river ebullition measurements linked to sediment methane formation. Environmental Science & Technology. 49: 13121-13129, doi: 10.1021/acs.est.5b01525.

Winterwerp, J. C., and W. G. M. van Kesteren. 2004. Introduction to the physics of cohesive sediment in the marine environment. Developments in sedimentology. 56: 466.

Wright, H. E. Jr. 1980. Coring of soft lake sediments. Boreas. 9: 107-114, doi.org/10.1111/j.1502-3885.1980.tb01032.x.

Wright, H. E. Jr. 1993. Core compression. Limnology and Oceanography. 38(3): 699-70, doi: 10.4319/lo.1993.38.3.0699.

Wyatt, C., and H. Miller. 2013. The use of high pressure waterjets to improve performance of rotary cutter head dredges from the inside out. In, WJTA-IMCA Conference and Expo, Texas, USA.

Xiao, S., Yang, H., Liu, D., Zhang, C., Lei, D., Wang, Y., Peng, F., et al. 2014. Gas transfer velocities of methane and carbon dioxide in a subtropical shallow pond. Tellus B: Chemical and Physical Meteorology. 66(1), doi: 10.3402/tellusb.v66.23795.

Yahiro, T., and H. Yoshida. 1974. On the characteristics of high speed water jet in the liquid and its utilization on the induction grouting method, p. 41-63. In, Proceedings of the 2nd International symposium on jet cutting technology.

Yamaguchi, S., and S. Shimizu. 1987. Erosion due to impingement of cavitating jet. Journal of Fluids Engineering. 109(4): 442-447, doi: 10.1115/1.3242686.

Yamamoto, S., Alcauskas, J. B., and T. E. Croxier. 1976. Solubility of methane in distilled water and seawater. Journal of Chemical & Engineering Data. 21(1): 78-80, doi: 10.1021/je60068a029.

Young, R. N., and J. B. Southard. 1978. Erosion of fine-grained marine sediments: sea-floor and laboratory experiments. Geological Society of America Bulletin. 89(5): 663-672, doi: doi.org/10.1130/0016-7606(1978)89<663:EOFMSS>2.0.CO;2.

Yvon-Durocher, G., Allen, A., Bastviken, D., Conrad, R., Gudasz, C., St-Pierre, A., Duc, N., and P. del Giorgio. 2014. Methane fluxes show consistent temperature dependence across microbial to ecosystem scales. Nature. 507:4 88-91, doi: 10.1038/nature13164.

Zarfl, C., Lumsdon, A. E., Berlekamp, J., Tydecks, L., and K. Tockner. 2014. A global boom in hydropower dam construction. Aquat. Sci. 77: 161-170, doi: 10.1007/s00027-014-0377-0.

Zeikus, J. G., and M. R. Winfrey. 1976. Temperature Limitation of Methanogenesis in Aquatic Sediments. Applied and Environmental Microbiology. 31(1): 99-107.

Zhang, S., Ge, T., Zhao, M., and C. Wang. 2017. The prediction of traveling jet trenching in stiff clay based on the erosion failure mechanism. Marine Georesources & Geotechnology. 35(7), 939-945, doi: 10.1080/1064119x.2016.1261311.

Zych, K. S., and J. Osnabrugge. 2017. Non-radioactive slurry density measurement for inland dredgers. In, Proceedings of CEDA Dredging Days 2017: Sustainable Dredging - Continued Benefits, Rotterdam, Netherlands.

## Declaration

I hereby declare that this thesis entitled “Characterization and Remobilization of Sediment Deposits in Reservoirs” is the result of my own work except where otherwise indicated. It has not been submitted for any other degree at another university or scientific institution.

Cologne, July 14th 2019 _____

Yannick Dück

# Curriculum Vitae


| | |
|---|---|
| Name | Yannick Dück (née: Ratke) |
| Date of birth | 21 March 1987 |
| Place of birth | Cologne (Germany) |
| Nationality | German |
| E-Mail | yannick.dueck@posteo.de |


**Background**

| | |
|---|---|
| 08/2014 – present | PhD Student at the Laboratory for Water and Environment at Cologne University of Applied Science (Cologne, Germany) |
| 02/2012 – 08/2014 | Master of Science in Business Administration and Civil Engineering at RWTH Aachen University of Technology (Aachen, Germany)<br><br>Study focus: Hydraulic Engineering and Water Resources Management |

## Acknowledgements

[redacted]

## Author Contributions

This thesis is based on four original research articles provided in Appendix I - IV which were conceived by all of the authors. I am the lead author of all articles. The contributions of all authors are explained in the following:

**DENSE: Semicontinuous Automated, Gravimetric Measurement Device for Suspended Sediment Concentrations**

Dück, Yannick; Fahlenbock, Timo; Frings, Roy and Christian Jokiel

Conception and design: YD, TF
Data acquisition: TF
Data analysis: YD, TF
Interpretation of results: YD, TF, RF, CJ
Writing the manuscript: YD, TF
Revising the manuscript: RF, CJ

**A novel freeze corer for characterization of methane bubbles and assessment of coring disturbances**

Dück, Yannick; Liu, Liu; Lorke, Andreas; Ostrovsky, Ilia; Katsman, Regina and Christian Jokiel

Designing of the freeze corer: YD, LL, AL, CJ
Data acquisition: YD, LL, RK
Data analysis: YD, LL
Interpretation of results: YD, LL
Writing the manuscript: YD, LL
Revising the manuscript: AL, LL, CJ, IO, RK

**Experimental Investigation of Impinged, Oblique Submerged Cavitating Water Jets with Pressure Measurement Sensing**

Dück, Yannick; Bolsenkötter, Laura; Lorke, Andreas and Christian Jokiel

Conception and design: YD
Data acquisition: YD
Data analysis: YD, LB
Interpretation of results: YD, LB, AL, CJ
Writing the manuscript: YD, LB
Revising the manuscript: LB, AL, CJ

**Laboratory and Field Investigations on Freeze and Gravity Core Sampling and Assessment of Coring Disturbances with Implications on Gas Bubble Characterization**

Conception and design: YD
Data acquisition: YD, JG
Data analysis: YD
Interpretation of results: YD, AL, CJ, JG
Writing the manuscript: YD
Revising the manuscript: AL, CJ

Yannick Dück (YD); Liu Liu (LL); Andreas Lorke (AL); Ilia Ostrovsky (IO); Regina Katsman (RK); Christian Jokiel (CJ); Laura Bolsenkötter (LB); Roy Frings (RF); Timo Fahlenbock (TF); Johannes Gierse (JG)

# Appendix I

**DENSE: Semicontinuous Automated, Gravimetric Measurement Device for Suspended Sediment Concentrations**

Dück, Yannick[1]; Fahlenbock, Timo[1]; Frings, Roy[2] and Christian Jokiel[1]

[1] Laboratory for Water and Environment, Cologne University of Applied Science
[2] Institute of Hydraulic Engineering and Water Resources Management, RWTH Aachen University

Please click on the following link to read the publication:
https://ascelibrary.org/doi/10.1061/%28ASCE%29HY.1943-7900.0001374

# Appendix II

**A novel freeze corer for characterization of methane bubbles and assessment of coring disturbances**

Dück, Yannick[1]; Liu, Liu[2]; Lorke, Andreas[2]; Ostrovsky, Ilia[3]; Katsman, Regina[4] and Christian Jokiel[1]

[1] Laboratory for Water and Environment, Cologne University of Applied Science, Cologne, Germany
[2] University of Koblenz-Landau, Institute of Environmental Sciences, Landau, Germany
[3] Israel Oceanographic and Limnological Research, The Yigal Allon Kinneret Limnological Laboratory, Migdal, Israel
[4] University of Haifa Faculty of Natural Sciences, The Dr. Moses Strauss Department of Marine Geosciences, Haifa, Israel

Please click on the following link to read the publication:
https://aslopubs.onlinelibrary.wiley.com/doi/abs/10.1002/lom3.10315

# Appendix III

**Laboratory and Field Investigations on Freeze and Gravity Core Sampling and Assessment of Coring Disturbances with Implications on Gas Bubble Characterization**

Dück, Yannick[1]; Lorke, Andreas[2]; Jokiel, Christian[1] and Johannes Gierse[1]

[1] Laboratory for Water and Environment, Cologne University of Applied Science, Cologne, Germany
[2] University of Koblenz-Landau, Institute of Environmental Sciences, Landau, Germany

# Laboratory and Field Investigations on Freeze and Gravity Core Sampling and Assessment of Coring Disturbances with Implications on Gas Bubble Characterization

Yannick Dück,[*1] Andreas Lorke,[2] Christian Jokiel[1] and Johannes Gierse[1]

[1] Institute of Hydraulic Engineering and Water Resources Management, Cologne University of Applied Science, Cologne, Germany

[2] Institute for Environmental Sciences, University of Koblenz-Landau, Landau, Germany

[*] Correspondence: yannick.dueck@th-koeln.de

**KEYWORDS**

Freeze Coring, Coring Disturbances, Sediment Sampling, CT Scan, Gas Bubbles

**RUNNING HEAD**

Coring disturbances of a freeze coring technique

**ABSTRACT**

The quantification of greenhouse gas emissions from aquatic ecosystems requires knowledge about the spatial and temporal dynamics of free gas in sediments. Freezing the sediment in situ offers a promising method for obtaining gas-bearing sediment samples, unaffected by changes in hydrostatic pressure and sample temperature during core withdrawal and subsequent analysis. This paper presents a novel freeze coring technique to preserve the in situ stratigraphy and gas bubble characteristics. Non-destructive X-Ray computed tomography (CT) scans were used to identify and characterize coring disturbances of gravity and freeze cores associated with gassy sediment, as well as the effect of the freezing process on the gas bubble characteristics. Real-time X-Ray CT scans were conducted to visualize the progression of the freezing process. Additional experiments were conducted to determine the freezing rate to assess the probability of sediment particle/bubble migration, and gas bubble nucleation at the phase transition of pore-water to ice. The performance of the freeze coring technique was evaluated under field conditions in Olsberg and Urft Reservoir (Germany). The results

demonstrate the capability of the freeze coring technique for the preservation of gas-bearing sediments and the analysis of gas bubble distribution pattern in both reservoirs. Nevertheless, the obtained cores showed that nearly all gravity and freeze cores show some degree of coring disturbances.

## INTRODUCTION

The ability to collect sediment samples from aquatic ecosystems that retain the in situ sedimentological properties is a fundamental prerequisite in various research and engineering fields, e.g., for the accurate quantification of sedimentation rates, organic matter mineralization rates, gas fluxes and determination of contaminated sediment layers. Consequently, it is necessary to preserve both the sediment structural integrity and ambient (in situ) conditions. Many authors have questioned the validity of results obtained from ex situ sediment analyses because of the sampling bias associated with the coring device used (Baxter et al. 1981; Blomqvist 1985; Buckley et al. 1994). The lack of validation studies for sediment coring techniques in shallow coastal environments has generated assumptions as the legitimacy of employing ex situ analyses on samples obtained in this way (Mogg et al. 2017).

In recent years, aquatic ecosystems (e.g., lakes, reservoirs, rivers and coastal waters) have been recognized as an important source of the potent greenhouse gas methane ($CH_4$) (Bastviken et al. 2011). $CH_4$ is formed in aquatic sediment through anaerobic decomposition of organic matter (Martens and Berner 1974), and can be stored and released as gas bubbles. Ebullition-mediated flux is often highly variable in space and time (Varadharajan and Hemond 2012; Maeck et al. 2014; Wilkinson et al. 2015), with sediment gas storage being an important parameter for explaining these dynamics (Liu et al. 2016). In addition, experiments demonstrated that gas formation and transport in sediments can be described as a function of gas bubble shape, orientation and size distributions (Algar et al. 2011; Boudreau et al. 2005; Liu et al. 2016). To apply these experimental and theoretical findings, in situ sediment gas content and bubble size distribution need to be analyzed and validated with in situ sediment cores.

The widespread demand for sediment coring has resulted in the development of a large variety of different sampling techniques in the last decades. Comparative assessments of coring techniques and how well they preserve the in situ conditions are limited of soft-bottom sediments (e.g. Blomqvist 1991; Environmental Protection Agency 1991; Chant and Cornett 1991). Those studies showed that sediment core sampling techniques, extraction, transport storage and specimen transportation are subject to various types of coring disturbances and therefore may not always represent the in situ sediment characteristics.

There is a special problem associated sampling of with gas-bearing sediment due to the change in hydrostatic pressure and sample temperature upon the sediment sample brought to the surface from a depth of several meters. The formation of free gas can occur over a few hours after the cores were taken due to the rise in temperature (the lake bottom is usually colder than the temperature at the surface of the lake or in the transportation vehicle), causing reduction in methane solubility (Lane and Taffs 2002) and resulting in an increase in gas production. None of traditional tube coring techniques (e.g., gravity or vibra corers) can take intact cores without causing significant disturbances to gas-bearing sediment and they are not applicable for collecting water-saturated sediment, if cohesion is low where the sample liquefies and can be lost during core recovery (Strasser et al. 2015).

The drawback of depressurization can be avoided by preserving in situ hydrostatic pressure. Pressure corers have been developed for characterizing gas-bearing sediment in Eckernförde Bay, Germany (Abegg and Anderson 1997). The in situ hydrostatic pressure was preserved by capping a pressure tight aluminum transfer chamber on the seabed floor with the help of divers. However, the application of pressure cores obtained by divers is limited to shallow depths (Abegg and Anderson 1997). Various pressure corers have been developed and deployed in marine environments, such as the Pressure Coring Barrel developed by the Deep Sea Drilling Project and the Pressure Coring Sampler developed by the Ocean Drilling Program (Li et al. 2016). Such pressure corer requires expertise and a proper platform to operate, which makes sampling complex and expensive.

As an alternative technique, freeze coring has been introduced to take sediment cores for the collection and detailed stratigraphic analysis, even if they have a low cohesion (Lisle 1989).

When taking freeze cores, sediment is frozen to the surface of the sampler, which is filled with a coolant such as dry ice (preferably mixed with ethanol) or liquid nitrogen (Pachur et al. 1984). In principle, this preserves sediment gas bubbles in frozen cores under in situ hydrostatic pressure and therefore prevents the sudden degassing of bubbles (Verschuren 2000). To our knowledge, no previous research has investigated the possibility of freeze coring for obtaining gas-bearing sediment and the determination of the different types and extent of coring disturbances between in situ frozen and unfrozen sediment samples for gas bubble analysis. However, even though freeze coring has been introduced as an alternative method for taking gas-bearing sediment cores, most of the previous studies did not investigate the effect of the freezing process on the sediment sample. Little is known about how and to what extent the structural integrity of the sediment, the gas content and bubble distribution is affected by freezing. Most of the theories and studies on the physical effects of freezing are focused on soil and pure water which may only be transferable to a limited extent to water-saturated or gassy sediments. Major conceptual frameworks were provided by Halde (1980) and Vesilind and Martel (1990), who reported that a slow freezing rate rejects particle by the moving ice-water interface, whereas a high freezing rate traps particle into the developing ice layer. Carte (1961) showed that air bubbles in ice could form from air originally dissolved in water before freezing.

In this paper, we analyzed X-ray CT scan images, which offers the possibility of a wide range of geological investigations and provides non-destructive three-dimensional visualization and characterization (Ketcham and Carlson 2001) of coring disturbances and gas bubbles. Additionally, for the first time spectral X-ray CT scans of freeze core samples were conducted, which allowed us to determine the effective atomic number ($Z_{eff}$) of each voxel within the core. Given that *in situ* stratigraphy dimensions are generally unavailable for comparison of recovered cores, comparative laboratory experiments of freeze and gravity cores with different sediment parameters, stratigraphy, and constant/inconstant penetration velocity were conducted. The experiments additionally included the measurement of the freezing rate and real-time CT scans to examine the freezing process of this coring technique with sediments, differing in grain size distribution (GSD), water content (WC) and organic matter (OM). Field

investigations were conducted to test the applicability and suitability of the freeze corer to characterize gas bubbles, and to determine the coring disturbances in comparison to those obtained in the laboratory studies.

This paper aims to provide more thorough documentation of the causes, effects, and extents of physical coring disturbances of a novel freeze coring technique, and to introduce certain disturbed structures that are rarely previously described in the literature. We first review different types of coring disturbances, before we describe the methods used for laboratory and field investigations. Examples of coring disturbances are given from selected laboratory and field cores. In particular, we focus on coring disturbances due to the freezing process of the sediment in situ and on the analysis of gas bubbles characteristics. Finally, we illustrate and discuss the scientific importance of the identification of coring disturbances, and we outline guidelines for the appropriate use of freeze or gravity corer under specific boundary conditions.

## CORING DISTURBANCES

In this section, we briefly review the most common causes and effects of coring disturbances, from descending the corer to the sediment surface to the handling of the core in the laboratory (Fig. 1).

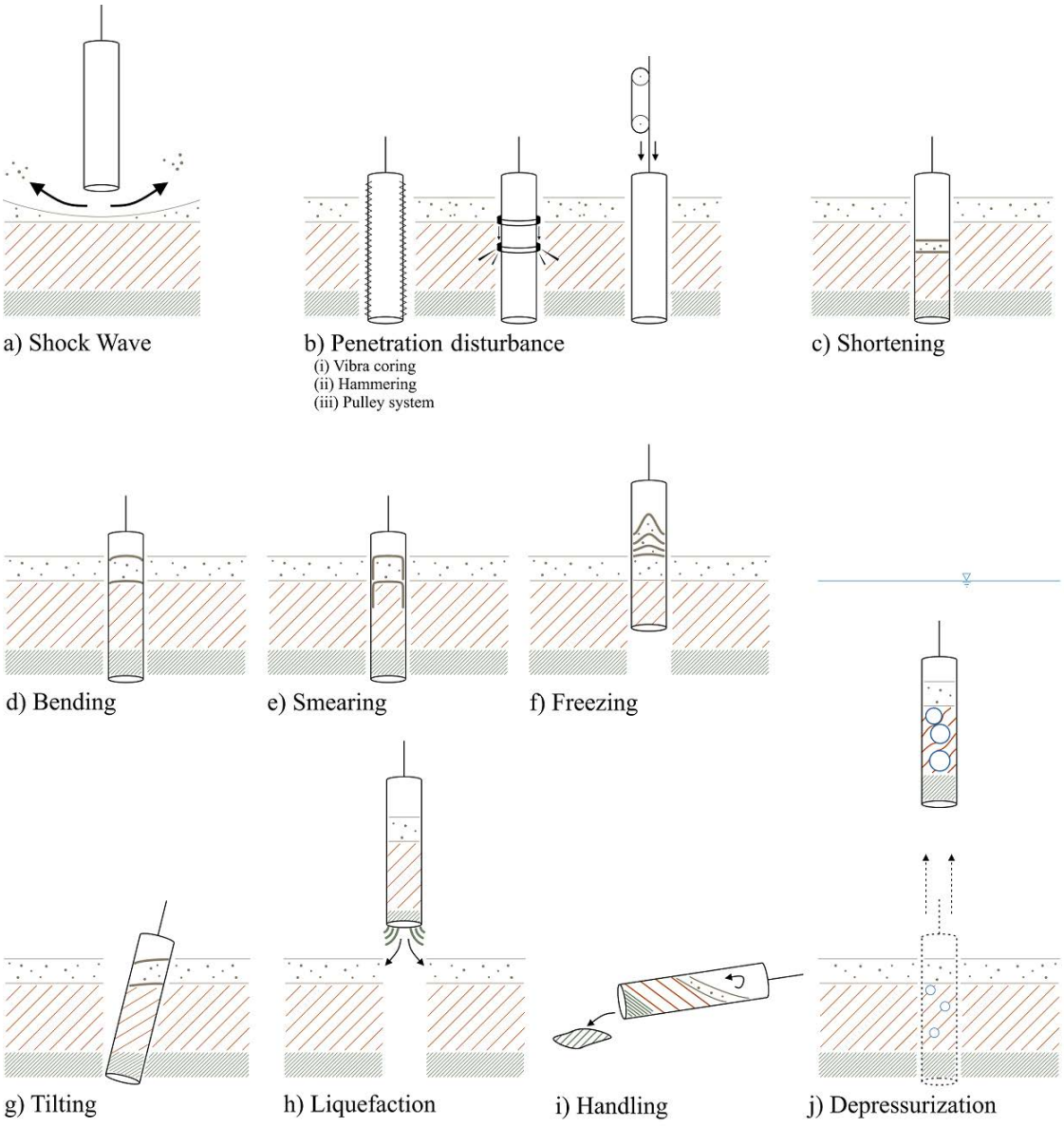


**Figure 1.** Schematic presentation of typical coring disturbances.

### *a) Shock Wave*

The corer can create a hydraulic shock wave (bow wave) in front of the orifice of the cutting-edge when the unimpeded water flow through the corer is restricted (Fig. 1 a). This shock wave

can wash away fluffy surficial sediment before the corer reaches the sediment-water interface. This source of error has been reported for open barrel gravity corers (McIntyre 1971; Elmgren 1973; Baxter et al. 1981; Jensen 1983; Leonard 1990) and piston corers (McCoy and von Herzen 1971; McCoy 1972, 1980; Stowe and Aksu 1978). Unimpeded water flow through the corer during descent and a careful lowering to the last few centimeters to minimize the dispersion of fine material due to a sample-induced shock wave is required (McIntyre 1971; Glew et al. 2001; Taft and Jones 2001).

***b) Penetration Disturbance***

Vibra coring uses (Fig. 1 b) high frequency - low amplitude corer vibration that liquefies a thin layer of water-saturated sediment at the core tube that, leading to a loss of sediment strengths and eases penetration (Glew et al. 2001). It is preferred for fine-grained sediment like sand, silt, and clay with average core compaction of over 40% (Smith 1992, 1998)

Gravity corers are inserted into the sediment using a hammering method (Fig. 1 b), whereby a ram or hydrostatic motor is used to lift and release a weight to hammer the corer into the sediment (Wang et al. 2011). Core shortening is a known problem of this method and its impact varies with the penetration velocity and sediment type (Parker and Sills, 1989).

By pulling a rope attached to the supporting stand (tripod) of the corer, the corer is constantly pulled into the sediment (Fig. 1 b). By using a tripod, the penetration velocity can be adjusted, since a slow penetration velocity reduces sediment deformation and compaction (Martin and Miller 1982; Wright 1993; Lane and Taffs 2002).

***c) Shortening***

Shortening is the reduction of the sediment core length compared to the actual length (Skinner and McCave 2003) by physical compaction, sediment thinning, sediment bypassing (Morton and White 1997) and/or partial loss of the sample during withdrawal of the corer from the sediment (Fig. 1 c). Core shortening occurs mainly due to friction between the sediment and inner tube wall of the corer. The pressure in the corer and the inner wall friction rises, as the sediment gradually becomes more compact. When the internal resistance of the sediment

inside the core is equal to the force of the sediment being penetrated, the sediment in front of the corer is forced aside and no material enters the tube. The corer begins to act partly as a plough and core shortening begins. It is also possible, that the plough force results in a down bending and stretching of layers, until they are finally cut, and the sediment enters the corer. Therefore, the effect of core compression must be extended by the possibility that sediment is pushed out of the way due to sampling resistance based on a high pressure inside the corer (Glew et al. 2001). Shortening typically occurs, if soft sediment is overlaid by stiffer matter, however, the former is more thinned than the latter (e.g. Piggot 1941; Hvorslev 1949; Hongve and Erlandsen 1979; Weaver and Schultheiss 1983). The soft sediments are driven aside as the core barrel containing high-density sediment penetrates deeper (Morton and White 1997). Clayey and silty sediments are compressed more than light, unconsolidated, organic sediments and a large core diameter minimizes shortening (Blomqvist 1991; Chaney and Almagor 2015).

Core shortening results in an altered representation of the sediment layers (Blomqvist 1985; Piggot 1941; Weaver and Schultheiss 1983). Studies have shown that core shortening patterns can be uniform (Emery and Dietz 1941; Richards and Keller 1961; Emery and Hülsemann 1964; Lebel et al. 1982), progressive over depth (Richards and Keller 1961; Weaver and Schultheiss 1983) or a mixture of different patterns (Parker and Sills 1990).

The subsequent analysis of sediment core data requires an adjustment of the core stratigraphy to remove the effects of shortening with respect to their natural position in order to avoid any over- or under-estimation. This coring disturbance produces a bias in samples, which is difficult to detect (Kallstenius 1958) and may severely bias the sampling (Emery and Dietz 1941; Piggot 1941; Hvorslev 1949; Richards and Keller 1961; Emery and Hülsemann 1964; Hongve and Erlandsen 1979; Lebel et al. 1982; Weaver and Schultheiss 1983; Blomqvist 1985; Blomqvist 1991). For example, sedimentation rates calculated from shortened cores maybe two to three times lower than rates calculated from unshortened cores (Nevissi et al. 1989; Crusius and Anderson 1991).

***d) Bending***

Bending is the result of coring-induced shear between the sediment and the corer (Skinner and McCave 2003) and/or the force of the partly filled corer, which is down-bending sediment layers (Fig. 1 d) ahead of the end of the cutting-edge as it penetrates the sediment (Emery and Dietz 1941). Kegwin et al. (1998) described this effect as a function of core barrel radius and degree of deformation. Bending can be recognized as downward dredging of a layer near to the core liner and the sediment.

***e) Smearing***

Smearing is the frictional downward dragging of overlying sediment material along the core tube wall into deeper layers (Fig. 1 e). It can occur when the tube penetrates the sediments and/or when the core is extruded from the core liner during sectioning in the lab. The risk of smearing increases with decreasing tube diameters (Nies et al. 1990).

Smearing may change the depth gradients of materials in the core from those present under in situ conditions (Chant and Cornett 1991), and, particularly in studies dealing with trace components, might also create a contamination problem (e.g. Stowe and Aksu 1978; Harvey et al. 1987; Chant and Cornett 1990). Smearing can be recognized as a smear of sediment along the inside of and near to the core barrel, whereas the flowage along the core liner is likely over long sections of the core.

***f) Freezing***

The sediment is being subjected to changes in physical properties, like density, pore space, shear strength, thermal properties and chemical properties of the particles and pore water due to the freezing process (Fig. 1 f). The majority of those effects are described in the literature for soil freezing under natural conditions or sludge freeze for the dewatering in the process industry. Due to this lack in literature, those phenomenon needs to be transferred, as far as the results are transferable, to sediment freezing.

During the phase transition, the density of water decreases rapidly, and the volume expands by about 9%. It is followed by a continuous decrease of volume until the sample achieves -

70°C; below this temperature, all sediment is frozen (Tsychovich 1975). Rutledge and Fleeger (1988) have shown a distortion of the vertical stratigraphy, whereas the extent and shape of distortion depend on the freezing rate, which is related to the chosen coolant. This effect can accumulate to a certain extent in vertical direction. Besides the freezing rate, it can be reasonably assumed that the vertical distortion of the sediment layer depends on various ambient conditions (e.g. hydrostatic pressure, water temperature, etc.) and sediment characteristics (WC, OM, GSD, etc.).

The ice crystal formation can be accomplished with the separation of particles and/or gas bubbles. Due to the compressibility and temperature-dependent volume change of gases, the gas volume can also change during the freezing process. Furthermore, Carte (1961) observed the nucleation and entrapment of gas bubbles by an advancing ice-water interface, since gas solubility in ice is at least two orders of magnitude smaller than in water (Killawee et al. 1998). Therefore, bubbles may form due to nucleation at the water-ice boundary when the water at the interface becomes supersaturated. Bubble concentration and sizes were found to be depending on the rate of freezing (Carte 1961).

***g) Tilting***

When the corer hits the lake-bed, vessel movement may tilt the corer (Fig. 1 g) and result in redistribution and resuspension of enclosed sediment as well as the loss of material (Blomqvist 1985, 1991). The sampler also may sink deeper into the sediment than its length and over-penetrate the sediment (e.g. Flannagan 1970; Blomqvist 1991). Therefore, a supporting stand, favorable weather conditions, high ship stability, and anchoring before sampling reduce the probability of this disturbance type.

***h) Liquefaction / Deformation due to core recovery and transport on deck***

Conventional sampling techniques to extract water-saturated sands, as well as unconsolidated silts and clays fail, if the cohesion of the sediment is low, resulting in a (partial) liquefaction of the sample (Fig. 1 h) (Schreiner and Kreysing 2013; Strasser et al. 2015). During corer recovery, the sample is exposed to pressure variations due to suction, while

pulling the corer out of the sediment and decreasing pressure while lifting the corer to the water surface (Blomqvist 1985). An acceleration of the corer may result in a resuspension leading to (partial) leaking out of the sample (Blomqvist 1991). Even a small amount of gas may cause large dissipation rates and increase the risk of momentary liquefaction in the soil considerably (Sumer and Fredsøe 2002).

***i) Sample Handling***

When the sediment core is pushed out of the corer for subsample processing, the sediment may be disturbed by forces and friction during extrusion and moisture changes (Fig. 1 i) (Hopper 1992). The force required to extrude the sample from the sampling tube is larger than the unconfined strength of clayey silt (e.g. Arman and McManis 1976), which can result in smearing or bending of the sediment layer. Tumbling and horizontal storage of the core on deck may also increase disturbances in the sample (e.g. mixing).

***j) Depressurization / Change in temperature***

The sediment core structure obtained with non-pressurized sampling techniques can be deformed by gas bubble expansion and ebullition upon lifting the corer through the water column (Fig. 1 j) (Wright 1993; Scandella et al. 2011). The change in hydrostatic pressure and sample temperature on the sediment sample being brought from the lake-bed to the surface causes a dissolution of gases, causes the formation of gas bubbles which rose to the top of the core and destroying the stratigraphy (Saarnisto et al. 1977; Rymer and Neale 1981; Swain 1978; Lane and Taffs 2002). Even hours after the core arrives was retrieved, an increase in gas production, expansion and subsequent escape of gas from sediment can occur (Flood et al. 1995). Wever et al. (1998) demonstrated that sediment gas content can increase by six times in half an hour after 0.5 bar pressure release. A number of authors have recognized that gas bubble migration destroys the stratigraphy (Förstner et al. 1968) or postulated that degassing after core retrieval result in elongated fissures and vertical cracks (Schubel 1974; Milkert 1993). Freezing the sample may be the only way to overtime those in situ disturbances (Rymer and Neale 1981).

## METHODS

### *Corer Design*

This study was performed in two phases: a laboratory phase, which focused on the identification of the causes, types, and extents of coring disturbances, and a field phase which focused on the feasibility and applicability of the freeze coring technique with an emphasis on sampling and characterization of gas-bearing and water-saturated sediment. Both, the laboratory experiments and field investigations were conducted with the novel, custom made freeze corer with a tripod and a gravity corer with hammering action (UWITEC, Austria) (Fig. 2).

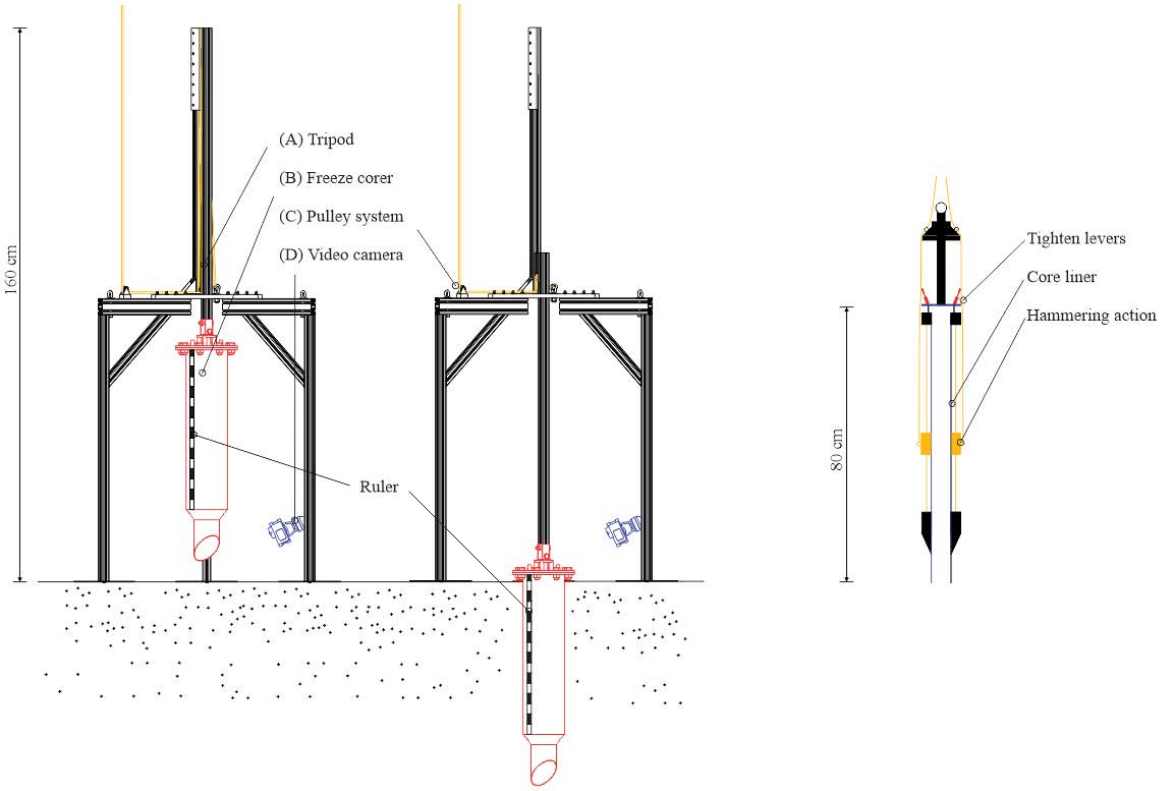


**Figure 2.** Left: Sketch of the tripod and the attached freeze corer with position before and after the penetration. The device consists of four main components: (A) tripod as a supporting frame; (B) freeze corer; (C) pulley system and (D) underwater video camera. The corer mainly consists of a (1) cutting edge; (2) a double-walled tube and a (3) corer head. (1) Cutting edge: To reduce the penetration resistance, the lower end of the corer was beveled to a 45° angle edge (inner diameter 72 mm, length 75 mm). Above the cutting edge, the tube outer diameter increases gradually from 76 to 100 mm to reduce the penetration force. The sharp cutting-edge of 0.1 mm with an edge

angle of 45° facilitates a smoother penetration of the freeze corer in contrast to the gravity corer with 1.8 mm wall thickness and a tip edge angle of 45°. (2) Double-walled tube: The double-walled tube is the container for the coolant, made of 2 mm thick stainless steel, and starts 75 mm above the cutting edge. Commercially available dry ice pellets (3 mm) and ethanol was used as coolant (temperature of approx. -78°C). The sediment core length can be up to 80 cm. The 72 mm inner diameter was chosen to allow the best ratio between minimal wall friction and short freezing time (<30 min, which was determined in this study). (3) Corer head: The corer head is a massive stainless steel flange. It is equipped with two overpressure valves and a junction to connect the corer to the tripod. The two overpressure valves mounted on the lid of the corer allow the release of gas formed during the sublimation of the dry ice. Right: Gravity Corer (Source: Uwitec) consists of a PVC core liner (80 cm long; 59 mm inner diameter) with hammering action. The penetration is controlled by its gravity and can be enhanced by hammering the corer with an attached weight into the sediment.

The newly designed freeze corer (Fig. 2) is a further development of the remote-controlled freeze corer described by Lotter et al. (1997). For a detailed description of the new corer design see Dück et al. (2019). The tripod is made of modular low-weight aluminum, which can easily be assembled and extended. All components can be transported in two cases with a total weight of 40 kg. The three bars, with stabilizing crossbars, have a length of 50 cm. The tripod is loosely tethered to a boat and unaffected by vessel motion to avoid disturbances before the corer actually enters the sediment (Hessler and Jumars 1974; Snider et al. 1984). Round plates with a diameter of 30 cm are mounted at the bottom of the tripod to prevent an over-penetration and tilting, which may cause disturbances (Flannagan 1970; Blomqvist 1991).

The corer is filled with the coolant and attached to the tripod. The tripod is lowered by a static rope into the water. To obtain the optimum position above the sediment surface and to avoid destroying the sediment structure, a low-cost underwater video camera (GoPro 4 Black: up to 4K/30 fps; waterproofed up to 40 m water depth) and an illumination system is mounted on the tripod. A coaxial cable transmits the WiFi signal under water for real-time video transmission on board of the boat. The video monitoring also allows the measurement of the penetration depth to determine the core shortening. It also allows the observation of gas bubbles release during penetration, that may bias the determination of the total gas content. After deployment on the sediment surface the corer is slowly lowered into the sediment by pulling

an additional static rope. With a 4-way pulley system, a transmission ratio of 1:4 is achieved and a precise penetration process can be facilitated. With this, a hydraulic shock wave induced by penetration process can be minimized and the risk of core shortening is reduced (Blomqvist 1991).

***Laboratory Experiments***

***a) Coring Disturbances***

Comparative laboratory experiments of the freeze and gravity corer were conducted to qualitatively and quantitatively evaluate coring disturbances under controlled conditions, where the initial sediment stratigraphy is known. Four types of homogenized sediments were used, differing in predominant GSD, OM and WC (Sand: $D_{50}$ = 325 µm, OM: 0.0%, WC: 24.8%; Silt: $D_{50}$ = 17 µm, OM: 2.4%, WC: 30.0%, and in situ sediment (see Field Investigations): Olsberg: $D_{50}$ = 65 µm, OM: 15.1%, WC: 65.0%; Urft: $D_{50}$ = 43 µm, OM: 13.6%, WC: 63.0%). Therefore, sediment was homogenized, filled into a common springform pan (inner diameter of 30 cm) and immediately frozen with dry ice and ethanol to prevent particles from settling down during the freezing process. The frozen sediment samples were stacked in the acrylic tube (Fig. 3) with an inner diameter of 30 cm and a height of 100 cm. The sediment layers were separated by thin (~1 mm) layers of fluorescent pigments (Components: Phosphorescent Pigment, Zinc sulfide, copper chloride-doped; $D_{50}$ = 21 µm; $\rho$ = 4100 kg $m^{-3}$) in different colors to allow the subsequent assignment of the specific layers during the analysis. The quantity of pigments was adequate to ensure a minimum influence on the mechanical properties of the sediment. After the sediment layers were stacked, the height of each layer was documented. The samples were thawed at room temperature (~20°C) and the height of each layer was measured again to quantify settlements.

Twelve sets of duplicate experiments - to ensure reproducible results - with different sediment characteristics (GSD, WC, and OM), constant/inconstant penetration velocity, and with/without ice crust inside the freeze corer (an ice crust is usually formed while the corer is lowered through the water column to the sediment surface) were conducted. A constant

penetration velocity (10 cm/s) was attained by using an electrical lift truck, even though the penetration force increases with penetration depth due to increased friction. An inconstant penetration velocity (~0.6-0.12 cm/s) was facilitated by using the tripod (as used in the field investigations). Since the penetration velocity of the gravity corer cannot be controlled in situ, it was not varied in the laboratory tests. The specifications of each experiment are summarized in Table 1. To exclude, that the diameter of the acrylic tube had an influence on the results, we conducted a preliminary examination (Set 0: *FC5_Silt_Tripod_0*; e.g. *FC5_Silt_Tripod_0* is the nomenclature for *Freeze Corer*, Experiment No. *5*, *Silt Sediment*, *Tripod* as inconstant penetration velocity and an ice crust of *0* mm), with a diameter of 50 cm. The preliminary examination has revealed that the diameter has no effect on coring disturbances.

**Table 1.** Main specifications of the laboratory experiments. $D_{50}$ denotes the median grain diameter, FC refer to freezer corer and GC to gravity corer. Set 0 is the preliminary experiment.

| ID | No. of experiments | Corer type | Sediment | $D_{50}$ (µm) | Water content (%) | Organic matter (%) | Penetration velocity (cm/s) | Sample diameter (cm) | Average shortening (%) |
|---|---|---|---|---|---|---|---|---|---|
| Set 0 | 1 | FC | Silt | 17 | 25.5 | 2.4 | 0.10 | 50 | 21 |
| Set 1 | 4 | FC | Silt | 17 | 28.3 ± 0.4 | 2.4 | 0.10 | 30 | 6 |
| Set 2 | 3 | GC | Silt | 17 | 26.8 ± 1.6 | 2.4 | 0.10 | 30 | 30 |
| Set 4 | 3 | FC | Silt | 17 | 27.6 ± 2.5 | 2.4 | 0.11 | 30 | 3 |
| Set 5 | 2 | FC | Silt | 17 | 28.6 ± 0.1 | 2.4 | 0.11 | 30 | 24 |
| Set 6 | 2 | FC | Silt/Sand | 17/325 | 27.0 ± 0.4 | 2.4 | 0.10 | 30 | 3 |
| Set 7 | 2 | FC | Silt/Sand | 17/325 | 29.0 ± 0.4 | 2.4 | 0.09 | 30 | 11 |
| Set 8 | 2 | FC | Silt/Sand | 17/325 | 27.8 ± 0.9 | 2.4 | 0.12 | 30 | 8 |
| Set 9 | 2 | GC | Silt/Sand | 17/325 | 26.6 ± 1.1 | 2.4 | 0.10 | 30 | 22 |
| Set 10 | 2 | FC | Olsberg | 17 | 65.4 ± 0.3 | 14.2 | 0.10 | 30 | 38 |
| Set 11 | 2 | FC | Olsberg | 17 | 69.1 ± 0.1 | 14.2 | 0.12 | 30 | 45 |
| Set 12 | 2 | FC | Olsberg | 17 | 63.0 ± 1.8 | 14.2 | 0.06 | 30 | 3 |
| Set 13 | 2 | GC | Olsberg | 17 | 66.7 ± 0.6 | 14.2 | 0.10 | 30 | 37 |

### *b) Freezing Rate*

Freezing rate experiments were conducted for practical reasons, to determine the time period needed for complete freezing of the sediment in field applications. Furthermore, the freezing

rate can give some indication on whether the freezing process may result in particle and bubble migration, as well as bubble nucleation. Freezing rate is defined as the speed at which the water-ice interface migrates radially through the sediment column (°C/min). For the experiments artificially sediments (*Silt* and *Sand Sediment*) and sediments taken from two reservoirs (*Olsberg* and *Urft Sediment*) were used. Additionally, tap water was tested and served as a reference sample. Duplicates of each experiment were done, to ensure reproducible results. Sediment were filled into a double-walled stainless steel tube with the freeze corer's dimensions. Sediment temperature was measured and logged with a temperature immersion sensor (Voltcraft DL-141 TH2k temperature logger, measuring range: -100°C to +1000°C; accuracy: 1°C), in the center and half the radius (R1/2) between the center of the core and the tube wall. All experiments started at ambient room temperature of approx. 20°C.

***c) Real-Time CT Scans***

Real-time CT scans (Philips IQon-Spectral CT, 120 kV; voxel dimension 0.126 $mm^3$) has been conducted to visualize the effect of freezing on the sediment structure (e.g. expansion of water, sediment particle and bubble migration). Real-time CT scans were obtained at a 10 s time interval. Samples were filled in graphite tubes (height: 250 mm; inner diameter: 75 mm; thickness: 2 mm) with similar dimensions of the freeze corer, surrounded by a coolant of dry ice pellets (3 mm) and ethanol. Graphite tubes (thermal conductivity $\lambda_{graphite\ tube}$: 119-165 W $m^{-1}$ $K^{-1}$) were used, since metallic materials ($\lambda_{metal}$: 15-58 W $m^{-1}$ $K^{-1}$) cause severe artifacts in X-ray CT scans. Plastic material ($\lambda_{plastic}$: < 0.5 W $m^{-1}$ $K^{-1}$) could not be used, as the thermal conductivity is significantly smaller than of the freeze corer (V2A stainless steel, $\lambda_{V2A}$: 21 W $m^{-1}$ $K^{-1}$).

***Field Investigations***

Sediment cores were obtained at Urft Reservoir (50°36'8''N, 6°25'8''O; Germany) in late August 2017 and at Olsberg Reservoir (51°20'54''N,8°29'17''O; Germany) in September 2017 (Fig. 3). All coring work was conducted aboard a floating platform, which was anchored at the coring position, using a three-point anchoring system.

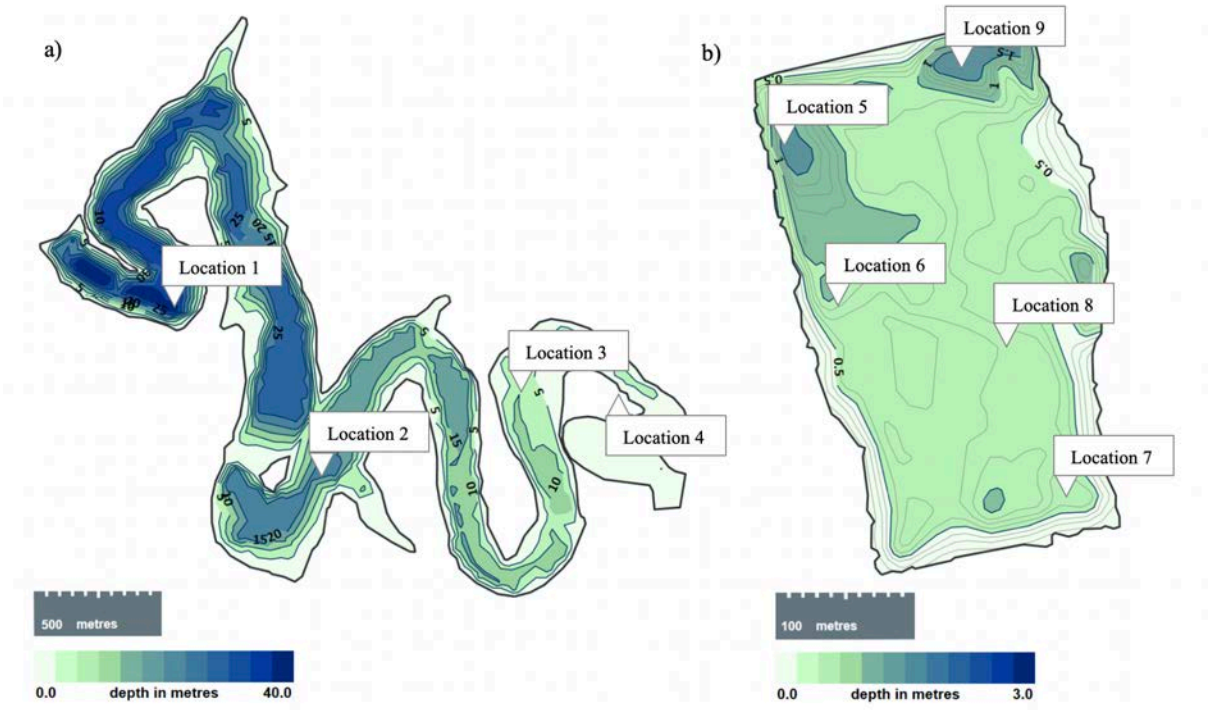


**Figure 3.** Bathymetry of Urft (a) and Olsberg (b) Reservoir. The sampling locations are marked on the map. The nomenclature for the field cores is for example: *Urft_GC1(frozen)_Hammering_0* is the nomenclature for *Gravity Core* (which has been frozen after the core was retrieved on deck), Sampling location *1*, *Hammering* was used for the penetration process, and no ice crust exists (*0* mm).

At Urft Reservoir, four sampling locations along the thalweg from deep-water to shallow depths were chosen, to cover a gradient of hydrostatic pressure, GSD and OM (see Table S1 for details). A pair of gravity cores (considered as duplicates) were taken some meters distant from the freeze cores (sampling location 1-3). After retrieving the gravity cores on deck, one core was immediately frozen with dry ice pellets and ethanol, and the other core was capped with a rubber bung and transferred to dark storage. This allows the identification of the freezing process related disturbances on the gas bubble structure with the same sampling technique. At sampling location 4, no gravity core could be obtained due to the high water-saturation of the sediment, resulting in liquefaction of the sample.

Five freeze and five gravity cores were sampled at Olsberg Reservoir. Sampling locations have been selected on the results of previous grab samples, which have shown a different spatial distribution of GSD, OM and ρ within the reservoir.

### *Assessment*

### *a) Core Preparation and Conditioning*

All sediment cores were X-Ray CT scanned after sampling in a local hospital. Additional X-Ray Spectral CT scans of the freeze cores were conducted five months after sampling due to the limited temporal availability of this scanner (there exists only one X-Ray Spectral CT scanner in Germany). Due to this large time difference between sampling and scan, the gravity cores could not be scanned, as an increase in bacterial production probably produce additional gas bubble and therefore causes a bias of the gas content. The core processing is shown in Figure 4.

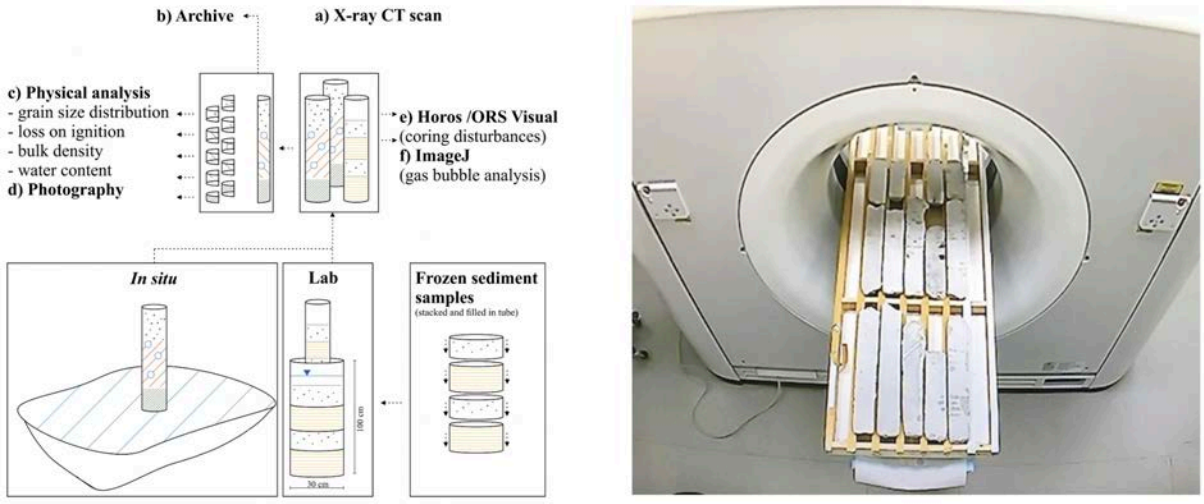


**Figure 4.** Right: Philips IQon-Spectral X-ray CT scanner with scanned freeze cores. Left: Schematic representation of the experimental procedure of the field and laboratory investigations: Cores were X-ray CT scanned (a) with a common CT scanner (Siemens AS, 120 kV) and with an X-ray Spectral CT scanner (Philips IQon-Spectral CT, 120 kV). The CT scans were analyzed with Horos, ORS Visual (e) and gas bubble were visualized with ImageJ (f). After scanning, the cores were split lengthwise with a circular saw into an archive (b) and a working half. The archive half was prepared for photography imaging (d) under natural and UV light (for visualization of the fluorescent pigment layer), and then the extent of vertical displacement was measured. The archive halves were inspected visually with a ZeissStemi SV8 microscope and an attached CCD-camera (Pentax K2). The working halves (c) were defrosted and used for the physical analysis of the GSD, WC, OM, and wet bulk density (ρ).

***b) X-Ray CT Data Acquisition***

The radiodensity for each voxel is commonly reported using the Hounsfield scale (Rogasik et al. 2003). The Hounsfield unit (HU) is calibrated using the absorption coefficient of distilled water (0 HU) and air (-1000 HU). A single energy CT scanner can only reveal the distribution of the linear attenuation coefficient (density), while the spectral CT scanner can represent the distribution of density along with the effective atomic number ($Z_{eff}$) of each voxel (Iovea et al. 2005). The spectral X-Ray CT scanner (Fig. 4) in this study uses one X-ray source and two stacked detectors, rotating around the scanned object which moves longitudinally and provides a sequence of consecutive scan slices, imaging the entire soil sample volume (Katcham and Carlson 2001). The two radiation detectors allow the detection of X-ray photons with a low and high level of energy. The differentiation enables the detection of $Z_{eff}$. This allows a determination between water, organic and inorganic material. $Z_{eff}$, is the average atomic number of the elements inside the voxel like the HU values.

***d) X-Ray CT Data Treatment***

Analyses and visualization of the X-ray CT data were conducted with Horos (Horosproject.org) and ORS Visual Lite software (Object Research Systems Inc.). For a qualitative description and measurement of the horizontal and vertical extension of the coring disturbances, and to visualize and analyze the bubble distribution in the sediment cores, a threshold technique, based on the HU and $Z_{eff}$ values, was used. The material in the cores was classified into three categories:

"gas bubbles" – gathered all HU and $Z_{eff}$ values associated to gas bubbles. Gas bubble HU values range from -1000 to -500, $Z_{eff}$ is <5.

"ice" – represents all kinds of frozen water. To account for the ice thresholds, calibration samples of different types (water was frozen at different freezing rates) and temperatures were used. Ice HU values ranged from -281 to 167. The ice calibration samples revealed a $Z_{eff}$ value of 7.7.

"sediment" – represents all kinds of solid material, ranging from highly organic to inorganic material. The sediment HU ranges from 167 to 3071. $Z_{eff}$ scans clearly reveal the presence of different types of sediments. The corresponding numerical values of $Z_{eff}$, lies between 7.7 (water) and 16.8 (pure quartz), confirming the grain size distribution as well as the mineralogical composition of sediments.

Bubble size ($D_{eq}$: mean equivalent sphere diameter) distribution and volumetric gas content ($\theta$) in the sediment cores of Olsberg and Urft Reservoir were analyzed using ImageJ. Gas bubbles were segmented in accordance with the intensity distribution of binary images by calculating the fraction of black area on each slice. A constant HU threshold for gas bubbles (-1000 to -500) was chosen for all cores. MorphoLibJ (ImageJ plugin) was used for morphological separation for the CT images of the binary images. Measurement of the 3D gas bubbles is facilitated by counting the number of voxels that constitute it, weighted by the volume of each individual voxel. 3D visualization of gas bubbles was created using the ImageJ 3D volume viewer.

***Evaluation of Coring Disturbances***

The vertical cross-sectional X-ray CT images were used to measure the sediment displacement from the initial to the post coring location. The distance between the initial sediment layer and the maximum vertical position after the coring is the *Height of Disturbance* (*HoD*) (Fig. S47). Based on the assumption that the sediment is generally horizontally layered, the difference in length of the interfacial layer in the disturbed core to the initial horizontal length of the undisturbed core was defined as the *Width of Disturbance* (*WoD*). The percentage of the number of layers affected by coring disturbance is the *Disturbance Occurrence Frequency* (*DOF*). In field cores, especially in gravity cores, the *DOF* could not be determined for all cores, because the lack of stratigraphic features.

## RESULTS AND DISCUSSION

### *Freezing Rate*

The freezing rate experiments revealed clear differences between the temperature dynamics during freezing of the samples, particularly for different WC (Fig. 5). This temporal difference might be due to the thermal conduction differences among the corer ($\lambda_{V2A}$: 21 W $m^{-1}$ $K^{-1}$) and the non-frozen sediment ($\lambda_{water}$: 0.6 W $m^{-1}$ $K^{-1}$) at the transition from the corer to the sediment. The pore water does not start to crystallize until the temperature drops to the temperature of spontaneous nucleation, which is usually a few degrees below the melting point of ice. Initially, the water is in a metastable equilibrium state. At this state, the free water (water that moves under gravity) between the particles freezes and bounds particles. This causes a release of latent heat during ice formation, resulting in a rise in temperature. After the majority of free water is frozen, bound water (unfrozen water film on the sediment particles) freezes and the sediment particles start to cool down. The increase of the thermal conductivity after the phase transition from water to ice ($\lambda_{ice}$: 2.3 W $m^{-1}$ $K^{-1}$) results in an acceleration of the freezing process. This effect can be observed at the phase transition, where the negative gradient of the curve increases for all samples (Fig. 5). The slope of the curves is related to the (bound) water content. The smaller the particles, the higher is the specific surface area and therefore a higher amount of unfrozen water can exist at temperature below the freezing point, which increases the time until the sample is completely frozen. This effect can be shown exemplarily in the temperature profile of *Olsberg Sediment* and *Urft Sediment* (WC: 72% and 69%), which have a significant higher WC than *Silt/Sand Sediment* (WC: 27% and 28%). Other parameters (e.g. salinity, mineralogy) may also influence the freezing time. However, the number of variations within the sediment parameters in this study is too small to draw a clear conclusion of the relevant parameter and to separate the effects of individual parameters and should be investigated in future studies.

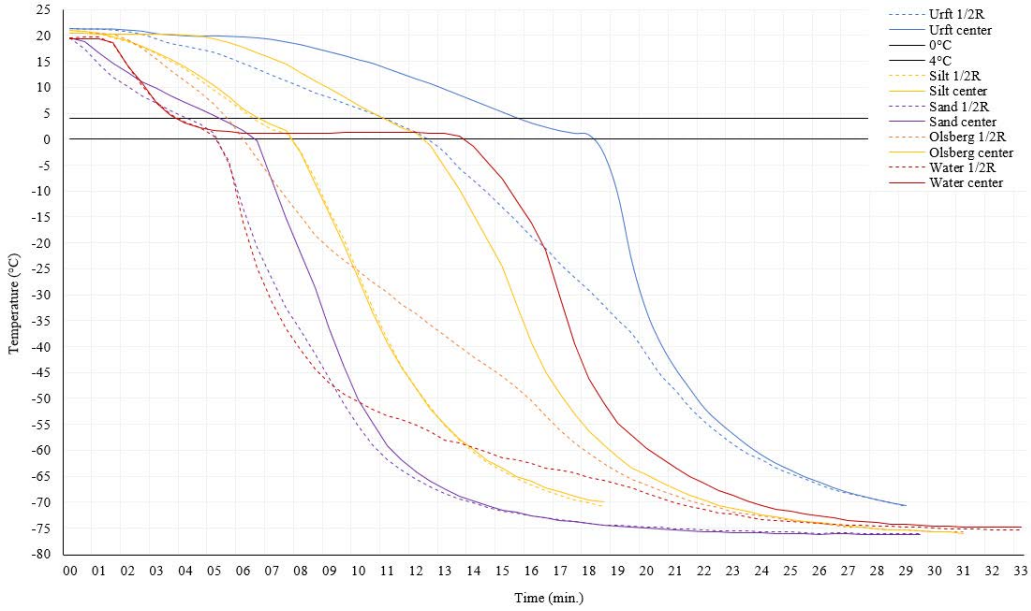


**Figure 5.** Time series of sediment temperature during freezing of *Silt Sediment*, *Sand Sediment*, *Olsberg Sediment* and *Urft Sediments*, as well as tap water as a reference. The temperature was measured in the center of the core (solid lines) and at a radial distance of 18 mm from the core center (R1/2, dotted lines). The time needed to cool down the sample from 0 to -70°C varied from 7:36 min for *Sand Sediment* to 16:00 min for *Urft Sediment*. The freezing rates of all samples varied from -14.8°C/min (R1/2) to -22.6°C/min (center). *Urft Sediment* has shown the slowest freezing rate (-0.6°C/min) during liquid state, and also the fastest freezing rate (22.6°C/min) in the center after phase transition from water to ice. After phase transition, the freezing rate of all samples increased. The higher the WC, the slower the freezing rate. A surprising result was, that the time difference between the R1/2 and center of pure water was highest of all samples.

The freezing rate results provide information about the time, which is required to entirely freeze the sediment samples under in situ conditions, to reduce the risk of a loss of the sample and to prevent the sediment structure being affected by changes in hydrostatic pressure and temperature. Furthermore, the freezing rate results allow to determine the probability of particle and bubble migration, as well as gas bubbles nucleation at the water-ice interface, when the concentration of dissolved gas reaches a critical value. Hung et al. (1997) and Lee and Hsu (1994) found that the freezing rate has a significant impact on particle migration in terms of dewatering of sludge by freeze-thaw treatment. However, particle migration is a complex phenomenon affected by many important variables besides the freezing rate, such as particle size, shape and dissolved solids concentration (Halde 1980). Due to mutual interactions

between these parameters, a “critical velocity”, where particles are rejected or entrapped at the propagating freezing front cannot be determined. It can be concluded, that the higher the freezing rate is, the lower is the risk of dislocation of sediment particle. A high freezing rate also reduces the size of gas bubbles that may form by nucleation at the water-ice interface (Carte 1961) if the ice-water interface becomes supersaturated (Boereboom et al. 2012). According to Lipp et al. (1987), the maximum radius of nucleated bubbles is < 20 µm at a freezing rate > 90 µm/s, and therefore smaller than the spatial resolution of the used X-Ray CT scanner. Generally, the higher the freezing rate, the less time is available for bubble growth after nucleation, i.e. before the bubbles become encapsulated in ice. Existing knowledge on bubble nucleation during freezing, however, is based on measurements in pure water. The effect of the sediment matrix on the nucleation microbubbles has not been investigated. This is an issue for future research to explore.

***Real-Time CT Scans***

The observations of the real-time CT scans (Fig. 6) revealed that a higher WC correlates to a slower freezing process and corroborates to the findings of the freezing rate experiments. The results have shown that *Silt Sediment* was frozen almost instantly throughout the entire horizontal cross-section, whereas a slowly propagating freezing front from the outside to the inside of the core was observed in the *Olsberg* and *Urft Sediment* cores. This slow freezing process results in a slightly change in density. This change in density is shown in the vertical cross-sectional CT scan images (Fig. 6) in a darker shade of grey in the center of the core (HU = 270), indicating a higher density after the freezing process in this region in contrast to the HU value of the entire core before freezing (HU = 245). The lateral shift in density may result from the crystallization process of the pore water. Growing ice crystals can displace solid particles and cause a rearrangement of the soil matrix (Singh and Niven 2013), which depends mainly on the freezing rate. There are three modes how sediment particles are affected by the freezing front: The freezing front pushes the sediment particles and segregate them in the last-freezing liquid or engulf particles after having pushed them over some distance or may engulf the particles instantaneously upon contact (Lipp et al. 1987). Vesiling and Martel (1990) stated

that various research studies confirmed that the smaller the solid particles, the more likely they are moved by advancing ice front, and, that the risk of particle relocation increases with decreasing freezing rate. Our findings are in accordance with those previous studies and show that an increasing WC negatively affects the uniform distribution of the density within the sediment column. Additionally, increasing WC and the related, relatively slower freezing rate increases the vertical displacement of sediment layer in an upward direction.

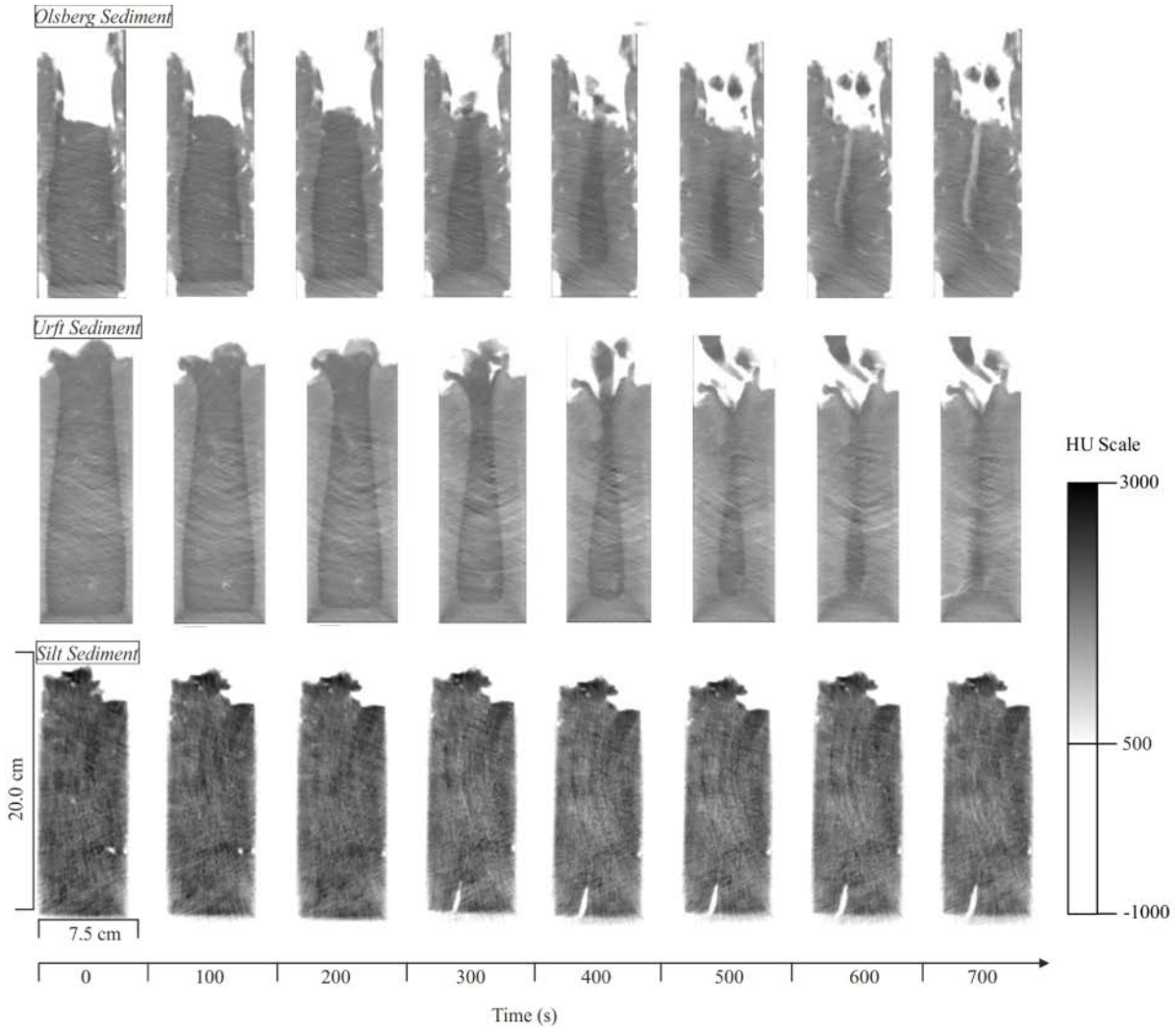


**Figure 6.** Image sequence of the real-time CT scans of *Olsberg Sediment*, *Urft Sediment* and *Silt Sediment* shown as vertical cross-sectional CT scan images. *Olsberg Sediment* and *Urft Sediment*: The continuous volume expansion due to the change in sample temperature and the rapid expansion at phase transition resulted in a vertical displacement of the sample in the center of the core. The displacement takes place in the direction of least resistance, as the sediment column freezes from the out- to the inside. Temperature of the dry ice and ethanol

mixture is lowest at the surface of the coolant between the double-walled tube, where the sublimation of dry ice takes place. This results in a conical freezing front (sharp interface in grey scale), which gradually converges from the top to the bottom of the sample. *Silt Sediment*: The sediment was completely frozen in a shorter time (t = 200 s) than *Olsberg Sediment* and *Urft Sediment* (t = 700 s). No conical shape can be seen in the images. The expansion of water caused a burst of the graphite pipe, which is shown as a crack at the lower left side of the pipe at t = 300 s).

## *Coring Disturbances*

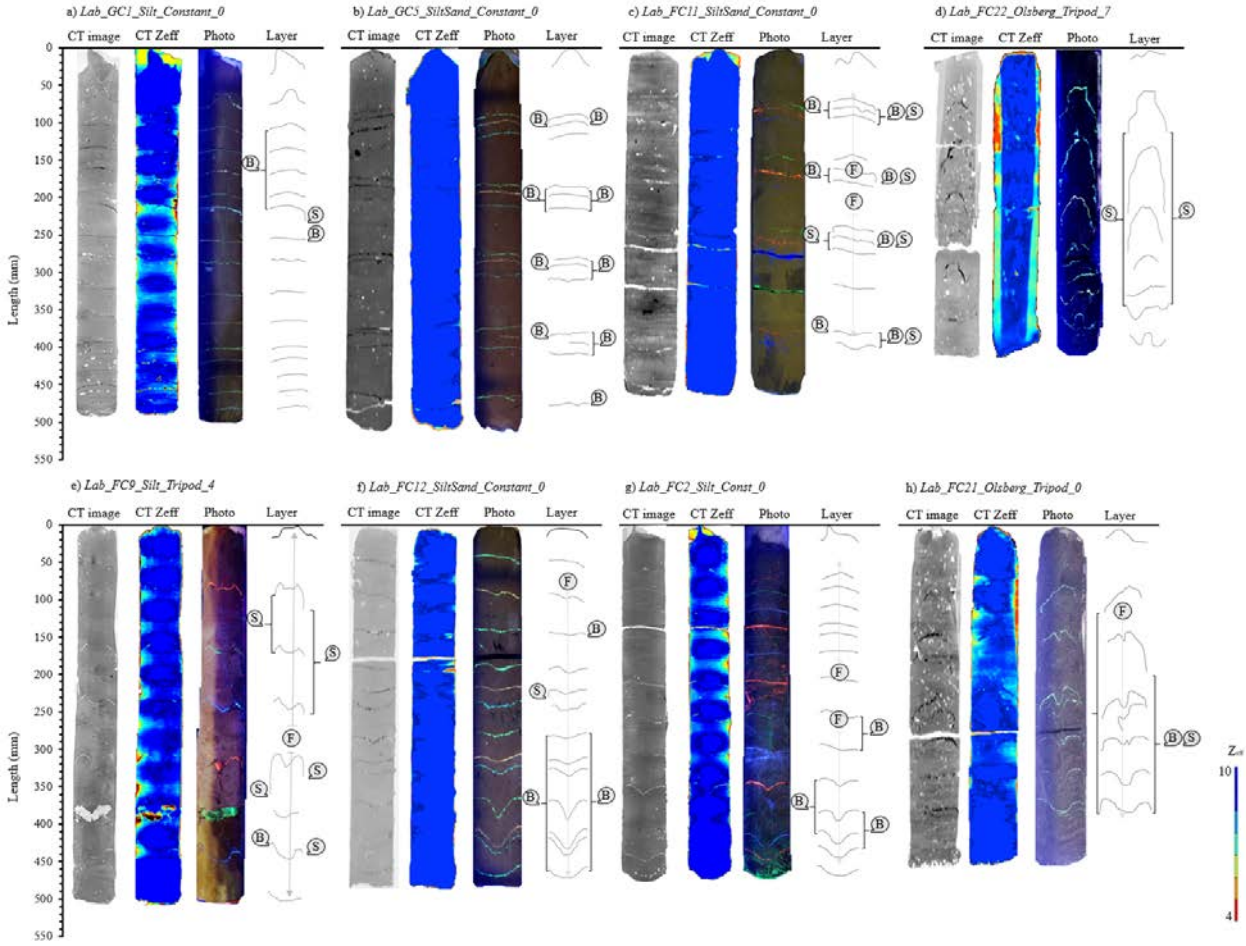


**Figure 7.** Selected laboratory cores (from left to right: X-Ray CT scan image, *Zeff* CT scan image, core photography under UV illumination, and digitized sediment layer) with artificially fluorescent laminated stratigraphy, shown as colored lines in the photos. To better visualize the coring disturbances, the layers have been digitized and labeled with the corresponding type of disturbance for each core. Four major types of disturbances were observed: (1) bending (B); (2) smearing (S); (3) freezing (F) (shown as an arrow in upward- and downward-direction) and (4) shortening. (a),(b) and (c): Bending: sediment layer are concavely formed and

slightly bended downward at the core margin; (d) Smearing: strong deformation due to shearing of the ice crust (which can be differentiated in the $Z_{eff}$ CT scan images; $Z_{eff}$ ranges from 7.2 to 7.4 for ice) against the sediment which occur in close distance to the rim of the core; smearing drags the sediment significantly downwards along the core margin (e) Smearing: Moderate deformation due to shearing of the freeze corer without ice crust against the; (f) Freezing: Vertical displacement of the sediment layer in downward direction. *HoD* increases with depth; (g) Freezing: Upward vertical displacement at the upper half and downward displacement at the lower half of the core. *HoD* increases with increasing depth (h) Freezing and Smearing: Upward displacement at the upper half and downward displacement of the layer in the lower half of the core. Smearing is the result of the friction between the ice crust and the freeze corer. The complete documentation of all laboratory experiments, including WC, penetration velocity, as well as incremental and cumulative shortening diagram are shown in the supplementary information (Fig. S7-S35).

### *a) Bending*

The results showed that both, the freeze and gravity core samples are affected by bending, which can be identified as layer deformation at the outer perimeter of the corer (Fig. 7 a, b, c). The *DOF* of the freeze cores is 31 ± 19 (mean and standard deviation) for *Silt Sediment* (n=9) and 41 ± 12 for *Silt/Sand Sediment* (n=6), whereas the *DOF* of the gravity cores is 14 ± 12 for *Silt Sediment* (n=3) and 62 ± 2 for *Silt/Sand Sediment* (n=2). *Olsberg Sediment* showed no significant bending for both corer types. *WoD* of the freeze cores is 5 ± 3 mm for *Silt Sediment* and 5 ± 1 mm for *Silt/Sand Sediment*, and therefore slightly higher than of the gravity cores with 3 ± 3 mm and 5 ± 0 mm, respectively. The *HoD* of the freeze cores is 3 ± 2 mm for *Silt Sediment* and 4 ± 1 mm for *Silt/Sand Sediment*, and slightly smaller than of the gravity cores with 4 ± 4 mm and 4 ± 1 mm, respectively. *WoD* and *HoD* vary considerably within a single core, where bending occurs more frequently in the upper half of the core than in the lower half. We speculate that this might be due to an increase in the frictional drag between the sediment and core liner with increasing penetration depth, as described by Skinner and McCave (2003). A constant penetration velocity increased the intensity of bending compared to an inconstant penetration velocity (Fig. S7-S35).

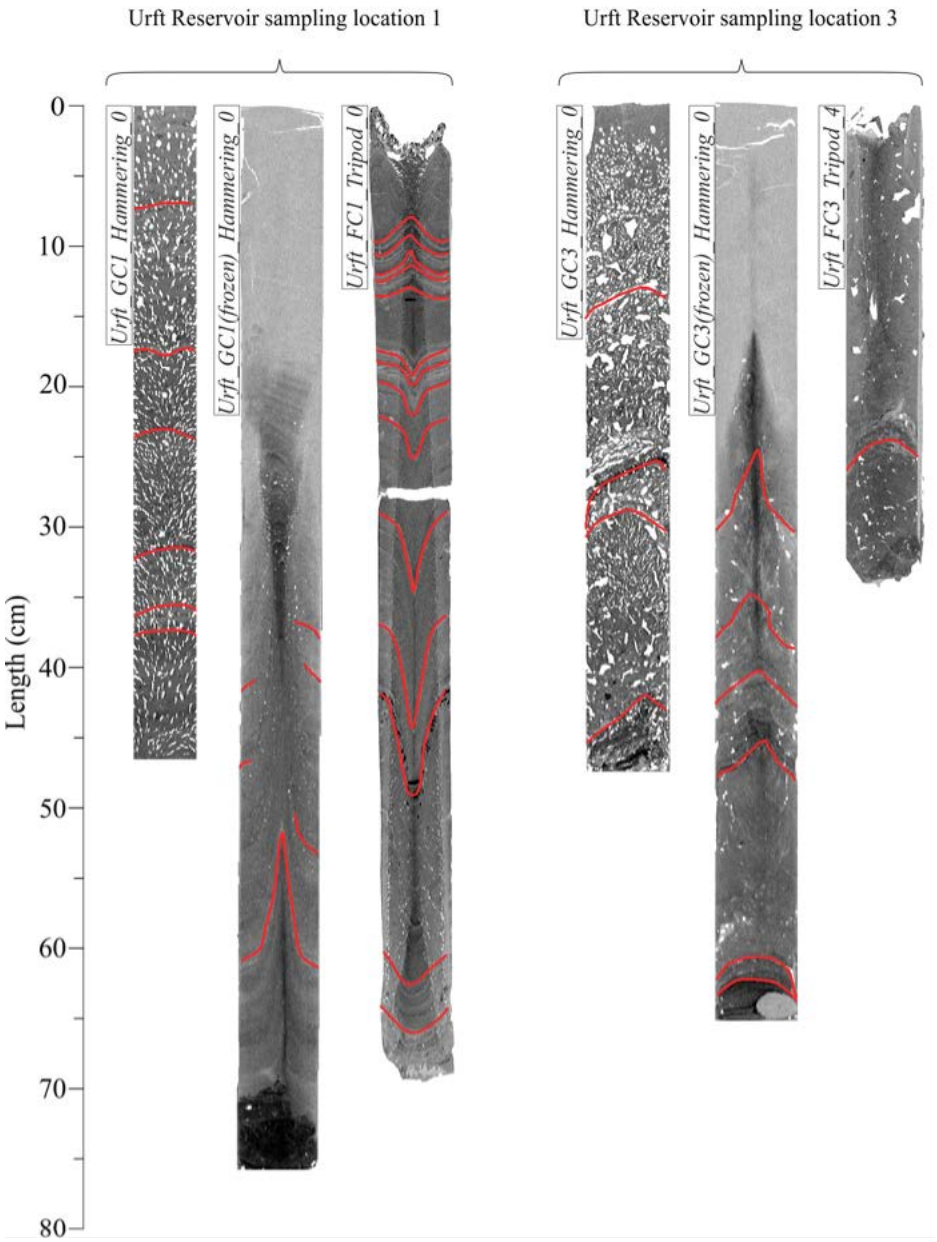


**Figure 8.** Vertical cross-sectional X-Ray CT scan images of Urft sampling location 1 and 3. Greyscale bar shows HU scale. Gas bubbles are shown as white spots. Core top is at 0 cm and indicates the position of the sediment-water interface. Coring disturbances (marked as red lines) are seen on all cores. Urft Reservoir gravity cores (*Urft_GC1_Hammering_0* and *Urft_GC3_Hammering_0*) shows bending at the core margin. Of particular note is the orientation of the bubbles in both gravity cores towards the core edge, originating from the symmetry axis of the core. This might be a result of a partial mid-core flow-out during withdrawal of the core. The adherence of the sediment at the core liner is higher than in the center of the core and therefore, the inner part of the core is more likely to flow out to a larger extent that the outer part. Freeze cores and frozen gravity cores shows an upward

displacement due to freezing process, except *Urft_FC1_Tripod_0* where the displacement is also in downward direction.

Field freeze cores showed no bending (Fig. S36-S44), whereas Urft and Olsberg Reservoir gravity cores showed a *DOF* of 100%, with *WoD* of 11 ± 4 mm and *HoD* of 7 ± 4 mm, where bending occurs predominantly in the lower half. This might be related to the reduced penetration force of the freeze corer due to the sharper design of the cutting-edge in contrast to the gravity corer. This assumption is in line with previous findings of Hvorslev (1941) showed the importance of the details of the cutting-edge design. This is in line with Clayton and Siddique (1999) who found that the most important factor governing coring disturbance is the combination of area ratio (ratio of displaced sediment area to the total sampler area) and cutting-edge angle (Clayton and Siddique 1999). A reason for this rather contradictory result, that bending occurs predominantly in the lower half of the cores compared to the laboratory results is not entirely clear. We assume that the consolidation of the in situ sediment increases with depth and therefore the frictional drag between the sediment and core liner increases, respectively. Consolidation in the laboratory cores were not given.

***b) Smearing***

*DOF* for freeze cores without ice crust (0% to 13%) was significantly smaller than cores with ice crust (30% to 50%; Fig. 7 d, e, h) and that of the gravity cores in *Olsberg Sediment* (31.3%). This might be related to the higher roughness of the ice crust surface in comparison to the stainless steel of the freeze corer and the PVC material of the gravity corer. The higher roughness causes a higher friction, which leads to enhanced shearing of sediment in direction of penetration. The maximum *WoD* of 13 mm and the maximum *HoD* of 39 mm of the freeze cores can be found in relatively short distances towards the core liner (e.g. Fig. S24, S28). Smearing can clearly be distinguished from bending, as the *HoD* is significantly higher and the *WoD* is smaller. This relies on the fact that smearing is an effect of dragging material along the core tube wall between adjacent sections into deeper layer (Chant and Cornett 1991).

Smearing in the field cores has only been observed in *Urft_FC2_Tripod_7* (Fig. 8), which has the thickest ice crust of all in situ freeze cores. This ice crust formed during the descent of

the corer, which took about 1 min. The results from the field investigation are consistent with those from the laboratory, where smearing predominantly appeared when an ice crust on the inside of the corer increased the shearing force between the sediment.

***c) Freezing***

All laboratory freeze cores (Fig. S7-S28) showed a vertical displacement of the sediment layer, which is probably the result of the freezing process, caused by radial freezing process from the outside to the inside of the core. It can be ruled out that the vertical deformation of the sediment layer in freeze cores is the result of friction between the corer and the sediment and can be clearly differentiated from bending and smearing (Fig. 7 f, g, h). Such deformation would appear as downward bends at the outer perimeter of the sediment core, which increases radially from the center of the core (Acton et al. 2002). An inconstant penetration velocity increased the *DOF*. *Olsberg Sediment*, which has a significantly higher WC shows the highest *DOF* of 61% to 78%, whereas *DOF* of *Silt Sediment* and *Silt/Sand Sediment* of 46% to 63% is slightly lower. *HoD* of all laboratory freeze cores is 34 ± 6 mm and *WoD* is 12 ± 4 mm.

This finding corroborates to the observation of the real-time CT scans, which have shown that the vertical displacement is a result of the expanding ice volume, primarily at phase transition from water to ice, which "squeezes" the non-frozen inner part of the core in the direction of least resistance. Our observations are in line with the concept of the freezing-induced deformation in soils, described by Grechichsev (1972, 1973). He distinguished three different multidirectional processes: Linear expansion (or contraction) of the soil-forming components, the continuous phase transition at the ice-water phase boundary, and the thermal deformation of the internal microstructures. Because expansion within the steel framed freeze corer is limited to the vertical direction, and the cores are frozen from the outside to the inside, the inner part of the core can only be relocated up- or downwards. This phenomenon has been described by Rutledge and Fleeger (1988), who found that the extent and shape of distortion strongly depend on the freezing rate. Accordingly, the fast freezing rate results in a significantly higher *DOF*, *WoD*, and *HoD* (e.g. *Olsberg Sediment*).

Figure 9 a) shows a conically shaped area in the vertical cross-sectional CT scan image of *Urft_FC1_Tripod_0*. Horizontal cross-sectional CT images (Fig. 9 b) shows that this area is bounded by accumulations of solid particles and gas bubbles. This observation corroborates the hypothesis of Stephenson et al. (1996), who stated that ice crystal formation causes a flux of sediment pore-water, excluding some solids. The boundary, where the circular arrangement occurred, also shows ice spikes (Fig. 9 c), which can be seen in the microscopic images. Ice spikes grow as tiny cracks in a radial direction from the core margin towards the center of the core, where spikes increase in size (max. length of 6 mm) and decrease in number. Parker et al. (1996) stated, that ice spikes can grow into the still unfrozen sludge in the direction of freezing at high freezing rates (> 21 µm/s), generally bypassing the sludge flocs, apparently without moving or altering them (Parker et al. 1996). The occurrence of ice spikes (Fig. 9) is consistent with our observations of the freezing rate experiments, which showed a freezing rate of > 20.8 µm/s. We have verified that by using microscopy images and produced similar results (e.g. Fig. S8, S9, S22, S14) where the conical shape coincided with the interface in the HU values. The results (Fig. 9) also indicate a lateral displacement of gas bubbles from the outer perimeter into the center of the core, where gas bubbles are circularly arranged. It cannot be ruled out that those gas bubbles originated from gas bubble formation from dissolved gas due to the phase transition. In this study, it cannot be excluded that nucleated gas bubbles grew or merged to form larger bubbles. According to Lipp et al. (1987), the maximum radius of nucleated bubbles is < 20 µm at a freezing rate > 90 µm/s. This bubble radius is significantly smaller than the spatial resolution of the X-Ray CT scans (voxel size: 0.1263 $mm^3$).

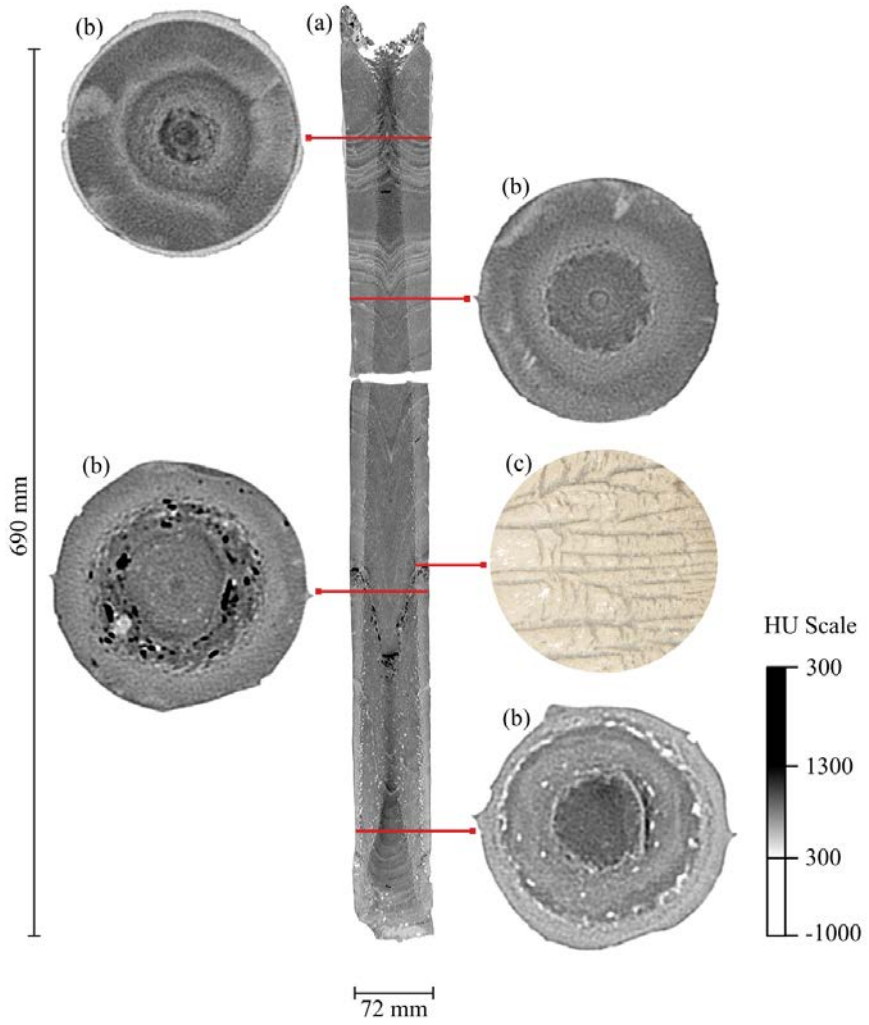


**Figure 9.** Vertical (a) and horizontal (b) cross-sectional CT scan images (HU scale according to the color bar) at different depths and microscopic pictures (c) of ice spikes formed in core *Urft_FC1_Tripod_0*. Core top is at 0 cm and indicates the position of the sediment-water interface. The cross-sectional images show a circular arrangement of solid particles (black spots) and gas bubbles (white spots), which may have formed during the freezing process. Of particular importance is the up- and downward vertical distortion of this core structure. The layers in the upper 13 cm are bent in an upward direction with a maximum *WoD* of 17 mm and a maximum *HoD* of 41 mm, whereas the layers below 13 cm depth are bent in a downward direction with a maximum *WoD* of 42 mm and a maximum *HoD* of 75 mm. The *HoD* upward and downward distortions increases with increasing core depth. The point, where the vertical displacement occurs, coincides with a sharp gradient of different X-ray absorption. This can be seen as a conical shape within the vertical cross-sectional image. HU values with a darker shade of grey are located inside of the conical arrangement (HU = 400 ± 150), whereas a brighter shade of grey (HU = 286 ± 127) can be seen outside.

Beside core *Urft_FC1_Tripod_0*, the shape of the layer distortion to other Urft Reservoir cores significantly differs by showing a more uniform expansion over the whole length of the core, with a *WoD* in an upward direction of 51 mm and a *HoD* of 23 mm. The effect of uniform expansion was also observed at Olsberg Reservoir freeze cores and in the real-time CT scans with *Olsberg Sediment*. The cores have *WoD* of 36 ± 6 mm and a *HoD* of 16 ± 6 mm. However, no correlation has been observed between the direction and extent of the layer displacement and WC, OM and ρ (Fig. S36-S44). This might be due to various sediment properties, which may influence each other and either enhance or mitigate the effect of freezing on the sediment structure.

***d) Shortening***

*DOF* of the freeze cores was 17 ± 20%, whereas the gravity cores showed a higher *DOF*, but with a lower variation with 30 ± 14% (Tab. 1). The *DOF* of the freeze core shortening for *Olsberg Sediment* (48%) was significantly higher than for *Silt Sediment* (28%) and *Silt/Sand Sediment* (25%). This finding of the current study do not support the results of Blomqvist (1991), where clayey and silty sediments are shortened more than light, unconsolidated sediments, such as *Olsberg Sediment*. *DOF* of gravity core shortening for *Silt/Sand Sediment* (22%) and *Olsberg Sediment* (37%) was lower than the freeze cores, whereas *Silt Sediment* is only marginally higher (30%). The gravity core shortening results are consistent with those of Morton and White (1997), who found a shortening factor of 30%, and inconsistent to earlier findings of Emery and Dietz (1941), and Emery and Hülseman (1964), who reported a shortening factor of up to 50%. However, our findings show that shortening increases with WC and OM, and support the idea of Emery and Dietz (1941) that the degree of shortening depends on sediment characteristics.

Our results showed that the shortening pattern (see bar charts, showing the shortening pattern in Fig. S7-35) in the laboratory experiments is not uniform throughout the core. The best correlation between shortening and physical sediment properties was found where GSD and WC changed within two subsequent sediment layers, which is given for *Silt/Sand Sediment*. Half of the cores exhibited this pattern, which is shown as a stair-step pattern of alternating

vertical lines and horizontal lines, representing the unshortened and shortened sections (Morton and White 1997). Besides this finding, we observed different shortening pattern, however, show poor correlation with WC, OM, and GSD is given (Fig. S36-S46).

Measurement of the in situ gravity core shortening was not possible, as stated by Kallstenius (1958) and Blomqvist (1991). No information of the effect of tilting and disturbances related to the penetration process and withdrawal could be obtained, as no observation during those processes was possible. Though, the freeze corer in combination with the tripod allowed the measurement of the in situ core shortening. However, even though the careful descend of the freeze corer was controlled by video monitoring, a hydraulic shock wave in front of the cutting-edge washed away a certain part of the flocculent surficial sediment layer at one sampling location (Fig. S6). As the descending velocity of the gravity corer is much higher than the one of the freeze corer, it can be assumed, that core shortening and a hydraulic shock wave of the gravity corer occurs more frequently and washes away more flocculent surficial material, resulting in coring disturbances.

***Gas Bubble Analysis***

3D gas bubbles visualization of Urft and Olsberg Reservoir freeze and gravity cores shows that the volumetric gas content ($\theta$), bubble size, and bubble distribution vary significantly between the sampling locations and different types of coring techniques (Fig. 10). It is obvious that gas bubble distribution and size did not follow a general pattern. For instance, bubbles in *Urft_FC1_Tripod_0* were found 5 cm below the sediment-water interface and below a depth of 40 cm, whereas the gravity core gas bubble distribution is almost constant over depth.

$\theta$ of Olsberg Reservoir gravity cores (4.5% to 12.4%) was significantly larger than of freeze cores (0.6 to 1.2%) at sampling depths between 0.8 m and 2.5 m (Fig. 10). $\theta$ of Urft Reservoir gravity cores decreases with decreasing water depth of the sampling locations, from 10.5% (31 m), 11.2% (22 m) and 10.9% (10 m), respectively. In contrast, $\theta$ of Urft Reservoir freeze cores increased from 0.2 (31 m), 0.2 (22 m), 2.0 (10 m) to 1.2% (5 m) with decreasing water level. $\theta$ of the frozen gravity core shows a similar trend, 0.3, 2.9 to 5.6%, respectively. The increasing $\theta$ from deeper to shallower parts of the Urft Reservoir corresponds to the findings

of Bastviken et al. (2008), Duc et al. (2010), Natchimuthu et al. (2016), Wik et al. (2013), where ebullition is often found most active in the littoral zone. The greater variability in $\theta$ between the three different coring techniques of Urft Reservoir in comparison to Olsberg Reservoir may be related to the deeper water depths and differences between the lake-bed temperature ($T_{Urft,Dam}$= 5.1°C, $T_{Urft,Inflow=}$ 7.9°C, $T_{Olsberg}$= 14.2°C) and ambient air temperature ($T_{Olsberg}$= 24.3°C; $T_{Urft}$= 21.2°C) of the thermally stratified Urft Reservoir. This may be explained by the observations of Lane and Taffs (2002) and Scandella et al. (2011), who found that the core can expand, and sediment structures disturbed by the expansion of gas bubbles due to the decrease in hydrostatic pressure during core recovery. Also, the decrease in hydrostatic pressure causes a considerable shift in the partitioning between dissolved $CH_4$ and the gaseous phase. $CH_4$ dissolute, as saturation concentration decreases significantly with pressure (Duan et al. 1992) and temperature. Additionally, even though the gravity cores were transported in a dark transport box, the temperature is higher than the in situ temperature of the sediment, and movements and vibrations during transport cannot be excluded, which may cause ebullition and bias the gas bubble characteristics. It might be also be attributed to an additional methane formation, as the methanogenesis is temperature dependent (Yvon-Durocher et al. 2014). Wilkinson et al. (2019) demonstrate that a 10°C temperature change can cause between a 1.6 to 7-fold change in methane production rate. Due to the short time difference (approx. 36 h) between sampling and CT scan, the effect of increasing methane production can be assumed to affect $\theta$, but to a minor extent. When comparing our results to those of Dück et al. (2019), who showed that freezing of gassy clay sediments under laboratory conditions caused a contraction in $\theta$ by 27 ± 6%, it can be concluded that the greater differences in our study can be related to the changes in hydrostatic pressure and sample temperature, as described above.

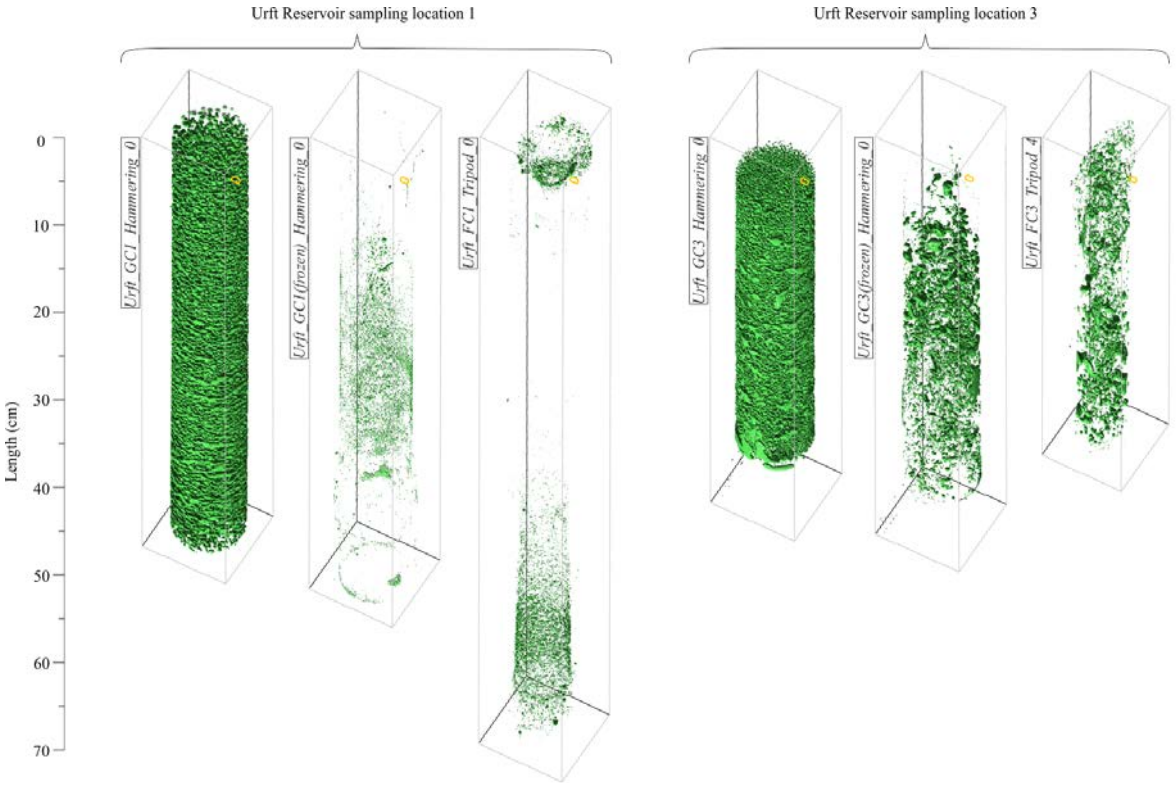


**Figure 10.** Exemplary 3D gas bubble visualization in gravity, frozen gravity and freeze cores of Urft Reservoir sampling locations 1 and 3 (see labels). In the gravity cores, gas bubbles are homogenously distributed over depth, whereas the gas distribution in the freeze and frozen gravity cores are different and more heterogeneous and obviously do not correlate to the gravity cores. Differences are more pronounced at sampling location 1 in contrast to sampling location 3, due to the greater differences in hydrostatic pressure and sediment temperature.

Bubble size ($D_{eq}$) was significantly smaller in the freeze cores (0.2 to 1.0 mm) and frozen gravity cores (0.1 to 1.0 mm) than in gravity cores (1.0 to 2.1 mm) at Urft Reservoir (Fig. 11). For instance, *Urft_GC3(frozen)_Hammering_0* contained few large bubbles, resulting in a relatively smaller $\theta$, comparing to *Urft_GC3 _Hammering_0*. $D_{eq}$ of the freeze core increased from 0.2 (31 m depth), 0.3 (22 m depth), 0.9 (10 m depth) to 1.0 mm (5 m depth), and in the frozen gravity cores from 0.1, 0.4 to 1.0 mm with decreasing water depth. This trend in bubble size was not observed in the gravity cores (ranging from 1.0, 2.1 to 1.1 mm from deep to shallow water depths). The same discrepancies in gas bubble distribution between frozen and unfrozen sediment cores were observed at Olsberg Reservoir. $D_{eq}$ of Olsberg Reservoir freeze cores (0.2 mm to 0.6 mm) was significantly smaller contrast to gravity cores (0.9 mm to 2.0 mm) at water depths between 0.8 m and 2.5 m.

Freezing can be expected to result in gas bubbles nucleation due to the two orders of magnitude smaller gas solubility in ice compared to water (Killawee et al. 1998). Due to the limitation in spatial resolution of the CT scan, the occurrence of this effect can neither be confirmed nor denied. In future investigations real-time CT scans with a higher spatial resolution may shed some light on this issue of nucleation and/or relocation of gas bubbles due to the freezing process.

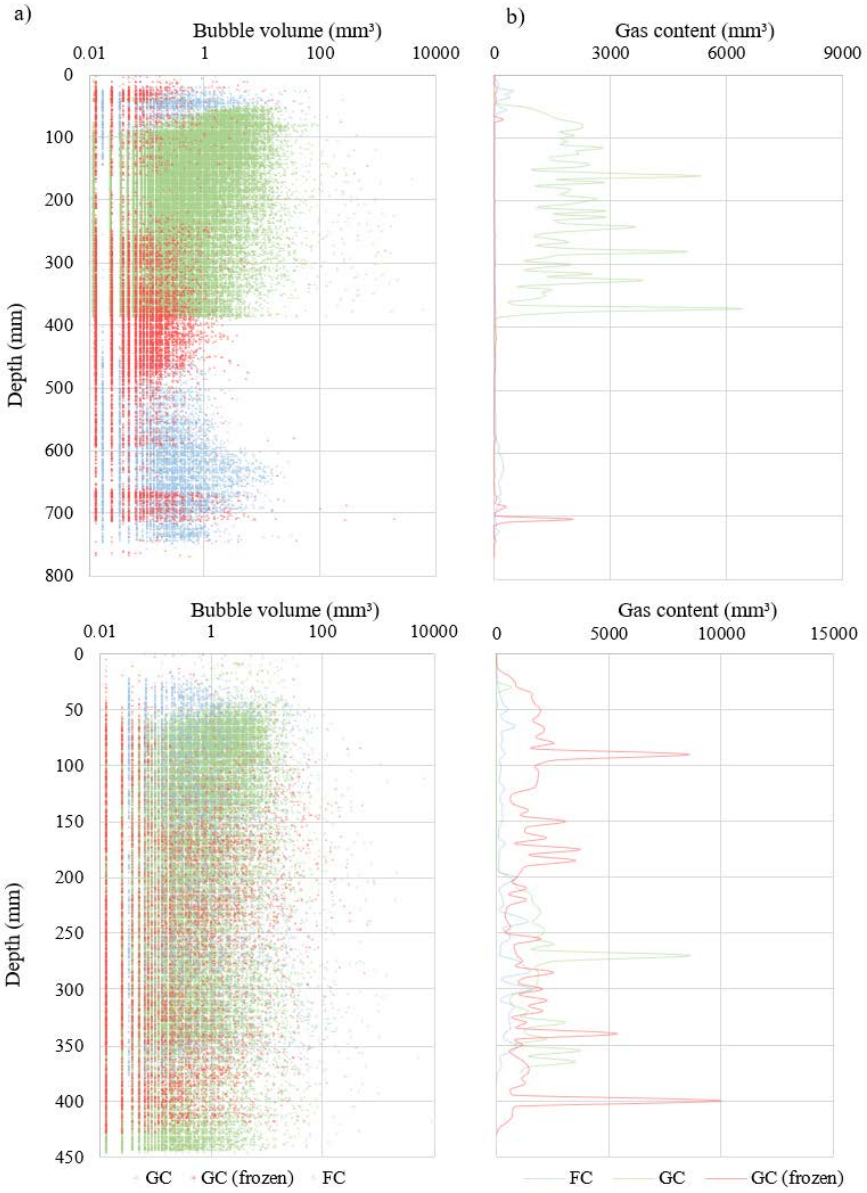


**Figure 11.** Bubble size and volumetric gas content ($\theta$) as a function of depth for Urft Reservoir sampling location 1 (a) and 3 (b). Green line/dots refer to gravity cores, red line/dots to frozen gravity cores, and blue line/dots to freeze cores.

## CONCLUSIONS

This study determined the causes, effects, and extent of coring disturbances between freeze and gravity coring techniques in comparative laboratory and field investigations. We demonstrated that the novel freeze coring technique facilitates an effective way for obtaining gas-bearing sediment samples and the combination with the non-destructive X-Ray CT scans made a visualization of the in situ sediment structure and gas bubble characteristics possible. Our findings suggest, that this freeze corer combined with X-ray CT analysis may open a new field for comparatively cost-efficient studies requiring a qualitative and quantitative understanding of the structure and quantity of gas bubbles in aquatic sediment. Spectral X-ray CT scans can provide additional information for the analysis and interpretation of sediment cores, which increases the informative value of existing X-ray CT scans (e.g., differentiation between organic and inorganic material).

Nevertheless, almost all cores showed coring disturbances and it was also shown that the identification of zones of coring disturbances is necessary, as this facilitates a necessary correction of analysis results. We identified four major types of coring disturbances: bending, smearing, freezing and shortening. Minor disturbances (e.g. tilting, liquefaction) can be assumed also to occur, however a clear identification or separation to other disturbances is often difficult due to missing appropriate measurement techniques.

The freeze coring technique reduces the risk of coring disturbances during core recovery, depressurization and handling. The design of our freeze corer prevents the typical conical shaped form of cores, which usually occurs by using tube- or wedge-shaped freeze corer (DIN ISO 2016). By using the tripod and underwater video camera it is possible to prevent the corer from being affected by tilting, allows the measuring core shortening and observation of the penetration process, where a possible gas release can be detected. Our results suggest, that freezing the sediment in situ preserves the gas characteristics better than the gravity coring technique. Due to the limited data on the gas bubble distribution in both investigated reservoirs, further research is needed to validate the results of the results obtained with the freeze coring technique to characterize gas bubbles in aquatic sediments under different conditions (e.g.

water depth, sediment composition) and compare those results with other coring methods (e.g. pressurized corer). Freeze coring affect the sediment stratigraphy in a regular way, i.e. by a gradual shifting of the inner relative to the outer part of the core. Such a gradual disturbance does not affect the general integrity of the sediment. Therefore, it is important to consider that gas bubbles and particles are rearranged due to the freezing process, and, freezing may result in the nucleation of gas bubbles that were not resolved in the X-ray CT measurements and should be investigated in future studies.

No type of sediment coring technique is applicable to all types of studies and conditions (Glew et al. 2001). Based on the results and experiences made within this study, we can state the following recommendation for the use of freeze and gravity coring:

1) The probability of a change in volumetric gas content, equivalent sphere bubble diameter and sediment stratigraphy due to the change in hydrostatic pressure during core recovery and sample temperature increases with sampling depth. To eliminate potential bias, the use of the freeze coring technique in low-cohesive and gas-bearing sediment is recommended. This recommendation is supported by results from field investigation, which showed that the discrepancies in $\theta$ and $D_{eq}$ between the gravity and freeze core increase with increasing hydrostatic pressure and difference in sample temperature.

2) Our results suggest that nearly all cores are affected by different types and extents of coring disturbances. The occurrence and extent of coring disturbances are highly variable and differs significantly between the coring techniques and boundary conditions. Undetected coring disturbances would lead to analytical bias resulting in possible erroneous or inaccurate conclusions. Therefore, the validity of various results obtained from field cores is questionable (e.g. Baxter et al. 1981; Blomqvist 1985; Buckley et al. 1994; Ostrovsky 2000). The extent of sampling bias will largely be the result of the choice of corer design, water depth and physical properties θ and of the sediment. With increasing water saturation, gravity coring has shown to be more susceptible to (partial) leakage or liquefaction during core recovery and for problems during sample handing in the laboratory. Thus, the freeze coring technique should be used for water-saturated sediment to prevent liquefaction. This leads to the conclusions that the analysis of core-specific disturbances is highly recommended and should become a routine

aspect of data analysis and publication reporting, dealing with sediment core data. We recommend a core-specific analysis of the type and extent of coring disturbances on the structural integrity of the subsequent analysis, as suggested by Liernur et al. (2017). A visual inspection of the core stratigraphy and an exclusion of a buffer zone around the corer (e.g. Franchini and Zeyer 2012; Strasser et al. 2015) only allow the identification of coring disturbances in texturally and structurally homogenous sediments of just one cross-section through the core, and does not take into account the spatial structure of disturbances.

3) Core shortening is an important disturbance for both the gravity and freeze coring techniques. The laboratory experiments indicate that core length has been changed during the penetration and withdrawal process, where the gravity coring technique seems to be more pronounced to shortening than the freeze coring technique. As the degree of core shortening is related to the core tube diameter, penetration velocity (Emery and Dietz 1941; Hvorslev 1949; Blomqvist 1985; Hongve and Erlandsen 1979; Blomqvist 1991) and sediment parameter, it is important to measure the penetration depth in situ. This allows adjusting the core stratigraphy to remove the effect of shortening to their natural position to reduce the risk of an under- or overestimation of the core data. Dück et al. (2019) have shown that video imaging method for visualization of the freeze corer penetration into the sediment can bring a benefit in terms of quantification of shortening and is recommended to be used. In cases where the visibility at the benthic boundary layer is not good, the use of an echo-sounding technique for the measurement of the penetration depth is recommended.

4) Gravity coring is a relatively easy, cost-efficient method and requires less effort than freeze coring. It can, therefore, be used for the analysis of the vertical distribution of physical sediment parameter (e.g. grain-size distribution, water content, organic matter, and wet bulk density). This technique should only be sued for gas bubble analysis when the difference in hydrostatic pressure and temperature is small, to avoid related bias.

## ACKNOWLEDGMENTS

The authors would like to thank Laura Bolsenkötter, Eric Zimmermann and Timo Fahlenbock for their help throughout the sediment core sampling in the field. We would also like to thank Patrick Püttmann and Thomas Fortmeier for their help during laboratory experiment preparation. We thank Bettina Baeßler, Annika Thillmann and Jasmin Holz for their assistance in X-Ray CT scans. All data are provided in the supporting information.

## FUNDING

This study was conducted in the framework of a project of the European Regional Development Fund / Investment for Growth and Employment, project number EFRE-0800107.

## AUTHOR CONTRIBUTION

Yannick Dück is responsible for the study design, data analysis and text. Andreas Lorke and Christian Jokiel support the entire process. Johannes Gierse support the data analysis.

## CONFLICT OF INTERESTS

The authors declare no conflict of interest. The funding agency had no role in the design of the study; in the collection, analyses, or interpretation of data; in writing the manuscript, and in the decision to publish the results.

## REFERENCES

Abegg, F., and A. L. Anderson. 1997. The acoustic turbid layer in muddy sediments of Eckernfoerde Bay, Western Baltic: methane concentration, saturation and bubble characteristics. Marine Geology. 137: 137-147, doi: doi.org/10.1016/S0025-3227(96)00084-9.

Acton, G. D., M. Okada, B. M. Clement, S. P. Lund, and T. Williams. 2002. Paleomagnetic overprints in ocean sediment cores and their relationship to shear deformation caused by piston coring. J. Geophys. Res. 107(B4), doi: 10.1029/2001JB000518.

Algar, C. K., B. P. Boudreau, and M. A. Barry. 2011. Initial rise of bubbles in cohesive sediments by a process of viscoelastic fracture. Journal of Geophysical Research: Solid Earth. 116: B04207, doi: 10.1029/2010JB008133.

Arman, A., and K. L. MacManis. 1976. Effects of Storage and Extrusion on Sample Properties. Symposium on Soil Specimen Preparation for Laboratory Testing. ASTM STP, 599: 66-87, doi: 10.1520/STP39076S.

Bastviken, D., J. J. Cole, M. L. Pace, and M. C. Van de Bogert. 2008. Fate of methane from different lake habitats: Connecting whole-lake budgets and CH4 emissions. Journal of Geophysical Research. 113: G02024, doi: 10.1029/2007JG000608.

Bastviken, D., L. J. Tranvik, J. A. Downing, P. M. Crill, and A. Enrich-Prast. 2011. Freshwater methane emissions offset the continental carbon sink. Science. 331: 50-50, doi: 10.1126/science.1196808.

Baxter, M. S., J. G. Farmer, I. G. McKinley, D. S. Swan, and W. Jack. 1981. Evidence of the unsuitability of gravity coring for collecting sediment in pollution and sedimentation rate studies. Environmental Science and Technology. 15: 843-846, doi: doi/pdf/10.1021/es00089a014.

Blomqvist, S. 1985. Reliability of core sampling of soft bottom sediment - an in situ study. Sedimentology. 32: 605-612, doi:10.1111/j.1365-3091.1985.tb00474.x.

Blomqvist, S. 1991. Quantitative sampling of soft-bottom sediments: Problems and solutions. Marine Ecology Progress Series. 72: 295–304, doi:10.3354/meps072295.

Boereboom, T., M. Depoorter, S. Coppens, and J.-L. Tison. 2012. Gas properties of winter lake ice in Norhtern Sweden: implication for carbon gas release. Biogeosciences. 9: 827-838, doi:10.5194/bg-9-827-2012.

Boudreau, B. P., C. Algar, B. D. Johnson, I. Croudace, A. Reed, Y. Furukawa, K. M. Dorgan, et al. 2005. Bubble growth and rise in soft sediments. Geology. 33(6): 517-520, doi: 10.1130/G21259.1.

Buckley, D. E., W. G. MacKinnon, R. E. Cranston, and H. A. Christian. 1994. Problems with piston core sampling: Mechanical and geochemical diagnosis. Marine Geology. 117: 95-106, doi: doi.org/10.1016/0025-3227(94)90008-6.

Carte, A. E. 1961. Air bubbles in Ice. Proceedings of the Physical Society. 77: 757-768, doi: doi.org/10.1088/0370-1328/77/3/327.

Chaney, R. C., and G. Almagor. 2015. Seafloor Processes and Geotechnology, 1st ed. CRC Press.

Chant, L. A., and R. J. Cornett. 1991. Smearing of gravity core profiles in soft sediments. Limnology and Oceanography. 67(7): 1492-1498, doi: doi.org/10.4319/lo.1991.36.7.1492.

Clayton, C. R. I., and A. Siddique. 1999. Tube sampling disturbance – forgotten truths and new perspectives. Geotech. Eng. 137: 127-135, doi.org/10.1680/gt.1999.370302.

Crusius, J., and R. F. Anderson. 1991. Core compression and surficial sediment loss of lake sediment of high porosity caused by gravity coring. Limnology and Oceanography. 36: 1021-1031, doi: 10.4319/lo.1991.36.5.1021.

Duan, Z., N. Møller, J. Greenberg, and J. H. Weare. 1992. The prediction of methane solubility in natural waters to high ionic strength from 0 to 250°C and from 0 to 1600 bar. Geochimica et Cosmochimica Acta. 56(4): 1451-1460, doi: doi.org/10.1016/0016-7037(92)90215-5.

Duc, N. T., P. Crill, and D. Bastviken. 2010. Implications of temperature and sediment characteristics on methane formation and oxidation in lake sediments. Biogeochemistry, 100: 185-196, doi: doi.org/10.1007/s10533-010-9415-8.

Dück, Y., L. Liu, A. Lorke, I. Ostrovsky, R. Katsman, and C. Jokiel. 2019. A novel freeze corer for characterization of methane bubbles and assessment of core disturbances. Accepted for publication in: Limnology and Oceanography: Methods.

Elmgren, R. 1973. Methods of sampling sublittoral soft bottom meiofana. Oikos. 15: 112-120.

Emery, K. O., and J. Hülsemann. 1964. Shortening of sediment cores collected in open-barrel gravity corers. Sedimentology. 3: 144-154, doi: doi.org/10.1111/j.1365-3091.1964.tb00639.x.

Emery, K. O., and R. S. Dietz. 1941. Gravity coring instrument and mechanics of sediment coring. Geological Society of America Bulletin. 53: 1685-1714, doi: doi.org/10.1130/GSAB-52-1685.

Environmental Protection Agency. 1991. Handbook: Remediation of contaminated sediments. EPA/625/6-91/028.

Flannagan, J. F. 1970. Efficiencies of various grabs and cores in sampling freshwater benthos. Journal of the Fisheries Research Board of Canada. 27: 1691-1700, doi: doi.org/10.1139/f70-191.

Flood, R. D., D. J. W. Piper, A. Klaus, et al. 1995. Proceedings ODP, Initial Reports, 155: College Station, TX (Ocean Drilling Program), doi: 10.2973/odp.proc.ir.155.1995.

Förstner, U., G. Müller, and H.-E. Reineck. 1968. Sediment und Sedimentgefüge des Rheindeltas im Bodensee. Neues Jahrb. Min. Abh. 109: 33-62.

Franchini, A. G., and J. Zeyer. 2012. Freeze-Coring Method for Characterization of Microbial Community Structure and Function in Wetland Soilds at High Spatial Resolution. Applied and Environmental Microbiology. 78(12): 4501-4504, doi: 10.1128/AEM.00133-12.

German Institute for Standardization (DIN) / International Organization of Standardization (ISO). (2016). Water quality - Sampling – Part 12: Guidance on sampling of bottom sediments (ISO/DIS 5667-12:2006).

Glew, J. R., J. P. Smol, and W. M. Last. 2001. Sediment Core Collection and Extrusion, p. 73-105. In Last W. M., and J. P. Smol [eds.], Tracking Environmental Change Using Lake Sediments, Springer.

Grechishchev, S. E. 1972. Study results of thermal deformations and prediction of frost cracking of soils. Proc. All-Union Sci. Conf. on Geocryology, Moscow: Mosk. Gos. Univ.

Grechishchev, S. E. 1973. The basic regularities of thermogeology and temperature cracking of frozen soils. Proc. 2nd Int. Conf. On Geocryology, Yakutsk: Yakutsk. Kn. Izd.

Halde, R. 1980. Concentration of impurities by progressive freezing. Water Research. 14: 575-580, doi: doi.org/10.1016/0043-1354(80)90115-3.

Harvey, B. R., M. B. Lovett, and S. J. Boggis. 1987. Some experiences in controlling contamination of environmental materials during sampling and processing for low-level actinide analysis. Journal of Radioanalytical and Nuceal Chemistry. 115: 357-368, doi: doi.org/10.1007/BF02037449.

Hessler, R. R., and P. A. Jumars. 1974. Abyssal community analysis from replicate cores in the central North Pacific. Deep Sea Research and Oceanographic Abstracts. 21(3): 185-209, doi: 10.1016/0011-7471(74)90058-8.

Hongve, D., and A. H. Erlandsen. 1979. Shortening of surface sediment cores during sampling. Hydrobiologia. 65: 283-287, doi: doi.org/10.1007/BF00038869.

Hopper, R. J. 1992. Effects and Implications of Sampling Clay Soils. Ph.D. thesis. University of Surrey.

Hung, W. T., W. H. Feng, I. H. Tsai, D. J. Lee, and S. G. Hong. 1997. Uni-directional freezing of waste activated sludges: vertical freezing versus radial freezing. Water Research. 31(9): 2219-2228, doi: doi.org/10.1016/S0043-1354(97)00067-5.

Hvorslev, M. J. 1949. Subsurface exploration and sampling of soils for civil engineering purposes. U. S. Army Corps of Engineers. Waterways Experimental Station. Vicksburg, Mississippi.

Iovea, M., G. Oaie, O. G. Duliu, M. Bodale, G. Mateiasi, and M. Neagu. 2005. Single and dual-energy X-ray computer tomography and digital radiography study of sedimentary cores, p. 1337-1348. In, Proceedings of the 7th International Conference on the Mediterranean Coastal Environment, MEDCOAST 2005.

Jensen, P. 1983. Meiofauna abundance and vertical zonation in a sublittoral soft bottom, with a test of the Haps corer. Marine Biology. 74: 319-326, doi: doi.org/10.1007/BF00403458.

Kallstenius, T. 1958. Mechanical disturbances in clay samples taken with piston samplers. Royal Swedish Geotechnical Institute.

Kegwin, L., D. Rio, and G. D. Acton. 1998. Intermediate depth Blake outer ridge. Proceedings Ocean Drill Program Initial Reports. 172: 77-156, doi: 10.2973/odp.proc.ir.172.104.1998.

Ketcham, R. A., and W. D. Carlson. 2001. Acquisition, optimization and interpretation of x-ray computed tomographic imagery: Applications to the geosciences. Computers and Geosciences. 27(4): 381-400, doi: 10.1016/S0098-3004(00)00116-3.

Killawee, J. A., I. J. Fairchild, J. L. Tison, L. Janssens, and R. R. Lorrain. 1998. Segregation of solutes and gases in experimental freezing of dilute solutions: Implications for natural glacial systems. Geochimica et Cosmochimica Acta. 62: 3637-3655, doi: doi.org/10.1016/S0016-7037(98)00268-3.

Lane. M. C., and K. H. Taffs. 2002. The LOG corer – a new device for obtaining short cores in soft lacustrine sediments. Journal of Paleolimnology. 27: 145-150, doi: doi.org/10.1023/A:1013547028068.

Lebel, J., N. Silverberg, and B. Sundby. 1982. Gravity core shortening and pore water chemical gradients. Deep Sea Research. 29: 1365-1372, doi: doi.org/10.1016/0198-0149(82)90014-0.

Lee, D. J., and Y. H. Hsu. 1994. Fast freeze/thaw treatment on excess activated sludges: floc structure and sludge dewaterability. Environ. Sci. Technol. 28: 1444-1449, doi: 10.1021/es00057a011.

Leonard, R. 1990. An assessment of sediment loss and distortion at the top of short gravity cores. Sedimentary Geology. 66: 57-63, doi: doi.org/10.1016/0037-0738(90)90006-F.

Li, L., J. Peng, Q. Gao, M. Sun, Y. Liu, M. Li, B. Chen, and K. Bo. 2016. Pressure retaining method based on phase change of coring of gas hydrate bearing sediments in offshore drilling. Applied Thermal Engineering. 107: 633-641, doi: doi.org/10.1016/j.applthermaleng.2016.06.174.

Liernur, A., A. Schomburg, P. Turberg, C. Guenat, R.-C. Le Bayon, and P. Brunner. 2017. Coupling X-ray computed tomography and freeze-coring for the analysis of fine-grained low cohesive soils. Geoderma. 308: 171-186, doi:10.1016/j.geoderma.2017.08.010.

Lipp, G., C. Körber, S. Englich, U. Hartmann, and G. Rau. 1987. Investigation of the behavior of dissolved gases during freezing. Journal of Cryobiology. 24: 489-503, doi: doi.org/10.1016/0011-2240(87)90053-8.

Lisle, T. E. 1989. Sediment transport and resulting deposition in spawning gravels, north coastal California. Water Resources Research. 25: 1303–1319, doi: 10.1029/WR025i006p01303.

Liu, L., J. Wilkinson, K. Koca, C. Buchmann, and A. Lorke. 2016. The role of sediment structure in gas bubble storage and release. Journal of Geophysical Research: Biogeosciences. 121: 1992-2005, doi: 10.1002/2016JG003456.

Lotter, A. F., I. Renberg, H. Hansson, R. Stöckli, and M. Sturm. 1997. A remote controlled freeze corer for sampling unconsolidated surface sediments. Aquatic Sciences. 59: 295-303, doi: doi.org/10.1007/BF02522360.

Maeck, A., H. Hofmann, and A. Lorke. 2014. Pumping methane out of aquatic sediments: Ebullition forcing mechanisms in an impounded river. Biogeosciences. 11: 2925-2938, doi: doi.org/10.5194/bg-11-2925-2014.

Martens, C. S., and R. A. Berner. 1974. Methane production in the interstitial waters of sulfate-depleted marine sediments. Science. 185: 1167-1169, doi:10.1126/science.185.4157.1167.

Martin, E. A., and R. J. Miller. 1982. A simple, diver-operated coring device for collecting undisturbed shallow cores. Journal of Sedimentary Petrology. 52: 641-642, doi: doi.org/10.1306/212F7FC2-2B24-11D7-8648000102C1865D.

McCoy, F. W. 1980. Photographic Analysis of Coring. Marine Geology. 38: 263-282, doi: 10.1016/0025-3227(80)90063-8.

McCoy, F.W. Jr. 1972. An analysis of piston coring through core head camera photography. Underwater soil sampling, testing, and construction control. Underwater Soil Sampling, Testing and Construction Control, ASTM Spec. Tech. Publ., 501, 90-105. DOI: 10.1520/STP38796S.

McCoy, F.W., and R.-P. von Herzen. 1971. Deep-sea core head camera photography and piston coring. Deep Sea Research. 18: 361-373, doi: doi.org/10.1016/0011-7471(71)90041-6.

McIntyre, A. D. 1971. Deficiency of gravity cores for sampling meiobenthos and sediments. Nature. 231(5300): 260, doi: doi.org/10.1038/231260a0.

Milkert, D. 1993. Auswirkungen von Stürmen auf die Sclicksedimente der westlichen Ostsee. Rep. Geol. Paläontol. Inst. Univ. Kiel. 66: 153.

Mogg, A. O., K. M. Attard, H. Stahl, T. Brand, R. Turnewitsch, and M. D. Sayer. 2017. The influence of coring method on the preservation of sedimentary and biogeochemical features when sampling soft-bottom, shallow coastal environments. Limnol. Oceanogr. Methods. 15: 905-915, doi: 10.1002/lom3.10211.

Morton, R. A, and W. A. White. 1997. Characteristics of and Corrections for Core Shortening in Unconsolidated Sediments. Journal of Coastal Research. 13(3): 761-769.

Natchimuthu, S., I. Sundgren, M. Gålfalk, L. Klemedtsson, P. Crill, A. Danielsson, and D. Bastviken. 2016. Spatio-temporal variability of lake CH4 fluxes and its influence on annual whole lake emission estimates. Limnology and Oceanography. 61: 13-26, doi: doi.org/10.1002/lno.10222.

Nevissi, A. E., G. J. Shott, and E. A. Crecelius. 1989. Comparison of two gravity coring devices for sedimentation rate measurement by 210Pb dating techniques. Hydrobiologia. 179: 261-269, doi: doi.org/10.1007/BF00006639.

Nies, H., H. Albrecht, V. Rechenberg, I. Goroncy, H. Dahlgaard, D. Weiss, and L. Brugmann. 1990. Intercomparison of sediment sampling techniques by means of radionuclide and heavy metal analyses. Dt. hydrogr. Z. 43: 27-53.

Ostrovsky, I. 2000. The upper-most layer of bottom sediments: sampling and artifacts. Arch Hydrobiol Spec Issues Advanc Limnol. 55: 243-255.

Pachur, H. J., H. D. Denner, and H. Walter. 1984. A freezing device for sampling the sediment-water interface of lakes. Catena. 11: 65-70, doi: doi.org/10.1016/S0341-8162(84)80006-5.

Parker P. J., A. G. Collins, and J. P. Dempsey. 1996. Incorporation and rejection of alum sludge flocs by an advancing freezing front, p. 757-767. In, Proceedings of the 8th International Cold Regions Conference.

Parker, W. R., and G. C. Sills. 1989. Observation of Corer Penetration and Sample Entry during Gravity Coring. Marine Geophysical Researchers. 12: 101-107, doi: doi.org/10.1007/BF00310566.

Piggot, C. S. 1941. Factors involved in submarine core sampling. Bulletin of the Geological Society of America. 52: 1513-1523, doi: doi.org/10.1130/GSAB-52-1513.

Richards, A. F., and G. H. Keller. 1961. A plastic-barrel sediment corer. Deep Sea Research, 8: 306-312, doi: doi.org/10.1016/0146-6313(61)90035-1.

Rogasik, H., I. Onasch, J. Brunotte, D. Jegou, and O. Wendroth. 2003. Assessment of soil structure using X-ray computer tomography. Geological Society, London, Special Publications: Home. 215: 151-165, doi: dx.doi.org/10.1144/GSL.SP.2003.215.01.14.

Rutledge, P. A., and J. W. Fleeger. 1988. Laboratory studies on core sampling with application to subtidal meiobenthos collection. Limnology and Oceanography. 33: 274-280, doi: doi.org/10.4319/lo.1988.33.2.0274.

Rymer, L., and J. Neale. 1981. Freeze coring as a method of collecting unconsolidated lake sediments. Australian Journal of Ecology. 6: 123-126, doi: doi.org/10.1111/j.1442-9993.1981.tb01279.x.

Scandella, B. P., C. Varadharajan, H. F. Hemond, C. Ruppel, and R. Juanes. 2011. A conduit dilation model of methane venting from lake sediments. Geophysical Research Letters. 38, doi: 10.1029/2011GL046768.

Schreiner, M., and K. Kreysing. 2013. Geotechnik Hydrogeologie, 4th ed. Springer.

Schubel, J. R. 1974. Gas bubbles and acoustically impenetrable, or turbid, character of some estuarine sediments, p. 275-298. In: I. R. Kaplan [eds.], Natural Gases in Marine Sediments. Plenum Press.

Singh, K. and R. K. Niven. 2013. Non-aqueous Phase Liquid Spills in Freezing and Thawing Soils: Critical Analysis of Pore-Scale Processes. Critical Reviews in Environmental Science and Technology. 43(6): 551-597, doi.org/10.1080/10643389.2011.604264.

Skinner, L. C., and I. N. McCave. 2003. Analysis and modelling of gravity- and piston coring based on soil mechanics. Marine Geology. 199: 181-204, doi: 10.1016/S0025-3227(03)00127-0.

Smith, D. G. 1992. Vibracoring: recent innovations. Journal of Paleolimnology. 7: 137-141, doi: doi.org/10.1007/BF00196868.

Smith, D. G. 1998. Vibracoring: a new method for coring deep lakes. Palaeogeography, Palaeoclimatology, Palaeoecology. 140: 433-440, doi: 10.1016/S0031-0182(98)00031-5.

Snider, L. J., B. R. Burnett, and R. R., Hessler. 1984. The composition and distribution of meiofauna and nanobiota in a central North Pacific deep-sea area. Deep Sea Research. 31: 1225-1249, doi: doi.org/10.1016/0198-0149(84)90059-1.

Stephenson, M., J. Klaverkamp, M. Motycka, C. L. Baron, and W. Schwartz. 1996. Coring artifacts and contaminant inventories in lake sediment. Journal of Paleolimnology. 15: 99-106, doi: doi.org/10.1007/BF00176992.

Stowe, D. AV., and A. E. Aksu. 1978. Disturbances in soft sediments due to piston coring. Marine Geology. 28: 135-144, doi: doi.org/10.1016/0025-3227(78)90101-9.

Strasser, D., H. J. Lensing, T. Nuber, D. Richter, S. Frank, N. Goeppert, and N. Goldscheider. 2015. Improved geohydraulic characterization of river bed sediments based on freeze-core sampling – development and evaluation of a new measurement approach. Journal of Hydrology. 527: 133-141, doi: 10.1016/j.jhydrol.2015.04.074.

Sumer, B. M., and J. Fredsøe. 2002. The Mechanics of Scour in the Marine Environment. World Scientific.

Taft, R. A., and C. Jones. 2001. Sediment Sampling Guide and Methodologies. State of Ohio. Environmental Protection Agency.

Tsytovich, N. A. 1975. The Mechanics of Frozen Ground, Scripta Book Company.

Varadharajan, C., and H. F. Hemond. 2012. Time series analysis of high resolution ebullition fluxes from a stratified, freshwater lake. Journal of Geophysical Research: Biogeosciences. 117: G02004, doi: 10.1029/2011JG001866.

Verschuren, D. 2000. Freeze coring soft sediments in tropical lakes. Journal of Paleolimnology. 24: 361-365, doi: doi.org/10.1023/A:1008191418497.

Vesilind, P. A., and J. Martel. 1990. Freezing of Water and Wastewater sludges. Journal of Environmental Engineering. 116: 854-862, doi: 10.1061/(ASCE)0733-9372(1990)116:5(854).

Wang, X.J., D. R. Hutchinson, S. G. Wu, S. X. Yang, and Y. G. Guo. 2011. Elevated gas hydrate saturation within silt and silty clay sediments in the Shenhu area, South China Sea. Journal of Geophysical Research. 116(5): B05102, doi: 10.1029/2010JB007944.

Weaver, P. P. E., and P. J. Schultheiss. 1983. Direction of penetration and sediment disturbance in open-barrel gravity cores. Journal of Sedimentary Petrology. 53: 649-564, doi: 10.1306/212F8256-2B24-11D7-8648000102C1865D.

Wever, T. F., F. Abegg, H. M. Fiedler, G. Fechner, and I. H. Stender. 1998. Shallow gas in the muddy sediments of Eckernförde Bay, Germany. Continental Shelf Research. 18: 1715-1739, doi: doi.org/10.1016/S0278-4343(98)00055-7.

Wik, M., P. M. Crill, R. K. Varner, and D. Bastviken. 2013. Multiyear measurements of ebullitive methane flux from three subarctic lakes. Journal of Geophysical Research: Biogeosciences. 118: 1307-1321, doi.org/10.1002/jgrg.20103.

Wilkinson, J., A. Maeck, Z. Alshboul, and A. Lorke. 2015. Continuous seasonal river ebullition measurements linked to sediment methane formation. Environmental Science and Technology. 49: 13121-13129, doi: 10.1021/acs.est.5b01525.

Wilkinson, J., P. Bodmer, and A. Lorke. 2019. Methane dynamics and thermal response in impoundments of the Rhine River, Germany. Science of The Total Environment. 659: 1045-1057, doi: doi.org/10.1016/j.scitotenv.2018.12.424.

Wright, H. E. Jr. 1993. Core compression. Limnology and Oceanography. 38, doi: 10.4319/lo.1993.38.3.0699.

Yvon-Durocher, G., A. P. Allen, D. Bastviken, R. Conrad, C. Gudasz, A. St-Pierre, et al. 2014. Methane fluxes show consistent temperature dependence across microbial to ecosystem scales. Nature. 507(7493): 488-491, doi: doi.org/10.1038/nature13164.

Supporting Information for

# Laboratory and Field Investigations on Freeze and Gravity Core Sampling and Assessment of Coring Disturbances with Implications on Gas Bubble Characterization

Y. Dück[1*], A. Lorke[2], C. Jokiel[1], J. Gierse[1]

[1] Cologne University of Applied Science, Institute of Hydraulic Engineering and Water Resources Management, Betzdorfer Str. 2, 50679 Cologne, Germany

[2] University of Koblenz-Landau, Institute for Environmental Sciences, Fortstr. 7, 76829 Landau, Germany

Corresponding author: Yannick Dück (yannick.dueck@th-koeln.de)

## Contents of this file

**Introduction**

Supplementary data herein includes the *in situ* sediment core physical properties (Table S1 and S2), gas bubble distribution of the field freezes cores (Fig. S1-S5), image sequence of the underwater camera showing the freeze corer sediment penetration process (Fig. S6), laboratory experiment sediment core data (Fig. S7-S35), field investigations sediment freeze core data (Fig. S36-S44), and CT scan images of Urft and Olsberg Reservoir (Fig. S45, S46), as well as a schematically representation of the coring disturbances evaluation (Fig. S47).

**Table S1.** Olsberg Reservoir sediment cores physical properties. FC refer to freezer corer and GC to gravity corer. * no data available

| Site | Sampling location | Corer type | Nomenclature | Water depth (m) | Mean water content (%) | Mean organic matter (%) | Mean wet bulk density (g/ml) | Volumetric gas content (%) |
|---|---|---|---|---|---|---|---|---|
| Olsberg | 1 | FC | Olsberg _FC1_ Tripod_0 | 1.7 | 62.7 | 10.1 | 1.269 | 0.6 |
| Olsberg | 1 | GC | Olsberg _GC1_Hammering_0 | 1.7 | 63.7 | 10.6 | 1.287 | 4.5 |
| Olsberg | 2 | FC | Olsberg _FC2_Tripod_0 | 0.8 | 66.5 | 12.6 | 1.232 | 0.6 |
| Olsberg | 2 | GC | Olsberg _GC2_Hammering_0 | 0.8 | * | * | * | 5.8 |
| Olsberg | 3 | FC | Olsberg _FC3_Tripod_0 | 0.8 | 63.9 | 17.6 | 1.304 | 1.2 |
| Olsberg | 3 | GC | Olsberg _GC3_Hammering_0 | 0.8 | * | * | * | 12.4 |
| Olsberg | 4 | FC | Olsberg _FC4_Tripod_0 | 0.8 | 60.5 | 22.5 | 1.320 | 0.3 |
| Olsberg | 4 | GC | Olsberg _GC4_Hammering_0 | 0.8 | * | * | * | 12.0 |
| Olsberg | 5 | FC | Olsberg _FC5_Tripod_0 | 2.5 | 69.5 | 12.5 | 1.191 | 0.6 |
| Olsberg | 5 | GC | Olsberg _GC5_Hammering_0 | 2.5 | 65.1 | 12.3 | 1.238 | 9.6 |

**Table S2.** Urft Reservoir sediment cores physical properties. FC refer to freezer corer and GC to gravity corer. * no data available

| Site | Sampling location | Corer type | Nomenclature | Water depth (m) | Mean water content (%) | Mean organic matter (%) | Mean wet bulk density (g/ml) | Volumetric gas content (%) |
|---|---|---|---|---|---|---|---|---|
| Urft | 1 | FC | Urft_FC1_Tripod_0 | 31.0 | 68.9 | 11.0 | 1.190 | 0.2 |
| Urft | 1 | GC | Urft_GC1_Hammering_0 | 31.0 | 61.7 | 12.7 | 1.214 | 10.5 |
| Urft | 1 | GC (frozen) | Urft_GC1(frozen)_Hammering_0 | 31.0 | * | * | * | 0.3 |
| Urft | 2 | FC | Urft_FC2_Tripod_7 | 22.3 | 62.5 | 13.2 | 1.170 | 0.2 |
| Urft | 2 | GC | Urft_GC2_Hammering_0 | 22.3 | 64.0 | 11.4 | 1.220 | 11.2 |
| Urft | 2 | GC (frozen) | Urft_GC2(frozen)_Hammering_0 | 22.3 | * | * | * | 2.9 |
| Urft | 3 | FC | Urft_FC3_Tripod_4 | 10.4 | 60.2 | 13.1 | 1.206 | 2.0 |
| Urft | 3 | GC | Urft_GC3_Hammering_0 | 10.4 | 69.4 | 14.7 | 1.152 | 10.9 |
| Urft | 3 | GC (frozen) | Urft_GC3(frozen)_Hammering_0 | 10.4 | * | * | * | 5.6 |
| Urft | 4 | FC | Urft_FC4_Tripod_4 | 5.1 | 67.9 | 16.9 | 1.212 | 1.2 |

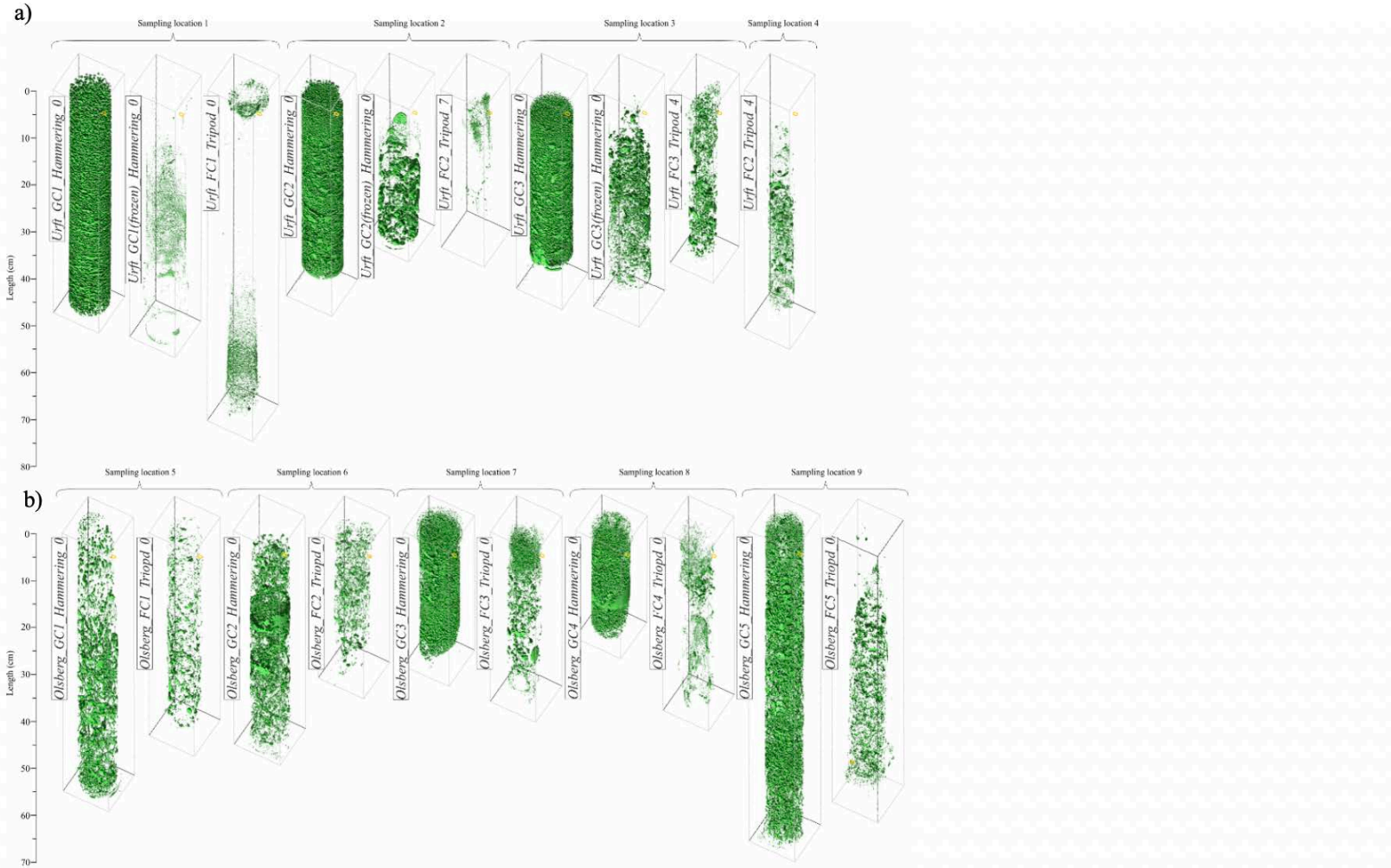


**Figure S1.** 3D gas bubble visualization of Urft (a) Olsberg Reservoir (b) sediment cores. 0 cm indicates the position of the sediment-water interface.

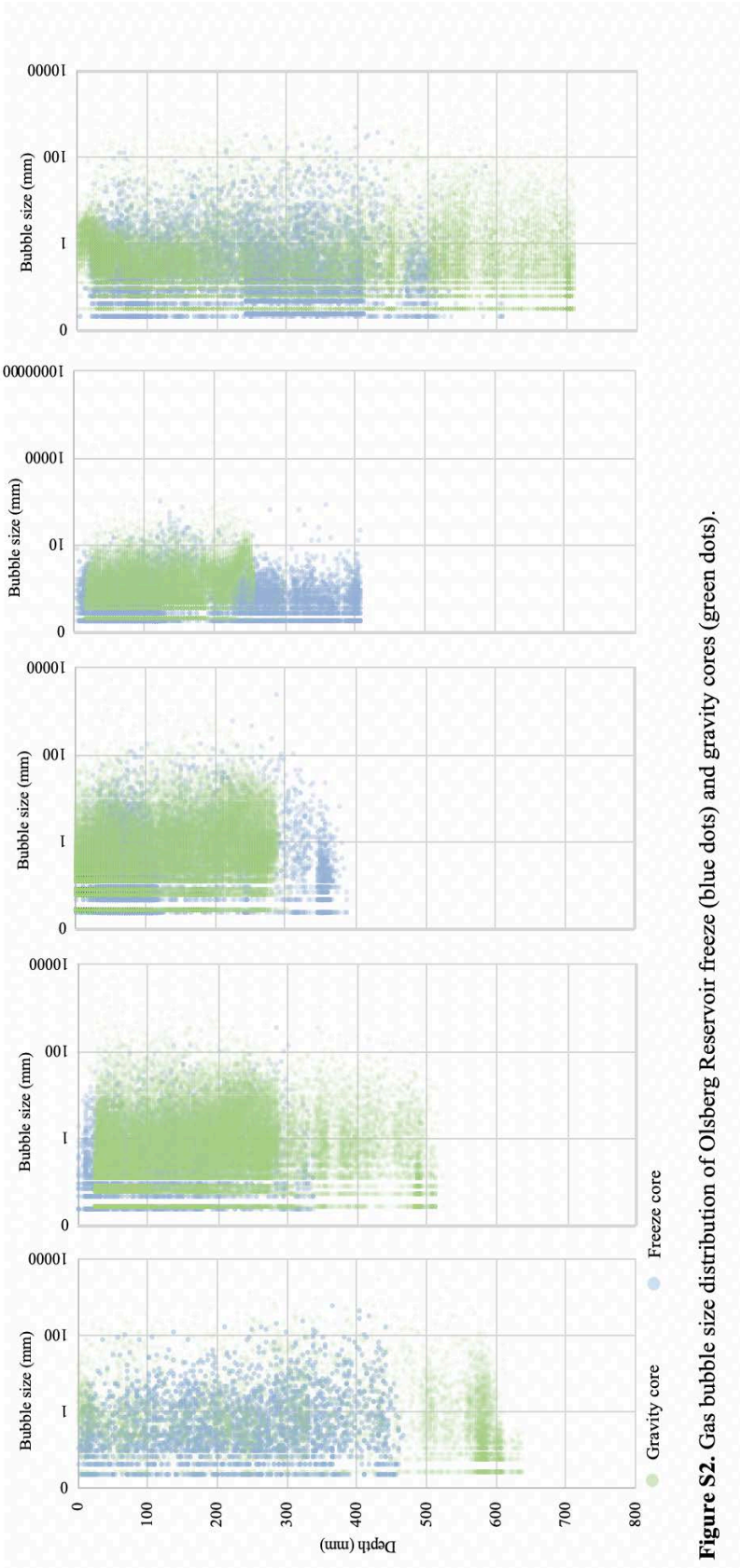


**Figure S2.** Gas bubble size distribution of Olsberg Reservoir freeze (blue dots) and gravity cores (green dots).

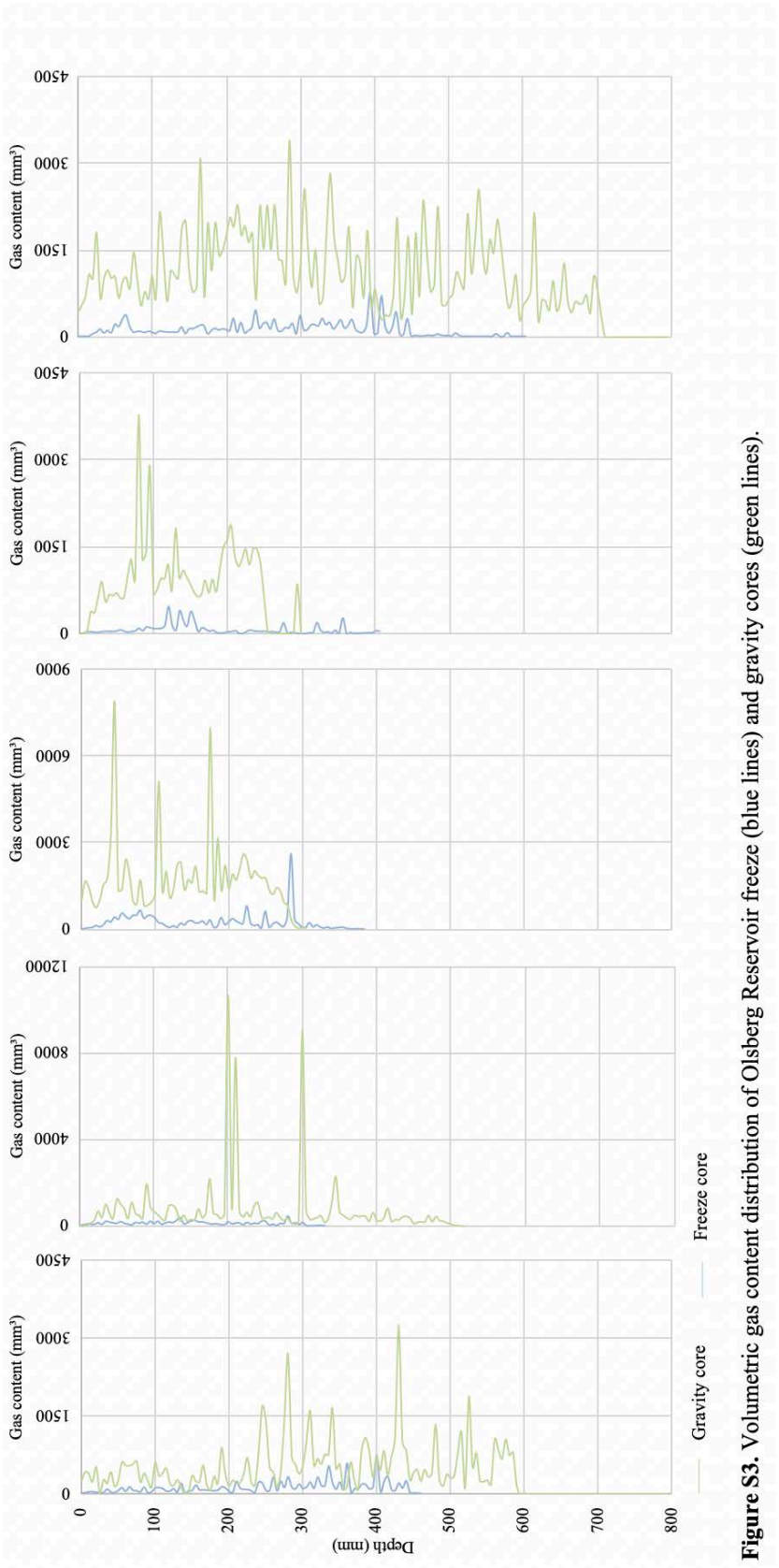


**Figure S3.** Volumetric gas content distribution of Olsberg Reservoir freeze (blue lines) and gravity cores (green lines).

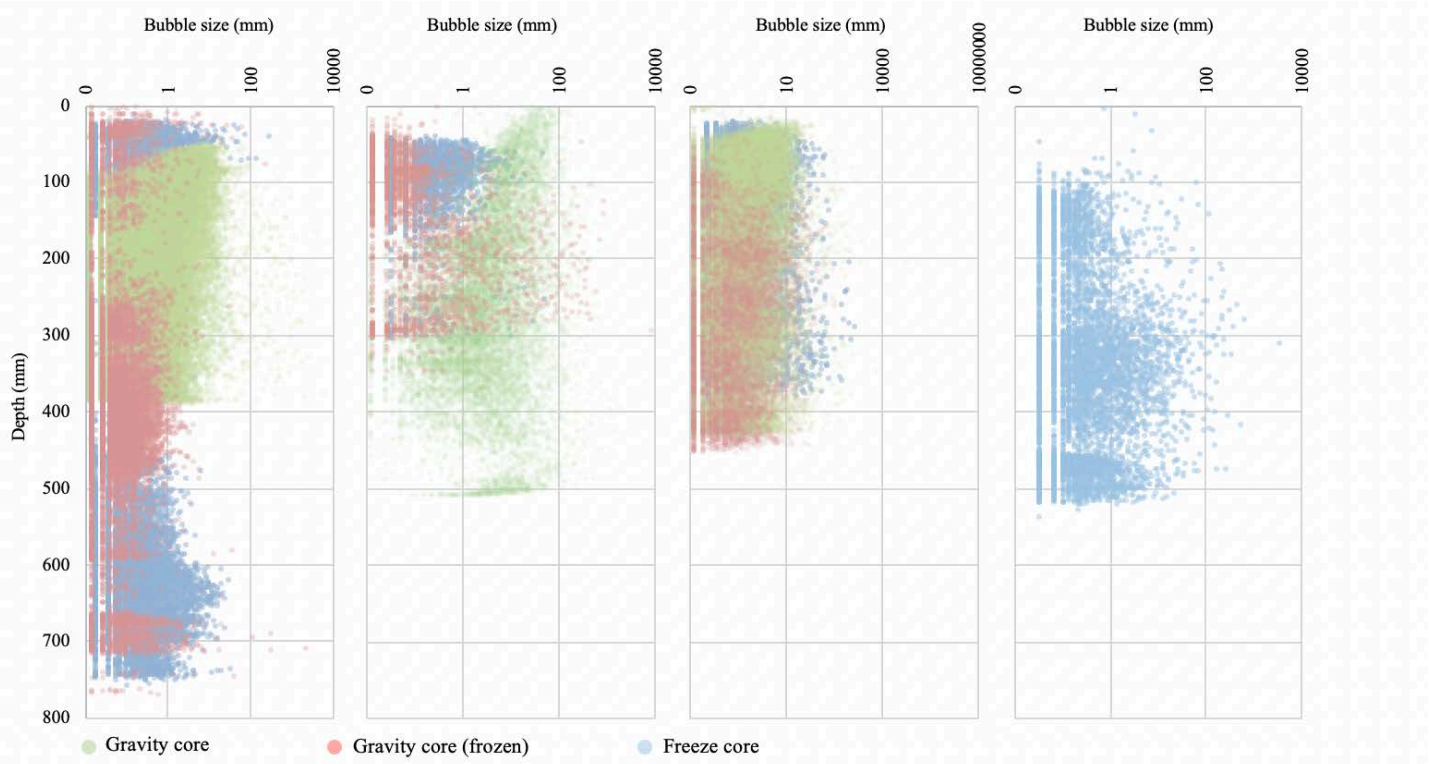


**Figure S4.** Gas bubble size distribution of Urft Reservoir freeze (blue dots), frozen gravity (red dots) and gravity cores (blue dots).

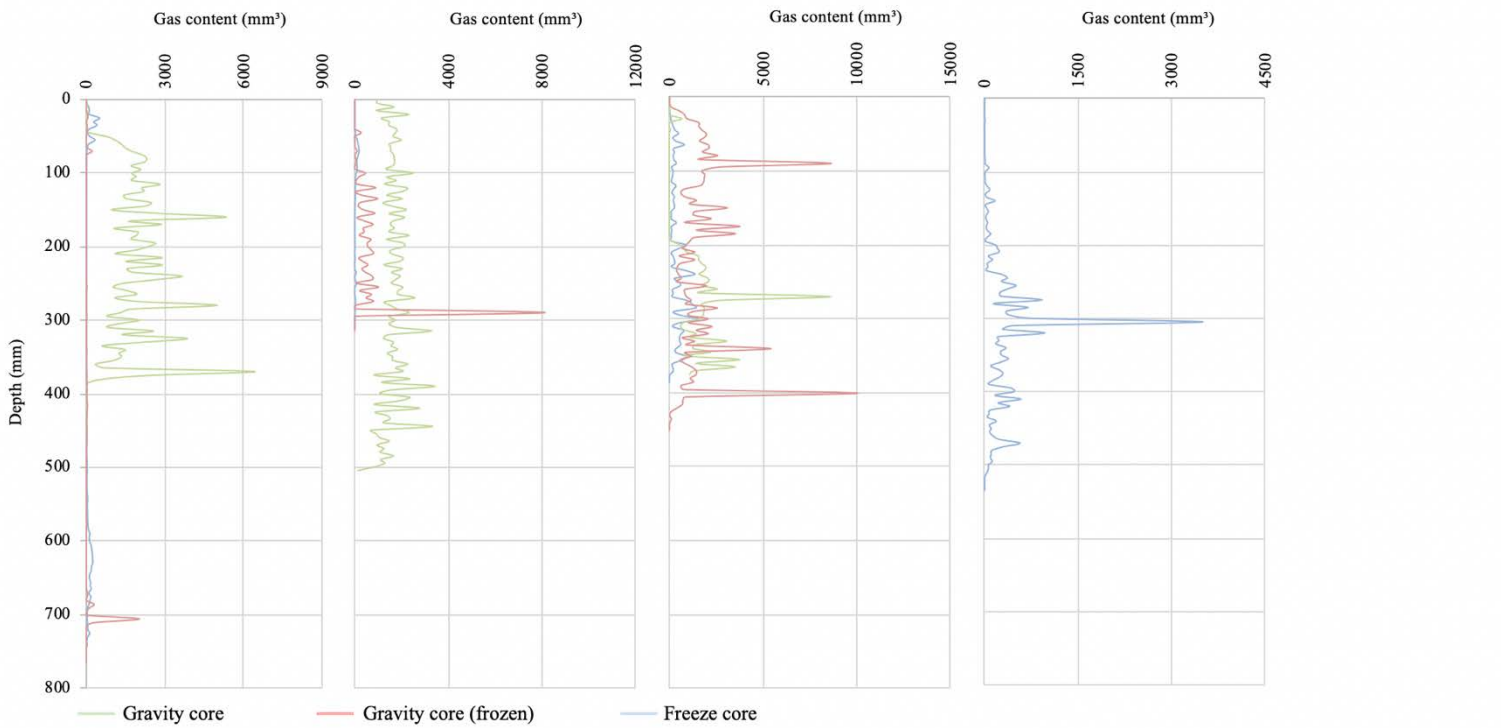


**Figure S5.** Volumetric gas content distribution of Urft Reservoir freeze (blue lines), frozen gravity (red lines) and gravity cores (green lines)

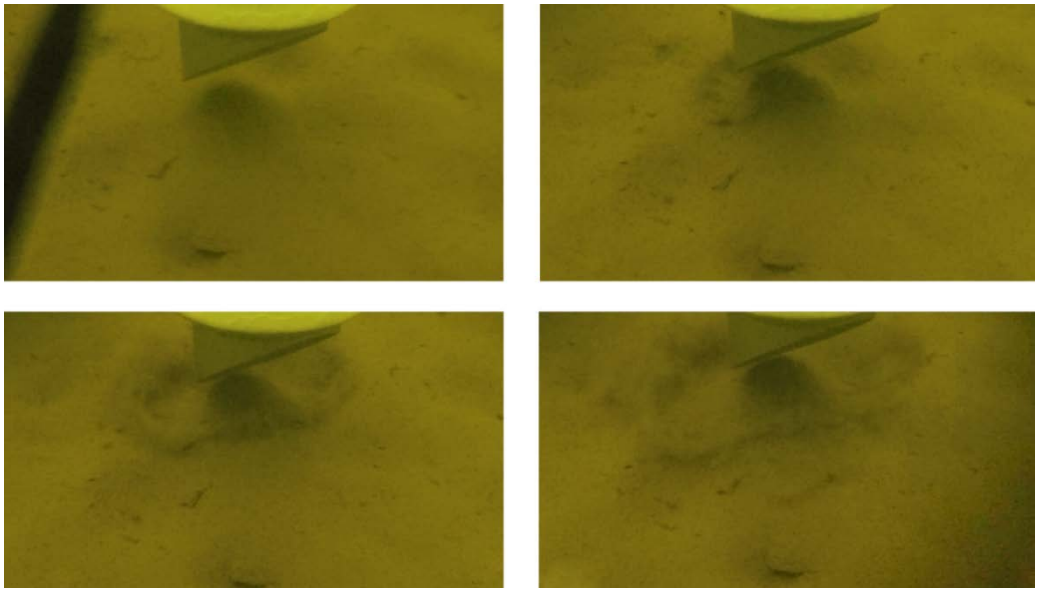

**Figure S6.** Image sequence showing the freeze corer penetration process at Urft Reservoir, recorded with an underwater camera (GoPro 4 Black: up to 4K/30 fps; waterproofed up to 40 m water depth) an illumination system. A hydraulic shock wave washed away the surficial, fluffy sediment.

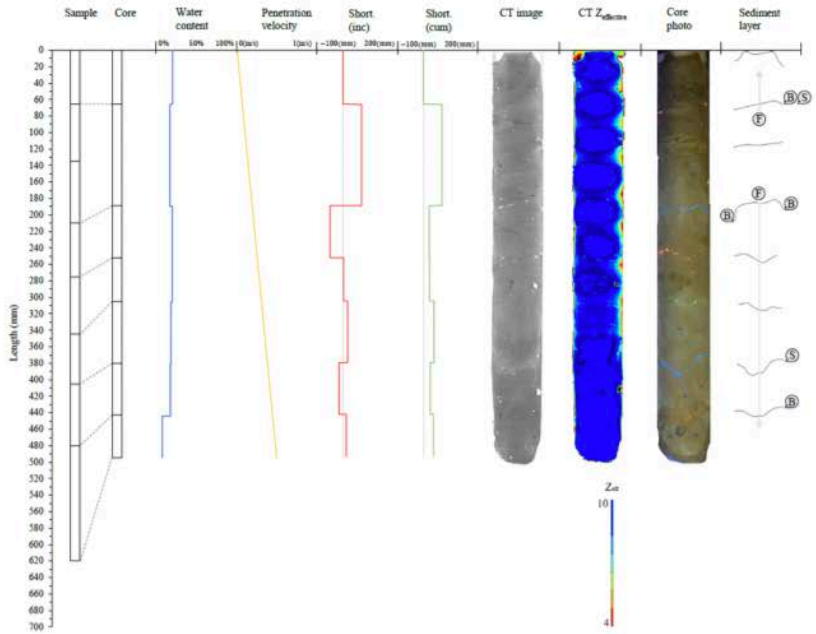


**Figure S7.** Laboratory experiment core: *Lab_FC1_Silt_Constant_0.* Bar chart shows the sediment stratigraphy before sampling and the stratigraphy of the core after sampling. Each horizontal line in the bar charts represents a fluorescent pigment layer. The dashed lines connect the (fluorescent) layer of the sediment sample and the core after sampling, thereby showing how each layer is affected by shortening. The blue line represents the water content distribution and the yellow line the penetration velocity over core length. The red and the green line is the incremental and cumulative shortening over core length, respectively, showing the shortening pattern. X-Ray CT scan image is shown as binary image. CT $Z_{eff}$ scan image shows of the effective atomic number distribution. Core photo shows the photography under UV light, while illuminating the fluorescent pigment layer. Sediment layer showing the digitized sediment layer and the type and location of the coring disturbances (bending (B), smearing (S), and freezing (F), where the relocation of the sediment layer are shown as an arrow in upward- and downward-direction), is shown.

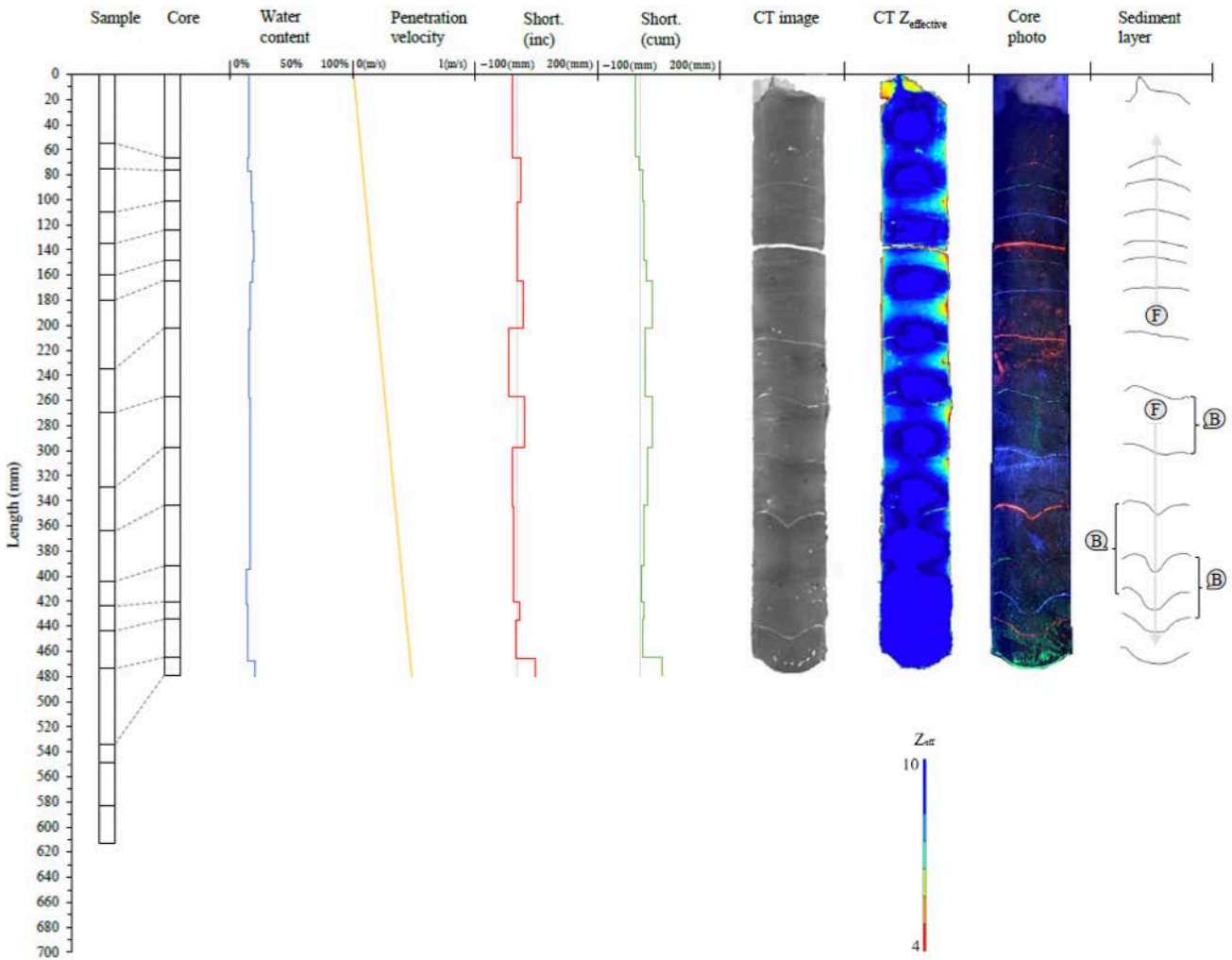


**Figure S8.** Laboratory experiment core: *Lab_FC2_Silt_Constant_0*.

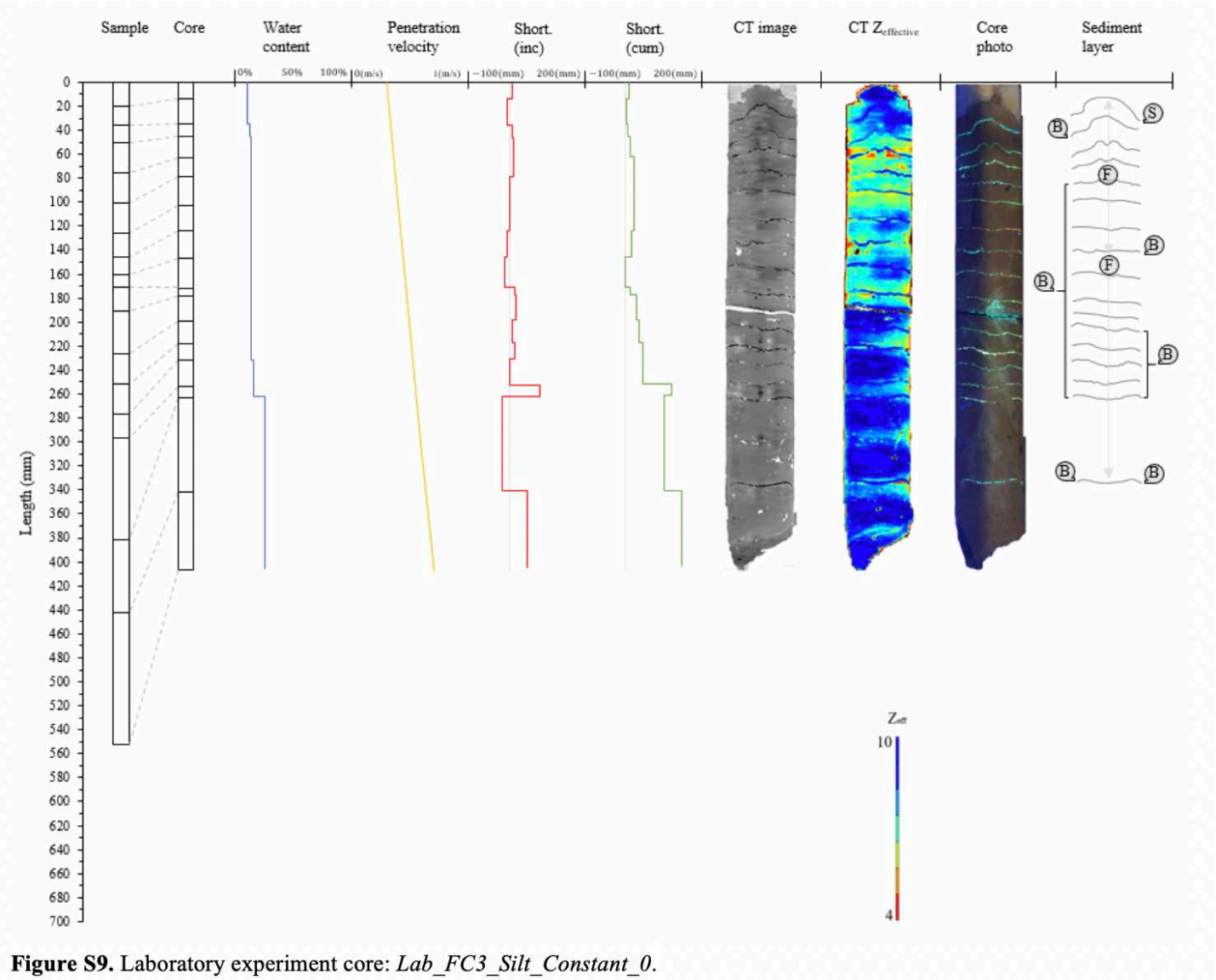


**Figure S9.** Laboratory experiment core: *Lab_FC3_Silt_Constant_0*.

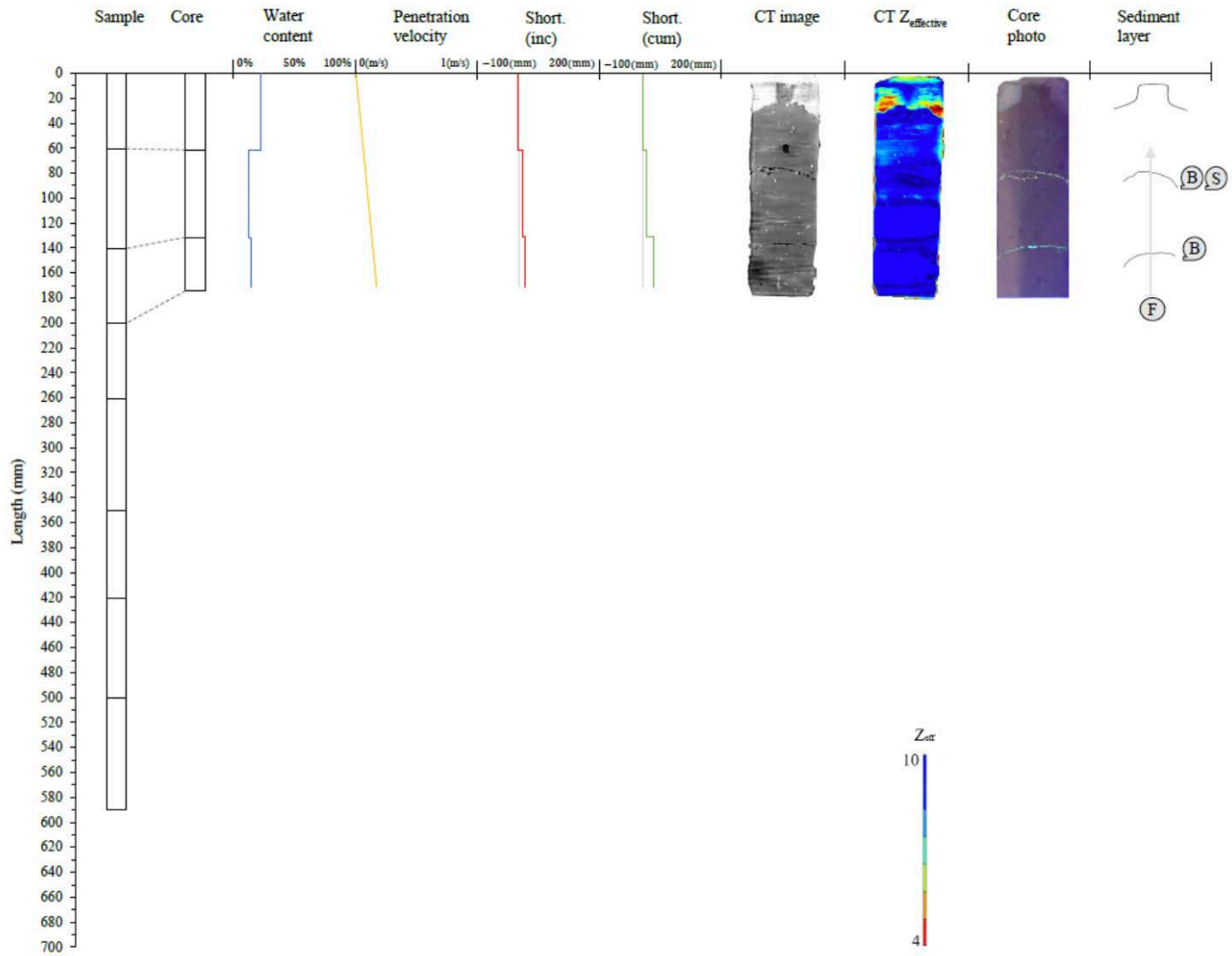


**Figure S10.** Laboratory experiment core: *Lab_FC4_Silt_Constant_0*.

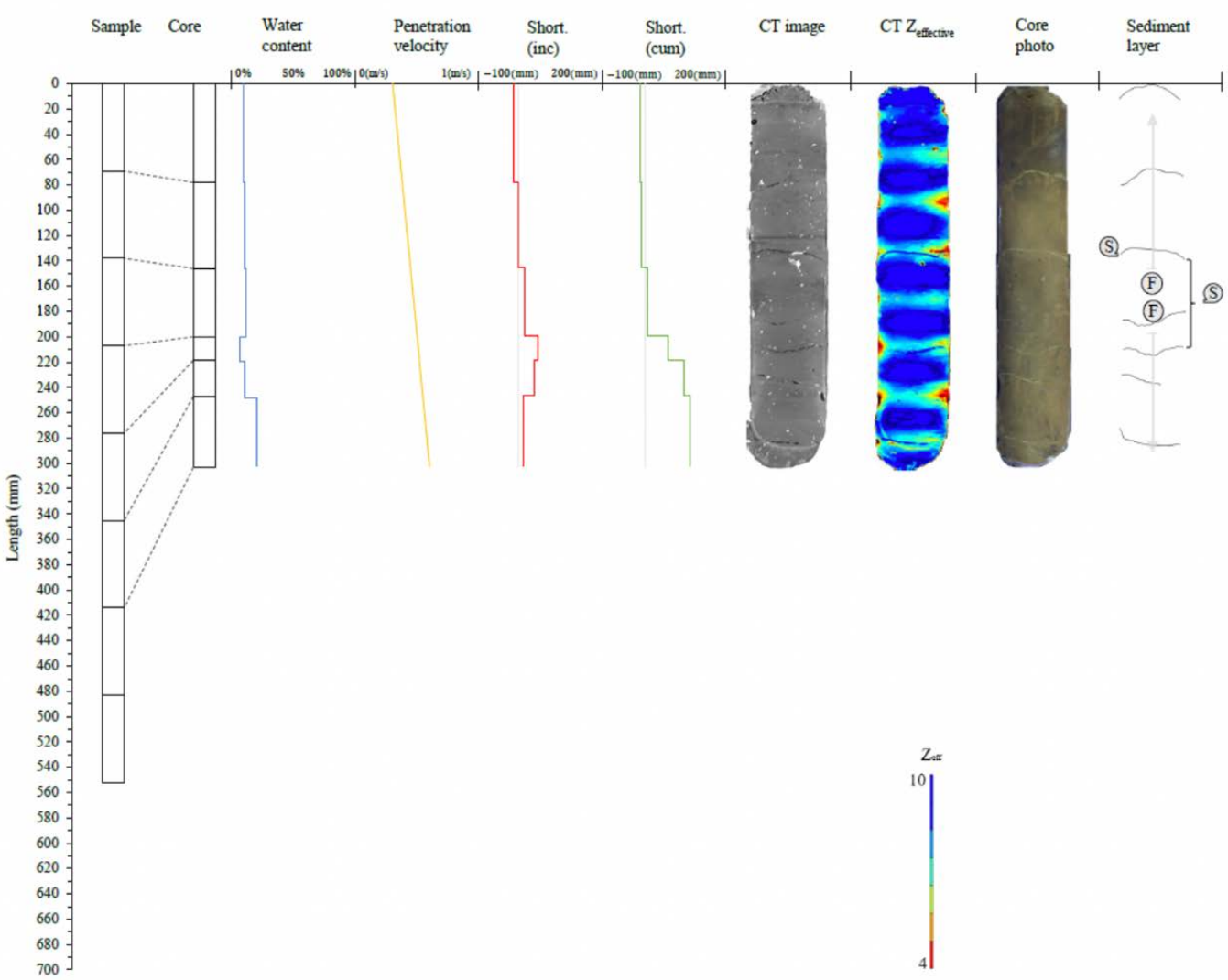


**Figure S11.** Laboratory experiment core: *Lab_FC5_Silt_Constant*.

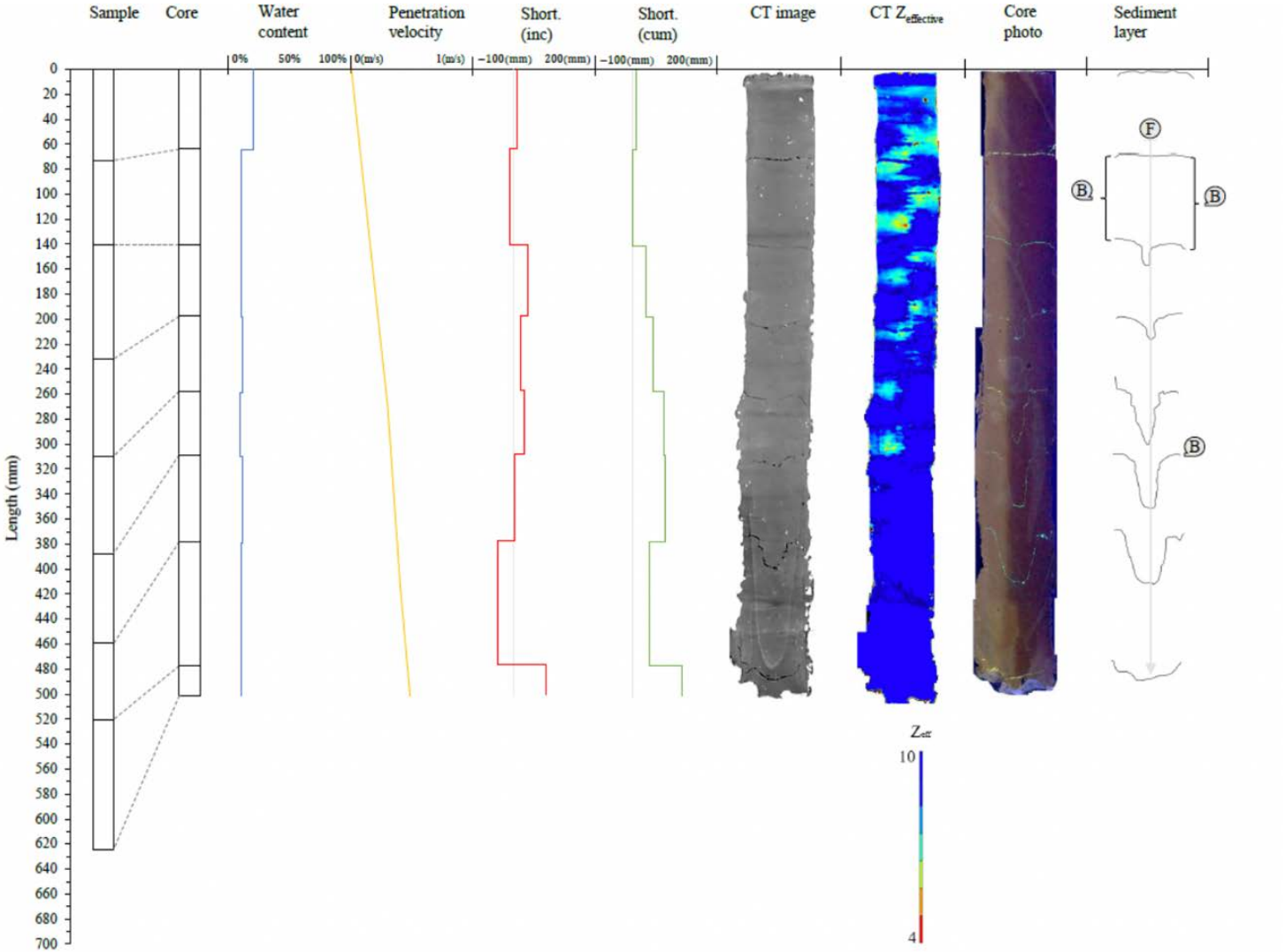


**Figure S12.** Laboratory experiment core: *Lab_FC6_Silt_Tripod_0*.

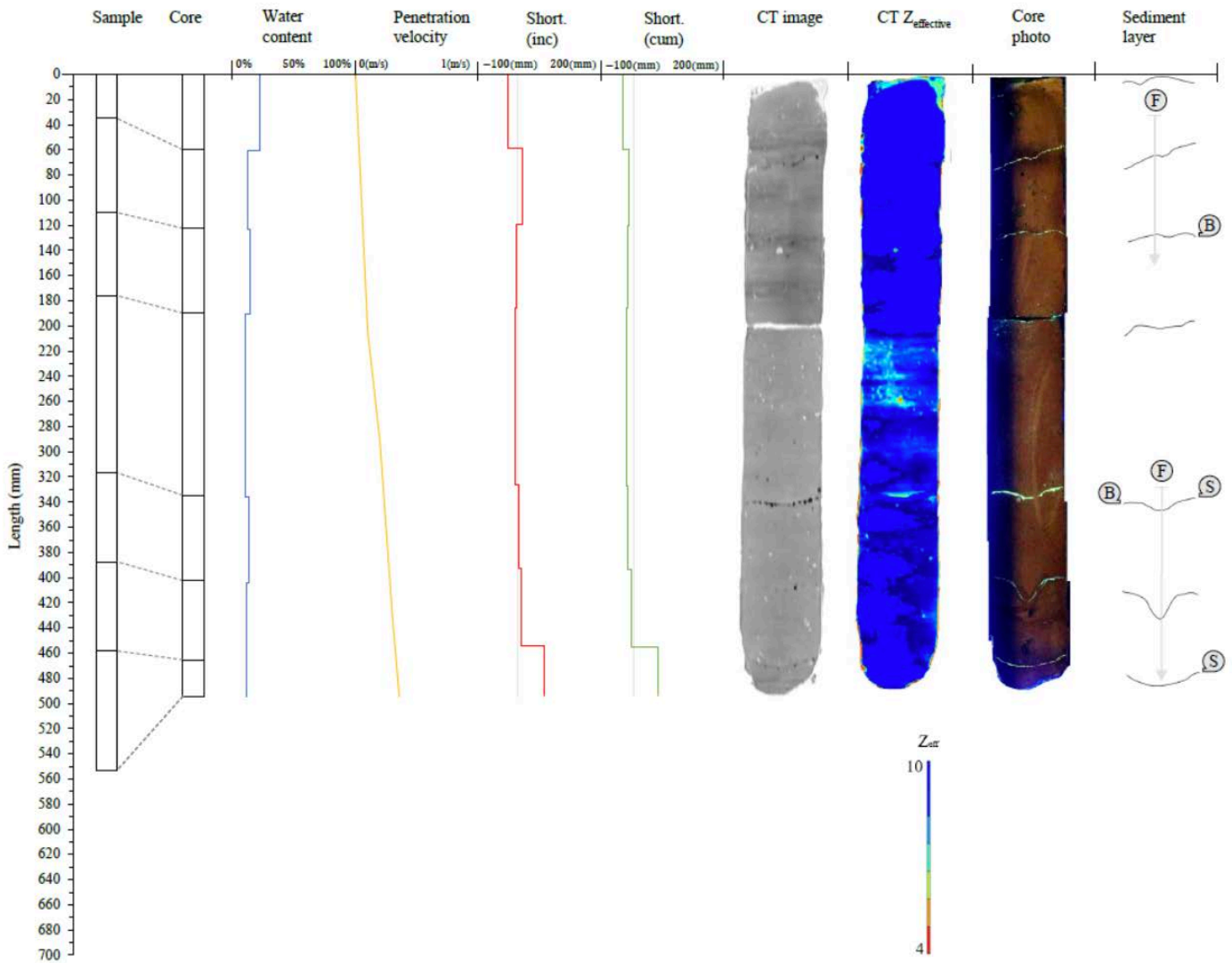


**Figure S13.** Laboratory experiment core: *Lab_FC7_Silt_Tripod_0*.

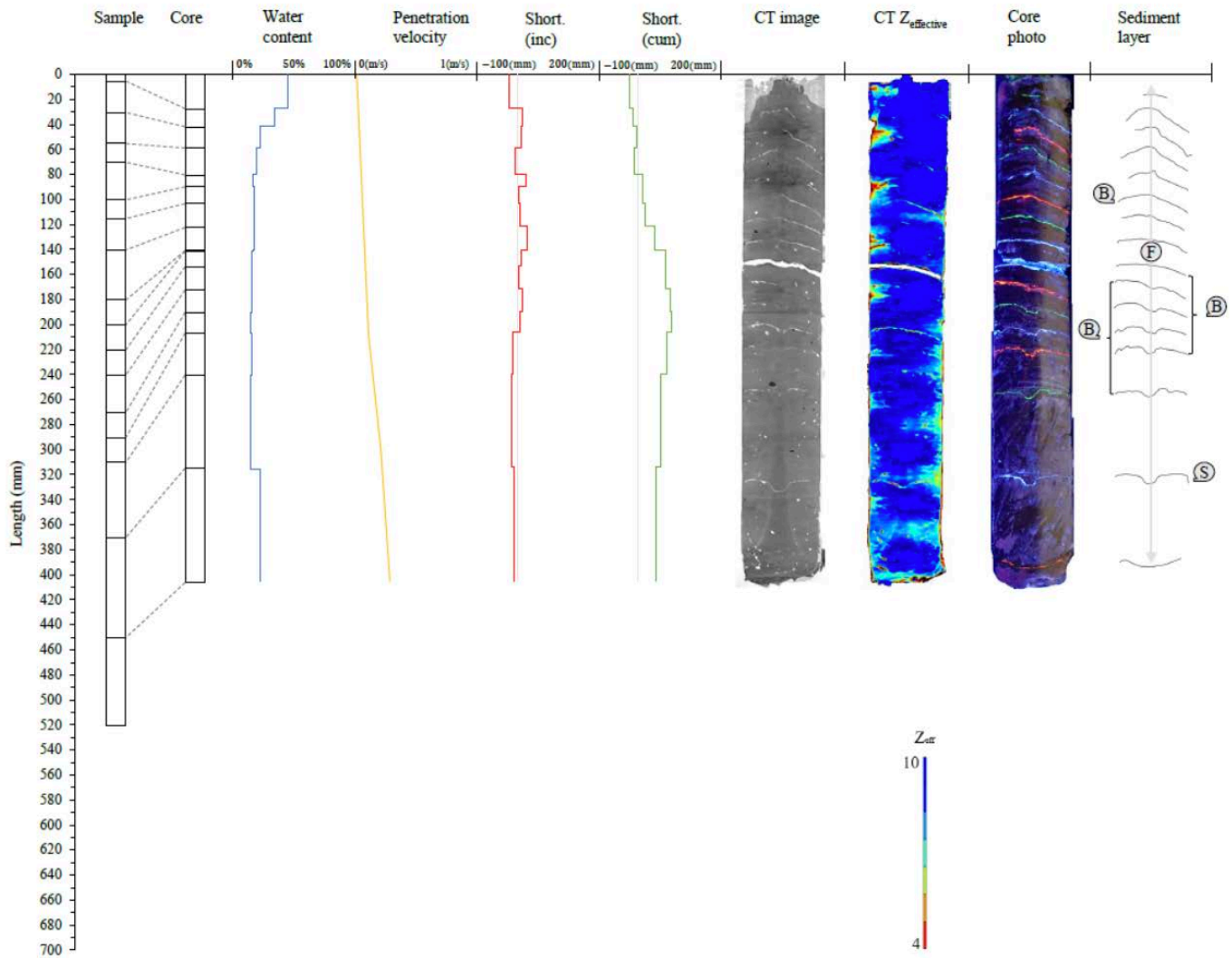


**Figure S14.** Laboratory experiment core: *Lab_FC8_Silt_Tripod_0*.

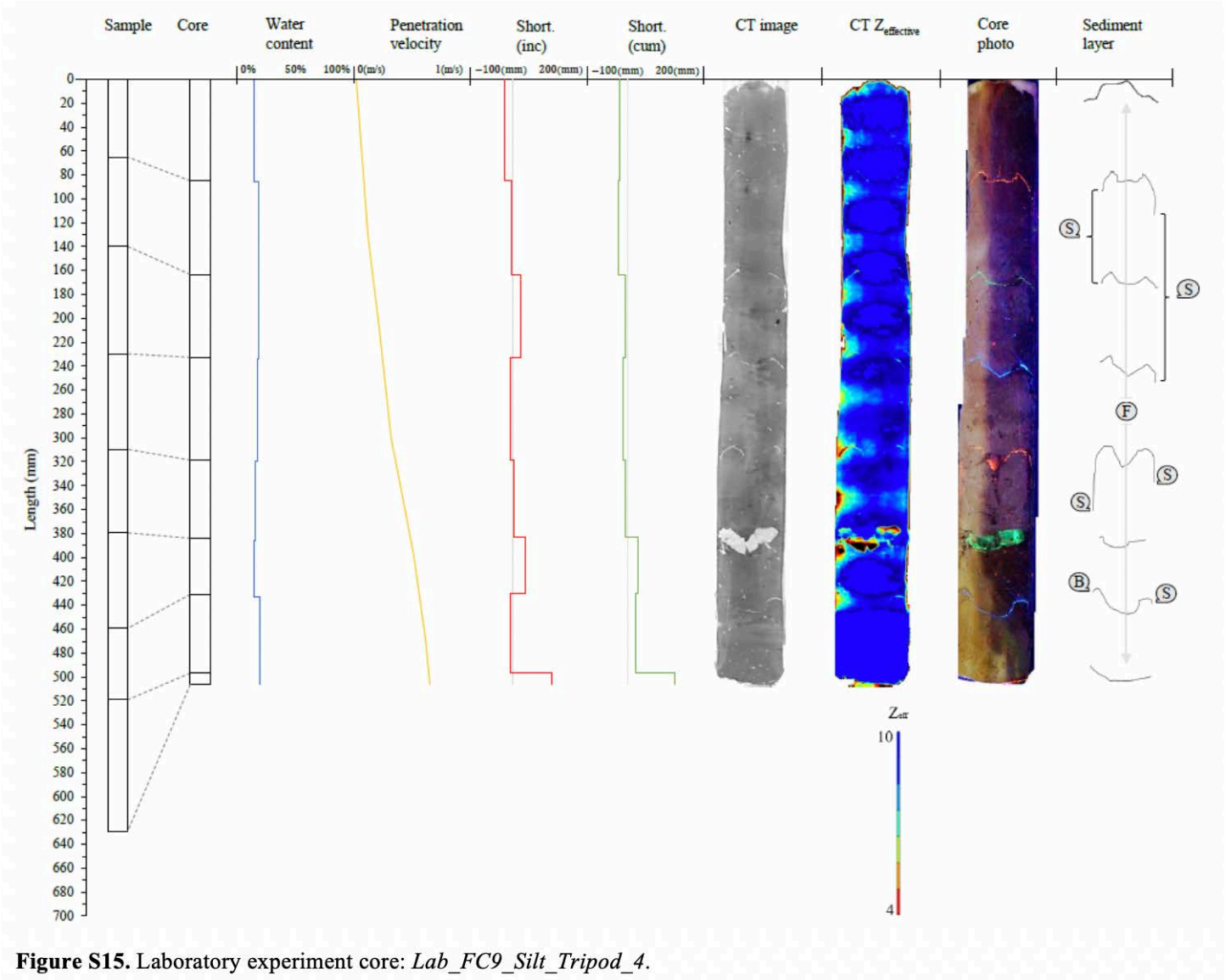


**Figure S15.** Laboratory experiment core: *Lab_FC9_Silt_Tripod_4*.

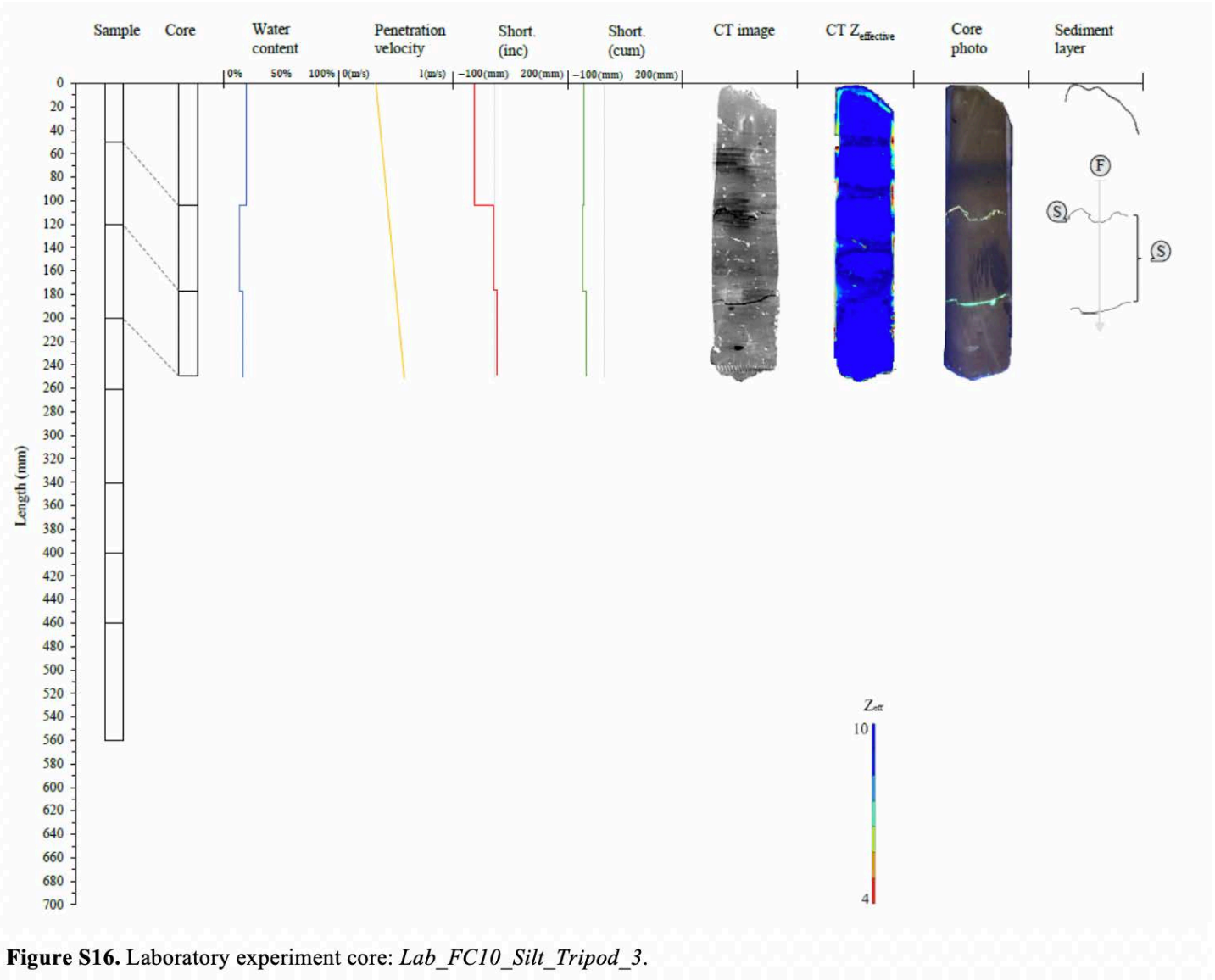


**Figure S16.** Laboratory experiment core: *Lab_FC10_Silt_Tripod_3*.

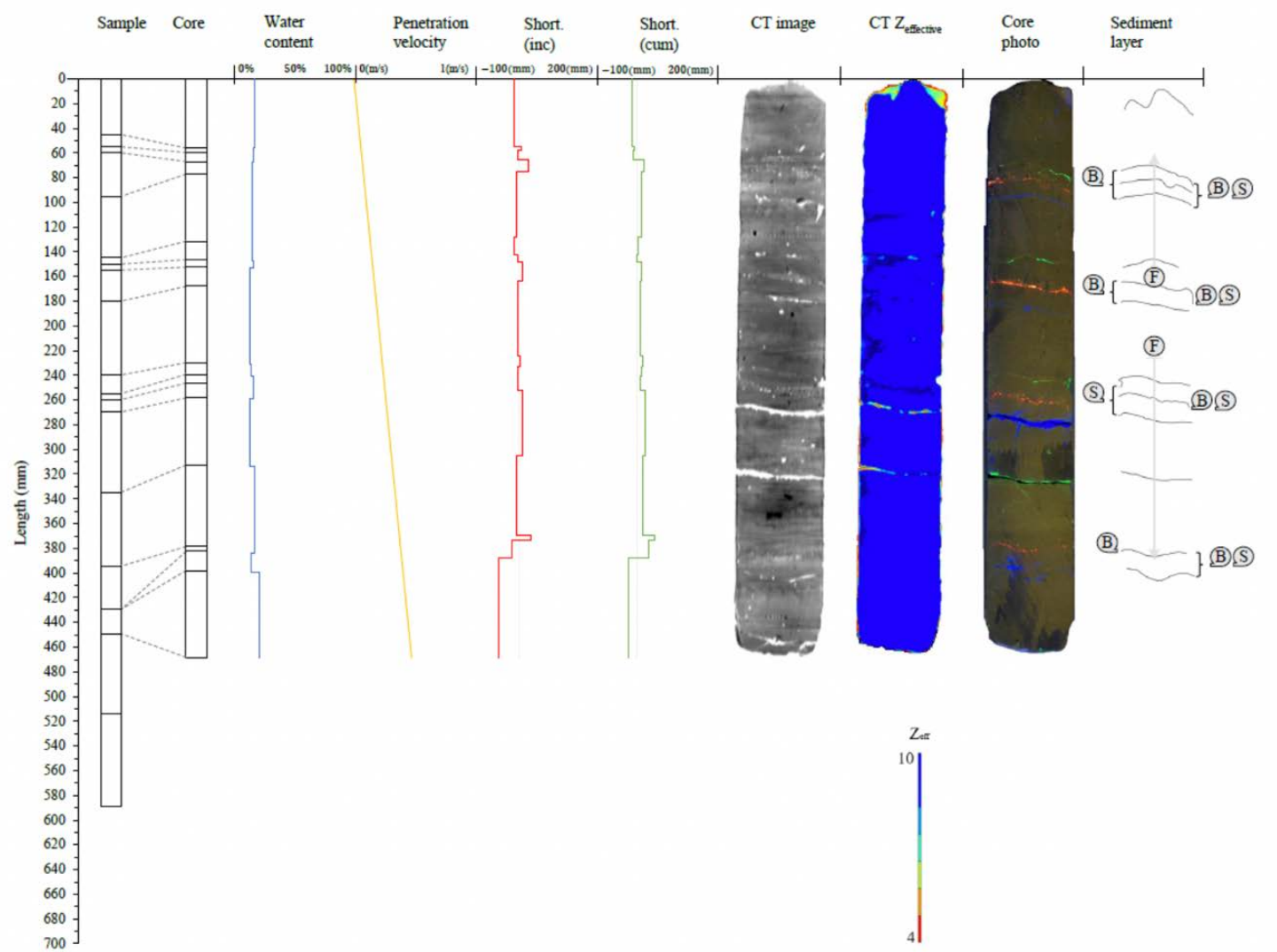


**Figure S17.** Laboratory experiment core: *Lab_FC11_SiltSand_Constant_0*.

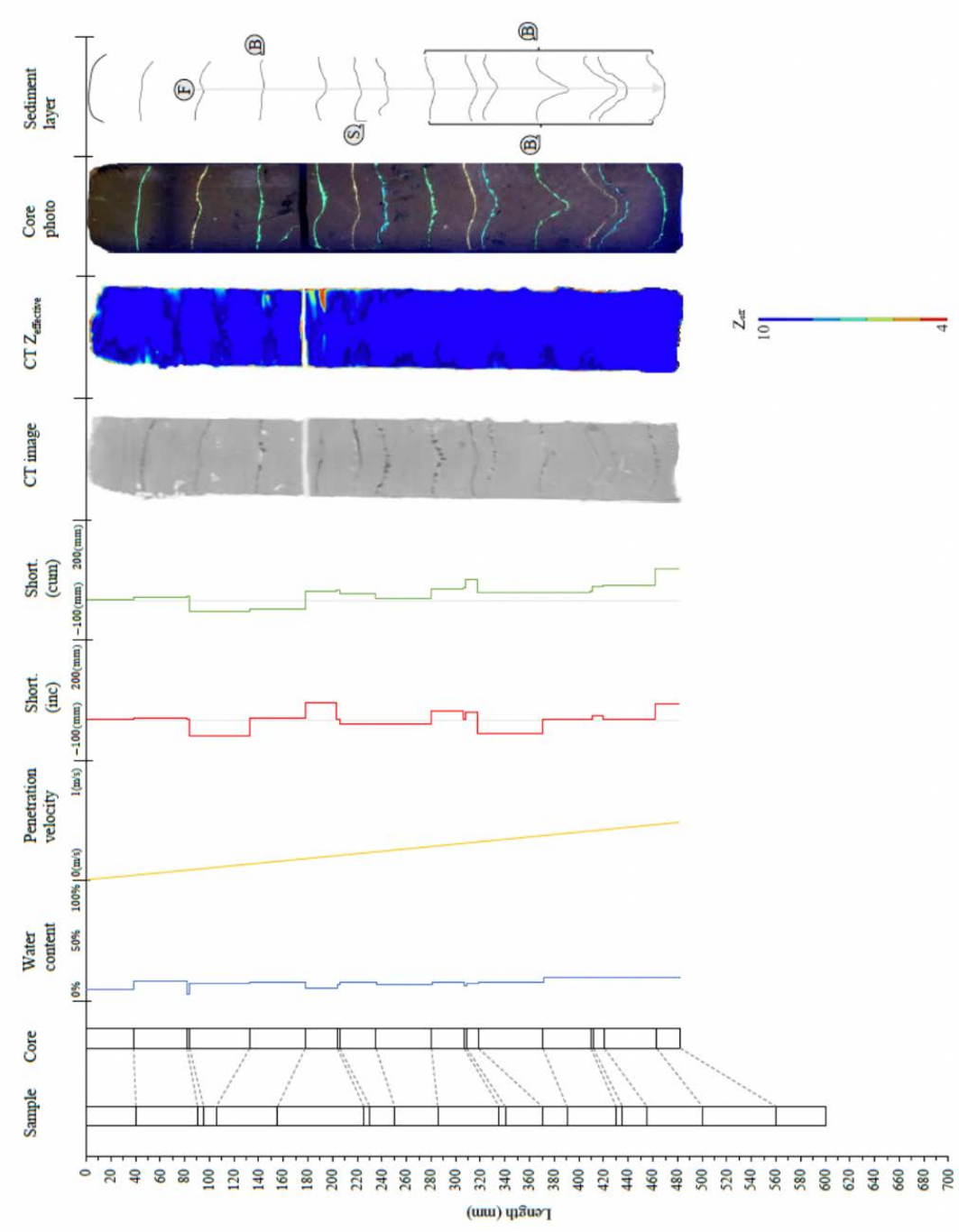


**Figure S18.** Laboratory experiment core: *Lab_FC12_SiltSand_Constant_0*.

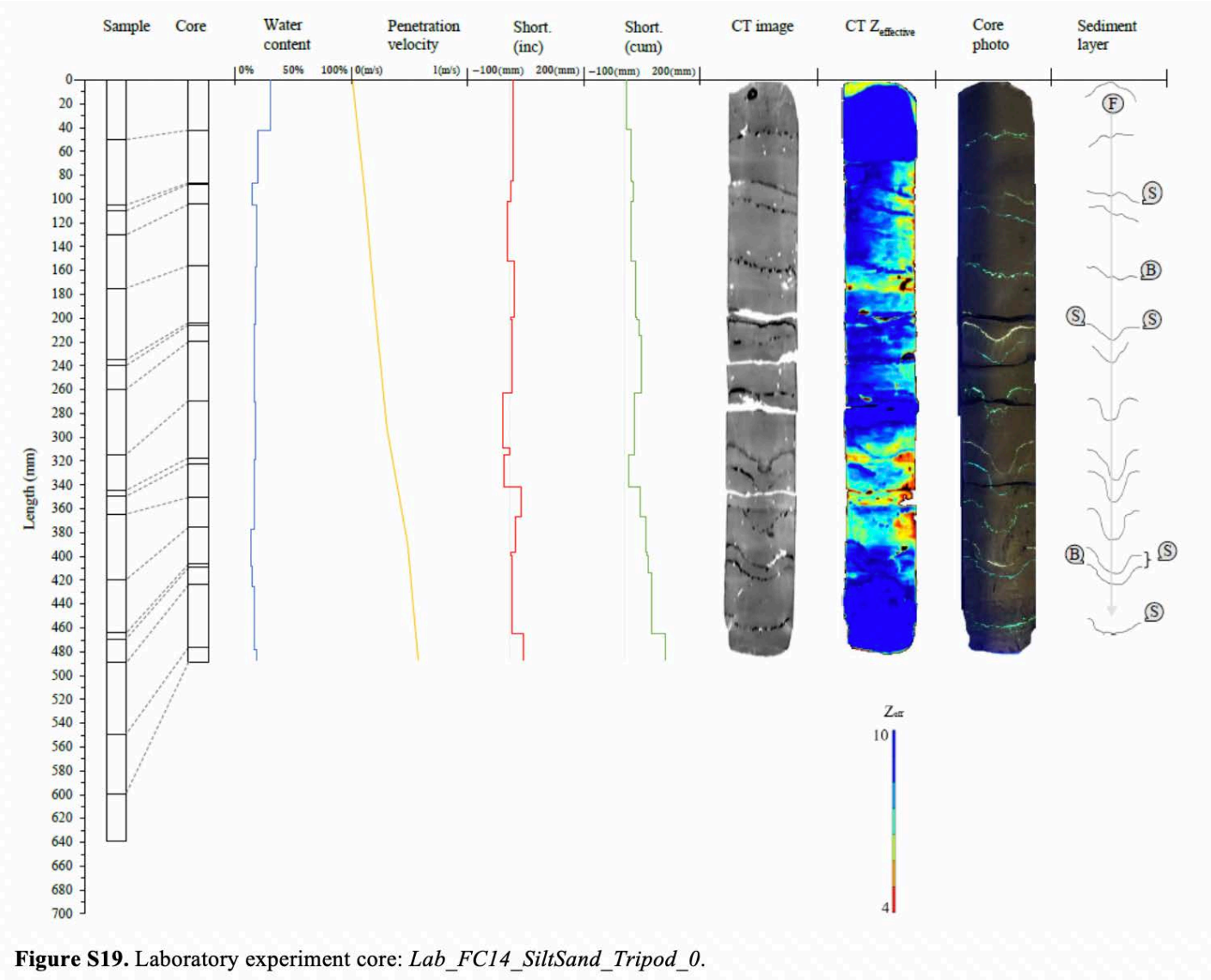


**Figure S19.** Laboratory experiment core: *Lab_FC14_SiltSand_Tripod_0*.

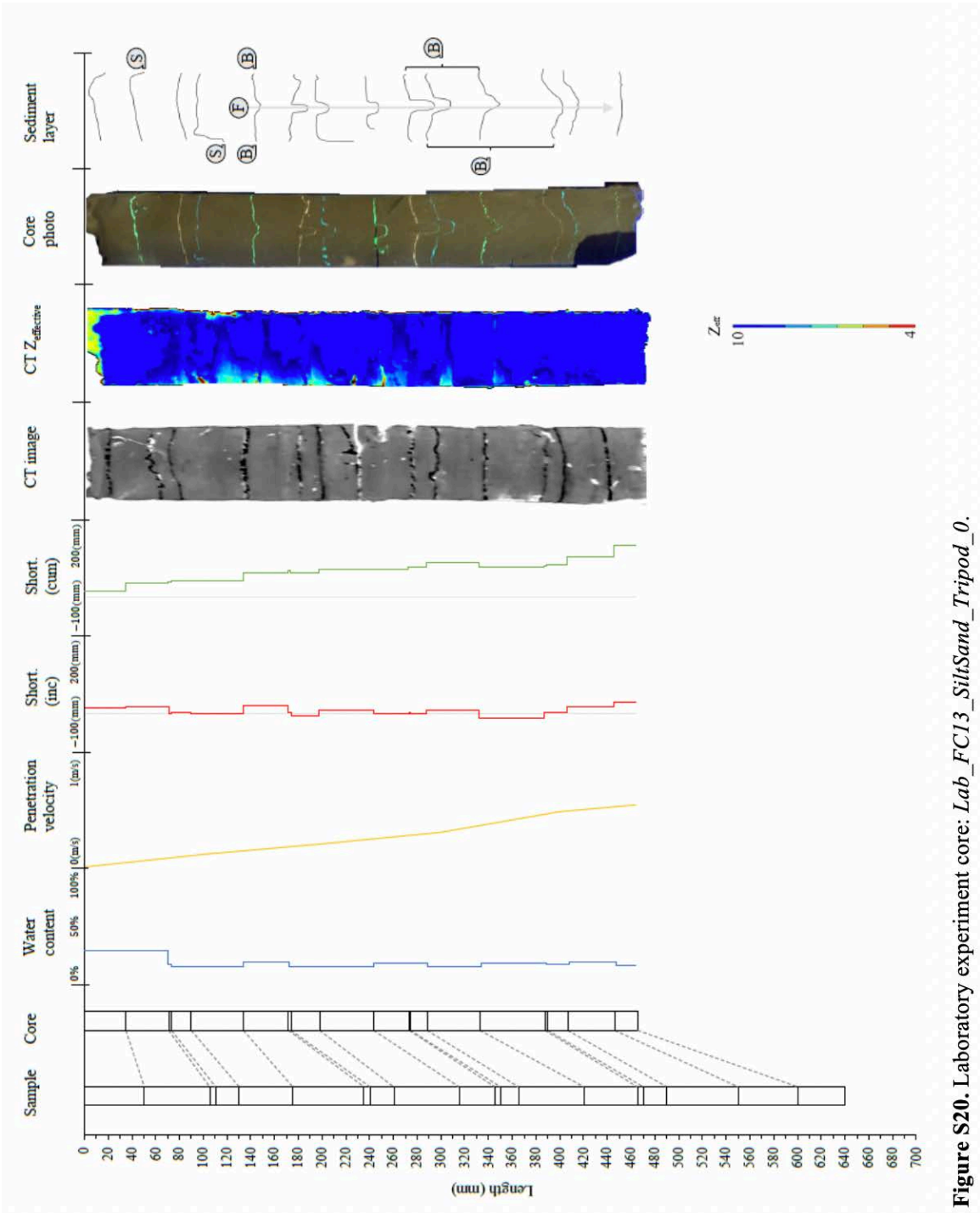


**Figure S20.** Laboratory experiment core: *Lab_FC13_SiltSand_Tripod_0.*

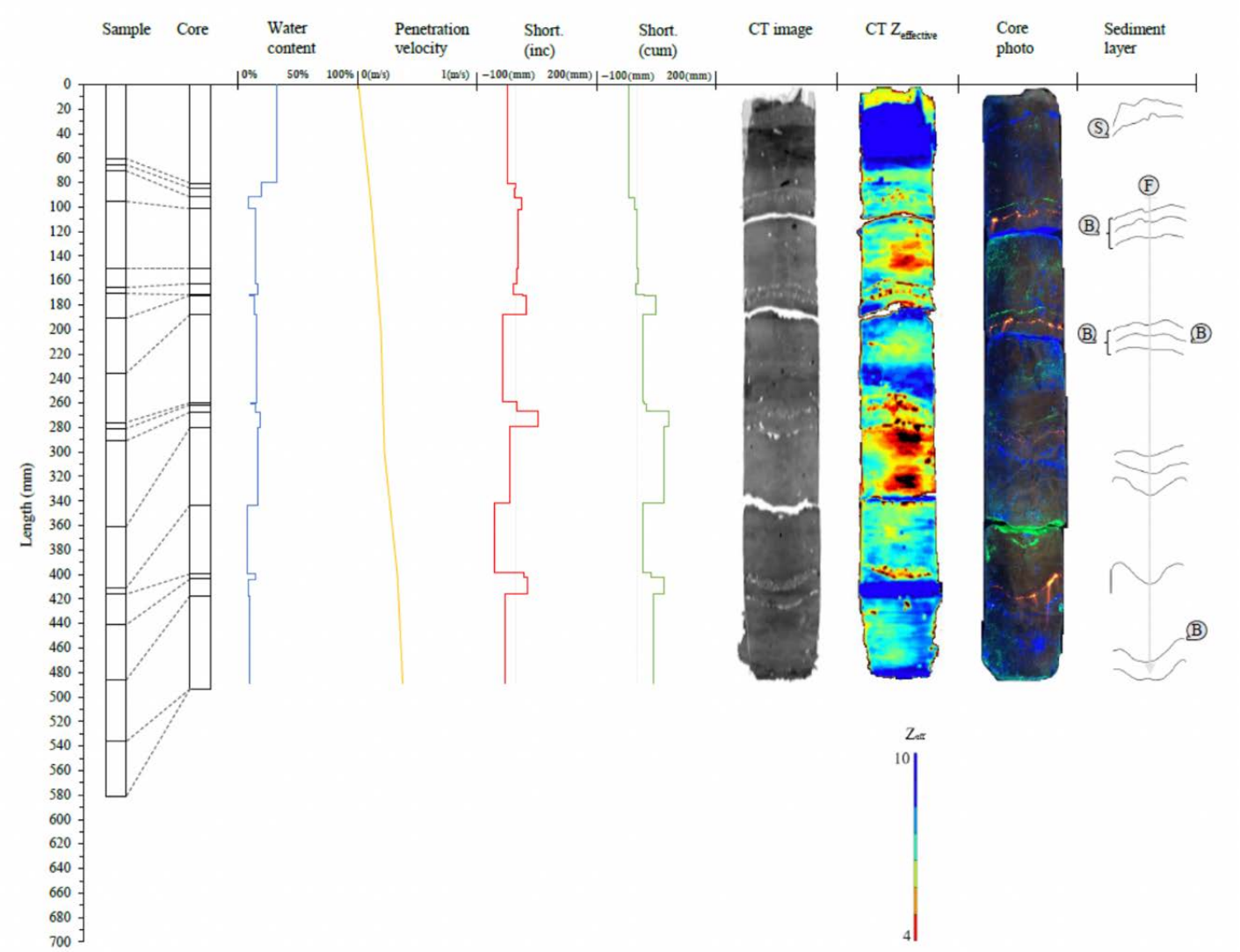


**Figure S21.** Laboratory experiment core: *Lab_FC15_SiltSand_Tripod_1*.

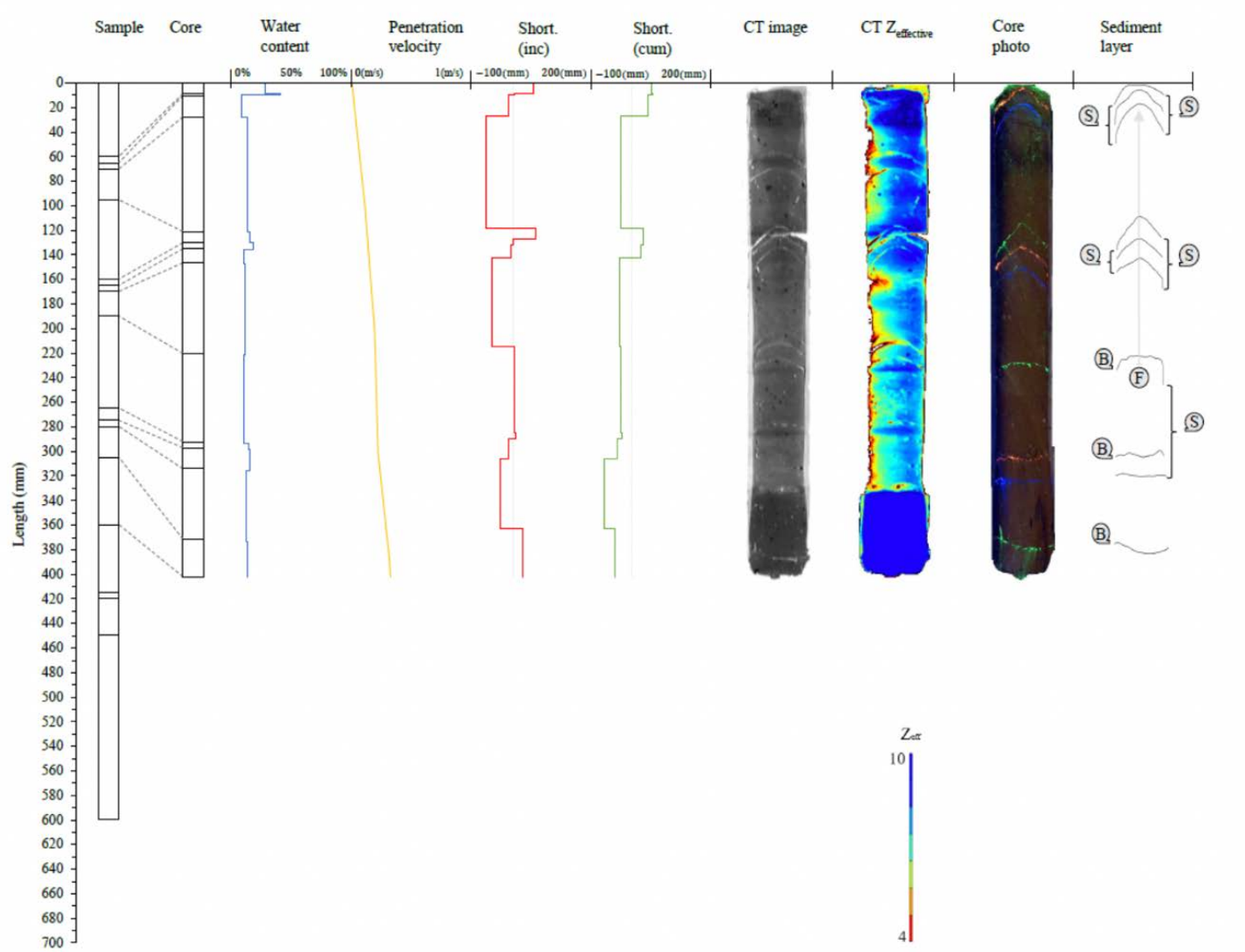


**Figure S22.** Laboratory experiment core: *Lab_FC16_SiltSand_Tripod_5*.

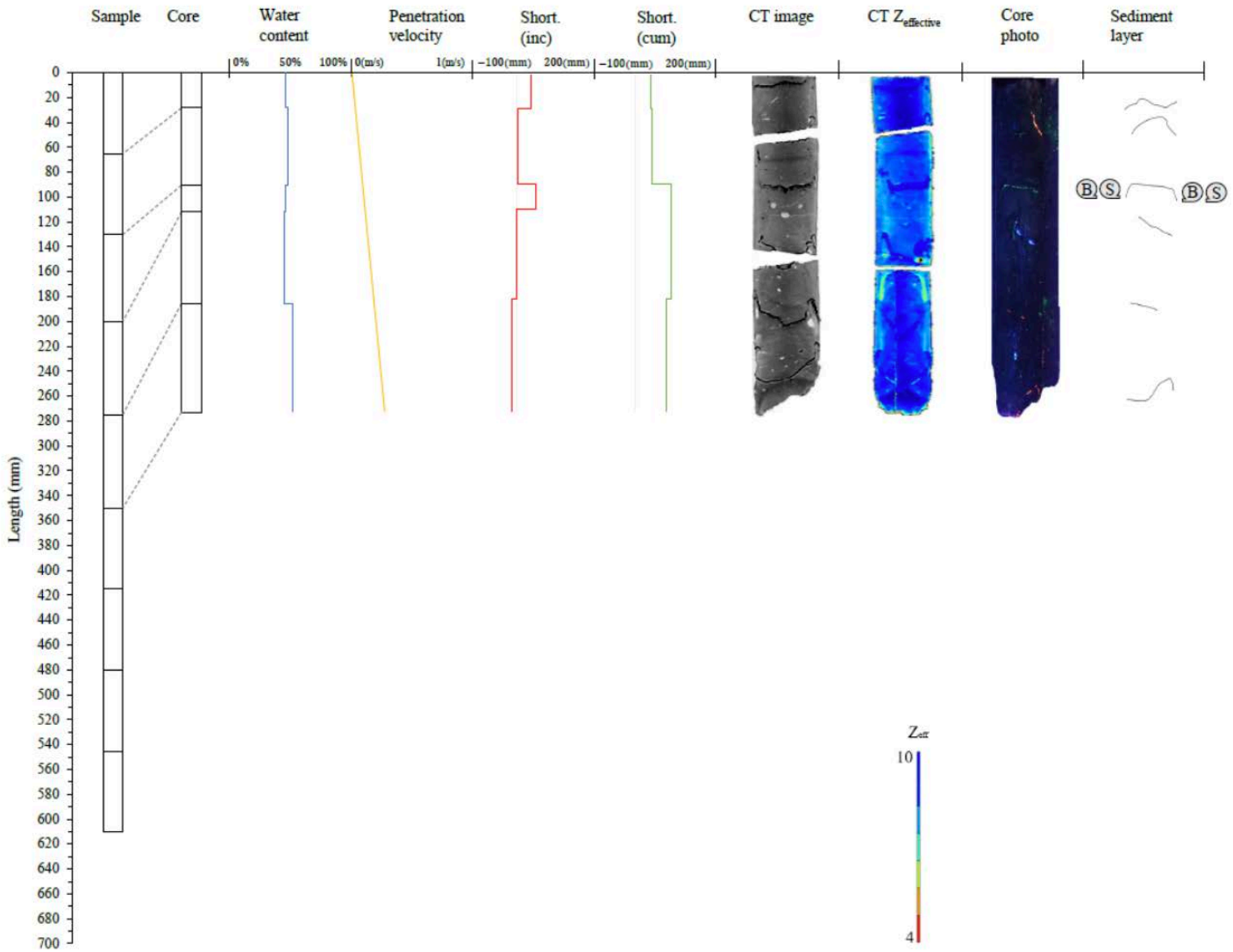


**Figure S23.** Laboratory experiment core: *Lab_FC17_Olsberg_Constant_0*.

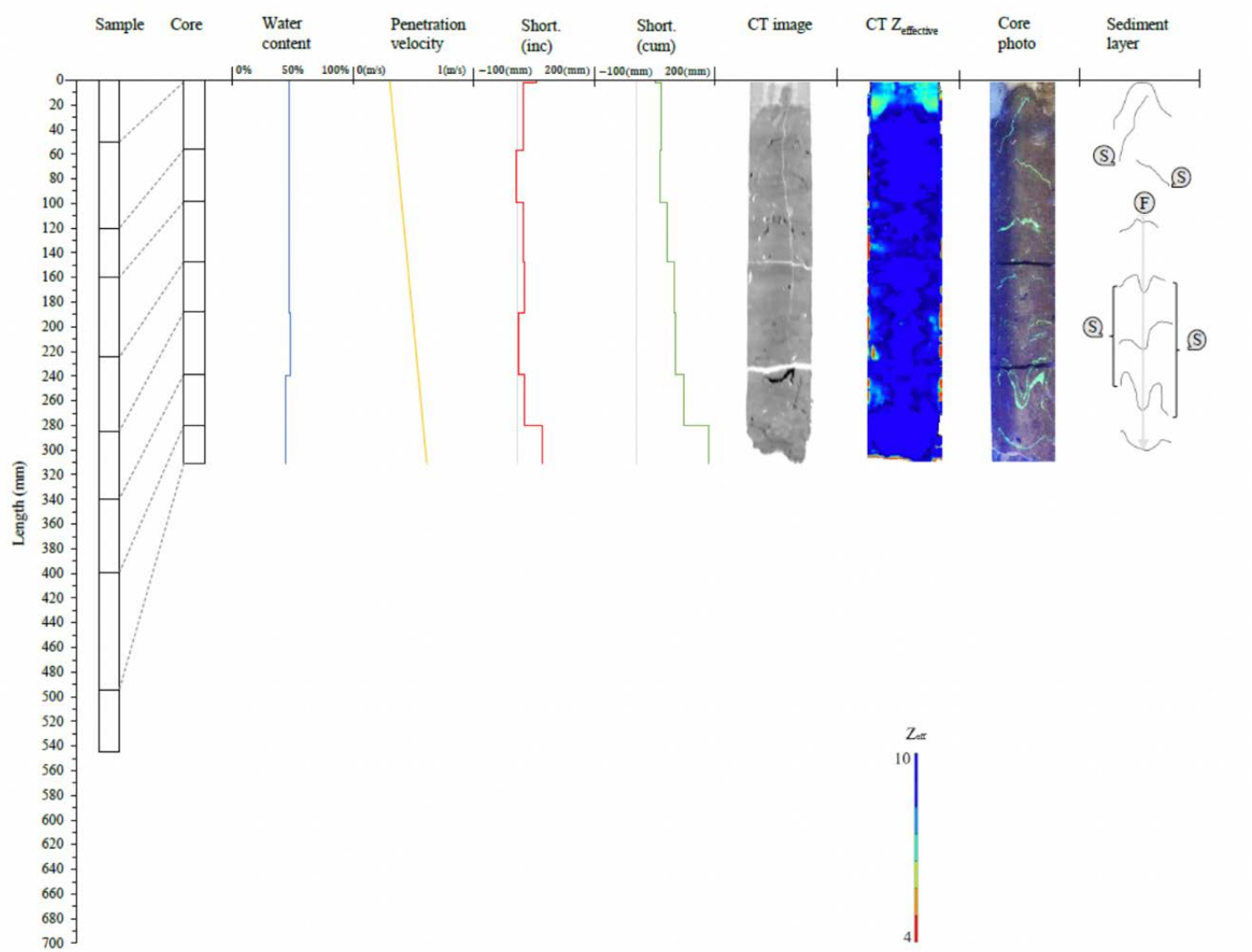


**Figure S24.** Laboratory experiment core: *Lab_FC18_Olsberg_Constant_0*.

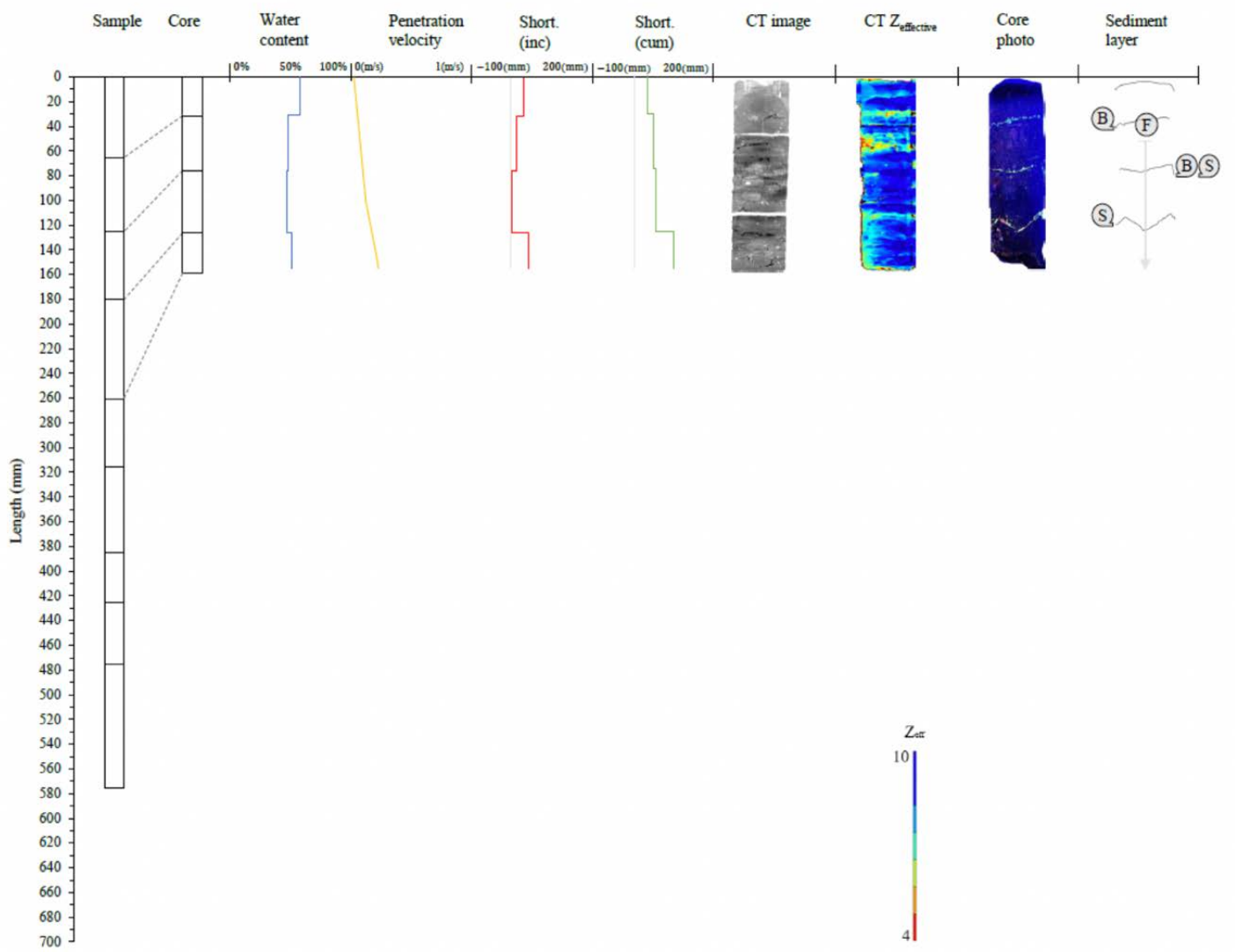


**Figure S25.** Laboratory experiment core: *Lab_FC19_Olsberg_Tripod_0*.

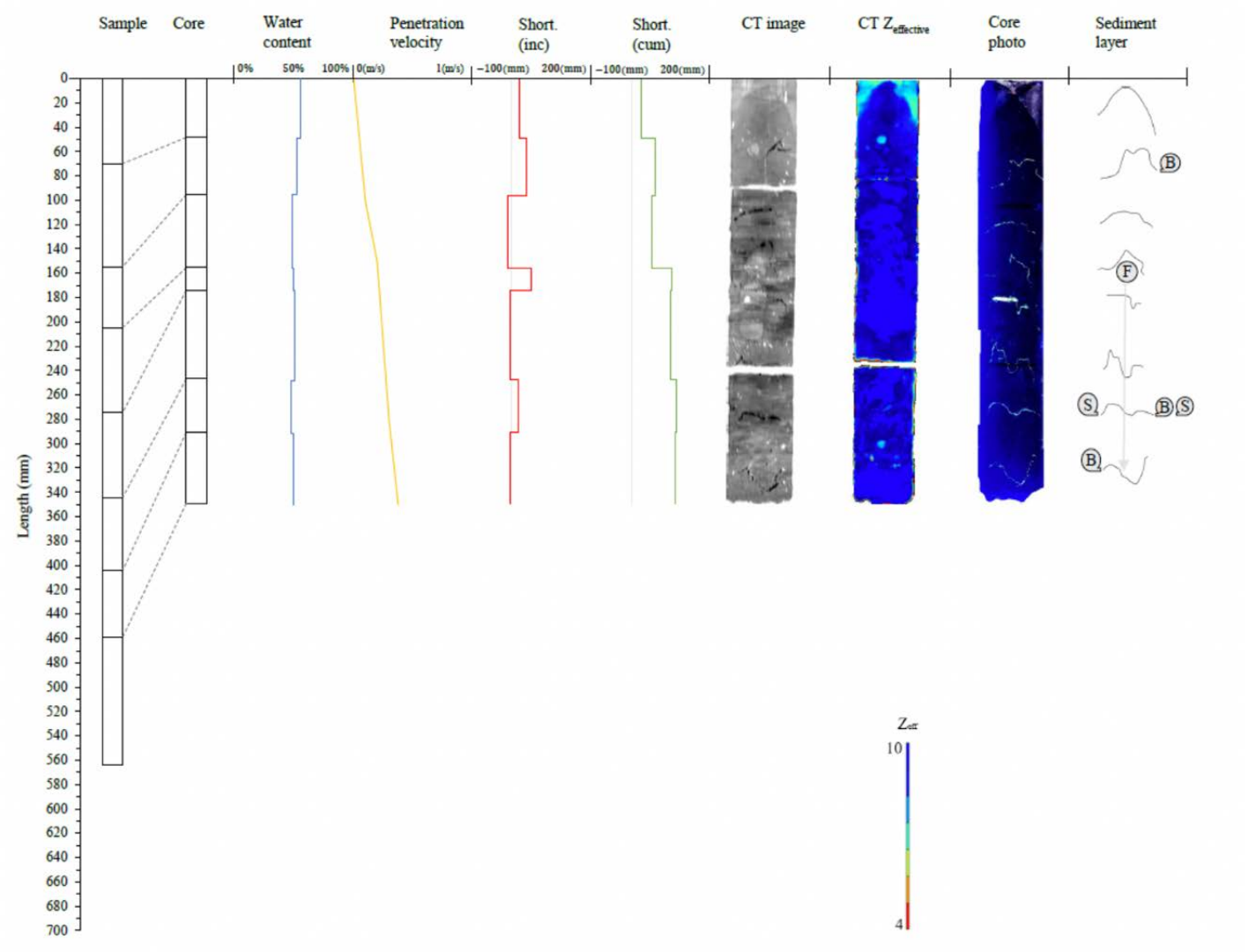


**Figure S26.** Laboratory experiment core: *Lab_FC20_Olsberg_Tripod_0*.

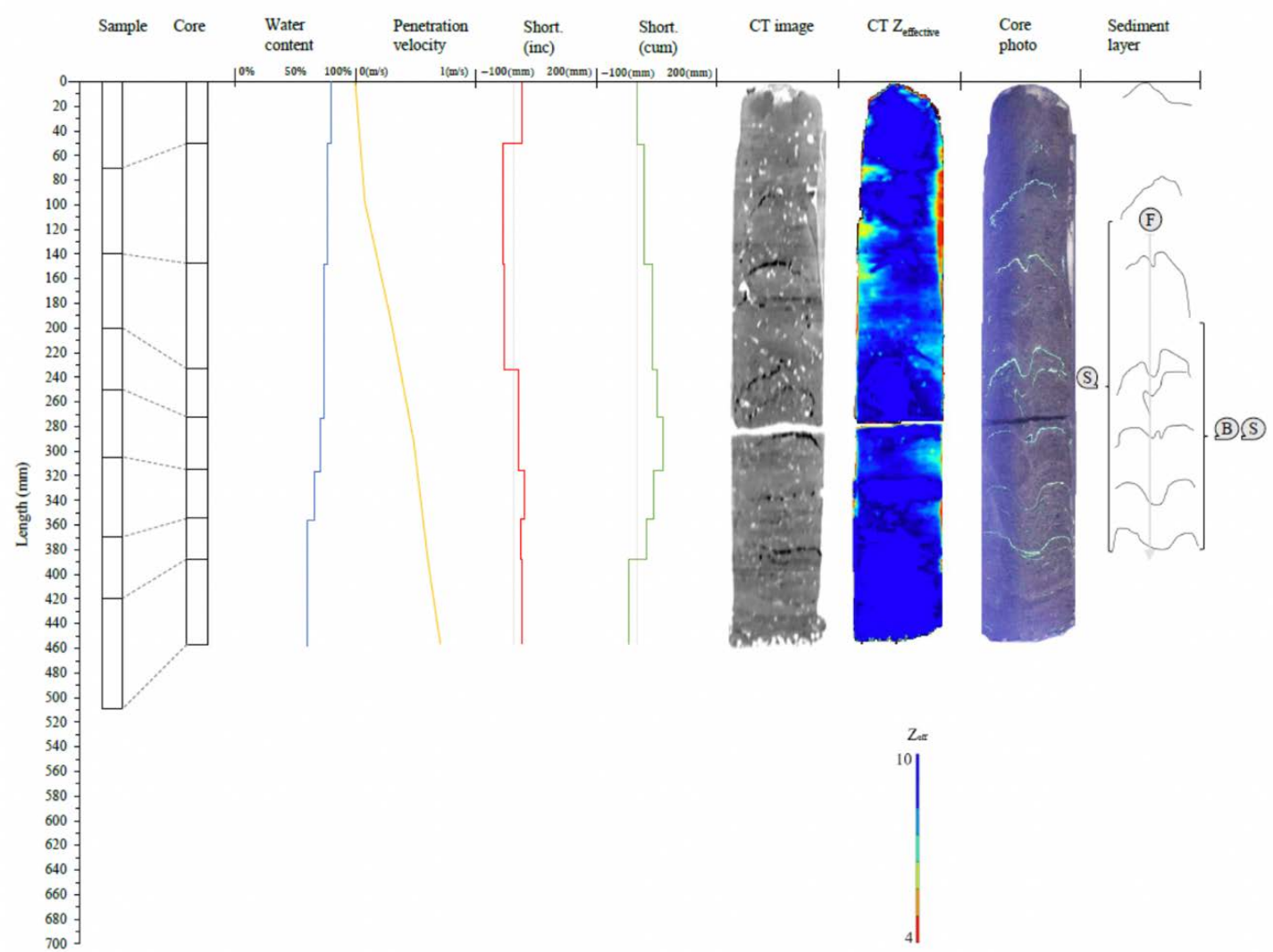


**Figure S27.** Laboratory experiment core: *Lab_FC21_Olsberg_Tripod_4*.

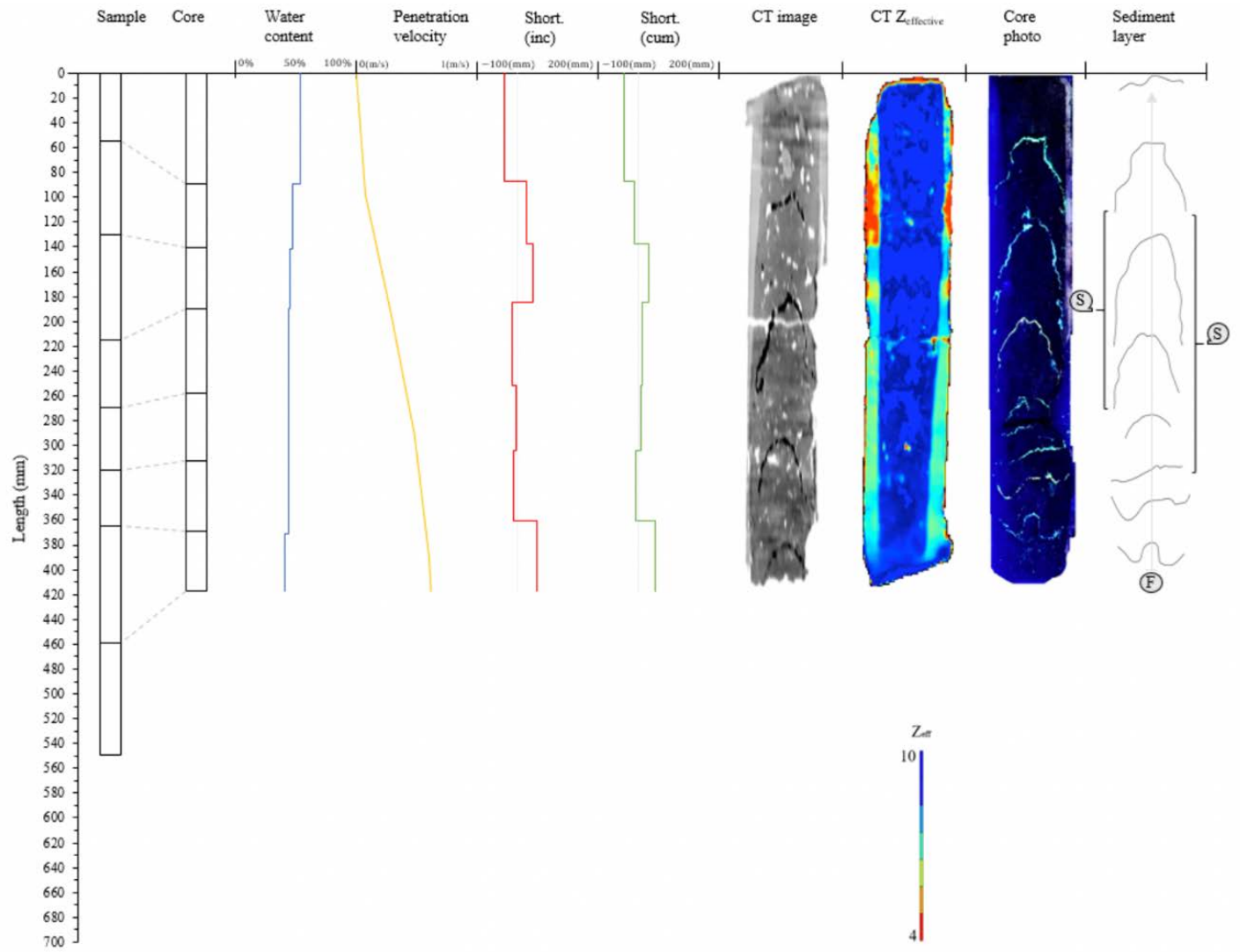


**Figure S28.** Laboratory experiment core: *Lab_FC22_Olsberg_Tripod_7*.

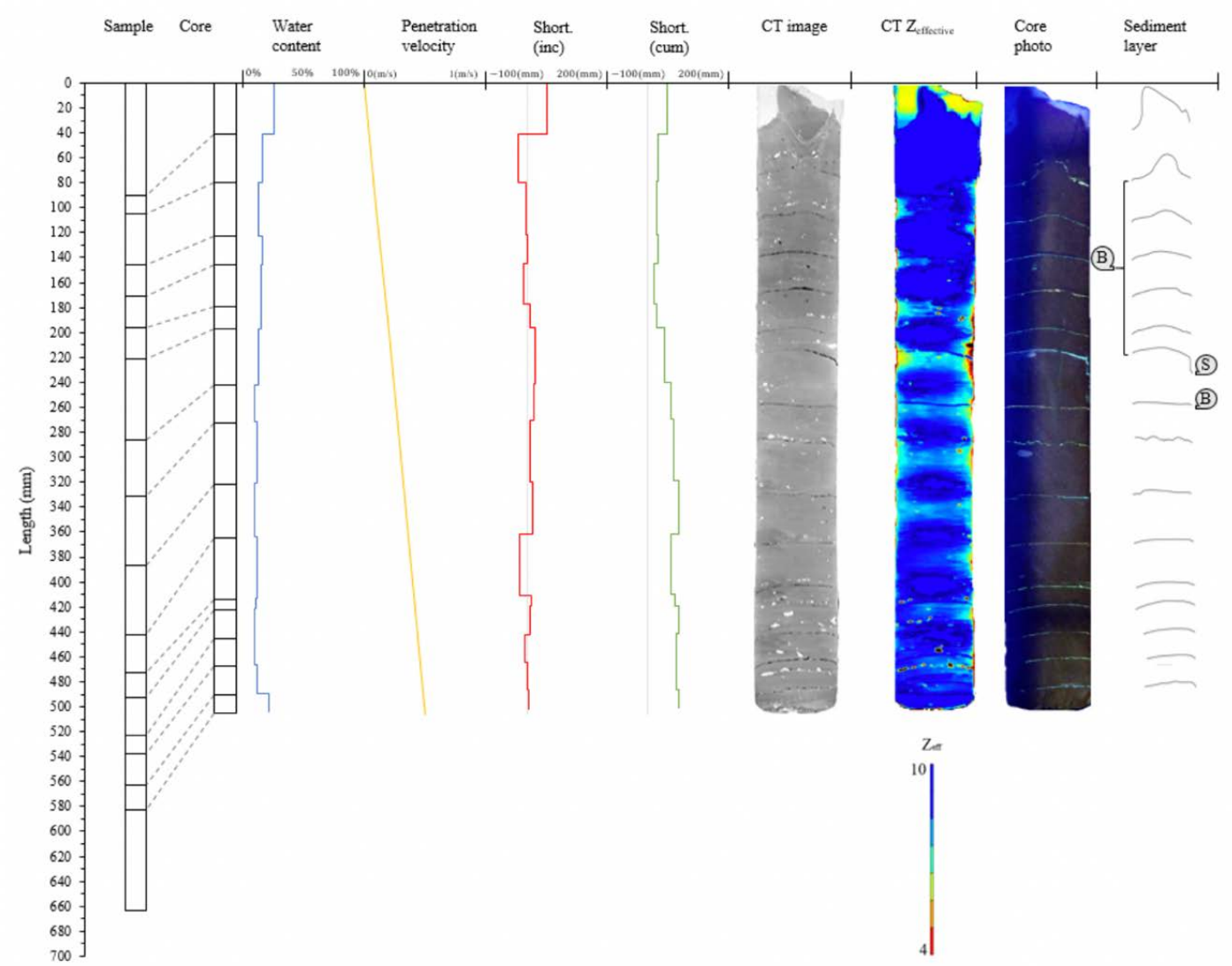


**Figure S29.** Laboratory experiment core: *Lab_GC1_Silt_Constant_0*.

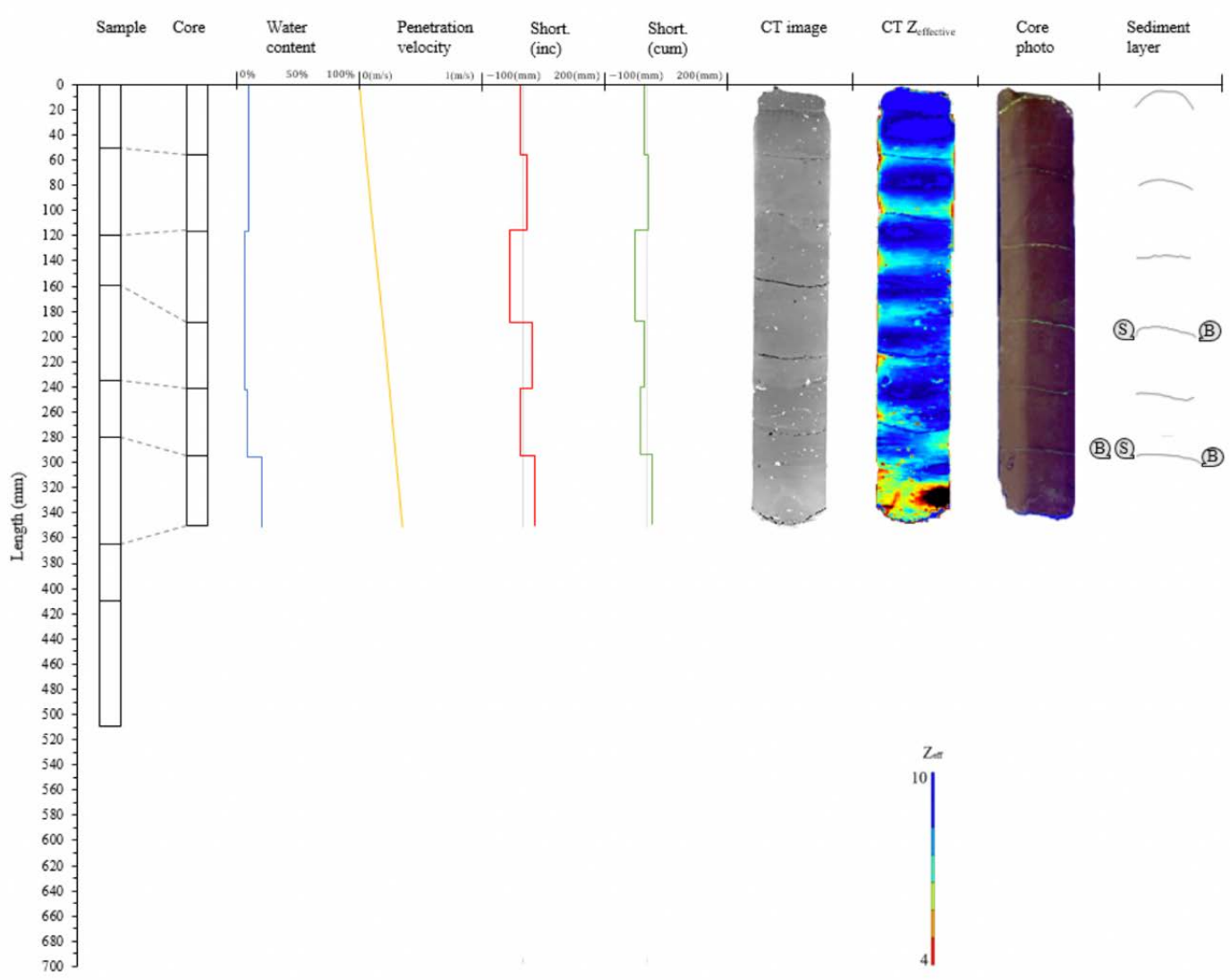


**Figure S30.** Laboratory experiment core: *Lab_GC2_Silt_Constant_0*.

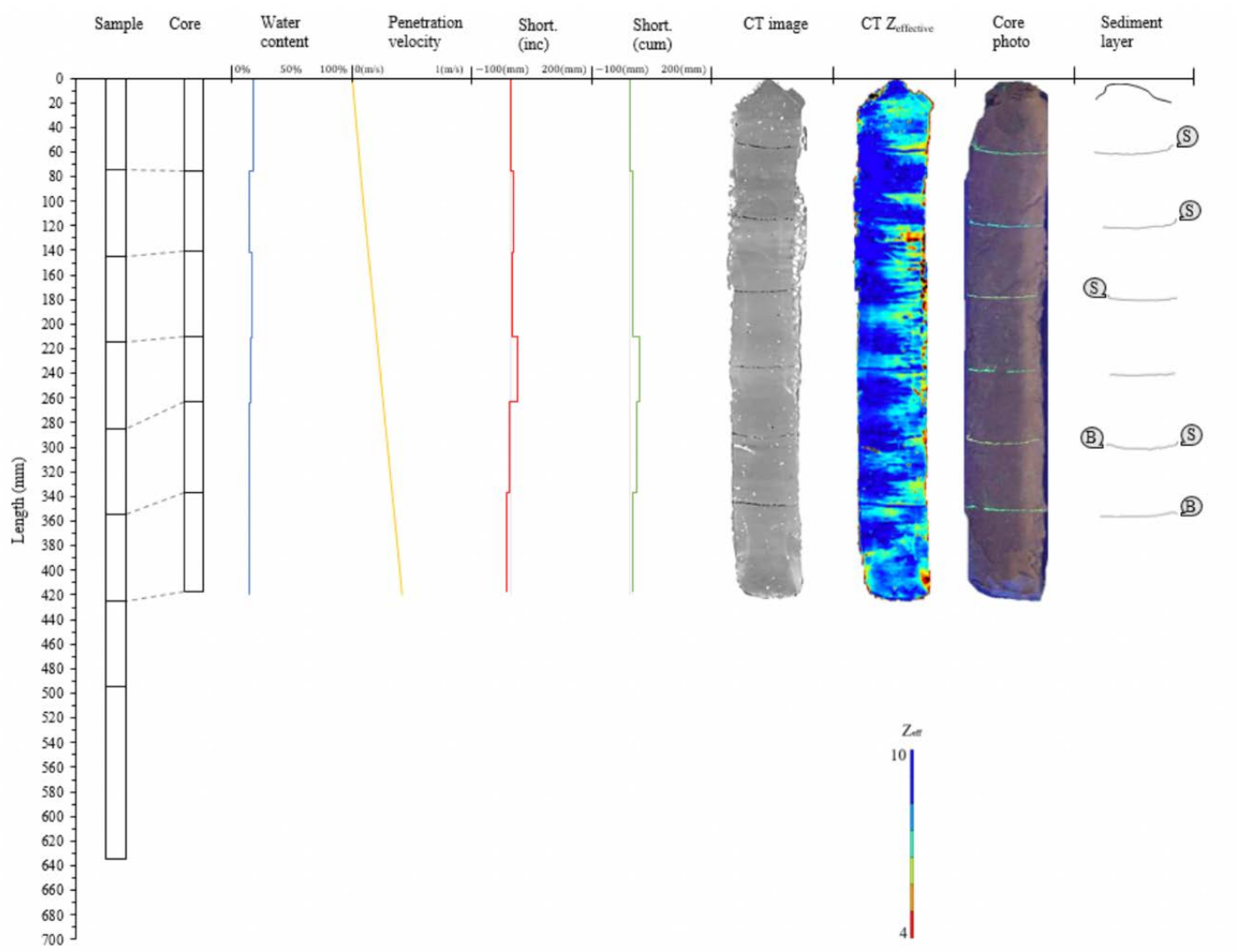


**Figure S31.** Laboratory experiment core: *Lab_GC3_Silt_Constant_0*.

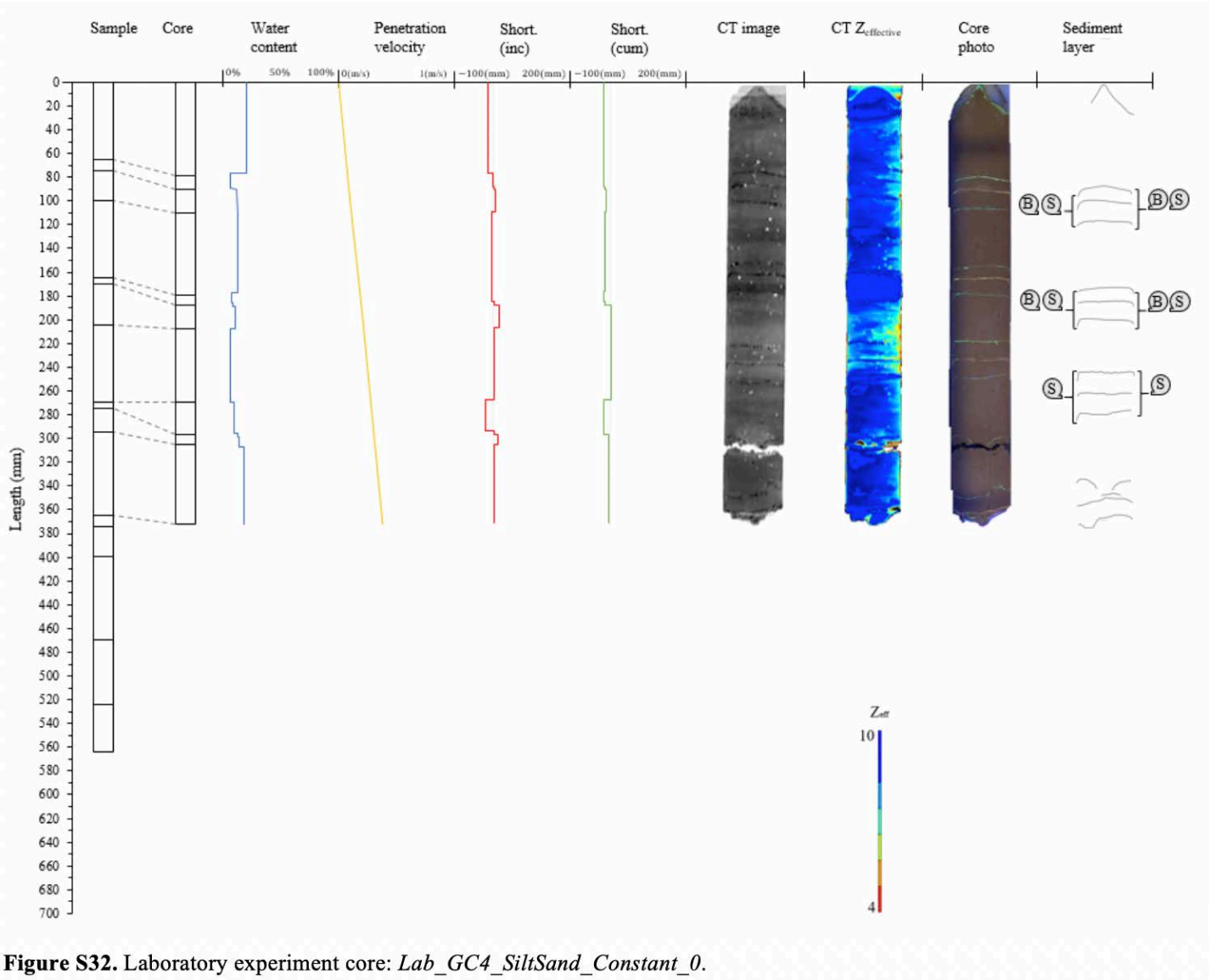


**Figure S32.** Laboratory experiment core: *Lab_GC4_SiltSand_Constant_0*.

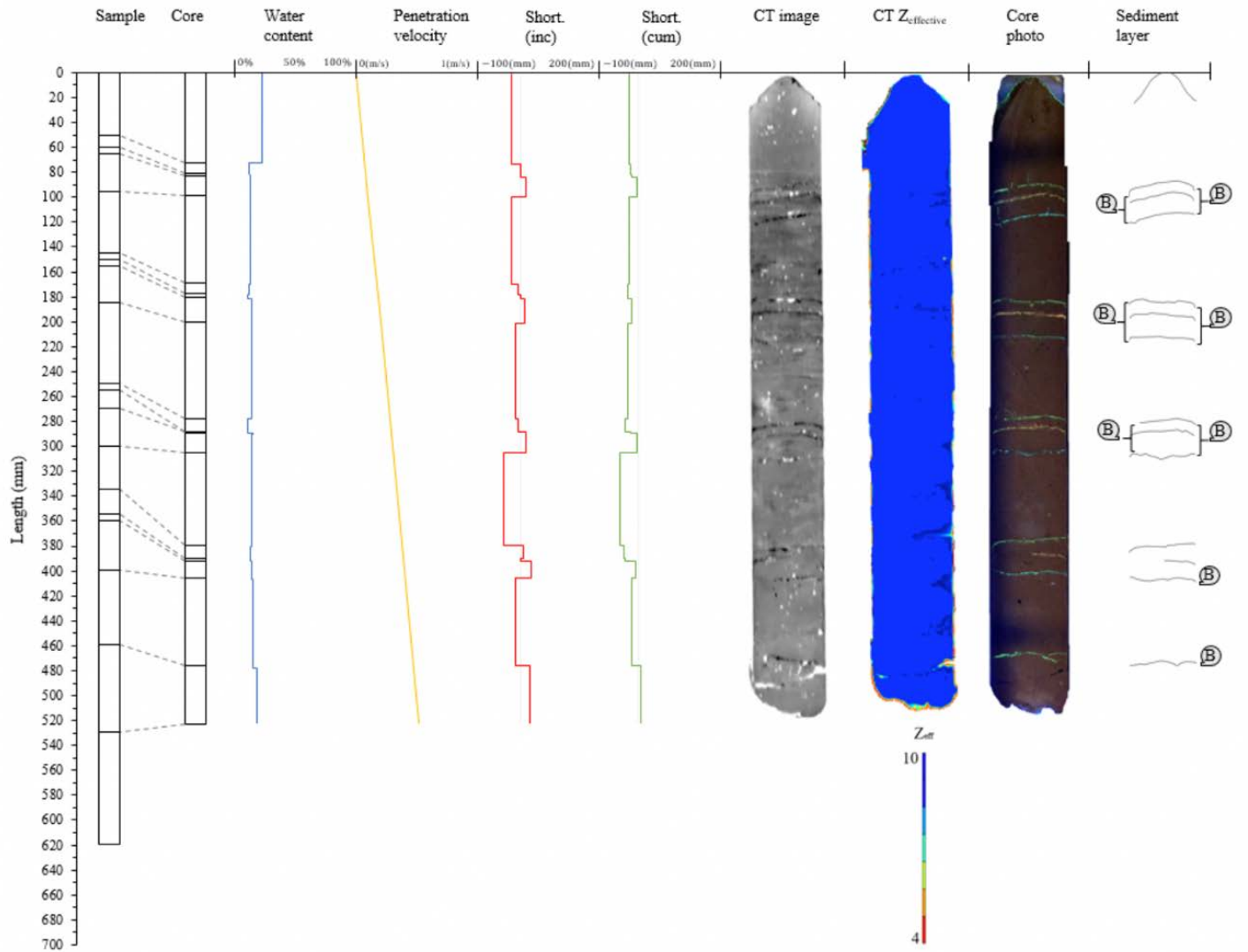


**Figure S33.** Laboratory experiment core: *Lab_GC5_SiltSand_Constant_0*.

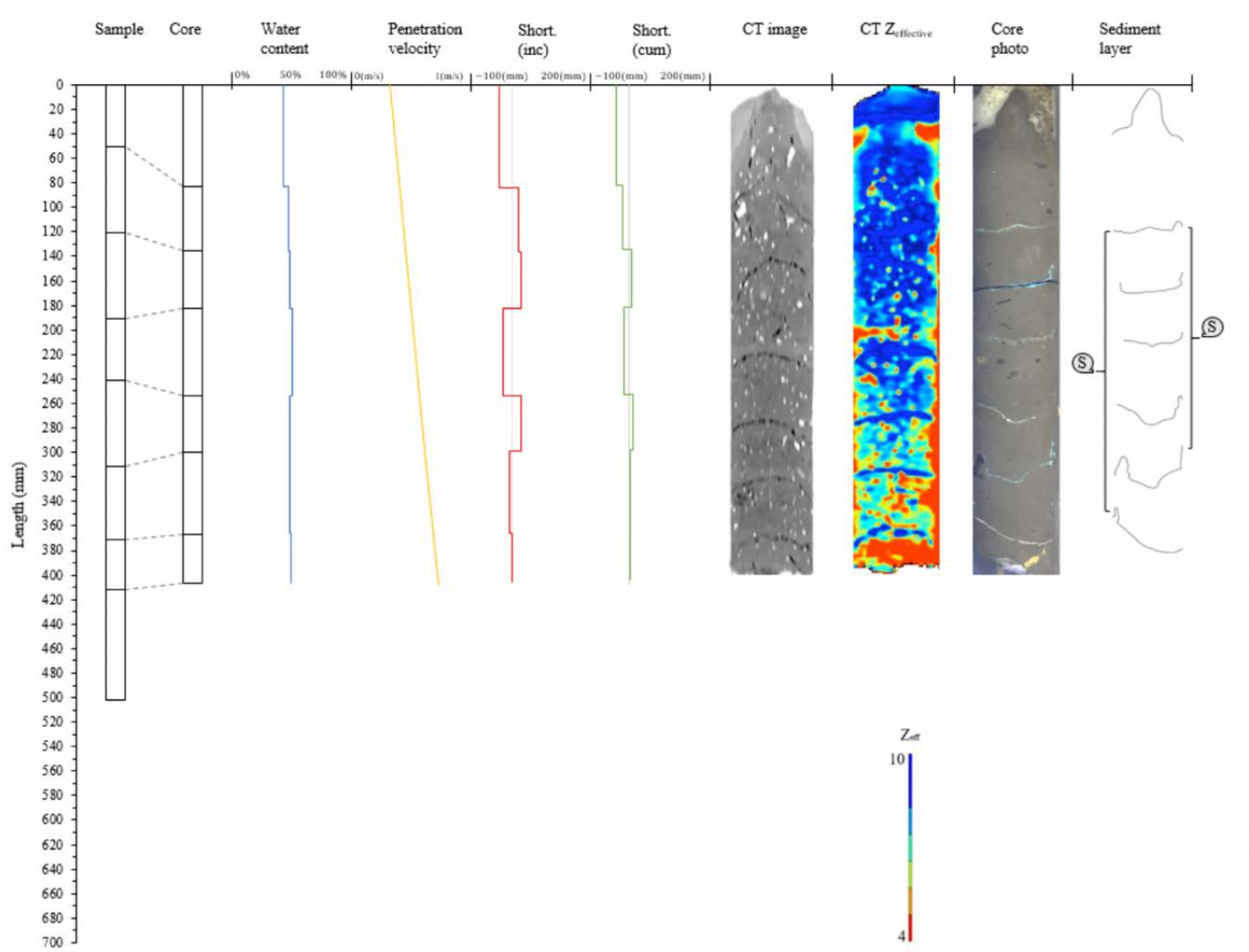


**Figure S34.** Laboratory experiment core: *Lab_GC6_Olsberg_Constant_0*.

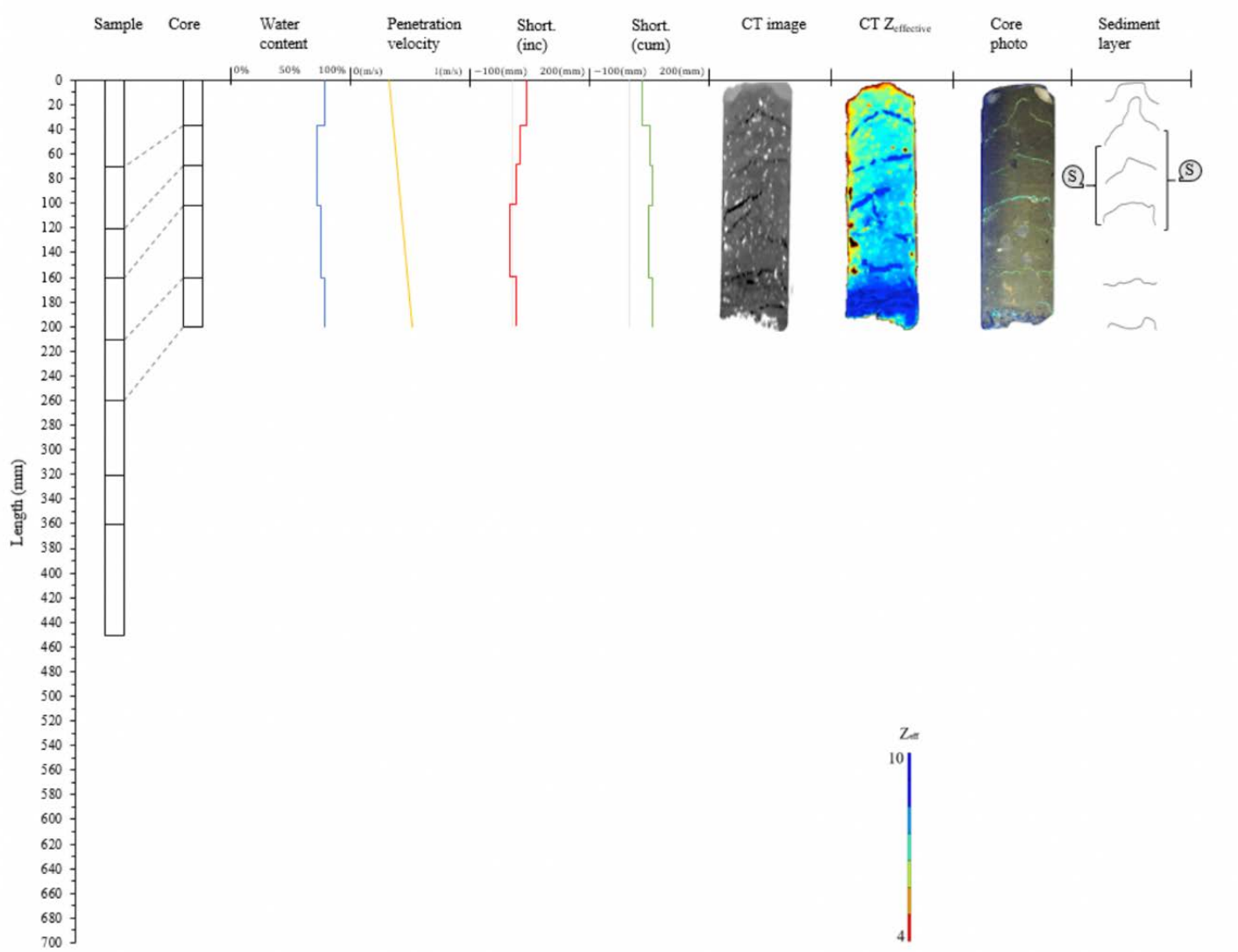


**Figure S35.** Laboratory experiment core: *Lab_GC7_Olsberg_Constant_0*.

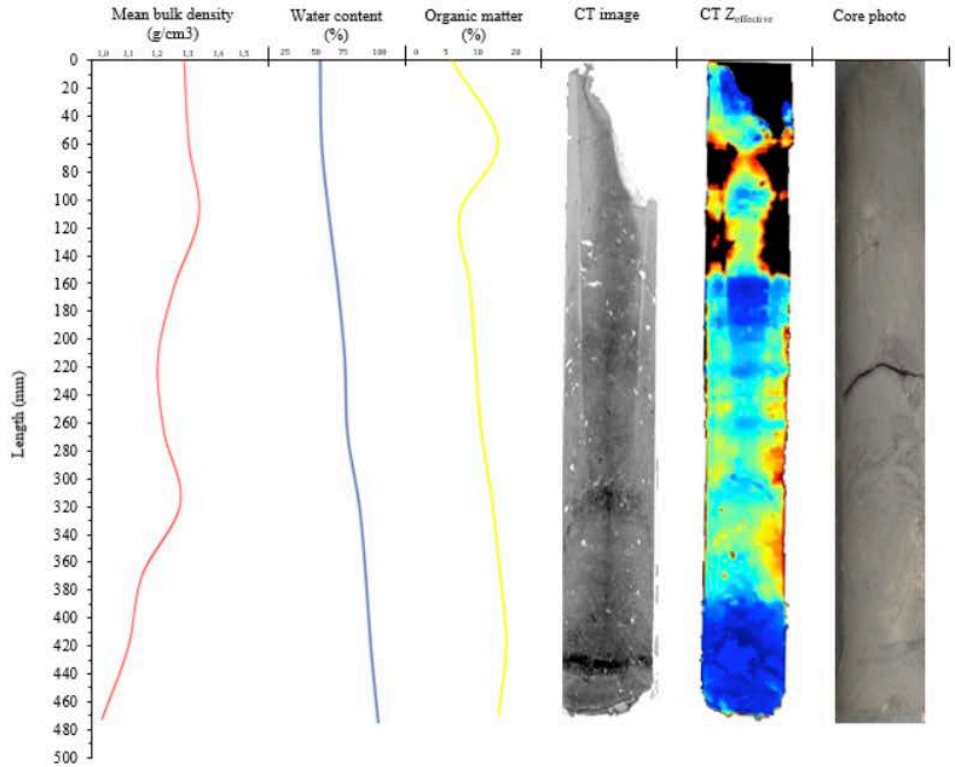


**Figure S36.** Field investigation core: *Olsberg _FC1_ Tripod_0.* The red line shows the mean bulk density, the blue line the water content, and the yellow line the organic matter distribution over core length. X-Ray CT scan image is shown as binary image. CT $Z_{eff}$ scan image shows the distribution of effective atomic number. Core photo shows the photography.

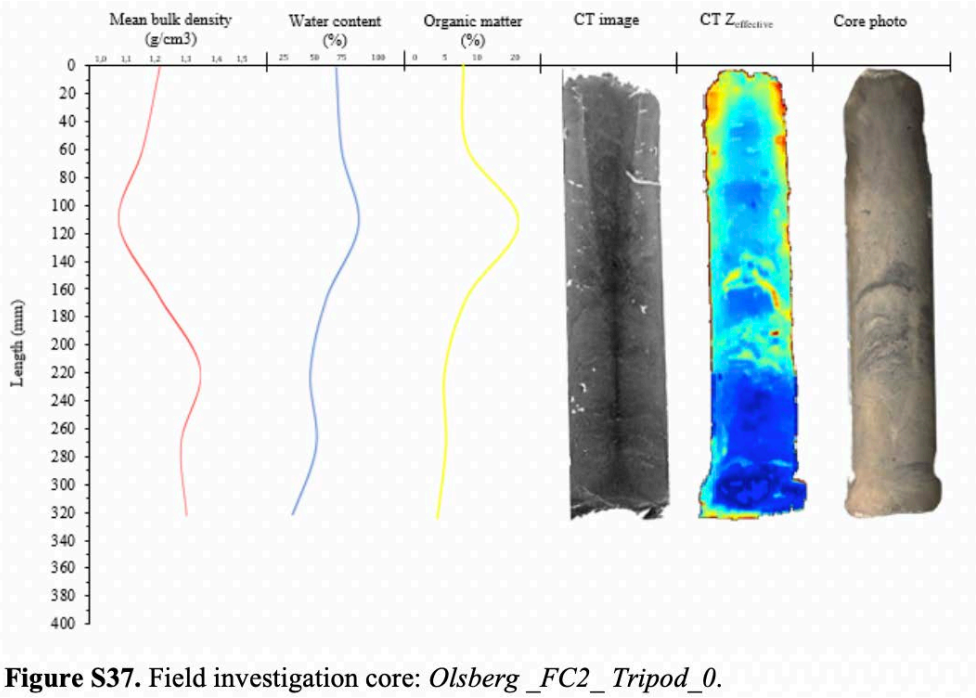


**Figure S37.** Field investigation core: *Olsberg _FC2_ Tripod_0*.

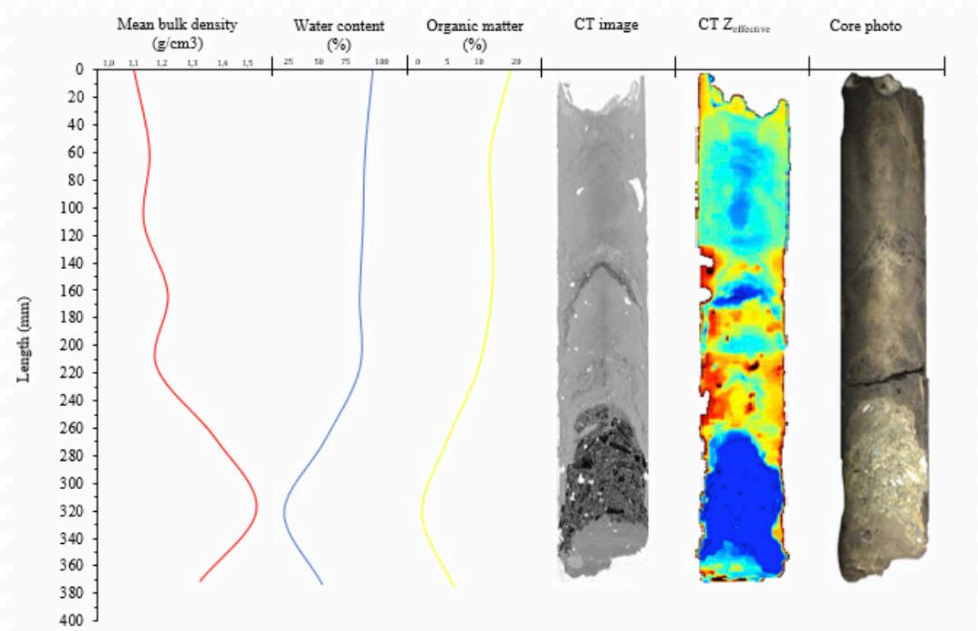


**Figure S38.** Field investigation core: *Olsberg _FC3_ Tripod_0*.

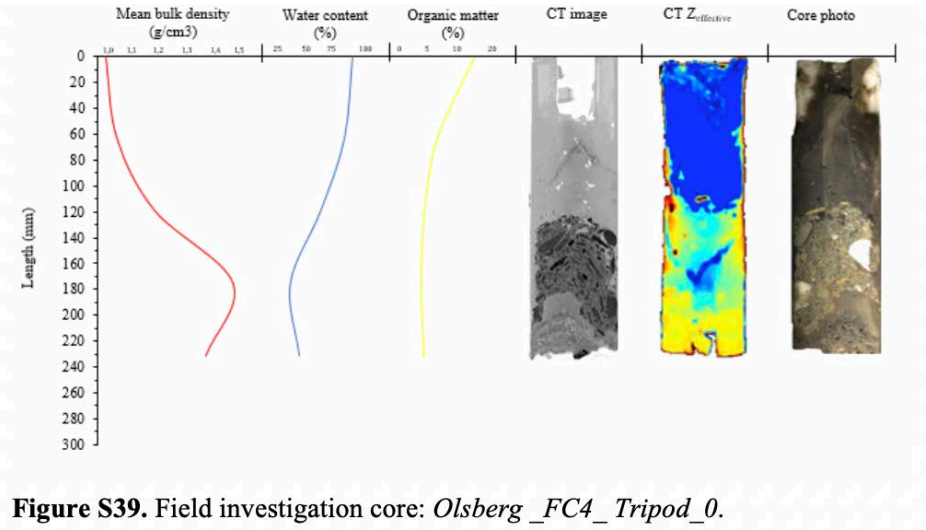


**Figure S39.** Field investigation core: *Olsberg _FC4_ Tripod_0.*

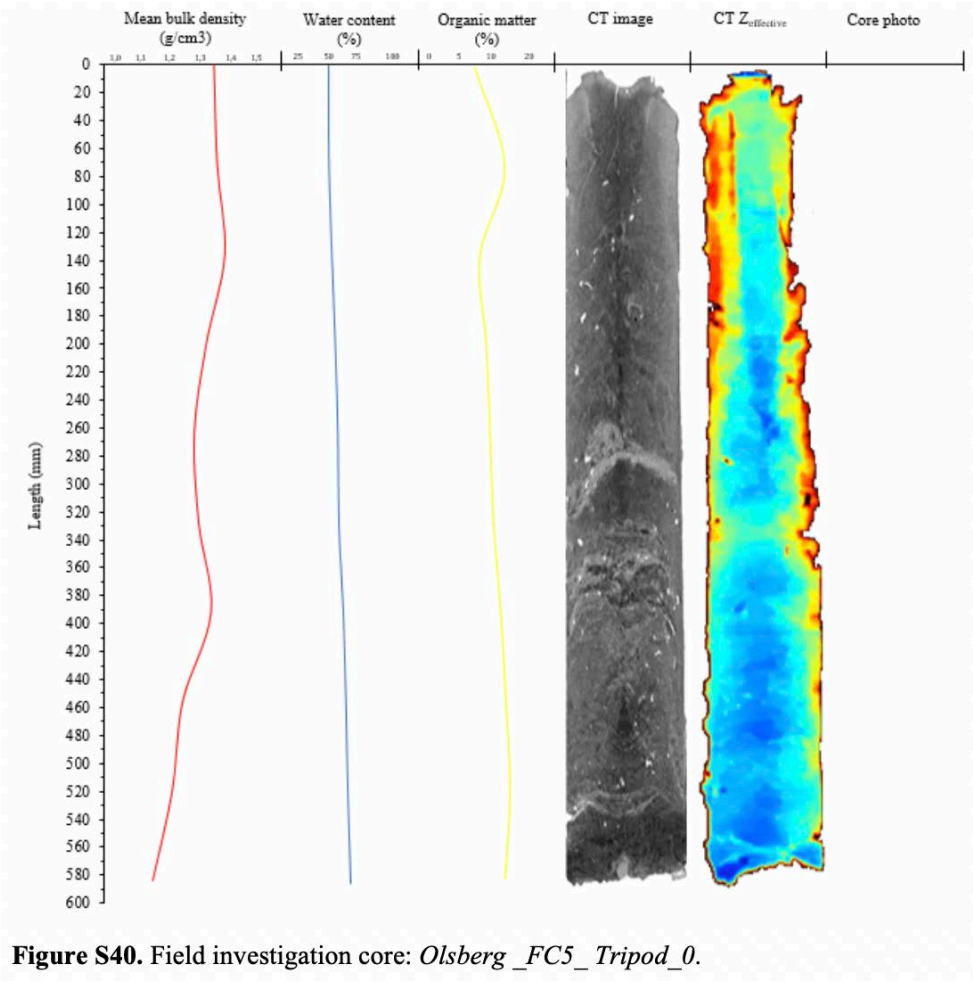


**Figure S40.** Field investigation core: *Olsberg _FC5_ Tripod_0*.

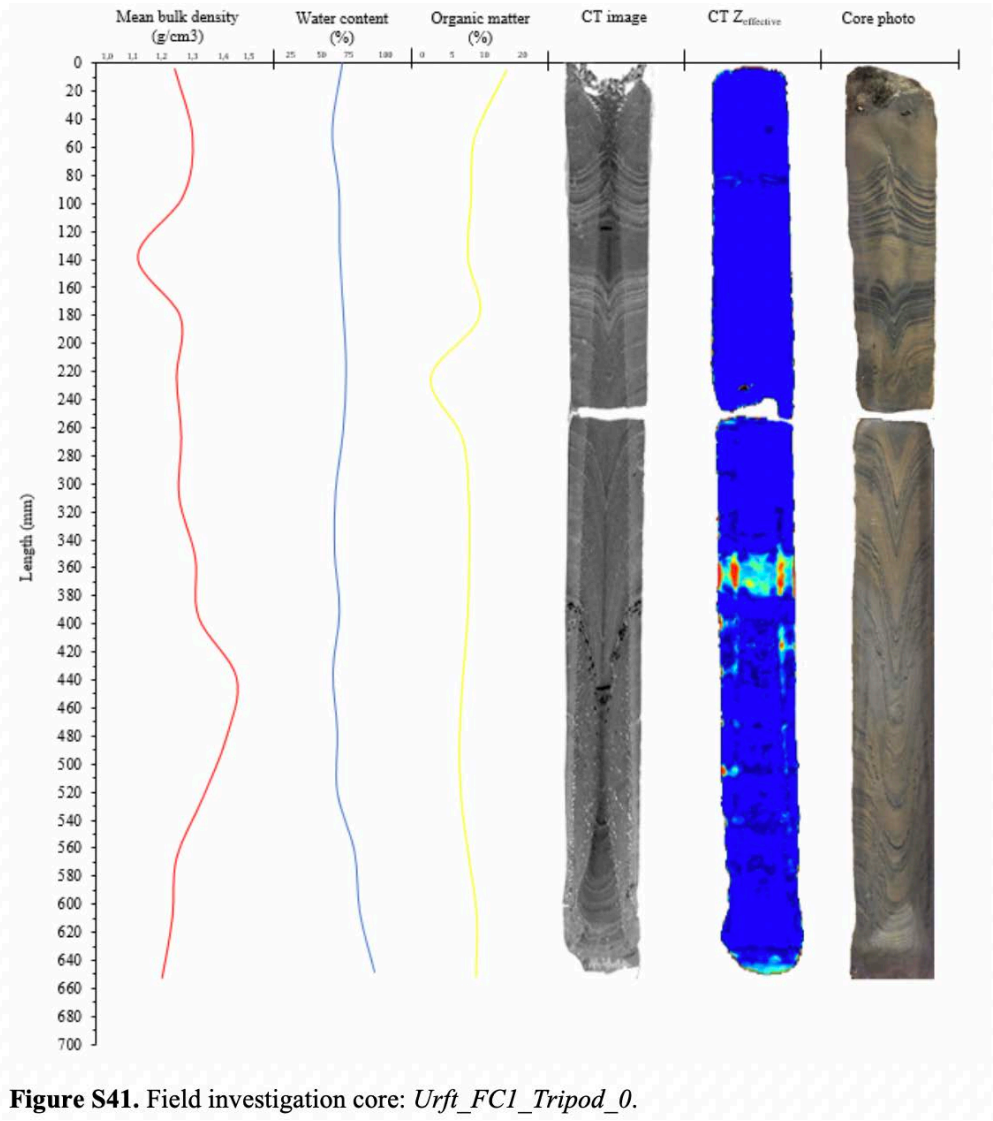


**Figure S41.** Field investigation core: *Urft_FC1_Tripod_0*.

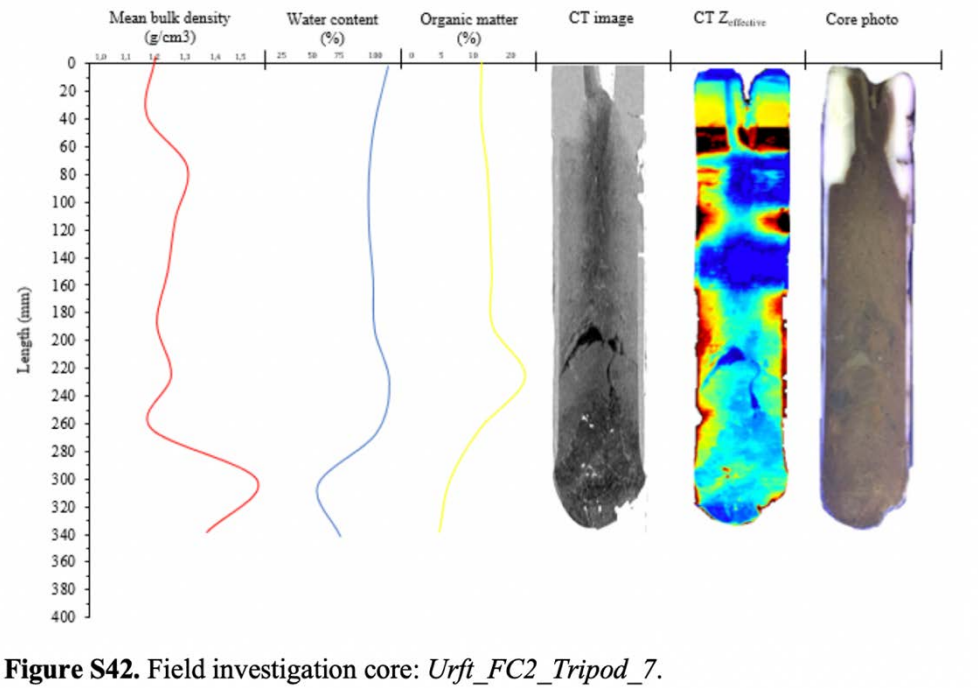


**Figure S42.** Field investigation core: *Urft_FC2_Tripod_7*.

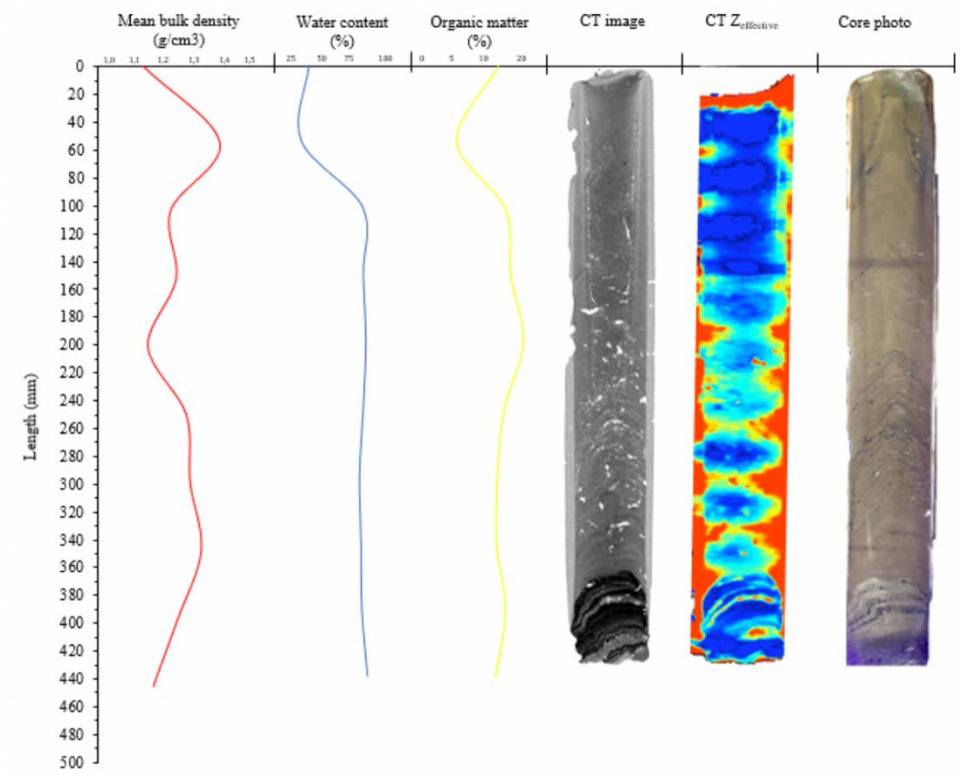


**Figure S43.** Field investigation core: *Urft_FC3_Tripod_4*.

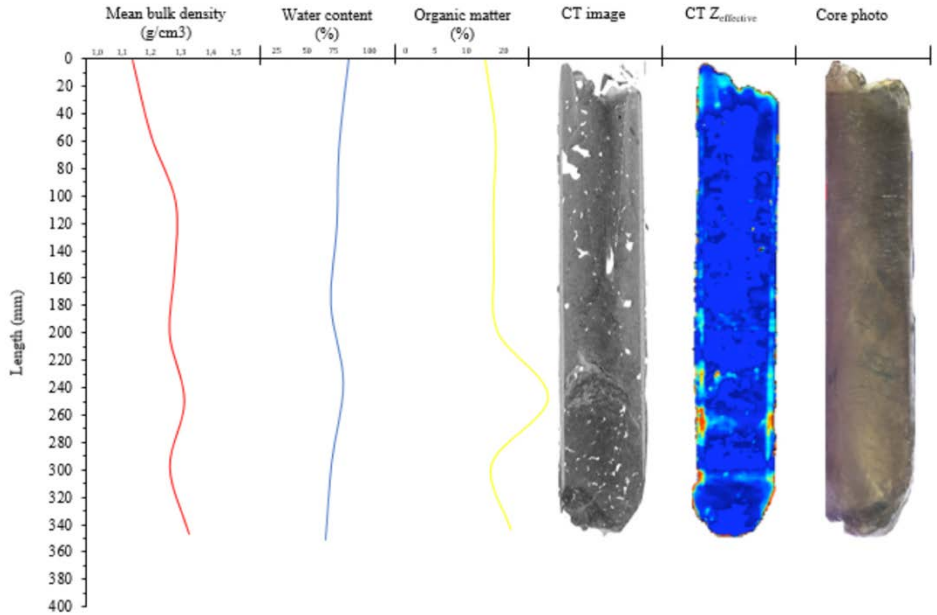


**Figure S44.** Field investigation core: Urft_FC4_Tripod_4.

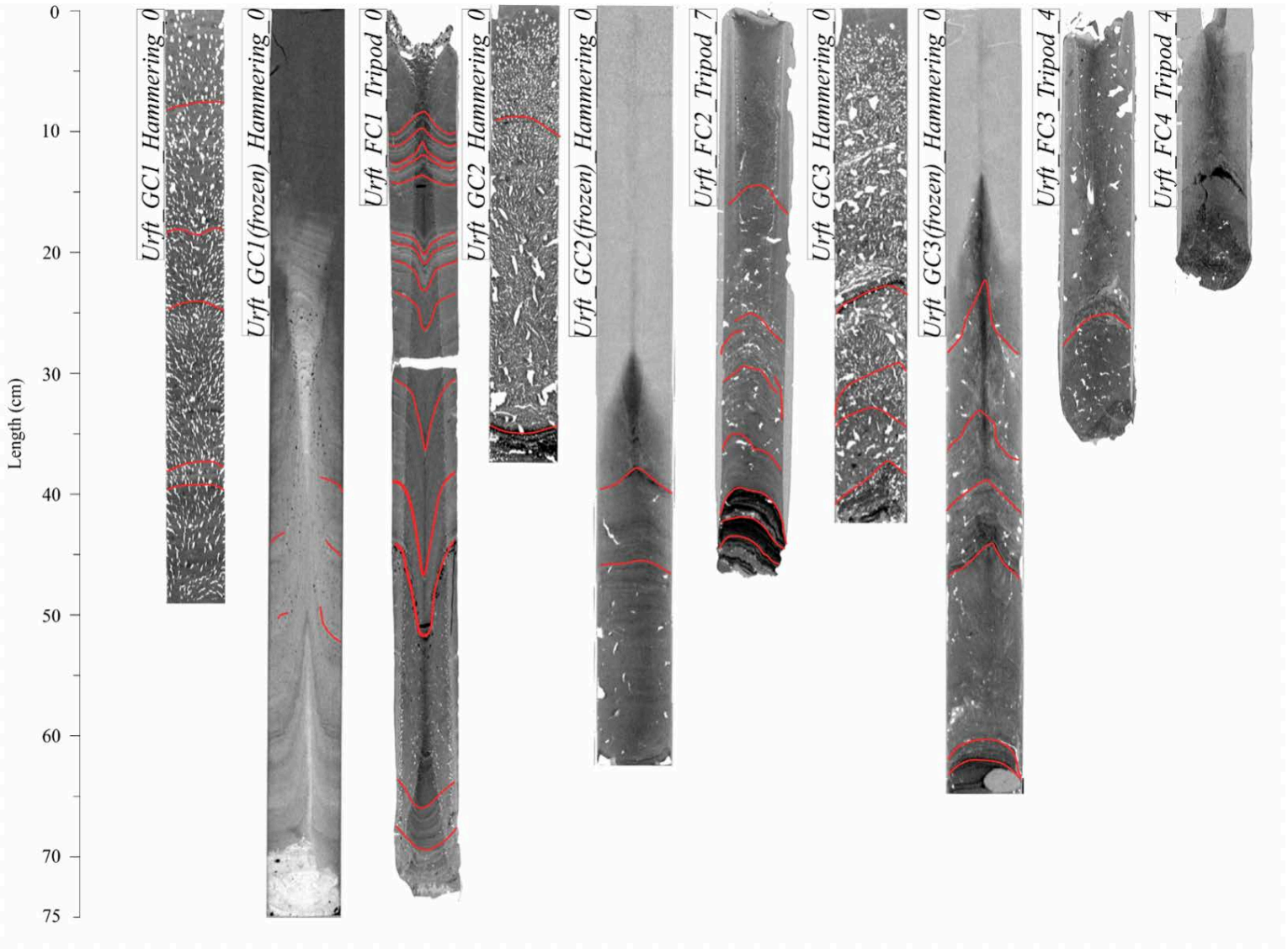


**Figure S45.** CT scan images of Urft Reservoir. Digitized sediment layers are marked in red. Gas bubbles are seen as white spots.

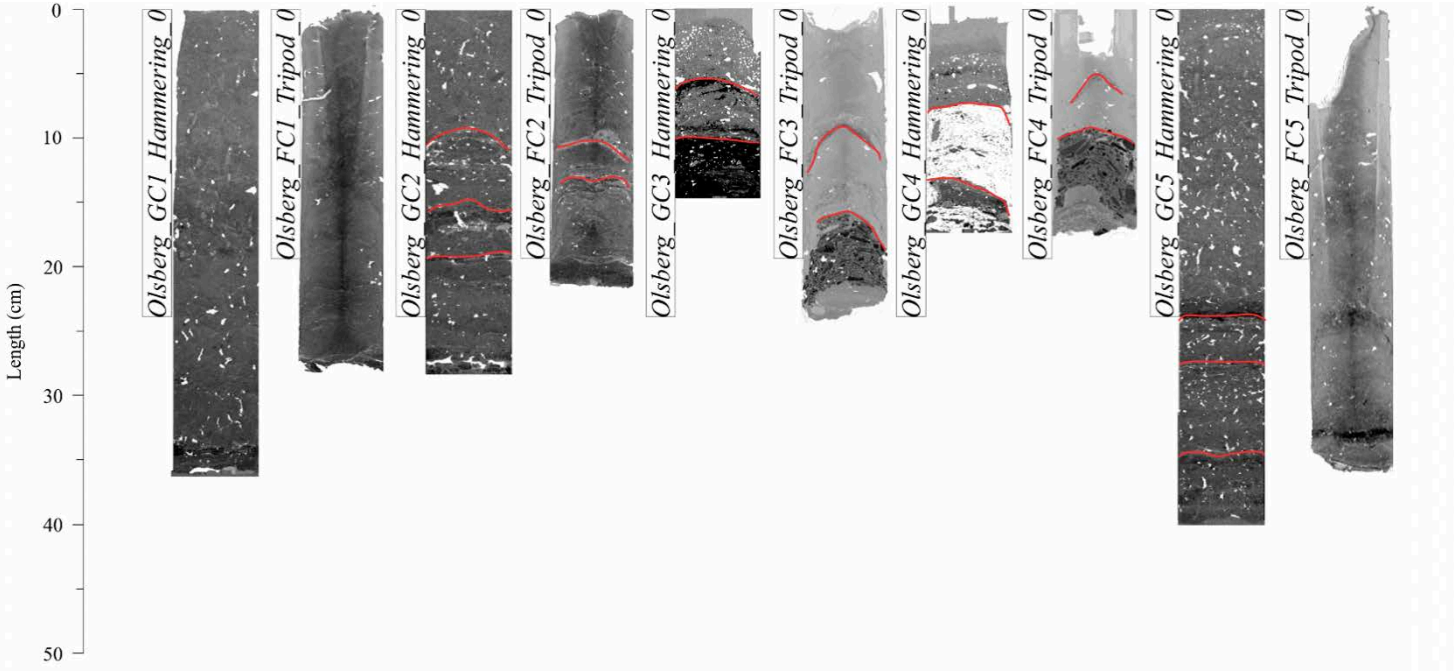


**Figure S46.** CT scan images of Olsberg Reservoir. Digitized sediment layers are marked in red. Gas bubbles are seen as white spots.

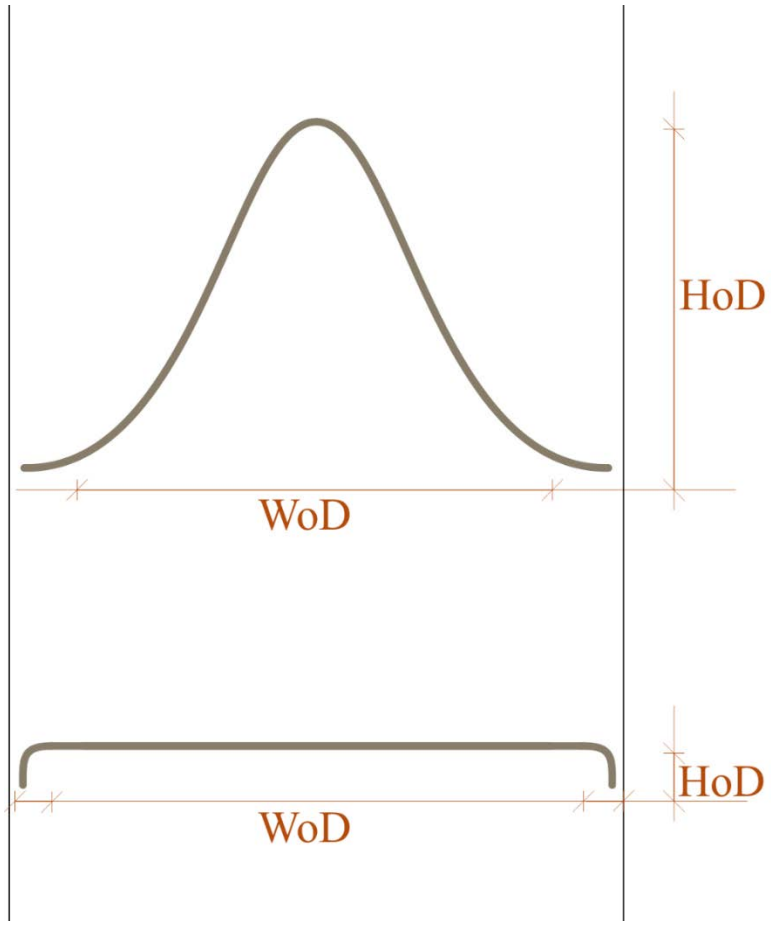


**Figure S47.** Schematically representation of the evaluation *(Width of Disturbance (WoD), Height of Disturbance (HoD))* of coring disturbances.

# Appendix IV

**Experimental Investigation of Impinged, Oblique Submerged Cavitating Water Jets with Pressure Measurement Sensing**

Dück, Yannick[1]; Bolsenkötter, Laura[2]; Lorke, Andreas[3] and Christian Jokiel[1]

[1] Laboratory for Water and Environment, Cologne University of Applied Science, Cologne, Germany
[2] DB Sediments GmbH, Bismarckstr. 142, 47057 Duisburg, Germany
[3] University of Koblenz-Landau, Institute of Environmental Sciences, Landau, Germany

# Investigation of Impinged, Oblique Submerged Cavitating Water Jets with Pressure Measurement Sensing

Yannick Dück

Institute of Hydraulic Engineering and Water Resources Management, Cologne University of Applied Science

Betzdorfer Straße 2, 50679 Cologne, Germany

Laura Bolsenkötter

DB Sediments GmbH, Bismarckstr. 142, 47057 Duisburg, Germany

Andreas Lorke, Dr. rer. Nat.

Institute for Environmental Sciences, University of Koblenz-Landau, Fort Str. 7, 76829 Landau, Germany

Christian Jokiel, Dr.-Ing.

Institute of Hydraulic Engineering and Water Resources Management, Cologne University of Applied Science

Betzdorfer Straße 2, 50679 Cologne, Germany

## ABSTRACT

In the dredging industry, water jets are often used in hydraulic dredging to erode (consolidated) sediment deposits and to bring sediment into suspension. Due to the high erosional forces, cavitating water jets are a promising technique to improve the dredging operation's efficiency and production rate. Objective of this study is the measurement of the impact pressure of those jets and the identification of the governing parameters, by using an adapted Pressure Measurement Sensing technique. The results obtained by this technique provide high spatial resolution data of the impact pressure distribution and has proven as an effective method for studying cavitating water jets with comparatively little effort to common pressure transducers. The results demonstrate that the impact pressure decreases with increasing spray angle and standoff distance. For a fixed standoff distance, impinging angle and spray angle, an increase in pump pressure correlates non-linearly to the impact pressure. However, the results show that an optimum of pump pressure exists. The results underline the importance of precise control and adjustment of the relevant jet parameters for an efficient dredging operation.

**INDEX TERMS**

Pressure Measurement Sensing; Sediment; Cavitating Water Jet; Dredging

## INTRODUCTION

In maintenance dredging of ports, waterways and channels as well as reservoirs, water jets at low pressure and high discharge (Nobel 2013) are widely used to remobilize sediment layers (Hogg et al. 1997). Through fluidizing the sediment, cutting forces of mechanical dredging devices are reduced, enhancing the production rate and making the water-sediment mixture more suitable for upward transportation (Weegenaar et al. 2015). Water jets remobilize the sediment deposits by exerting a jet flow with a high shear stress causing a high erosion velocity (Nobel and Talmon 2012). The resistance of the sediment against the shear stress is affected by multiple interacting parameters. The effects of those parameters are still not fully understood and analytical approaches can hardly handle the involved uncertainties (Silva et al. 2017). Therefore, the knowledge of both characteristics – the water jet and the sediment – is the key to develop and implement suitable and efficient dredging techniques. Besides dredging, water jets are further used for jet cutting, underwater cleaning, preparation of surfaces, disintegrations of biological material, removal of coatings and in many other applications (e.g. Guha et al. 2011; Zeleňák et al. 2015).

When jet pressure is low, the resistance of ambient water will clearly hinder the jet development and even destroy the integrity of the jet stream, whereas, at high jet pressure, the water jet can sustain itself over a long distance away from the nozzle (Liu et al. 2017). At high jet pressure, cavitation can occur forming a cloud of bubbles around the jet, which decreases the momentum exchange between the jet and the ambient water. As a result, the decay of the jet velocity, and thus the stagnation pressure decreases with jet distance (Soyama and Lichtarowicz 1996; Yahiro and Yoshida 1974). This effect increases the impact pressure of the cavitating water jet. Two characteristic effects are believed to be mainly responsible for the destructive action of the jet towards an obstacle: the generation of a high-speed liquid jet directed towards the boundary, and the emission of shock waves upon cavitation bubble collapse (Nobel 2013). The cavitation bubbles collapse due to pressure peaks near the (solid) boundary and result in a destructive force. The material destruction due to this implosion is caused by complex physical processes during the jet impact (Zeleňák et al. 2015). Therefore, a cavitating, high-speed water jet represents a progressive, recently developed technology enabling disintegration

of most existing materials, and an increased penetration depth of the jet in sediments. The impact pressure distribution of cavitation impacts on an impinging wall is important in predicting the range of erosion caused by those jets (Peng et al. 2018). Despite the amount of research on cavitating jets, the literature does not provide a description of the velocity and stagnation pressure development (Nobel and Talmon 2012).

The simulation of cavitating water jets with computational fluid dynamics is complex due to the generation and collapse of cavitation bubbles (Wang et al. 2015) and the fact, that the cavitation region of the flow is compressible, while in the non-cavitating regions the flow is incompressible (Nobel 2013). Therefore, the numerical prediction of cavitation evolution is still suffering from debate and uncertainties. Studies of physical measurements on submerged cavitating water jets encompass high-speed photography (e.g. Soyama and Lichtarowicz 1996; Dular and Petkovšek 2015; Sato et al. 2009), measurements with pressure transducers (Shen and Sun 1988; Mortensen 2013; Nobel and Talmon 2012) and the analyses of the cavitation impact damage pattern on metallic specimens (Peng et al. 2018). Thus, the accurate inverse estimation of impact pressure from the specimens requires the assumption of the possible pulse pressure profile induced by cavitation bubbles (Peng et al. 2017) or those measurements only provide limited spatial information (pressure transducers).

Maximizing the efficiency of a cavitating jet is not trivial, since many parameters have an influence on the shear stress, including pump pressure, inside diameter of the nozzle, standoff distance, jet shape and impingement angle (Mortensen 2013). An impinging jet can be depicted in four zones (Fig. 1). Zone 1 is described as the “zone of flow establishment,” where a water jet potential core exists. Eddies are formed as the jet entraining the surrounding, stagnant fluid. This zone ends, when the jet becomes completely turbulent. Zone 2 is defined as the “zone of established flow.” Zone 3 is the “deflection zone,” in which the jet impacts the planar surface and a transition from a vertical to a horizontal jet develops. A stagnation point occurs along the centerline of the jet at the planar boundary. At this stagnation point, pressure is at maximum and shear stress is zero. Zone 4 is defined as the “wall jet zone,” in which the flow of the jet is parallel to the planar boundary. The thick black line (Fig. 2) represents the potential erosional pattern by the water jet in sediment.

This paper attempts to determine and visualize the impact pressure distribution of submerged cavitating water jets under varying standoff distances and angles to the impinging surface, pump pressure, as well as the spray angle of flat fan nozzles. The present work extends the range of existing experimental data by using an adopted design of a Pressure Measurement Sensing (PMS) technique to determine the erosional behavior of the jets. In

addition, Particle Image Velocimetry (PIV) images are used to qualitatively describe the flow behavior and visualize cavitating bubbles.

## METHODS

Experiments were performed to determine the impact pressure distribution of different flat fan nozzle characteristics (varying jet spray angle β) with respect to pump pressure (P), standoff distance (h) and impinging angle (α) of the water jet to PMS. Table 1 outlines the experimental parameters, which were tested in all (192) combinations.

**Table 1.** Parameters of the laboratory experiments (the nomenclature of the experiments is shown exemplary for one test as follows: FS20_120_150_22.5 is a fan jet with β=20°, P=120 bar, h=150 mm and α=22.5°).

| Parameter | Values | Unit |
|---|---|---|
| Spraying angle (β) | 20, 40, 80, 120 | [°] |
| Nozzle diameter (d) | 1.04 | [mm] |
| Pump pressure (P) | 30, 60, 90, 120 | [bar] |
| Standoff distance (h) | 50, 100, 150, 200 | [mm] |
| Impinging angle (α) | 0.0, 22.5, 45.0 | [°] |
| Pump discharge (Q) | 10 | [l/s] |

A schematic view of the experimental setup is shown in Fig. 1. The tank is 1180 mm in length, 560 mm in width and has a height of 560 mm. A 1.8-kW pump with pressure regulation provided the pressure of the water jet. Flow rate was measured by a float-type flow meter with an accuracy of 2.5%. The test water was tap water. The pump sucks water from the tank to maintain a constant water level. Thus, the water jet is exempted from influence of water level oscillations and the possibility of air being entrained in the jet from the surface is eliminated. The water jet discharges horizontally into the water tank. The flat fan water jet nozzles (Manufacturer: BETE Germany GmbH; High Pressure Flat Fan Nozzle; Tungsten carbine insert; ¼'' stainless steel housing; ¼'' male screw; technical drawing and photo of the water jets are shown in Fig. S1) were originally designed for its application in air. The standoff distance is defined as the distance from the nozzle to the wall along the jet centerline in streamwise direction. I denotes the measurement of the impact pressure, perpendicular to the PMS. The impingement angle was varied by adjusting the angle of the PMS.

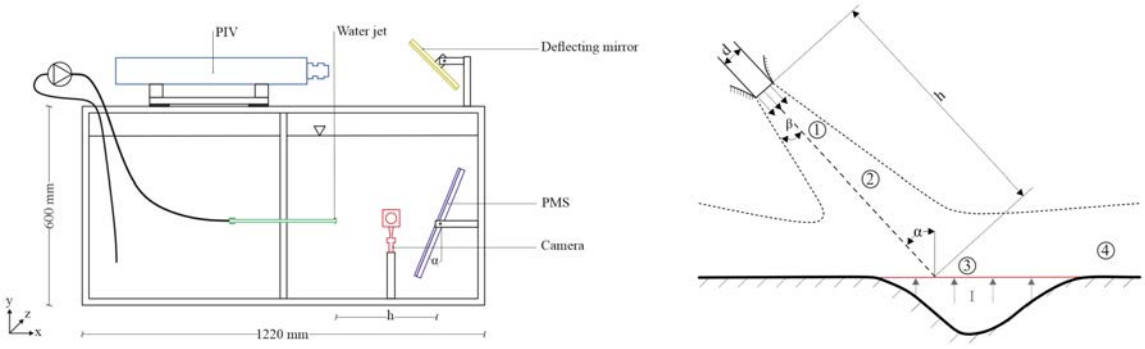


**Fig. 1.** Left: Schematic representation of the experimental rig. Right: Characteristics of an oblique impinging water jet.

### *Pressure Measurement Sensing*

Conventional pressure transducers have been found to be insufficient for the purpose of this study, as the sensing area is too large and inaccurate to fulfill the requirements of this study. Therefore, the PMS technique with a capacitive pressure sensing matrix (PX200:100:100.10; XSENSOR Technology; see specification in Table 2) was used to increase the spatial resolution. The authors adapted this technology for underwater measurements, which is usually applied in medicine, tire tread analysis and other industrial applications. As there is no factory calibration for the application under water available, the calibration which has been done at ambient air conditions to convert the measured signals into N/cm². The PMS was jetted with each nozzle for 60 seconds with a sampling frame rate of 1 frame/s. A lower threshold of 0.008 N/cell was used to neglect pressures that occurred due to minimal water surface turbulences.

**Table 2.** Specification of the PMS model PX200:100:100.10.

| Attribute | Data |
|---|---|
| Sensing Technology | Capacitive Pressure Imaging |
| Pressure Range | 0.1 – 10.3 N/cm² at normal atmospheric pressure |
| Sensing Area | 25.4 x 25.4 cm |
| Sensing Points | 10000 |
| Spatial Resolution | 2.54 mm |
| Accuracy | ± 10% full scale |
| Sampling Frame Rate | 1 frames/s |

### *Particle-Image-Velocimetry*

The 2D flow measurements were performed using a PIV Nd:YAG laser (YAG135-15-LIT Litron, 135 mJ, 15 hZ, 532 nm) with a light sheet for water jet illumination. Images were captured with an 8 MP Camera (TSI PowerView) with a 50 mm lens. Water was seeded with spherical hollow glass particles (12 µm) as tracer particles.

### *Statistics*

Possible relationships between average and peak impact pressure, and the water jet parameter were tested statistically by one-way analysis of variance (ANOVA) technique. Significance level is 5%. Average and peak impact pressure data was not normally distributed and therefore a log-transformation was applied to achieve normality.

The Multiple Linear Regression (MLR) was used to generate a prediction model for the impact pressure. A further description and background information about linear regression analysis can be found in Montgomery et al. (2012). The data were analyzed with the statistical software Origin. According to the results presented, h, P, α and β were used as parameter for the MLR. P and h were not normally distributed and therefore log-transformed to fulfill the requirements for the MLR analysis. As the PMS only measures pressure perpendicular to the wall, the cosine of β was used in the MLR.

## RESULTS AND DISCUSSION

### *Standoff Distance*

The water jet width, shown as cavitation cloud, shows a normal distribution (Fig. 2). Under conditions of cavitation, a cone of bubbles forms in the vicinity of the nozzle, expands significantly within several millimeters and the cavitation cloud develops over some length (Fig. 2 b & c), what is called the zone of flow establishment. After the cavitation cloud is developed, the effectiveness of the water jet is roughly constant and at a certain distance, the jet velocity decreases such that the conditions for cavitation are no longer satisfied and no new bubbles are formed in the zone of established flow. The cavitation cloud tends to disappear with increasing β and h. In Fig. 2 a), similarity is evident for the β=20° and β=40°, as well as for the β=80° and β=120° spray angle curve. Both, the β=20° and β=40° curve correspond almost to the theoretical β=40° spray width curve (grey dotted line, calculated by trigonometry functions) and the width of β=80° and β=120° curve is considerably smaller than

the theoretical spray width curve. However, the spray width is considerably different at h=150 mm for β=80° and β=120° spray angle jet. A twofold increase of β from 20° to 40° increases the spray width by 16%, whereas a duplication from β=40° to β=80° leads to an increase in spray width by 52%. A threefold increase from β=40° to β=120° increases the water jet width by nearly 100 %. The results have shown that the pump pressure P has no effect on the spray width.

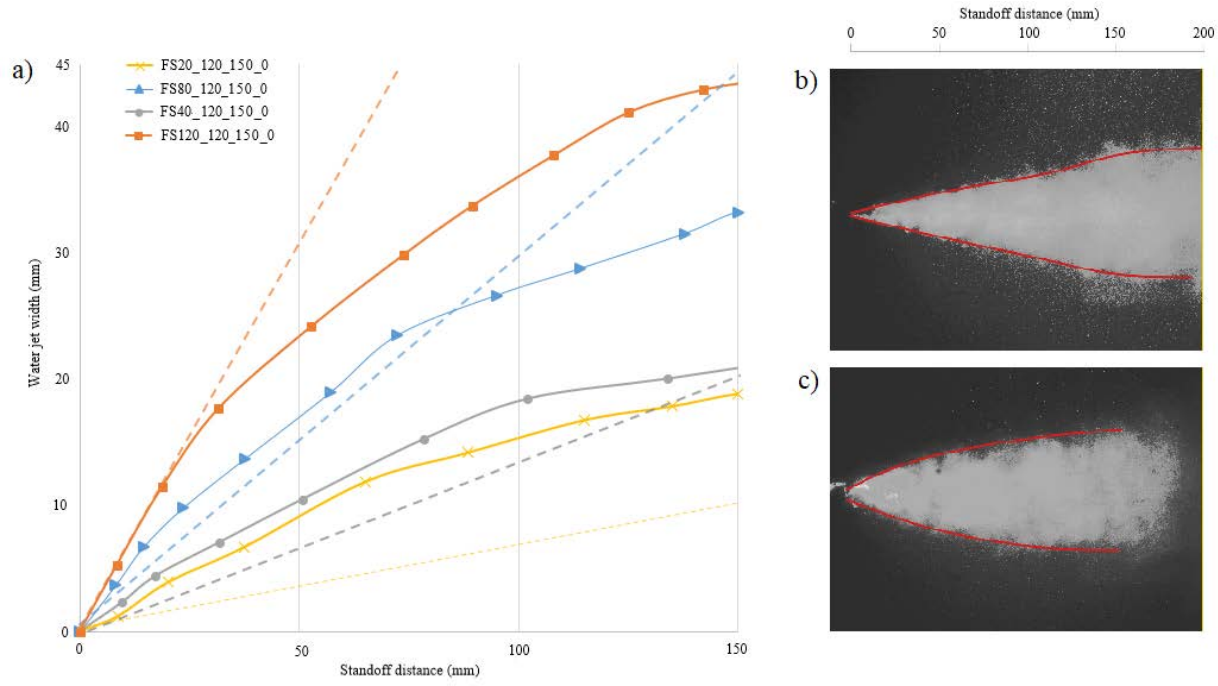


**Fig. 2.** (a) Variation of water jet width (solid lines) for different β (20°, 40°, 80° and 120°) and its theoretical spray pattern (dotted lines) at constant P (120 bar) and h (150 mm), approaching to the wall (marked by the yellow line). Streamwise direction of the water jet is from the bottom to the top. (b), (c) PIV images shows the cavitation cloud boundaries (red lines).

The decay in impact pressure of all experiments is less pronounced with increasing h (Fig. 3). This strongly non-linear effect is also shown for the impinging area. The ANOVA (one-way) showed that the decline in average impact pressure is only significant between h = 200 mm and h ≤ 150 mm, and the decline in peak impact pressure is only significant from h=50 mm to h=100 mm. An increase in h from 50 mm to 100 mm decreases the average impact pressure by 33% and the peak pressure by 45%. An increase in h to 200 mm decreases the impact pressures by 73% (peak) and 55% (average), respectively. This corroborates to the findings of Nobel & Talmon (2012), that after a certain distance of the jet towards a boundary, the jet velocity decreases and therefore the conditions for cavitation are no longer satisfied and no new bubbles are formed, therefore the impact pressure of the cavitating

jet decreases. At a short h, the impact pressure is at highest, because the water jet is already developed and the cavitation bubbles enhance the impact pressure. When the cavitating jet hits the surface, shock waves and micro jets are produced due to the bubble collapse, which cause a significant impact force.

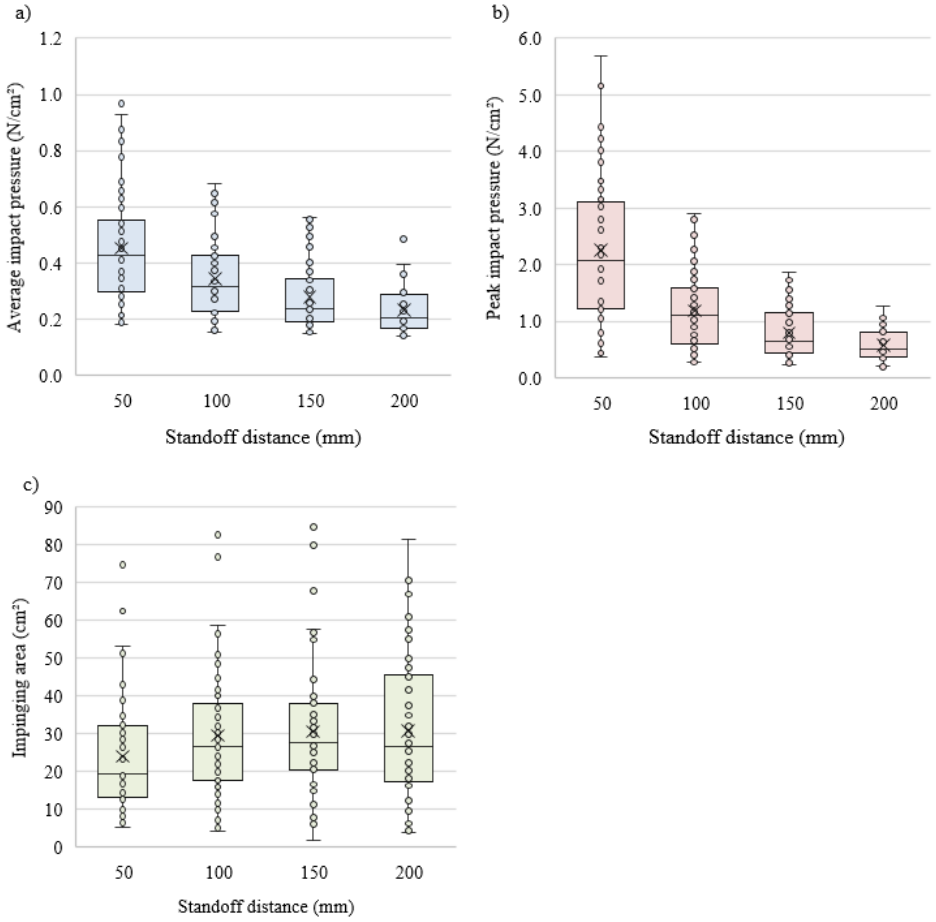


**Fig. 3.** Box plots showing average (a) and peak (b) impact pressure on the impinging area; as well as the impinging area (c) of all experiments (data for β, P, h and α were combined). Bottom and top of boxes show 25$^{th}$ (first quartile) and 75$^{th}$ (third quartile) percentiles, respectively. Whiskers show maximum and minimum, except when outliers are present. Outliers are shown as hollow dots and are 1.5 times below the first quartile and 1.5 times above the third quartile, respectively.

A sharp, but not significant increase in impinging area from h = 50 mm (MdN = 21.5 cm²) to h = 100 mm (Mdn = 30.9 cm²) can be seen in Fig. 3 c). A further increase in h resulted in not significant increase in impinging area, however, the measured data are further distributed.

### *Pump Pressure*

Pump pressure and impact pressure are not connected in a linear manner (Fig. 4). An increase of P by 100% increases the average impact pressure by 7%, 9% and 33%, and 10%, 83% and 15% for the peak pressure, respectively. PIV images showed that an increase in P results in the formation of additional cavitation bubbles. The authors assume that with an increase in jet pressure, the pressure gradient required for cavitation extends over a longer distance. Hence, the length of the cavitation cloud increases with jet pressure (Nobel 2013). Our results are in line with Liu et al. (2017), who stated that with low jet pressure, the resistance of the ambient water will clearly hinder the jet development even destroy the integrity of the jet stream.

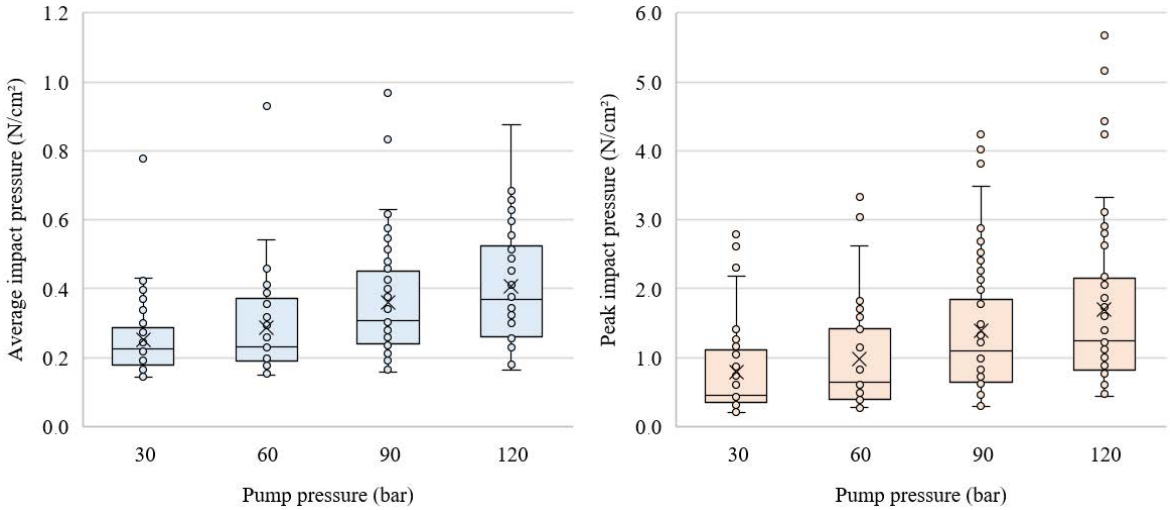


**Fig. 4.** Box plots shows the effect of a P on average and peak impact pressure of all measurement data.

Surprisingly, between P=60 bar and P=90 bar the increase in impact pressure is highest and the number of formed bubbles and the development of the water jet is assumed to be maximized. Therefore, the maximized output by minimized input (energy), under economic aspects, is achieved in this range. A further increase in P results only in a comparatively smaller increase in impact pressure.

### *Impinging Angle*

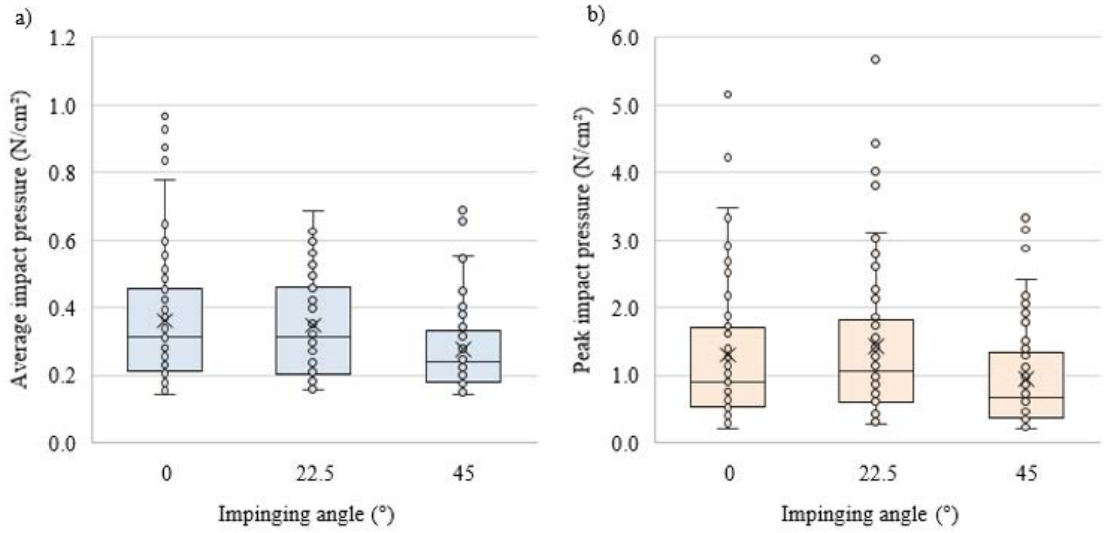


**Fig. 5.** Box plots show the effect of α on the average and peak impact pressure of all measurement data.

Average and peak impact pressure for α=22.5° ($Mdn_{avg}$=0.37; $SD_{avg}$=0.15; $Mdn_{peak}$=1.15; $SD_{peak}$=1.13) was slightly, but not statistically significantly higher than for α=0° ($Mdn_{avg}$=0.34; $SD_{avg}$=0.19; $Mdn_{peak}$=0.85; $SD_{peak}$=1.07) (Fig. 5). In contrast to α=45° ($Mdn_{avg}$=0.26; $SD_{avg}$=0.13; $Mdn_{peak}$=0.69; $SD_{peak}$=0.74) the average and impact pressure is significantly lower than for α=0°. It can thus be suggested that a water jet inclination changes the flow direction and velocity at the deflection zone, causing a change in impact pressure. In order to clarify such transient flow behavior of this zone, the cross-sectional impact pressure distribution in the center of the impinging area (where the maximum of the sum of all cells in a row of the PMS is) and the flow characteristics of PIV images (β=20°, h=50 mm and P=120 bar; wall marked by the yellow line, a: α=0°; b: α=22.5°; c: α=45°) is shown in Fig. 6. The impact pressure distribution is not normally distributed. The maximum impact pressure of 3.5 N/cm² for α=0° is slightly lower than the 3.8 N/cm² for α=22.5°. A collapse of cavitation bubbles may be caused by the pressure reduction in the near impinging wall region. The similarity of the curves indicates that α has significant effect on the impact pressure distribution (this trend is also shown in the other experimental results; Fig. S2 - S5). With decreasing distance to wall the cavitation cloud (the higher the cavitation bubble density, the brighter the cloud) tends to disappear. Only a few bubbles, shown as light grey region, are redirected along the wall.

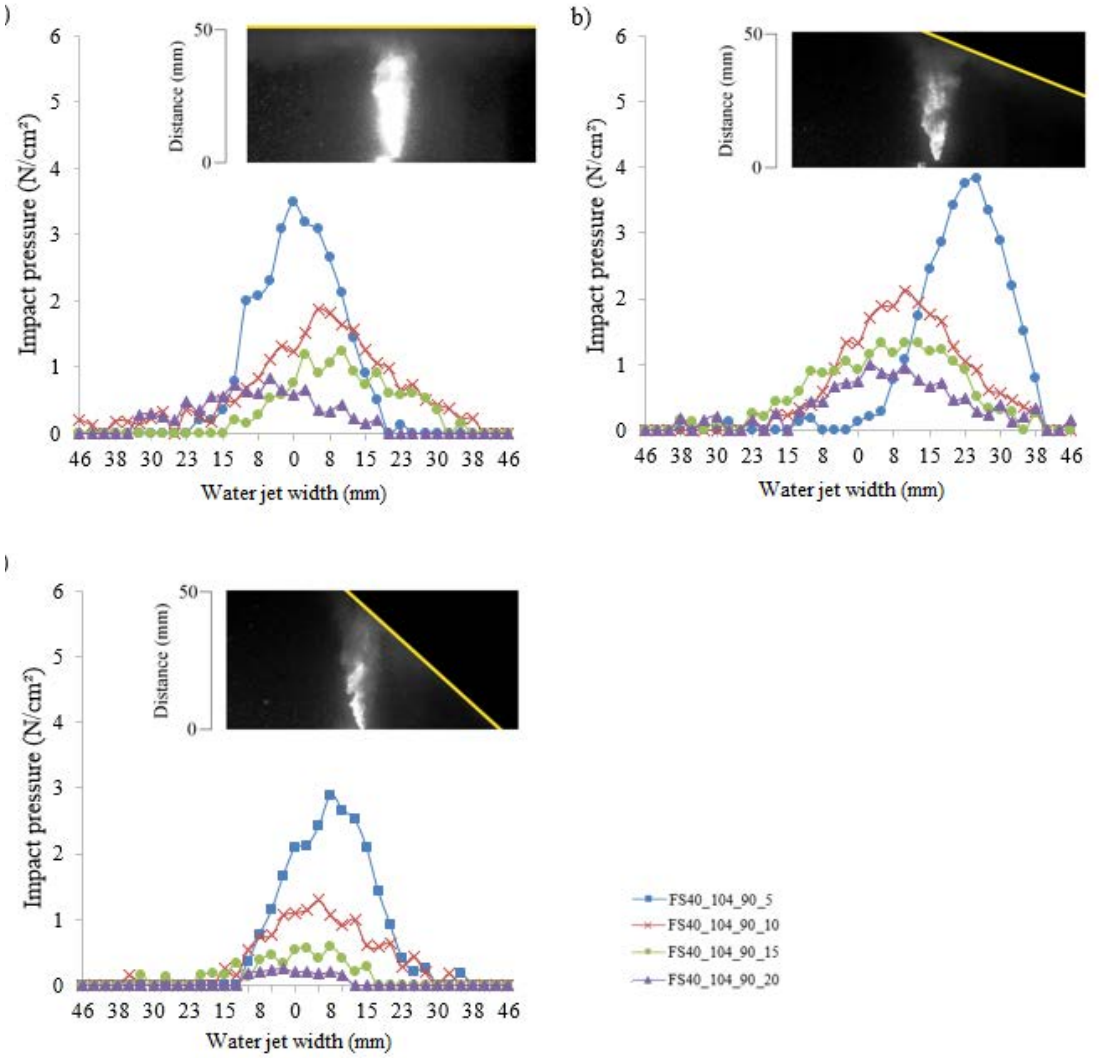


**Fig. 6.** Impact pressure distribution along a cross-section of water jets (β=20°, P=120 bar, h=50 mm) with variation in α=0° (a), α=22.5° (b) and α=45° (c).

Once the water jet is approaching the wall, it loses its x-axial velocity and the jet flow direction turns radially. The x-axial velocity component decreased and is transformed into a new reflected velocity vector with an x- and y-component (deflection zone). The jet flows in y-direction along the wall (wall jet zone), which can be seen in Fig. 6 as a less brighter cavitation cloud in y-direction in contrast to the cavitation cloud in x-direction. Within the deflection zone vortexes of various sizes are developed. With decreasing velocities of the jet flow in front of the wall, the cavitation bubbles get rapidly shrunk, causing a collapse of cavitation bubbles. This collapse generates an extremely large shock pressure (Nakamura et al. 2001). At a perpendicular jet impingement (α=0°) reflection components in backwards x-direction are most pronounced as well as the turbulent zone. It is assumed that the

approaching x-axial velocity is decreased at a larger distance towards the wall and therefore the collapse of the cavitation bubbles occurs also at larger distances. This could have the reducing effect on the resulting impact pressure. The overall average impact pressure is lowest within the experiments at an impinging angle of 45°. The authors assume that this effect is due to the reduced vertical impact pressure components and an increased orientation parallel to the wall overcompensating the effect of a reduced “cushion zone”. Further investigations are necessary to validate this assumption that can be drawn from this study.

### *Nozzle Spray Angle*

As shown in Fig. 7, the smaller β is, the higher is the impact pressure, which corresponds to the observations of the PIV images. There are no significant differences ($p<0.05$) between the average impact pressure of β=20°($Mdn_{avg}$=0.34; $SD_{avg}$=0.15) and β=40 ($Mdn_{avg}$=0.32; $SD_{avg}$=0.19), as well as for the peak impact pressure of β=20°($Mdn_{peak}$=1.17; $SD_{peak}$=1.21) and β=40 ($Mdn_{peak}$=1.15; $SD_{peak}$=1.03), respectively. This is similar to the observation of the standoff distance effect, where the flow characteristics of both, β=20° and β=40° showed similarity. With β=80° a relatively lower average ($Mdn_{avg}$=0.25; $SD_{avg}$=0.14) and peak impact pressures ($Mdn_{peak}$=0.68; $SD_{peak}$=0.67) are generated. An increase in β to 120° decreases the average impact pressure ($Mdn_{avg}$=0.25; $SD_{avg}$=0.05) and impinging area (Mdn 0 46.4 cm²) significantly in comparison to the lower spray angles, where the peak impact pressures ($Mdn_{peak}$=0.52; $SD_{peak}$=0.35) does not differ significantly.

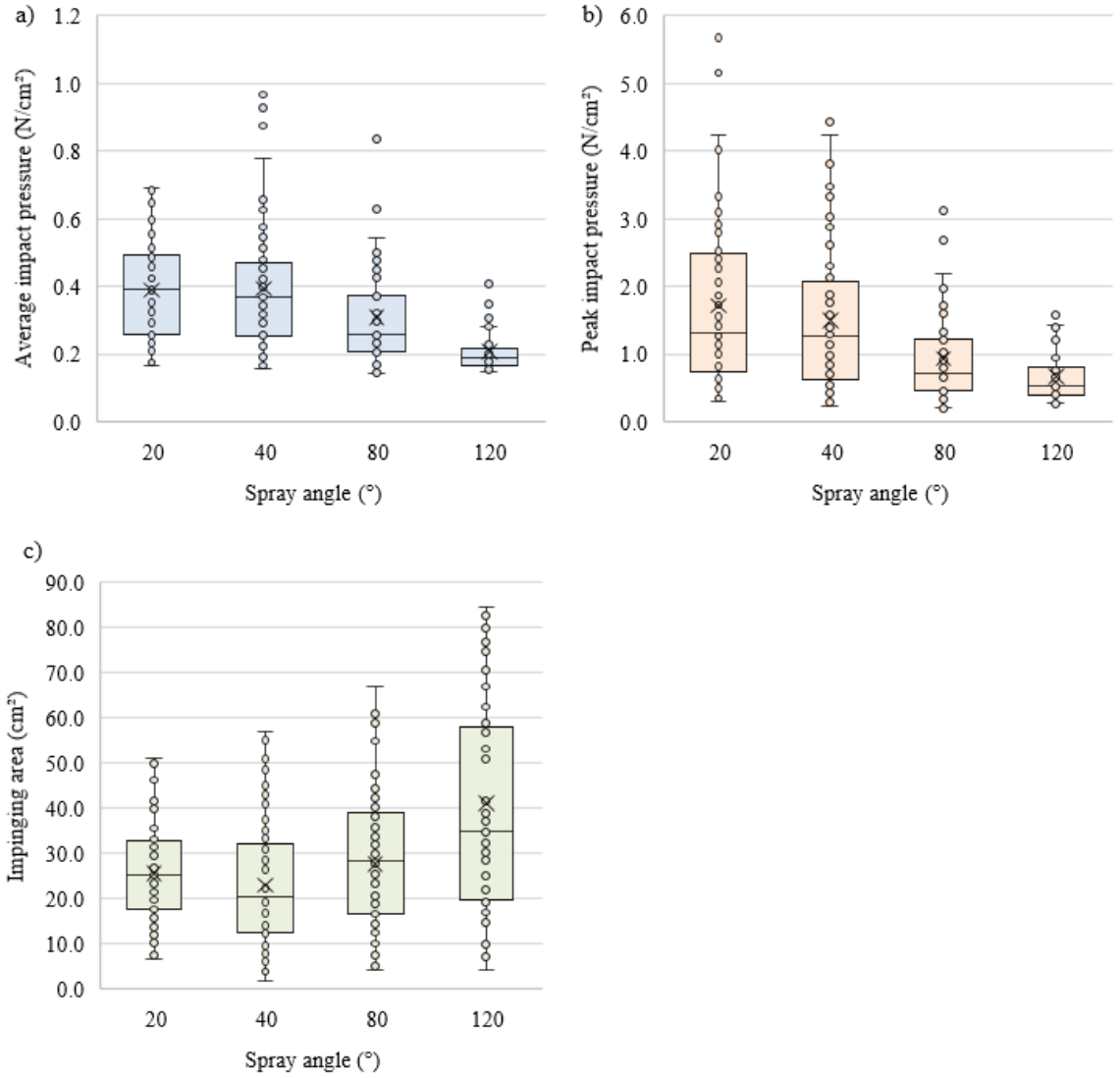


**Fig. 7.** Box plots show the influence of β on the average (a) and peak impact pressure (b), as well as impinging area (c) of all measurement data.

Spray angles of 80° and 120° show a more pronounced flat fan jet spray pattern, in terms of an elliptical impact pressure distribution, as compared to β=20° and β=40° (only β= 20° and 80° are exemplary shown in Fig. 8; see Fig. S6 - S10 for other spray pattern). It was assumed that all tested water jets show a flat fan jet spray pattern, as this was observed by tests of the manufacturer of the jets at air. The 20° spray pattern shows more defined edges, even at different standoff distances, in contrast to β=80°, where the contours blur with increasing h (Fig. 8). This is in line with the observation in the PIV images, where the cavitation characteristics significantly decrease, especially at larger standoff distances (Fig. 2).

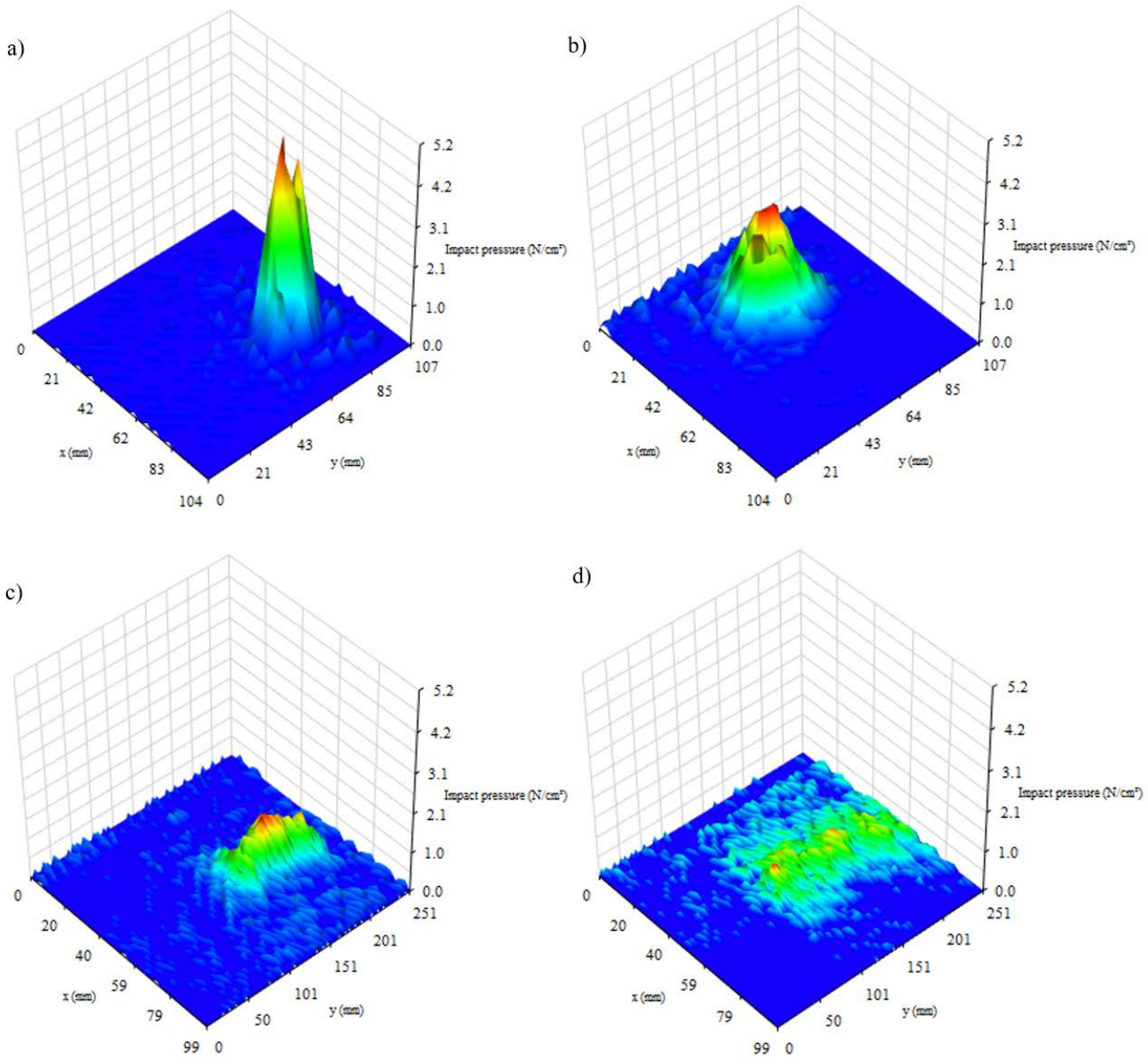


**Fig. 8.** Impact pressure distribution of a water jet with β=20°, P=120 bar, h=50 mm (a), 100 mm (b) and β=80°, P=120 bar, h=50 mm (c), 100 mm (d).

## Multiple Regression Model

As a result of the MLR, with four regression coefficients (α, β, h and P), the following equation to predict the average (Eq. 1) and peak (Eq. 2) impact pressure are derived :

$$\log(y_{average}) = 0.941+0.415*\log(P) - 0.486*\log(h) - 0.173*\beta + 0.393*\cos(\alpha) \quad \text{Eq. 1}$$

$$\log(y_{peak}) = -0.561 + 0.780*\log(P) - 0.981*\log(h) - 0.253*\beta + 0.584*\cos(\alpha) \quad \text{Eq. 2}$$

The correlation coefficient ($R^2$) for the average and peak impact pressure is around 0.81 and 0.86, respectively indicating a good correlation. The comparison between the predicted and the measured values is illustrated in Fig. 9. According to the $R^2$-values and Fig. 9 it can be seen, that the predictive power of the model is strongest for the peak impact pressure (Eq. 2). Interestingly, outliers (shown in red circle) are related to β=40°, P=30-120 bar, h=50 mm at α=0°, and to β=80°, P=90 bar, h=50 mm at α=0°. It can be assumed that at h=50 mm the water jet is in the transition between the zone of flow establishment and zone of established flow, where high turbulences resulted in measurement fluctuations. The analyses of this study show, that a prediction of impact pressure according to the defined water jet parameters is possible.

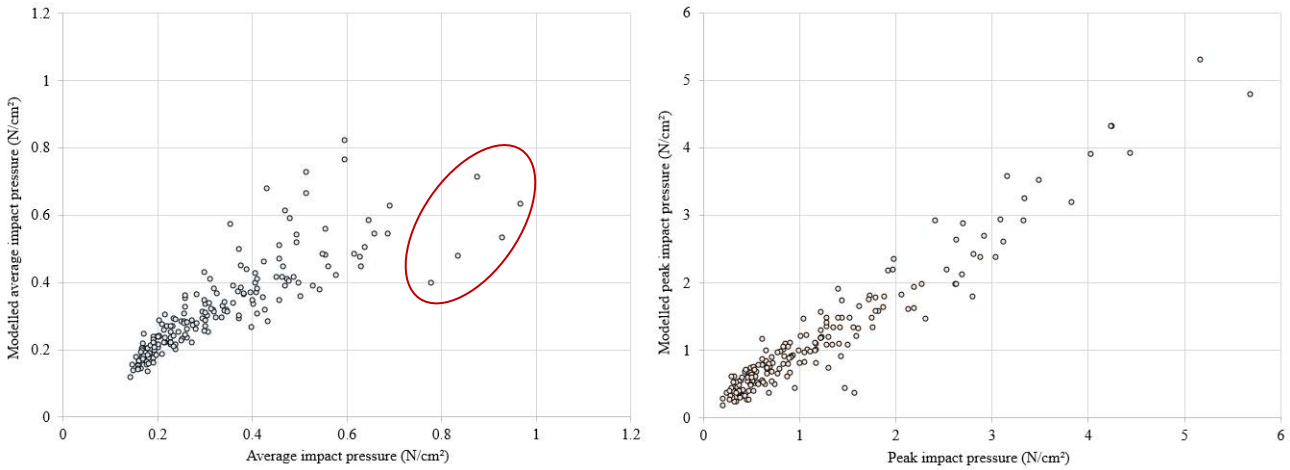


**Fig. 9.** Comparison of measured and modelled average (left) and peak (right) impact pressure. Red circle shows outliers.

Peak impact pressure decreases approximately reciprocally with standoff distance and the average impact pressure reciprocally with the square root of standoff distance. P and cos(α) have a positive impact on peak and average pressure whereas the spray angle shows a weak negative dependency.

## CONCLUSION

The experimental results show that the PMS is an innovative and applicable method for the measurement and visualization of submerged cavitating water jets impact pressures. The PMS technique has been used for the first time to investigate submerged water jets to enhance the high spatial resolution. The implosion of cavitation bubbles and the high-speed flow velocity towards the boundary of the wall are assumed to be responsible for the destructive action of this cavitating water jets. Thus, in order to improve the water jets and according dredging operations efficiency, it is necessary to control the impact pressure on the sediment by controlling the parameter and therefore establish a precise sediment removal technique. The model derived from the MLR-analyses allows the prediction of the resulting impact pressure according to set parameter configuration and therefore dredging optimization. If the erodibility of the sediment deposits is known, the model and the impact pressure distribution plots of the PMS measurement can be used to identify specific water jets to either provide higher impact pressures on a small area or lesser impact pressures at a larger area.

Further research is needed to investigate the relationship between the erodibility of sediment and the impact pressure of submerged cavitating water jets. However, the interaction of a water jet with sediment is a complex and dynamic process. As this paper describes an experimental method for impact pressure measurements on an impermeable planar, non-erodible and non-deforming wall, a sediment penetrating water jet is a clearly different situation. Erosion processes of natural sediment constantly change the penetrating ground conditions varying with dredging depth. In addition, a traversing water jet at a constant speed may also affect the dredging efficiency.

The PMS technique was initially calibrated for measurement in air and by making the PMS impervious to water, the calibration may be affected. Future investigations are necessary to calibrate the PMS technique under water to qualify and quantify potential differences between measurements in air and water. Further research purposes should further incorporate comprehensive PIV measurements and analysis and a subsequent comparison with PMS data. However, PIV measurements proved to be difficult in the studied situations. The PIV setup, pre- and post-processing needs to be readapted to the region of cavitation cloud extending, cloud preserving and cloud shrinking in each experimental setup. The constantly changing three-dimensional cavitation cloud structure makes the measurement setup and processing additionally difficult.

## DATA AVAILABILITY STATEMENT

Some or all data, models, or code generated or used during the study are available from the corresponding author by request. Items:

- Pressure Measurement Sensing data
- Particle-Image-Velocimetry images


## ACKNOWLEDGMENTS

The authors would like to thank Simon Ludwig for his help throughout the measurements.


## NOTATION

*The following symbols are used in this paper:*

d = Inner diameter of the water jet nozzle

h = Distance between the nozzle and the impact wall

I = Impact pressure on the Pressure Measurement Sensor

Mdn = Median

P = Pump pressure

SD = Standard deviation

α = Slope angle of the water jet at its issuing point

β = Spray angle of water jet nozzle

## SUPPLEMENT DATA

**Fig. S1.** Technical drawing (left) and photo of the flat fan water jet (right).

**Fig. S2.** Cross-sectional impact pressure distribution of water jets with spray angle β=20° and pump pressure P=90 bar with varying standoff distance (h) and impinging angle (α).

**Fig. S3.** Cross-sectional impact pressure distribution of water jets with spray angle β=40° and pump pressure P=90 bar with varying standoff distance (h) and impinging angle (α).

**Fig. S4.** Cross-sectional impact pressure distribution of water jets with spray angle β=80° and pump pressure P=120 bar with varying standoff distance (h) and impinging angle (α).

**Fig. S5.** Cross-sectional impact pressure distribution of water jets with spray angle β=1200° and pump pressure P=120 bar with varying standoff distance (h) and impinging angle (α).

**Fig. S6.** Impact pressure distribution of water jets with β=20°, P=120 bar and α=0° with varying standoff distance (a) h=50 mm, (b) h=100 mm, (c) h=150 mm, and (d) h=200 mm.

**Fig. S7.** Impact pressure distribution of water jets with β=20°, P=90 bar and h= 50 mm with varying impinging angle (a) α=0°, (b) α=22.5°, and (c) α=45°.

**Fig. S8.** Impact pressure distribution of water jets with β=40°, P=90 bar and α=0° with varying standoff distance (a) h=50 mm, (b) h=100 mm, (c) h=150 mm, and (d) h=200 mm.

**Fig. S9.** Impact pressure distribution of water jets with β=40°, P=90 bar and α=22.5° with varying standoff distance (a) h=50 mm, (b) h=100 mm, (c) h=150 mm, and (d) h=200 mm.

## REFERENCES


Dular, M., and Petkovšek, M. (2015). "On the mechanisms of cavitation erosion – Coupling high speed videos to damage patterns." *Experimental Thermal and Fluid Science*, 68, 359-370, doi: doi.org/10.1016/j.expthermflusci.2015.06.001.

Guha, A., Barron, R., and Balachandar, R. (2011). "An experimental and numerical study of water jet cleaning process." *Journal of Materials Processing Technology*, 211, 610–618, doi: 10.1016/j.jmatprotec.2010.11.017.

Hogg, E., Huppert, H., and Dade, W. (1997). "Erosion by planar turbulent wall jets." *Journal of Fluid Mechanics*, 338, 317-340, doi: 10.1017/S0033223097005077.

Liu, H., Kang, C., Zhang, W., and Zhang, T. (2017). "Flow structures and cavitation in submerged waterjet at high jet pressure." *Experimental Thermal and Fluid Science*, 88, 504-512, doi: 10.1016/j.expthermflusci.2017.07.003.

Montgomery, D. C., Peck, E. A., & Vining, G. G. (2012). Introduction to linear regression analysis (Vol. 821). John Wiley & Sons.

Mortensen, J. (2013). “Resistance of Protective Coatings and Pipe Linings to High-Pressure Water Jets Used for Invasive Mussel Removal and Cleaning.” Hydraulic Laboratory Technical Memorandum PAP-1074.

Nakamura, Y. (2001). “Residual stress improved by water jet peening using cavitation for small-diameter pipe inner surfaces.” *Proc, 9th International Conference on Nuclear Engineering*, Nice, France.

Nobel, A. J. (2013). “On the excavation process of a moving vertical jet in cohesive soil.” PhD Thesis, TU Delft, Delft University of Technology.

Nobel, A. J., and Talmon, A. M. (2012) “Measurements of the stagnation pressure in the center of a cavitating jet.” *Experiments in Fluids*, 52(2), 403, doi: 10.1007/s00348-011-1231-y.

Peng, K., Tian, S., Li, G., and Alehossein, H. (2018). “Mapping cavitation impact field in a submerged cavitating jet.” *Wear*, 396–397, 22-33, doi: 10.1016/j.wear.2017.11.006.

Sato, K., Sugimoto, Y., and Ohjimi, S. (2009). “Pressure-wave formation and collapses of cavitation clouds impinging on solid wall in a submerged water jet.” Proc., *7th International Symposium on Cavitation*, Ann Arbor, Michigan, USA.

Shen, Z., and Sun, Q. (1988). “Study of Pressure Attenuation of a Submerged, Nonfree Jet and a Method of Calculation for Bottomhole Hydraulic Parameters.” *Society of Petroleum Engineers*, 3(1), doi:10.2118/14869-PA.

Silva, A. S. R., Noack, M., Schlabing, D., and Wieprecht, S. (2017) “A data-driven fuzzy approach to simulate the critical shear stress of cohesive sediments.” *Proc., International Symposium of River Sedimentation*, Stuttgart, Germany.

Soyama, H., and Lichtarowicz, A. (1996) “Cavitating jets-similarity correlations.” *Journal of Jet Flow Engineering*, 13, 9-19.

Wang, X., Niu, G.-P., Yuan, S.-Q., Zheng, X., Soon, J., and Soon, T. (2015) “Experimental investigation on the mean flow field and impact force of a semi-confined round impinging jet.” *Fluid Dynamics Research*, 47, 025501, doi: 10.1088/0169-5983/47/2/025501.

Weegenaar, R., Keetels, G., Winkelman, M. and van Rhee, C. (2015). “Sand erosion with a traversing circular jet.” *Proceedings of the Institution of Civil Engineers: Maritime Engineering*, 168, 76-83, doi: 10.1680/maen.14.00004.

Yahiro, T., and Yoshida, H. (1974) “On the characteristics of highspeed water jet in the liquid and its utilization of injection grounting method.” Proc., *2nd International Symposium on Jet Cutting Technology*, Cambridge University, Cambridge.

Zeleňák, M., Zeleňák, F., Scucka, J., Hloch, J., Zdenek, S., and Zdenek, R. (2015) “Visualisation and measurement of high-speed pulsating and continuous water jets.” *Measurement*, 72, 1-8, https://doi.org/10.1016/j.measurement.2015.04.022.

**Supporting Information:** Investigation of Impinged, Oblique Submerged Cavitating Water Jets with Pressure Measurement Sensing

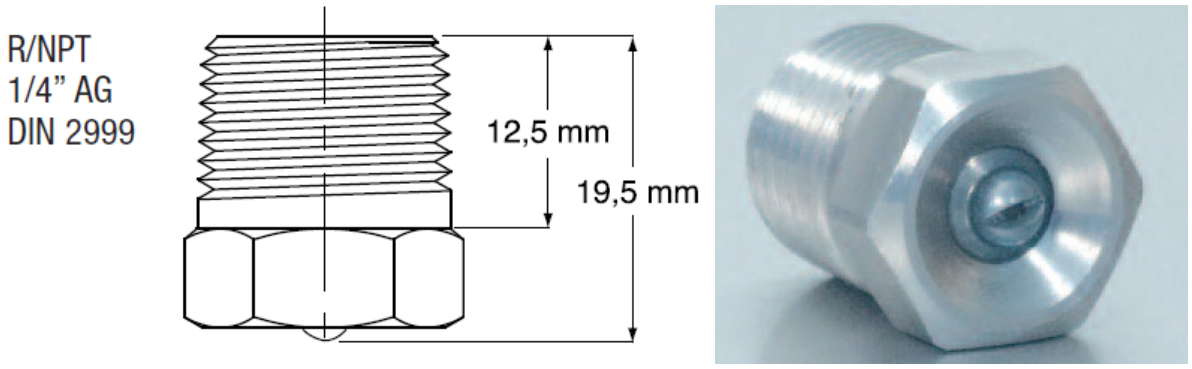


**Fig. S1.** Technical drawing (left) and photo of the flat fan water jet (right).

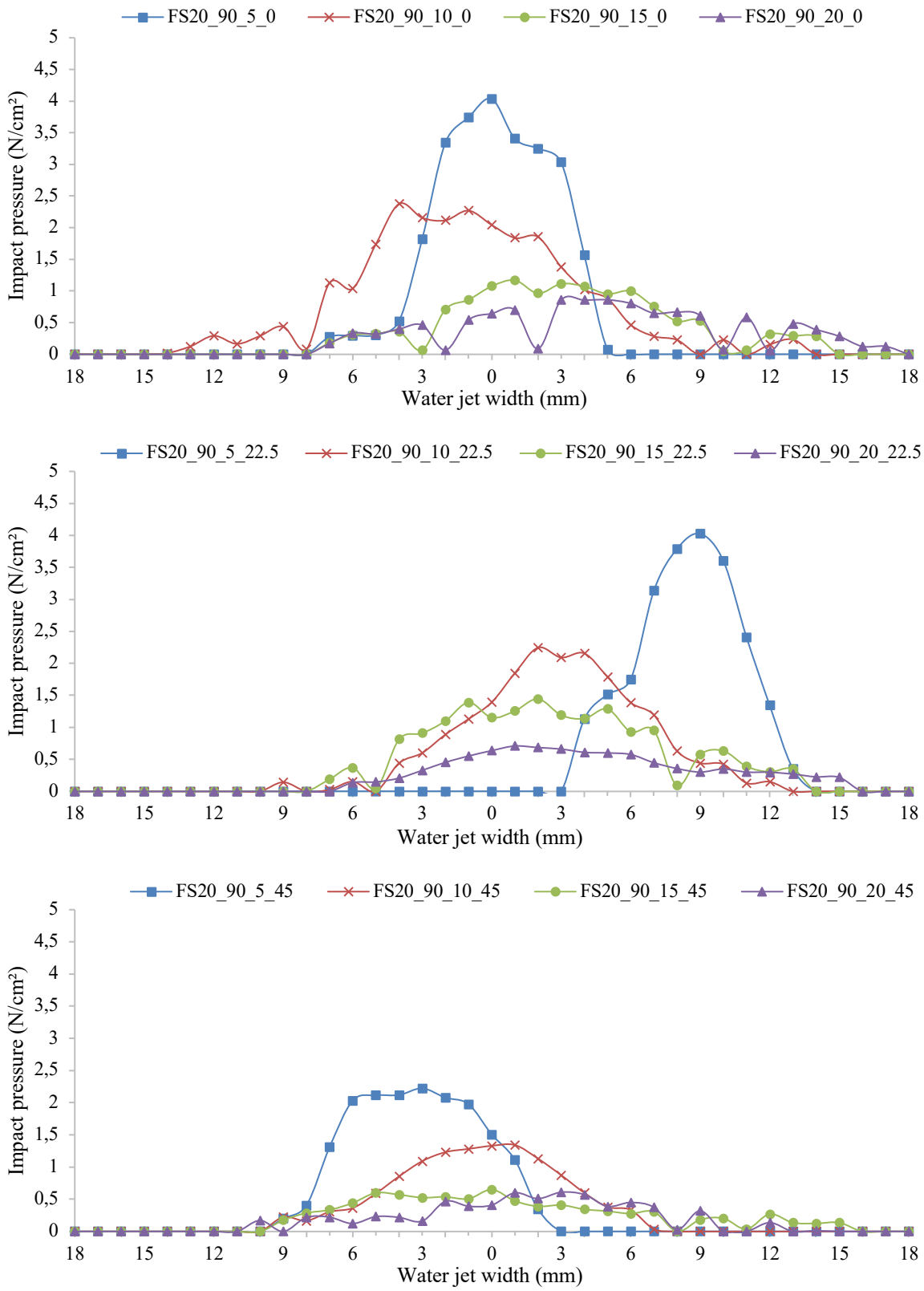


**Fig. S2.** Cross-sectional impact pressure distribution of water jets with spray angle β=20° and pump pressure P=90 bar with varying standoff distance (h) and impinging angle (α).

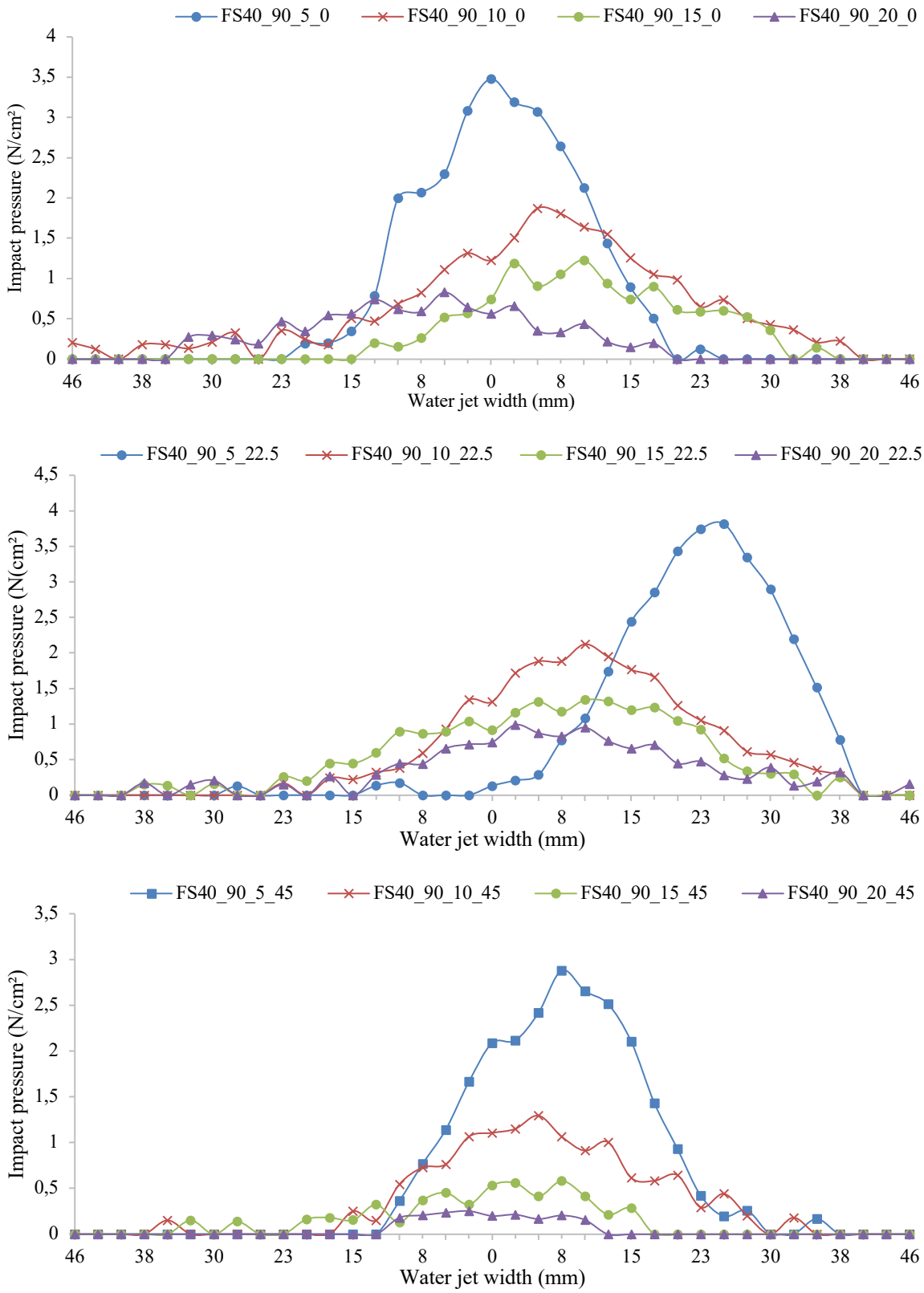


**Fig. S3.** Cross-sectional impact pressure distribution of water jets with spray angle β=40° and pump pressure P=90 bar with varying standoff distance (h) and impinging angle (α).

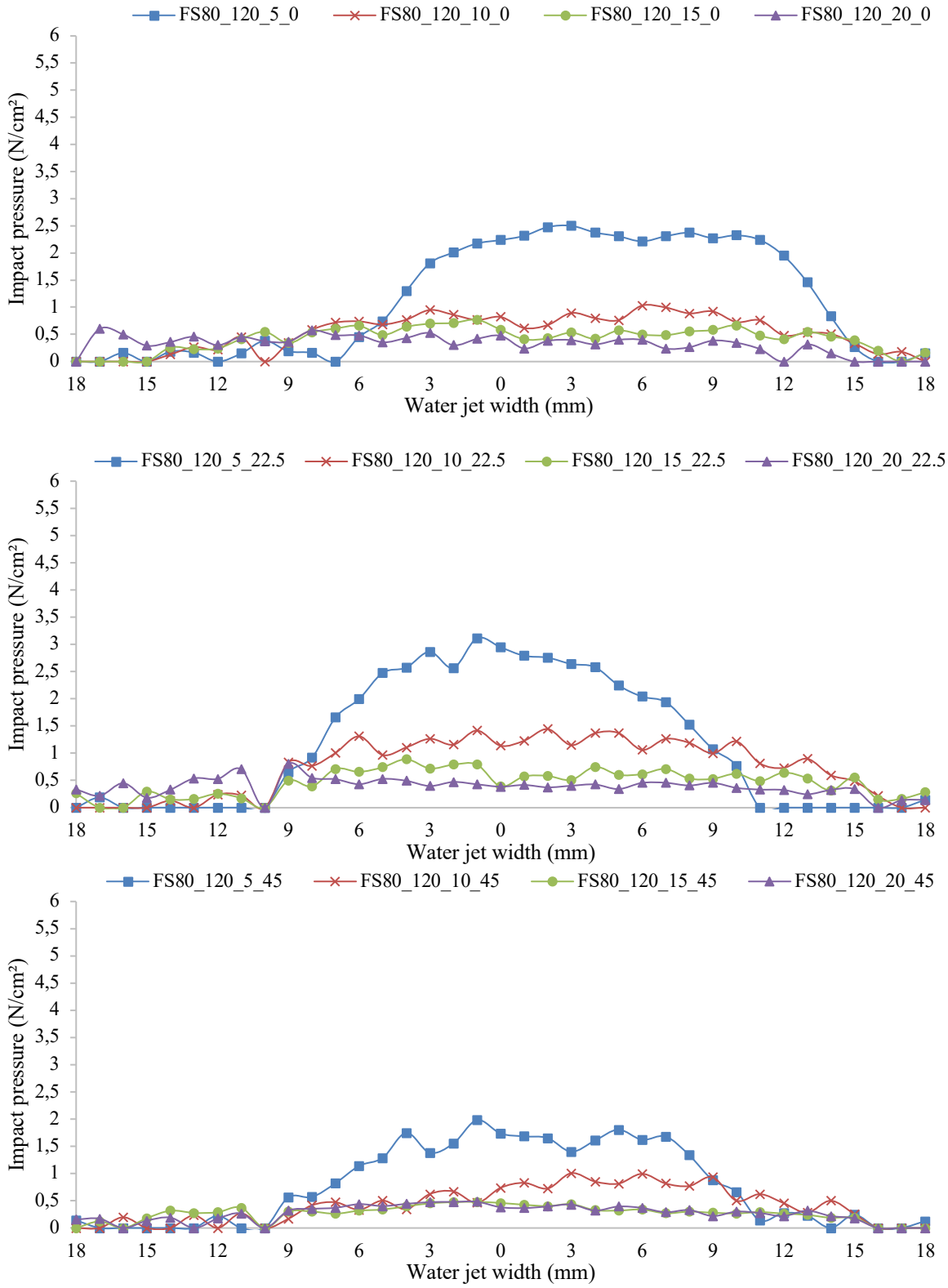


**Fig. S4.** Cross-sectional impact pressure distribution of water jets with spray angle β=80° and pump pressure P=120 bar with varying standoff distance (h) and impinging angle (α).

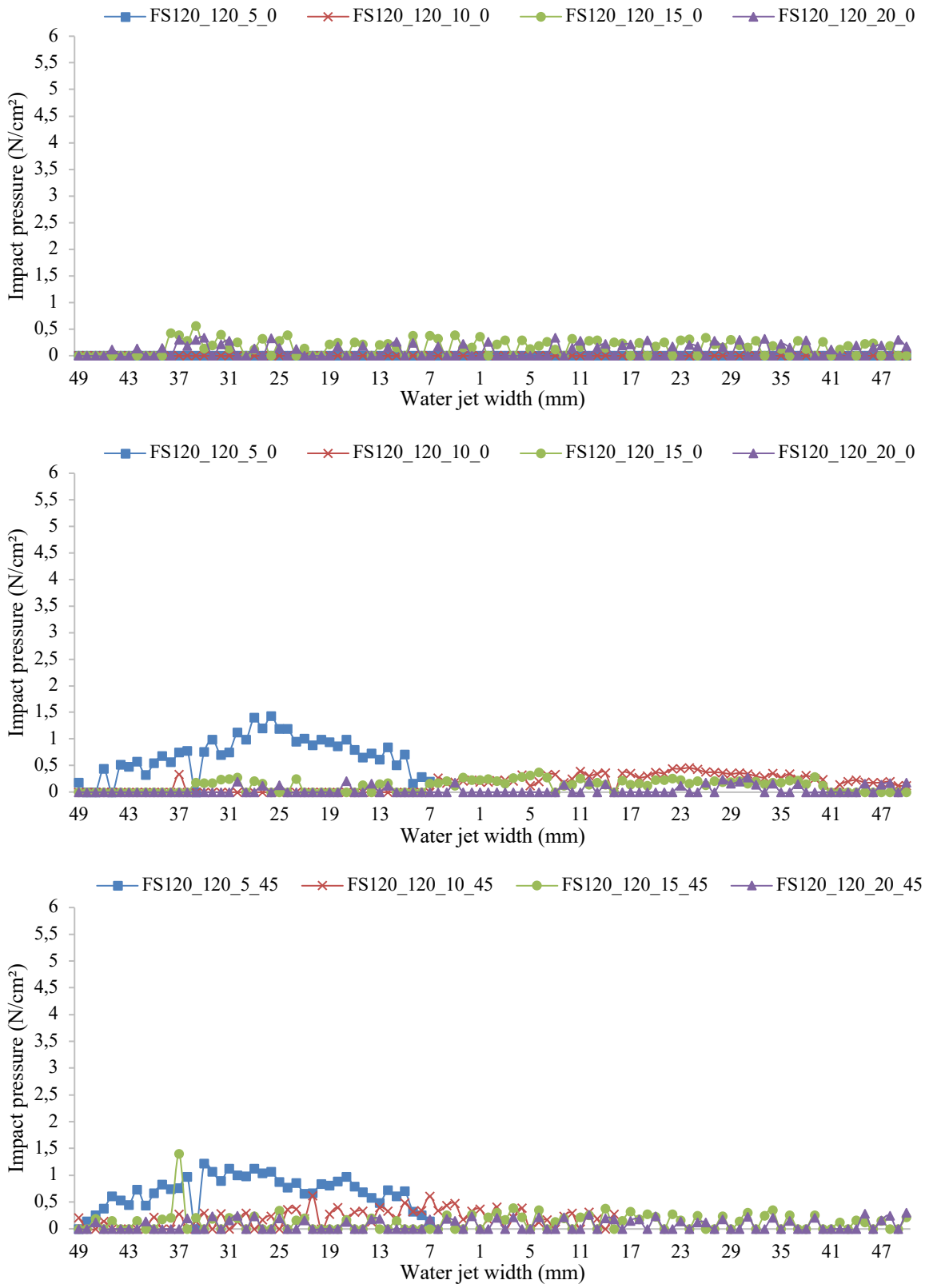


**Fig. S5.** Cross-sectional impact pressure distribution of water jets with spray angle β=1200° and pump pressure P=120 bar with varying standoff distance (h) and impinging angle (α).

a)

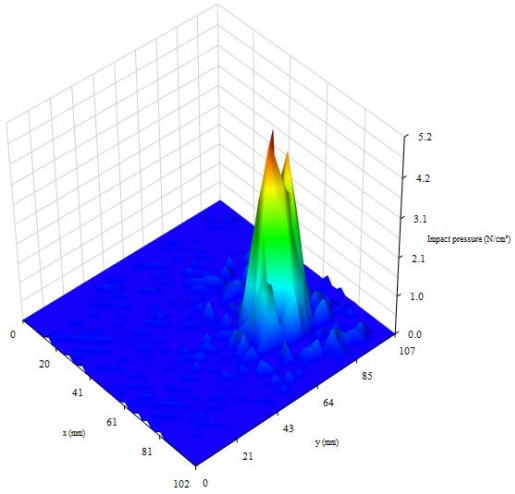


b)

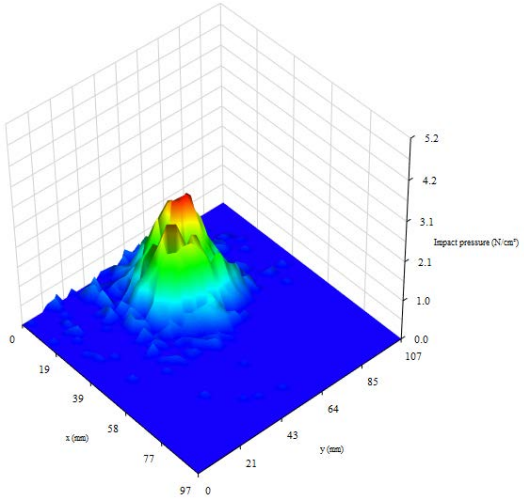


c)

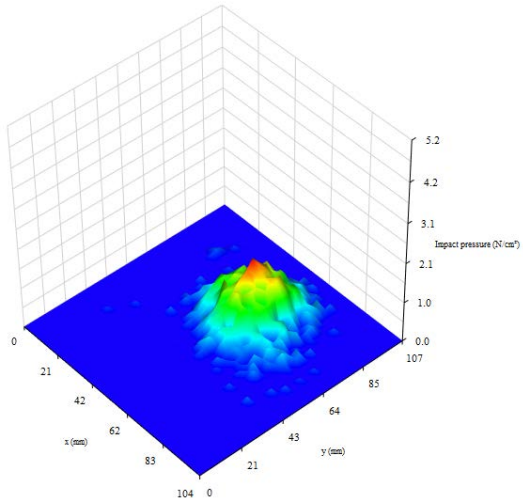


d)

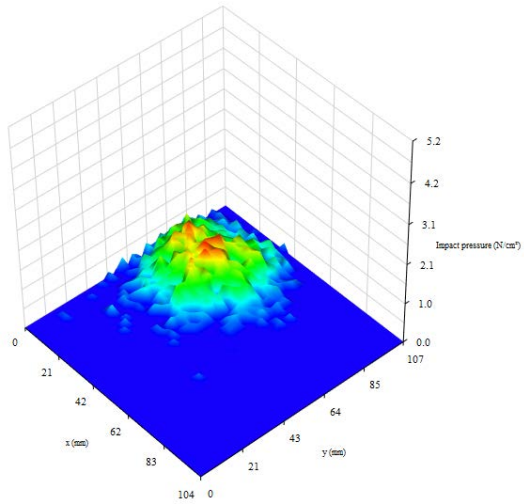


**Fig. S6.** Impact pressure distribution of water jets with β=20°, P=120 bar and α=0° with varying standoff distance (a) h=50 mm, (b) h=100 mm, (c) h=150 mm, and (d) h=200 mm.

a)

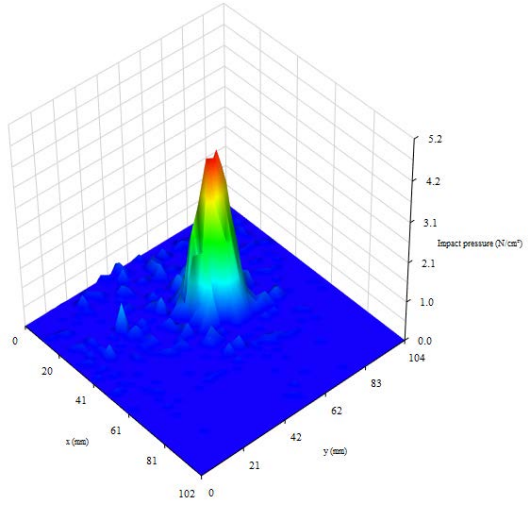


b)

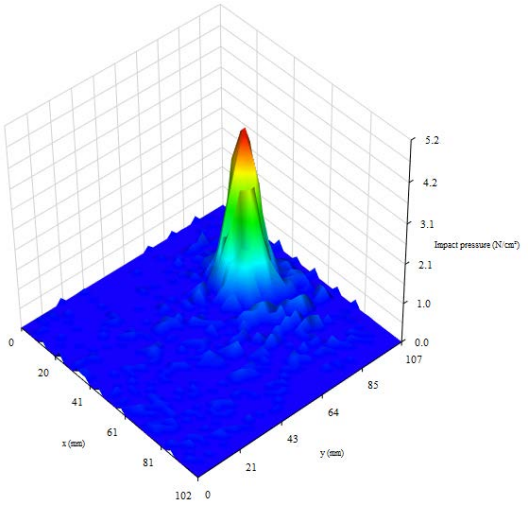


c)

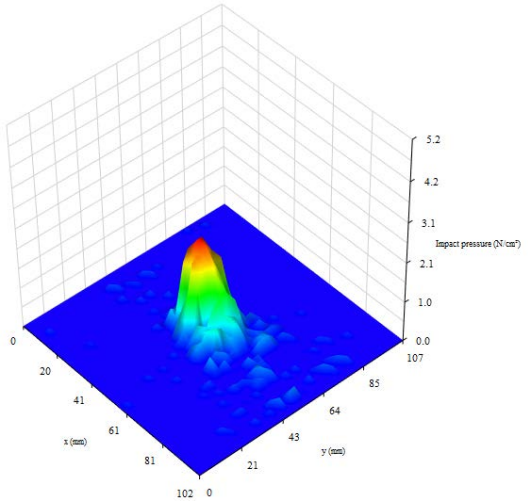


**Fig. S7.** Impact pressure distribution of water jets with β=20°, P=90 bar and h= 50 mm with varying impinging angle (a) α=0°, (b) α=22.5°, and (c) α=45°.

a)

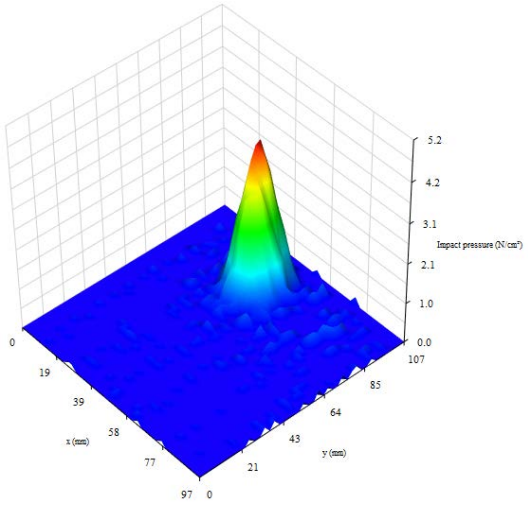


b)

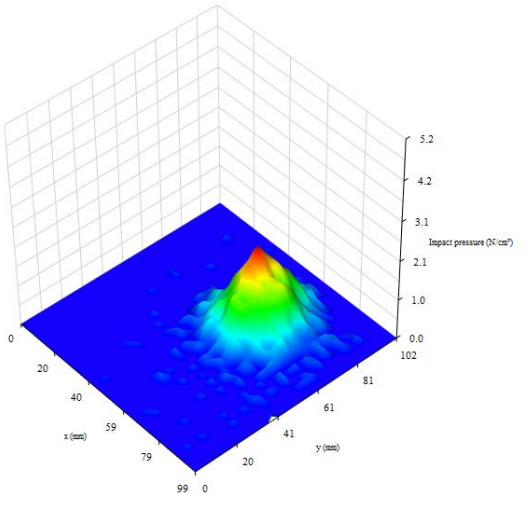


c)

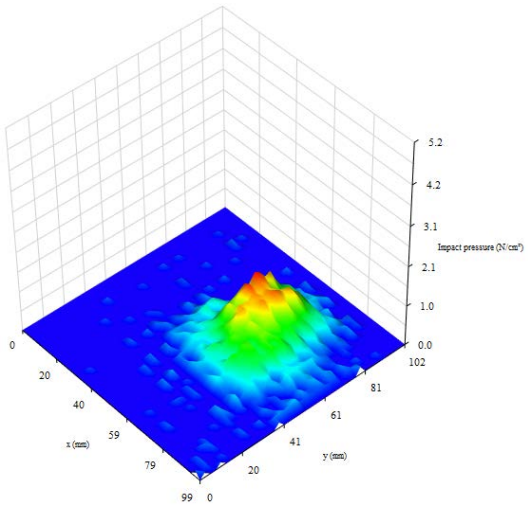


d)

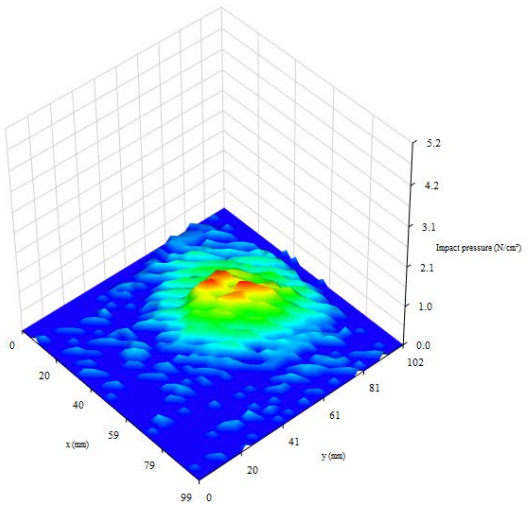


**Fig. S8.** Impact pressure distribution of water jets with β=40°, P=90 bar and α=0° with varying standoff distance (a) h=50 mm, (b) h=100 mm, (c) h=150 mm, and (d) h=200 mm.

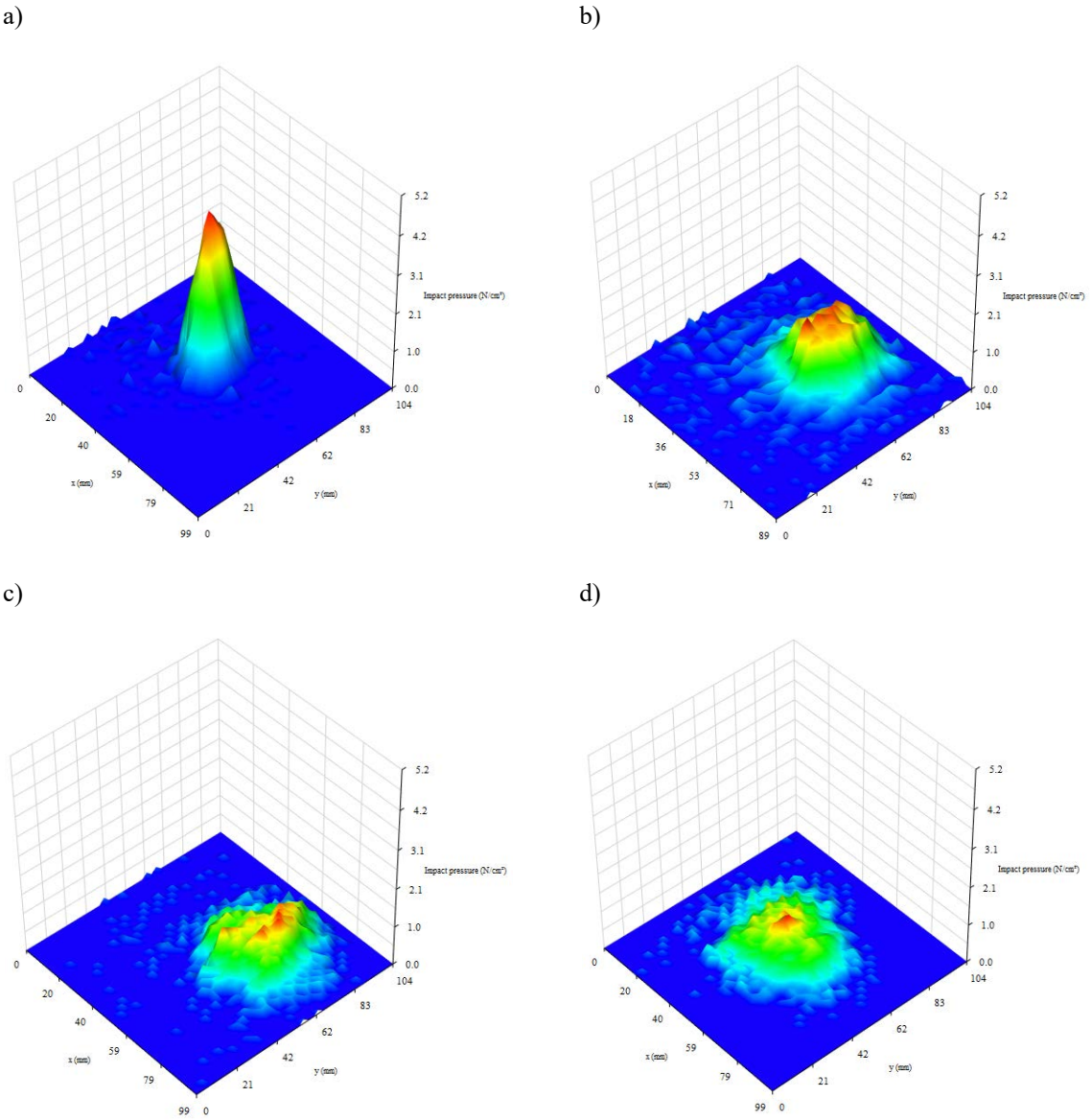


**Fig. S9**. Impact pressure distribution of water jets with β=40°, P=90 bar and α=22.5° with varying standoff distance (a) h=50 mm, (b) h=100 mm, (c) h=150 mm, and (d) h=200 mm.

a)

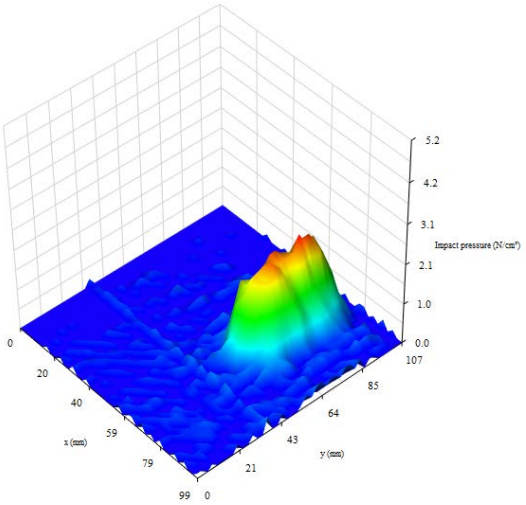


b)

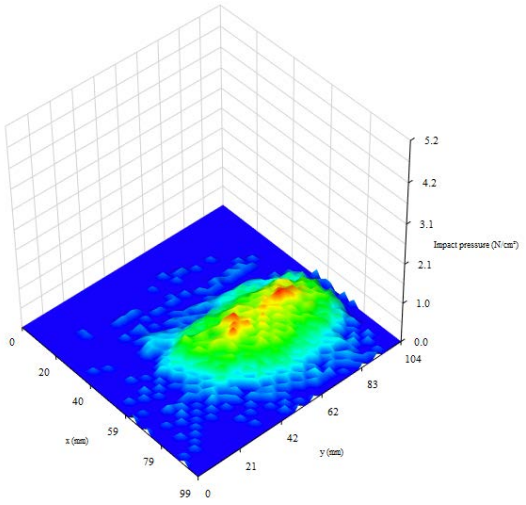


c)

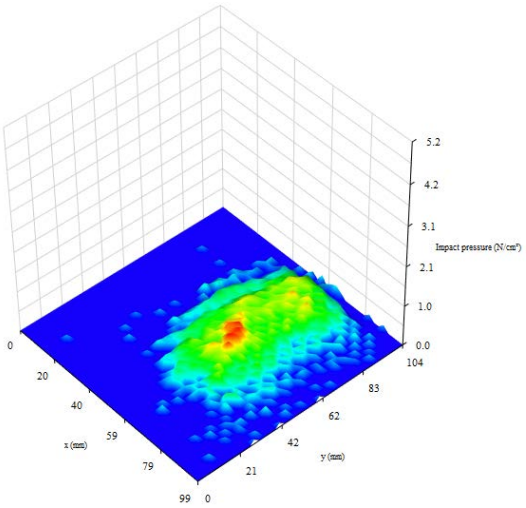


d)

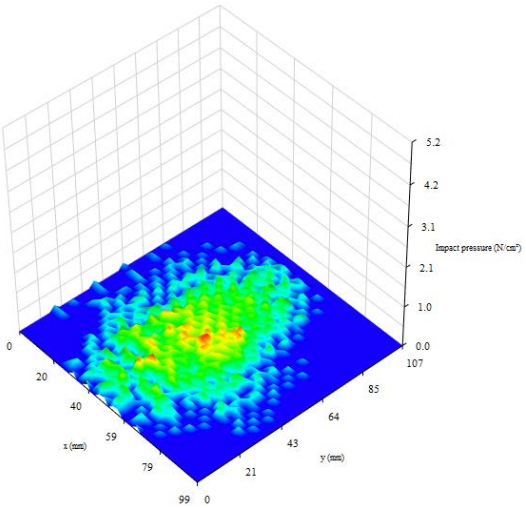


**Figure S10.** Impact pressure distribution of water jets with β=80°, P=120 bar and α=0° and varying standoff distance (a) h=50 mm, (b) h=100 mm, (c) h=150 mm, and (d) h=200 mm.